Improving the performance of causality analysis techniques for automated fault diagnosis in mineral processing plants

Brian Siegfried Lindner

Dissertation presented for the degree of
Doctor of Philosophy (Extractive Metallurgical Engineering)
in the Faculty of Engineering at Stellenbosch University

Supervisor: Dr. Lidia Auret
Co-supervisor: Prof. Margret Bauer, University of Pretoria

April 2019

Declaration

By submitting this dissertation electronically, I declare that the entirety of the work contained therein is my own, original work, that I am the sole author thereof (save to the extent explicitly otherwise stated), that reproduction and publication thereof by Stellenbosch University will not infringe any third party rights and that I have not previously in its entirety or in part submitted it for obtaining any qualification.

Date: April 2019

Plagiarism declaration

1. Plagiarism is the use of ideas, material and other intellectual property of anothers work and to present is as my own.
2. I agree that plagiarism is a punishable offence because it constitutes theft.
3. I also understand that direct translations are plagiarism.
4. Accordingly all quotations and contributions from any source whatsoever (including the internet) have been cited fully. I understand that the reproduction of text without quotation marks (even when the source is cited) is plagiarism.
5. I declare that the work contained in this dissertation, except where otherwise stated, is my original work and that I have not previously (in its entirety or in part) submitted it for grading in this dissertation or another document.

Initials and surname: B.S. Lindner

Date: April 2019

Abstract

Modern mineral processing companies are driven towards improving productivity by leveraging existing processes optimally. This can be achieved by improving diagnosis of faults that degrade process performance to provide insightful and actionable information to process engineers.

In mineral processing plants, units and variables are connected to each other through material flow, energy flow, and information flow. Faults propagate through a process along these interconnections, and can be traced back along their propagation paths to their root causes. Techniques have been developed for extracting these causal connections from historical process data. These techniques have proven successful for fault diagnosis in chemical processes. However, they have not been widely accepted by industry due to lack of automation of the techniques, complicated implementation, and complicated interpretation.

This dissertation investigated the limitations of the causality analysis procedures currently available to process engineers as fault diagnosis tools and developed improvements on them. Improvements were developed and tested using a combination of simulated case studies and real world case studies of operational faults occurring in a mineral processing plant.

Objective I: was to *investigate* the factors that affect performance of causality analysis techniques. The use of transfer entropy for fault diagnosis in a minerals processing concentrator plant was demonstrated. The desired performance criteria of causality analysis techniques were then defined in terms of: general applicability; automatability; interpretability; accuracy; precision; and computational complexity. The impact of process conditions on the performance of Granger causality and transfer entropy were then investigated. An analysis of variance (ANOVA) was performed to investigate the impact of process dynamics, fault dynamics, and the parameters on the accuracy of transfer entropy.

Objective II: was to *design* a systematic workflow for application of causality analysis for fault diagnosis. The ANOVA was used to develop a novel relationship between the optimal transfer entropy parameters and the process and fault dynamics. This relationship was then placed within a systematic workflow developed for the application of transfer entropy for oscillation diagnosis, addressing the need for clear procedures and guidelines for data selection and parameter selection. The workflow was applied to an oscillation diagnosis case study from a minerals concentrator plant, and shown to provide a systematic approach to accurately determining the fault propagation path.

Objective III: was to *design* a tool to aid the decision of which causality analysis method to select. A comparative analysis of Granger causality and transfer entropy for fault diagnosis based on the performance criteria defined was performed. The comparison showed that transfer entropy was more precise, generalisable, and visually interpretable. Granger causality was more automatable, less computationally expensive, and easier to interpret. Guidelines were developed from these comparisons to aid users in deciding when to use Granger causality or transfer entropy.

Objective IV: was to *present* tools for interpretation of causal maps for root cause analysis. Methods for construction of causal maps from the results of the causality analysis calculation were presented, and methods for interpretation of causal maps. The usefulness of these techniques for diagnosis of real world case studies was demonstrated.

Uittreksel

Mineraalprosesseringsmaatskappye plaas hul fokus op die verhoging van produktiwiteit deur bestaande prosesse te optimeer. Dit word bereik deur op 'n meer doeltreffende manier foute op te spoor wat prosesprestasie hinder en sodanig insiggewende inligting aan prosesingenieurs oor te dra.

Proseseenhede en veranderlikes word verbind aan mekaar in 'n mineraalproseseringsaanleg deur die vloei van material, energie en inligting. Foute word deur 'n proses voortgesit deur die verbintenis van die proseseenhede aan mekaar, en die kernoorsaak van 'n fout kan opgespoor word deur terug te werk deur prosesverbintenisse. Tegnieke is ontwikkel om oorsaaklike verbintenisse te onttrek vanuit historiese prosesdata. Hierdie tegnieke word as suksesvol geag vir foutdiagnose in chemiese prosesse. Hulle is egter nie in die mineraalprosesseringsbedryf aanvaar nie weens die tekort aan die moontlikheid van outomasie, die ingewikkelde implementasie daarvan, asook ingewikkelde interpretasie.

Hierdie verhandeling ondersoek die beperkinge van beskikbare oorsaaklikheidsanalisemetodes as foutdiagnosegereedskap vir prosesingenieurs en ontwikkel verbeteringe op die metodes. Verbeterings is ontwikkel en getoets deur 'n kombinasie van gesimuleerde gevallestudies en werklike gevallestudies van 'n mineraalprosesseringsaanleg.

Doel I: was om faktore te *ondersoek* wat die prestasie van oorsaaklikheidsanalises affekteer. Die gebruik van oordragsentropie vir foutdiagnose in 'n mineraalprosesserings konsentrasie-eenheid is gedemonstreer. Die gewenste prestasiekriteria van oorsaaklikheidsanalises is toe gedefinieer in terme van: algemene toepaslikheid; outomiseerheid; interpreteerbaarheid; akkuraatheid; presisie; en berekeningkompleksiteit. Die impak van prosestoestande op die prestasie van Granger oorsaaklikheid en oordragsentropie is toe ondersoek. 'n ANOVA variansieanalise is toe uitgevoer om die impak van prosesdinamika, foutdinamika, en geselekteerde parameters op die akkuraatheid van oordragsentropie te ondersoek.

Doel II: was om 'n systematiese werksvloei te *ontwerp* vir die toepassing van oorsaaklikheidsanalises op foutdiagnose. Die ANOVA was gebruik om 'n nuwe verhouding te ontwikkel tussen die optimale oordragsentropieparameters en die proses- en foutdinamika. Hierdie verhouding is toe in 'n sistematiese werksvloei geplaas ontwikkel vir die toepassing van oordragsentropie vir ossillasiediagnose, wat die nodigheid vir duidelike prosedures en riglyne vir data- en parameterseleksie addresseer het. Die werkvloei is toegepas op 'n ossilasiediagnose gevallestudie van 'n mineralekonsentrasieaanleg, en is gewys om 'n systematiese benadering te verskaf om die foutvoortplantingspad akkuraat vas te stel.

Doel III: was om gereedskap te *ontwerp* om te help besluit tussen oorsaaklikheidsanalisemetodes. 'n Vergelykende analise van Granger oorsaaklikheid en oordragsentropie vir foutdiagnose gebaseer op gedefinieerde prestasiekriteria is uitgevoer. Die vergelyking het getoon dat oordragsentropie meer presies, veralgemeenbaar en visueel interpreteerbaar is. Granger oor-

saaklikheid is meer outomeerbaar, minder berekeningsintensief en makliker om te interpreteer. Riglyne is ontwikkel vanuit hierdie vergelykings om verbruikers te help kies tussen Granger oorsaaklikheid en oordragsentropie.

Doel IV: was om gereedskap *voor te stel* vir die interpretasie van oorsaaklikheidskaarte vir kernoorsaakanalises. Metodes om oorsaaklikheidskaarte op te stel vanuit die resultate van oorsaaklikheidsanaliseberekeninge is voorgestel, asook metodes vir die interpretasie van oorsaaklikheidskaarte. Die nut van hierdie tegnieke vir die diagnosering van werklike gevallestudies is gedemonstreer.

Acknowledgements

The author wishes to acknowledge the following people and institutions for their various contributions towards the completion of this work:

- The supervisors of this project, Dr. Lidia Auret and Prof. Margret Bauer, for their support, guidance, feedback, and advice for this project.
- Anglo American Platinum Limited, for their extensive support of this project. This support included funding, access to data, and access to process expertise from process engineers.
- Dr. J.W.D Groenewald at Anglo American Platinum Limited, for support and guidance during this project, for contributing useful industrial perspective to the project, and for contributing as co-author on two of the papers published on this research.
- ABB Corporate Research Centre in Ladenburg, Germany, for facilitating a research exchange visit.
- Dr. Moncef Chioua at ABB Corporate Research in Ladenburg, Germany, for his useful guidance and insights for this project, and for contributing as co-author on one of the papers published on this research.
- Stone Three Digital, and my colleagues there for support during my project, and for allowing me the freedom to complete the project part time.
- My girlfriend, Patsy, for her continuous support during this project.
- My family for support and encouragement during this project.

Table of Contents

Abstract **v**

Uittreksel **vii**

Acknowledgements **ix**

Glossary **xvii**

List of Reserved Symbols **xix**

List of Abbreviations **xxi**

List of Figures **xxiii**

List of Tables **xxvii**

1 Introduction **1**

1.1 Background 1

1.2 Informal problem description 2

1.3 Dissertation aim 2

1.4 Dissertation objectives 2

1.5 Significance and novel contributions of this dissertation 2

1.6 Publications 3

1.6.1 Conference papers 3

1.6.2 Journal publications 4

1.7 Dissertation organisation 4

2 Critical literature review: Causality analysis for fault diagnosis **5**

2.1 Chapter introduction 6

2.2 Chapter objectives 6

2.3 Connectivity and causality in processes 8

2.4 Representing causality and connectivity . . . 9
2.5 Uses for causality and connectivity analysis for process engineers . . . 9
2.5.1 Topology modelling and system identification . . . 10
2.5.2 Process monitoring . . . 10
2.5.3 Consequential alarm identification . . . 11
2.5.4 Risk analysis . . . 11
2.5.5 Control structure design . . . 12
2.6 Causality analysis in the context of fault diagnosis . . . 12
2.6.1 Fault detection . . . 13
2.6.2 Fault identification . . . 14
2.6.3 Process recovery . . . 15
2.7 Resources for causality and connectivity information . . . 15
2.8 Capturing connectivity from process knowledge . . . 16
2.8.1 Connectivity from first principles and empirical mathematical models . . . 16
2.8.2 Manual construction of connectivity maps from human knowledge . . . 16
2.8.3 Extraction of topology from process schematics . . . 17
2.9 Capturing causality from historical process data . . . 17
2.9.1 Granger causality . . . 18
2.9.2 Transfer entropy . . . 19
2.9.3 Cross-correlation . . . 24
2.9.4 Partial directed coherence . . . 26
2.9.5 Convergent cross-mapping . . . 27
2.9.6 k-Nearest neighbours . . . 28
2.10 Combining knowledge and data-based connectivity and causality . . . 29
2.11 Summary of causality analysis literature . . . 31
2.11.1 Applications by industry . . . 33
2.11.2 Application by technique . . . 34
2.11.3 Applications by fault type . . . 35
2.12 Critical literature review of components of causality analysis based fault diagnosis 36
2.12.1 Data selection . . . 37
2.12.2 Causality analysis calculation . . . 37
2.12.3 Significance testing . . . 42
2.12.4 Causal map construction . . . 44
2.12.5 Causal map interpretation . . . 48
2.13 Components of causality analysis based fault diagnosis that require improvement 52

2.14 Chapter conclusions 53

3 Overview of dissertation methodology 55

3.1 Chapter introduction 55
3.2 Demonstrating the effectiveness of causality analysis for fault diagnosis 57
3.3 Investigating the factors that affect causality analysis 57
3.4 Developing a workflow for the application of causality analysis 57
3.5 Comparative analysis of Granger causality and transfer entropy 57
3.6 Tools for interpretation of causality analysis 58

4 Demonstrating the use of transfer entropy for oscillation diagnosis 59

4.1 Chapter introduction 59
4.2 Chapter objectives 60
4.3 Methods 60
4.3.1 Transfer entropy 60
4.3.2 Nonlinearity index 61
4.4 Description of case study 62
4.4.1 Flotation circuit operation and control 62
4.4.2 Oscillations in the flotation circuit 63
4.5 Results and discussion 64
4.5.1 Transfer entropy results 64
4.5.2 Nonlinearity index results 66
4.5.3 Discrepancy of different methods and further analysis 66
4.5.4 Shortcomings of causality analysis approach 69
4.6 Chapter conclusion 69

5 Defining desired performance of causality analysis techniques 71

5.1 Chapter introduction 71
5.2 Chapter objectives 72
5.3 Performance criteria for causality analysis 72
5.3.1 Accuracy and precision of causality analysis 72
5.3.2 Automatability of causality analysis 73
5.3.3 Interpretability of causality analysis 74
5.3.4 Computational complexity of causality analysis 75
5.3.5 Applicability for different process characteristics 75
5.4 Factors affecting performance of causality analysis 76

5.4.1 Noise and significance testing . . . 76
5.4.2 Fault type . . . 76
5.4.3 Process interactions . . . 77
5.4.4 Time series characteristics . . . 78
5.4.5 Time frame and parameter selection . . . 79
5.5 Chapter conclusion . . . 80

6 Investigating the impact of perturbations on causality analysis measures 81
6.1 Chapter introduction . . . 81
6.2 Chapter objectives . . . 82
6.3 Methodology . . . 82
6.3.1 Two-tank simulation used to generate experimental time series data . . . 83
6.3.2 Expected performance of causality analysis . . . 84
6.4 Results for system under influence of oscillatory perturbations . . . 85
6.5 Results for system under influence of step perturbations . . . 89
6.6 Chapter conclusions . . . 89

7 Developing guidelines for selection of parameters in causality analysis 91
7.1 Chapter introduction . . . 91
7.2 Chapter objectives . . . 92
7.3 Workflow for application of transfer entropy for oscillation diagnosis . . . 93
7.3.1 Detect fault . . . 95
7.3.2 Perform spectral analysis (optional) . . . 95
7.3.3 Select data for transfer entropy analysis . . . 95
7.3.4 Determine process dynamics (optional) . . . 96
7.3.5 Select parameters for transfer entropy analysis . . . 96
7.3.6 Perform transfer entropy analysis . . . 96
7.4 Establishing guidelines for transfer entropy application . . . 97
7.4.1 Selecting the number of samples . . . 97
7.4.2 Selecting the sampling time . . . 98
7.4.3 Selecting embedding parameters . . . 99
7.4.4 Selecting prediction horizon and time interval . . . 100
7.4.5 Final guidelines for parametrisation . . . 101
7.5 Demonstrating workflow on real case study . . . 103
7.5.1 Detect fault . . . 103
7.5.2 Perform spectral analysis (optional) . . . 104

7.5.3 Select data for transfer entropy . . . 104
7.5.4 Determine process dynamics (optional) . . . 105
7.5.5 Select parameters for transfer entropy . . . 106
7.5.6 Perform transfer entropy analysis . . . 106
7.6 Chapter conclusion . . . 110

8 Comparative analysis between transfer entropy and Granger causality 111
8.1 Chapter introduction . . . 111
8.2 Chapter objectives . . . 112
8.3 Comparing the features of Granger causality and transfer entropy . . . 113
8.3.1 Accuracy and precision of causality analysis techniques . . . 113
8.3.2 Automatability of causality analysis techniques . . . 113
8.3.3 Interpretability of causality analysis techniques . . . 114
8.3.4 Computational complexity of causality analysis . . . 115
8.3.5 Applicability for different process characteristics . . . 116
8.4 Comparing the accuracy and precision of Granger causality and transfer entropy in a simulated system . . . 117
8.4.1 Description of simulated process case study . . . 117
8.4.2 Comparison of Granger causality and transfer entropy to ground truth in simulated case study . . . 118
8.4.3 Summary of simulated case study comparing Granger causality and transfer entropy . . . 122
8.5 Decision flow for application of Granger causality or transfer entropy . . . 122
8.6 Illustrating the features of Granger causality and transfer entropy on an industrial case study . . . 124
8.6.1 Case study description . . . 124
8.6.2 Transfer entropy results . . . 125
8.6.3 Granger causality results . . . 128
8.6.4 Summarising the difference between Granger causality and transfer entropy for the industrial case study . . . 129
8.7 Chapter conclusion . . . 130

9 Development of visual and algorithmic graph interpretation tools for fault diagnosis 133
9.1 Chapter introduction . . . 133
9.2 Chapter objectives . . . 134
9.3 Graph layouts . . . 134
9.4 Graph pruning using transitive reduction . . . 137

9.5 Assigning node and edge attributes . . . 139
9.5.1 Assigning edge weights based on connection strength . . . 139
9.5.2 Grouping nodes according to variable location . . . 140
9.5.3 Grouping nodes according to variable categories . . . 144
9.6 Assigning node importance . . . 146
9.7 Graph complexity metrics . . . 146
9.8 Graph traversal . . . 147
9.9 Recommended causal map interpretation procedure . . . 150
9.10 Chapter conclusion . . . 150

10 Conclusions **153**
10.1 Dissertation summary . . . 153
10.2 Objective I conclusion . . . 153
10.3 Objective II conclusion . . . 155
10.4 Objective III conclusion . . . 155
10.5 Objective IV conclusion . . . 156
10.6 Fulfilment of overall project aim . . . 156
10.7 Appraisal of dissertation contributions . . . 157
10.8 Suggestions for future work . . . 157

A Analysis of variance for parametrisation relationships **167**

B Transfer entropy application procedure **171**
B.1 Detect fault . . . 171
B.2 Perform spectral analysis . . . 171
B.3 Select data for transfer entropy . . . 171
B.4 Determine process dynamics . . . 172
B.5 Select parameters for transfer entropy . . . 172
B.6 Perform transfer entropy analysis . . . 172

Glossary

Adjacency matrix Matrix representation of a graph. Square matrix whose rows and columns correspond to nodes, and binary entries represent the edges.

Causality Links between elements in a process, so that a change in one element cause a change in another, and the direction of the influence is known.

Causality map Graph with nodes representing measured variables, and edges representing causal connections between them.

Connectivity Links between elements in a process, so that changes in either variable influence the other.

Cross correlation Causality measure base on lagging two time series to find the time lag at which the correlation between them is at a maximum

Convergent cross-mapping Causality measure based on the mutual prediction ability of embedding manifolds

Depth-first search Algorithm for graph traversal. Works by beginning at a start node, and discovering adjacent nodes sequentially until the algorithm encounters a node where all the adjacent nodes have already been visited. At this point, the search backtracks along the discovered path to the closest previously discovered node without a discovered neighbour. This is implemented recursively until all nodes reachable from the start node have been visited.

Diffeomorphism Isormorphism of smooth manifolds.

Edge Connection between nodes in a graph. Also called *arc* In causality maps it indicates a causal connection between two measured variables.

Fault Abnormal event occurring in a process that causes measured variables or KPIs to deviate from desired values, possibly causing performance or safety degradation.

Fault detection Procedure for determining whether a fault is present in a process or not.

Fault diagnosis Combination of fault detection and identification.

Fault identification Procedure for determining the type, magnitude and location of a fault.

Granger causality Causality measure based on autoregressive models. Quantifies the prediction improvement of a variable when including past values of another variable.

Graph A mathematical model of pairwise relationships between elements. Consists of *nodes* representing the elements, and *edges* representing the relationship between the elements.

Hazard and operability analysis Risk analysis performed typically during process design phase to identify all potential safety and performance degradation risks.

Inflow Number of edges entering a node.

Isomorphism Mapping that can be reversed using the inverse of the mapping.

k-Nearest Neighbours In this dissertation this refers to a causality measure based on prediction of a variable based on its nearest neighbours.

Node Element in a graph. Also called *vertex*. In a causality map it represents measured variables.

Outflow Number of edges exiting a node.

Partial directed coherence Causality measure based on frequency-domain autoregressive models.

Process monitoring Strategy for analysing process behaviour to determine performance.

Process recovery Corrective action taken to return a process to its desired state after deviation from this state has been diagnosed.

Process topology The way in which constituent parts of the model are interconnected. May be described in terms of connectivity or causality of the variables in the process.

Reachability Ability to negotiate from one node to another within a graph

Root cause analysis Procedure for isolating the location of a fault.

Smearing effect The effect of a fault spreading throughout a process and affecting numerous variables and units.

Strongly connected component A subgraph of of a graph, G, where all the nodes in the subgraph are mutually reachable.

Subgraph A subgraph of a graph, G, is a graph made of a subset of the nodes and edges of G.

Transfer entropy Information theoretic causality analysis approach. Quantifies the reduction in uncertainty of one variable given past values of another variable.

Transitive reduction The transitive reduction of a graph G, is another graph, $G_{reduction}$, with the same number of nodes, but the fewest edges, so that $G_{reduction}$ has the same reachability as G.

Vertex See *Node*.

List of Reserved Symbols

Symbols in this dissertation conform to the following font conventions:		
A	Symbol denoting a variable	(Upper case letter)
a	symbol denoting a scalar	(Lower case letter)
$\mathbf{a}$	Symbol denoting a vector	(Bold lower case letter)
$\mathbf{A}$	Symbol denoting a matrix	(Bold upper case letter)

Symbol	Meaning
α_k	Random phases added for AAFT
$\mathbf{A}$	Coefficient matrix for full AR model
B	Regression coefficient for reduced AR model
$D_i(x)$	Predictability factor for k-nearest neighbours
$d_{i,j}$	Distance between two embedded vectors, i and j
$\mathbf{E}$	Prediction error matrix for autoregressive model
ϵ	Prediction error in autoregressive model
$F_{x_i \to x_j}$	Granger causality from variable x_i to variable x_j
$H(y_{i+h}\|\mathbf{y}_i^{(K)})$	Shannon entropy for y conditioned on past values of itself
$H(y_{i+h}\|\mathbf{y}_i^{(K)}, \mathbf{x}_i^{(L)})$	Shannon entropy for y conditioned on past values of x and y
h	Prediction horizon for transfer entropy
$\eta(x\|y)$	Dependence measure for k-nearest neighbours
$\eta_{x \to y}$	Causality measure for k-nearest neighbours
ι	Imaginary unit
K	Embedding dimension for output variable Y in transfer entropy calculation
k	Model order for Granger causality calculation
κ	Number of nearest neighbours
L	Embedding dimension for input variable X in transfer entropy calculation
M	Number of variables
$\mathbf{M}$	Embedded matrix (manifold)
μ	Mean
N_S	Number of samples
$p(.)$	Probability density function
$p(.\|.)$	Conditional probability density function
$\hat{\pi}_{ij}(\omega)$	partial directed coherence between variable i and variable j, at frequency, ω
ρ	Cross-correlation function
$\bar{\mathbf{r}}(t)$	iAAFT surrogate time series
$\bar{\mathbf{R}}(\omega)$	Frequency domain representation of $\bar{\mathbf{r}}(t)$
σ	Standard deviation
$\bar{\mathbf{s}}(t)$	AAFT surrogate time series
$S_{x \to y}$	Significance threshold for transfer entropy from x to y

T_S	Sampling time
$T_x \rightarrow y$	Transfer entropy from variable x to variable y
τ	Time interval for transfer entropy
τ_p	Residence time of process
$\mathbf{x}_i^{(L)}$	Embedded vector for variable x, at time step i, with embedding dimension, L
y_{i+h}	Value of variable y at time step $i + h$
ω	Frequency

List of Abbreviations

AAFT: Amplitude Adjusted Fourier Transform

AIC: Akaike Information Criterion

AML: Automation Markup Language

APC: Advanced Process Control

ANOVA: ANalysis Of VAriance

AR: AutoRegressive

CCM: Convergent Cross Mapping

CSTR: Continuous Stirred Tank Reactor

CV: Controlled Variable

DTE: Direct Transfer Entropy

DTF: Directed Transfer Function

FFT: Fast Fourier Transform

HAZOP: HAZard and OPerability

iAAFT: iterative Amplitude Adjusted Fourier Transform

KPI: Key Performance Indicator

KDE: Kernel Density Estimation

LSD: Least Significant Difference

MV: Manipulated Variable

NOC: Normal Operating Conditions

PCA: Principal Component Analysis

PDC: Partial Directed Coherence

PDF: Probability Density Function

PID: Proportional Integral Derivative

P&ID: Piping & Instrumentation Diagram

PGM: Platinum Group Metal

PV: Process Variable

RCA: Root Cause Analysis

SDG: Signed DiGraph

SDNTE: Symbolic Dynamic-based Normalised Transfer Entropy

SCC: Strongly Connected Component

VAR: Vector AutoRegressive

XML: eXtensible Markup Language

XRF: X-Ray Fluorescence

List of Figures

2.1 Process monitoring overview 7
2.2 Simple causal map example 9
2.3 Process monitoring loop 13
2.4 Causal map with indirect connections 22
2.5 Density estimation comparisons 24
2.6 Gaussian kernel density estimation example 25
2.7 Literature summary by industry 34
2.8 Literature summary by method 35
2.9 Overview of components of causality analysis 36
2.10 Example of layered layout of causality maps 45
2.11 Example of circle layout of causality maps 46
2.12 Example of force layout of causality maps 46
2.13 Causal map with indirect connections 47
2.14 Transitive reduction illustration 48
2.15 Transitive reduction illustration with cycles 49
2.16 Straightforward causality map example 49
2.17 Causality map demonstrating maximum flow attriute 49
2.18 Example of shortest path found between $Node7$ and $Node3$ 51
2.19 Overview of chapters addressing components of causality analysis 52

3.1 Overview of chapters addressing components of causality analysis 56

4.1 Transfer entropy basic methodology 60
4.2 Causal map example 61
4.3 Flotation circuit flow diagram 62
4.4 Flotation case study oscillatory time series 63
4.5 Flotation case study transfer entropy propagation paths 65
4.6 Cyclone pressure disturbance 68

5.1 Example of a cyclical graph 75
5.2 Illustration of sensor and process noise 76
5.3 Causal map for control loop 77
5.4 Causal map with confounding connections 78
5.5 Time frame for Granger causality and transfer entropy 80

6.1 Diagram of simulated tank with heat exchange system 82
6.2 Response of T_1 to perturbations T_{1in} 84
6.3 Expected response of causality measures to perturbations 85
6.4 Impact of oscillatory perturbations on Granger Causality and transfer entropy . 88
6.5 Impact of step perturbations on Granger causality and transfer entropy 90

7.1 Workflow for application of transfer entropy for oscillation diagnosis 94
7.2 Transfer entropy response to number of samples 98
7.3 Transfer entropy response to sampling time 99
7.4 Transfer entropy response to process dynamics 100
7.5 Linear relationship between optimal time interval (τ_{max}) and oscillation period (P) 101
7.6 Linear relationship between oscillation period (P) and time delay (T_D), and optimal time interval (τ_{max}) 102
7.7 Linear relationship between P and distance between τ peaks 102
7.8 Flotation circuit flow diagram 103
7.9 Flotation circuuit oscillatory time series 104
7.10 Power spectra showing oscillation frequency 105
7.11 Flotation case study transfer entropy parametrisation propagation path 108
7.12 Flotation case study cyclone pressure 109

8.1 Computational time required to calculate transfer entropy significance for one pair of variables as a function of number of samples. System used: 32 GB RAM, 3.33 GHz processor. The computational time was found to be well approximated by $CPU_{time} = 34 \times N^{0.5}$ 116
8.2 Diagram of simulated two tank process. Two tanks in series with heat exchangers. Tank levels are controller by the flow of cold water into the tank, tank temperatures are controlled by the steam flow rate through the heating coils. Random noise was added to the signals. 119
8.3 Oscillations in signals in two tank process. 120
8.4 Distributions of true connection rates and relative true connection rates for Granger causality and transfer entropy in the simulated two-tank process. 120
8.5 Granger causality and transfer entropy results from repeated simulated experiments compared to true propagation path. Results shown from minimum, median, and maximum true connection rates. 121

8.6 Decision flow for application of Granger causality or transfer entropy for fault diagnosis. . . . 123
8.7 Simplified process flow diagram showing the primary milling circuit, the rougher flotation section and the secondary milling section. . . . 125
8.8 Trends for all variables showing oscillation at period of 69 minutes. This includes variables from primary milling circuit, rougher flotation circuit, and secondary milling circuit. . . . 126
8.9 Transfer entropy propagation paths for oscillations in the primary milling, flotation, and secondary milling circuits. Values displayed on edges and edge width represent the transfer entropy value calculated. Colours on nodes indicated the section of the plant where the variables are located. . . . 127
8.10 Time series plots of sump variables at start of oscillation. . . . 128
8.11 Granger causality propagation paths for oscillations in the primary milling, flotation, and secondary milling circuits. . . . 129

9.1 Different layours for causality maps . . . 136
9.2 Transitive reduction for the primary milling oscillation . . . 138
9.3 Causality map for plant wide oscillation visualising connection strength using edge width . . . 139
9.4 Causality map for both banks in flotation circuit . . . 141
9.5 Propagation paths for oscillations in the flotation circuit . . . 142
9.6 Causality map coloured according to plant sections . . . 143
9.7 Flotation circuit oscillations treating CVs and MVs separately . . . 145
9.8 Causality map for primary mill oscillation with maxflow highlighted . . . 146
9.9 Shortest path from $SU1LevelPV$ to $SU5Density$ . . . 148
9.10 All nodes reachable from $SU1LevelPV$, found using the depth-first search . . . 149
9.11 Procedure for interpretation of causal maps for fault diagnosis . . . 150

10.1 Overview of chapters addressing components of causality analysis . . . 154

A.1 ANOVA results for different levels of each factor . . . 169

List of Tables

2.1 Comparing characteristics of knowledge and data-based causality 31
2.2 Causality analysis literature summary 31
2.2 Causality analysis literature summary 32
2.2 Causality analysis literature summary 33
2.3 Summary of decisions and parameter selection methods used for transfer entropy in literature 39

4.1 Flotation case study nonlinearity index results 67
4.2 Flotation case study oscillation start times 67

6.1 Tank simulation model parameters 83
6.3 Ranges of perturbations used for sensitivity analysis 84
6.4 Means and standard deviations of Granger causality and transfer entropies shown in Figure 6.4. 86

7.1 Guidelines for transfer entropy parametrisation 101
7.3 Time delay between level variables 106
7.4 Time delay between outflow variables 106
7.5 τ between level variables 107
7.6 τ between outflow variables 107
7.7 Flotation case study oscillation start times 109

8.1 Means and standard deviations of true connection rates and relative true connection rate shown in Figure 8.4. 118

9.1 Maxflow for nodes in primary mill oscillation causal map 147

A.1 ANOVA design 167
A.2 ANOVA results 168

CHAPTER 1

Introduction

Contents

1.1 Background 1
1.2 Informal problem description 2
1.3 Dissertation aim 2
1.4 Dissertation objectives 2
1.5 Significance and novel contributions of this dissertation 2
1.6 Publications 3
1.6.1 Conference papers *3*
1.6.2 Journal publications *4*
1.7 Dissertation organisation 4

This dissertation investigates the use of causality analysis for fault diagnosis in mineral processes.

1.1 Background

Modern mineral processing companies are driven towards improving productivity. Rather than initiating large capital expenditure projects, mineral processing companies are interested in leveraging existing processes optimally. One of the ways to optimise process productivity is to improve process monitoring. In Deloitte's article titled 'The Future of Mining in Africa' [Deloitte, 2018], the major challenges that need to be addressed in the industry involve improving visibility on actions to be taken to improve the a process:

> 'Mining processes lack visibility to real time, accurate information. This hinders the ability to track resource performance and increase equipment uptime. More complete, timely, and insightful information and leading indicators enables leadership and frontline teams to intervene more proactively. Incorporating smart workflows that highlight process deviations will trigger the desired response mechanisms and support the required behavioural change.'

Process monitoring that provides insightful and actionable information is therefore paramount to improving process productivity. Accurate fault diagnosis can be used to investigate process changes and determine the required corrective action.

In mineral processing plants, units and variables are connected to each other through material flow, energy flow and information flow. Knowledge of this interconnection of the process can be a useful tool for process engineers. One of the uses for this information is fault diagnosis. Faults propagate through a process along these interconnections, possibly causing performance or safety degradation. With knowledge of the connections a fault may be traced back to its root cause along these propagation paths. This information can then be used to determine what corrective action needs to be taken.

Causality analysis techniques can be used for fault diagnosis. These techniques infer causal connections between measured variables from historical process data. This dissertation investigates and improves on existing causality analysis techniques for fault diagnosis.

1.2 Informal problem description

Techniques have been developed for extracting causality information from historical process data. The variations of causality analysis include: transfer entropy [Duan *et al.*, 2013]; Granger causality [Yuan & Qin, 2014]; cross-correlation [Bauer & Thornhill, 2008]; partial directed coherence [Landman *et al.*, 2014]; convergent cross-mapping [Luo *et al.*, 2017]; and k-nearest neighbours [Stockmann *et al.*, 2012]. Numerous authors have demonstrated successful fault diagnosis using these techniques. However, data-based causality analysis has not been widely accepted by industry as a solution for automated fault diagnosis. The reason for industry's reluctant adoption can be ascribed to: the complex implementation procedures of the techniques; the sensitivity of their performance to process conditions; and the difficult interpretation of the results of the causality analysis. These shortcomings need to be addressed to make these techniques accessible to industry practitioners.

1.3 Dissertation aim

The aim of this dissertation is to improve performance of data based causality analysis methods for fault diagnosis by developing systematic procedures and clear guidelines fo application of the techniques and interpretation of their results. Improvements will be developed and evaluated using a combination of simulated case studies and real world case studies from a mineral processing plant.

1.4 Dissertation objectives

The following objectives will be pursued in this dissertation:

Objective I. To *investigate* the factors that affect performance of causality analysis techniques.

Objective II. To *design* a systematic workflow for application of causality analysis for fault diagnosis.

Objective III. To *design* a tool to aid the decision of which causality analysis method to select.

Objective IV. To *present* tools for interpretation of causal maps for root cause analysis.

1.5 Significance and novel contributions of this dissertation

The improvements to causality analysis based fault diagnosis to be developed in this dissertation aim to make the tools more accessible for engineers in the processing industries. This improved accessibility will allow engineers to diagnose faults in a process rapidly, and implement corrective action. According to Reis & Gins [2017], reducing the time taken for diagnosis of the faults after they have been detected presents a significant potential improvement in the time taken from when a fault occurs to when it is corrected. This means that the detrimental impact of the fault will be limited to a shorter time. This means that processes can become more efficient, extracting more value from the raw materials, and utilising less energy for processing. The safety of the processes will also be improved, since some faults pose a potential degradation in safety, as well as performance.

The novel contributions of this project are:

1. Application of causality analysis is complicated, with multiple decision-making steps that could affect the results. In the literature of causality analysis for fault diagnosis, no systematic framework addressing these numerous, complicated steps has been presented. Chapter 7 provides a systematic workflow incorporating these steps.

2. The accuracy of causality analysis techniques is sensitive to data selection and parameter selection. Chapter 7 provides an analysis of variance on the impact that process and fault dynamics and calculation parameters have on transfer entropy. These results are used to provide guidelines for the above-mentioned workflow. This approach of parametrisation of causality analysis techniques based on process dynamics is novel, and is shown to be effective.

3. The comprehensive comparative analysis of Granger causality and transfer entropy based on all desired performance criteria for causality analysis techniques presented in Chapter 8 is novel. This comparison was used to provide useful guidelines for selection of which causality analysis technique to use and how to interpret the results.

4. Construction and interpretation of causality maps is an important step for root cause analysis using these methods that has been neglected in fault diagnosis literature, with most authors providing *ad-hoc* interpretations of results. Chapter 9 provides novel guidelines for construction and interpretation of causality maps based on existing techniques.

1.6 Publications

Sections of this dissertation have been submitted for publication in peer-reviewed conference proceedings, and in peer-reviewed journals.

1.6.1 Conference papers

The following papers based on this work were published in peer-reviewed conference proceedings:

1. Lindner B, Auret L & Bauer M, 2017a, Investigating the Impact of Perturbations in Chemical Processes on Data-Based Causality Analysis. Part 1: Defining Desired Performance of Causality Analysis Techniques, IFAC-PapersOnLine, 50(1), pp. 3269-3274.[Lindner *et al.*, 2017a]

2. Lindner B, Auret L & Bauer M, 2017b, Investigating the Impact of Perturbations in Chemical Processes on Data-Based Causality Analysis. Part 2: Testing Granger Causality and Transfer Entropy, IFAC-PapersOnLine, 50(1), pp. 3275-3280.[Lindner *et al.*, 2017b]

3. Lindner B, Chioua M, Groenewald J, Auret L & Bauer M, 2018b, Diagnosis of Os cillations in an Industrial Mineral Process Using Transfer Entropy and Nonlinearity Index, IFAC-PapersOnLine, 51(24), pp. 1409-1416.[Lindner *et al.*, 2018b]

1.6.2 Journal publications

The following papers based on this work have been submitted for publication in peer-reviewed journals:

1. Lindner B, Auret L & Bauer M, 2018, A systematic workflow for oscillation diagnosis using transfer entropy, Manuscript accepted by IEEE Transactions on Control Systems Technology. [Lindner *et al.*, 2018a]

2. Lindner B, Auret L, Bauer M & Groenewald JWD, Comparative analysis of Granger causality and transfer entropy to present a decision flow for the application of oscillation diagnosis. Manuscript accepted pending revision. Journal of Process Control.

1.7 Dissertation organisation

This dissertation is organised as follows: Chapter 2 presents the relevant background on causality analysis in the context of fault diagnosis; Chapter 3 present an overview of the research methodology followed to address the objectives of the dissertation; Chapter 4 presents an example of causality analysis used to isolate the root cause in an industrial case study to demonstrate the effectivity of the techniques; Chapter 5 discusses the desired performance of causality analysis techniques; Chapter 6 investigates the impact of process conditions on the performance of Granger causality and transfer; Chapter 7 develops a systematic workflow for application of causality analysis techniques, including a novel procedure for optimal parametrisation based on fault and process dynamics; Chapter 8 presents a comparative analysis of Granger causality and transfer entropy for fault diagnosis based on the performance criteria defined, to provide guidelines for the decision of which causality analysis technique to use; Chapter 9 presents algorithmic and visual techniques for interpreting causality analysis results; and finally, Chapter 10 presents the conclusions of the study and future recommendations based on the conclusions.

CHAPTER 2

Critical literature review: Causality analysis for fault diagnosis

Contents

2.1 Chapter introduction . . . 6
2.2 Chapter objectives . . . 6
2.3 Connectivity and causality in processes . . . 8
2.4 Representing causality and connectivity . . . 9
2.5 Uses for causality and connectivity analysis for process engineers . . . 9
2.5.1 Topology modelling and system identification . . . *10*
2.5.2 Process monitoring . . . *10*
2.5.3 Consequential alarm identification . . . *11*
2.5.4 Risk analysis . . . *11*
2.5.5 Control structure design . . . *12*
2.6 Causality analysis in the context of fault diagnosis . . . 12
2.6.1 Fault detection . . . *13*
2.6.2 Fault identification . . . *14*
2.6.3 Process recovery . . . *15*
2.7 Resources for causality and connectivity information . . . 15
2.8 Capturing connectivity from process knowledge . . . 16
2.8.1 Connectivity from first principles and empirical mathematical models . . . *16*
2.8.2 Manual construction of connectivity maps from human knowledge . . . *16*
2.8.3 Extraction of topology from process schematics . . . *17*
2.9 Capturing causality from historical process data . . . 17
2.9.1 Granger causality . . . *18*
2.9.2 Transfer entropy . . . *19*
2.9.3 Cross-correlation . . . *24*
2.9.4 Partial directed coherence . . . *26*
2.9.5 Convergent cross-mapping . . . *27*
2.9.6 k-Nearest neighbours . . . *28*
2.10 Combining knowledge and data-based connectivity and causality . . . 29
2.11 Summary of causality analysis literature . . . 31
2.11.1 Applications by industry . . . *33*
2.11.2 Application by technique . . . *34*

2.11.3 Applications by fault type 35
2.12 Critical literature review of components of causality analysis based fault diagnosis 36
2.12.1 Data selection 37
2.12.2 Causality analysis calculation 37
2.12.3 Significance testing 42
2.12.4 Causal map construction 44
2.12.5 Causal map interpretation 48
2.13 Components of causality analysis based fault diagnosis that require improvement 52
2.14 Chapter conclusions 53

2.1 Chapter introduction

Modern technological advances have presented the mineral processing industry with opportunities for improving process monitoring. Improved monitoring can be leveraged to improve efficiency, safety, quality, and throughput of a process. Advances in data storage, sensing technology, computational technology, and analytics, associated with the Big Data and Industry 4.0 movements, have been instrumental in providing the means for this improvement [Reis & Gins, 2017].

Figure 2.1 illustrates the flow of information for operational performance monitoring. The process can consist of multiple operations, including: processing steps; automatic control; and optimisation strategies. Within this process, multiple sensors are employed to measure process variables. For example, measurements may include temperatures, flow rates, and pressures. These measurements can be combined into a dataset that can be analysed to monitor the performance of the process operations. Poor performance may be characterised by unstable controlled variables, sub-optimal key performance indicators, or unwanted variation in key operational measurements. The results of this performance analysis can then be used to signal alarms or generate performance reports to alert plant engineers of the performance state of the process.

Process monitoring can have different objectives. Process data can be analysed to identify areas for optimisation and improvement of the process to meet targets from a control, production, or safety perspective. Process data can also be used for offline or online fault detection and identification. This function of process monitoring is to diagnose problems that originate due to abnormal process behaviours, sensor failures, controller failure, equipment failure, measurement gross random errors, or even more subtle problems, such as measurement biases [Hodouin, 2011].

This chapter presents a discussion of the theory of causality analysis as it is used for large scale industrial processes. The main focus of this thesis is the use of causality analysis for fault diagnosis.

2.2 Chapter objectives

The objectives of this chapter are:

I To *conduct* a critical review of the relevant literature on causality analysis for fault diagnosis, to *identify* areas that require improvement to aid industrial implementation.

II To *present* the relevant background information of causality analysis techniques.

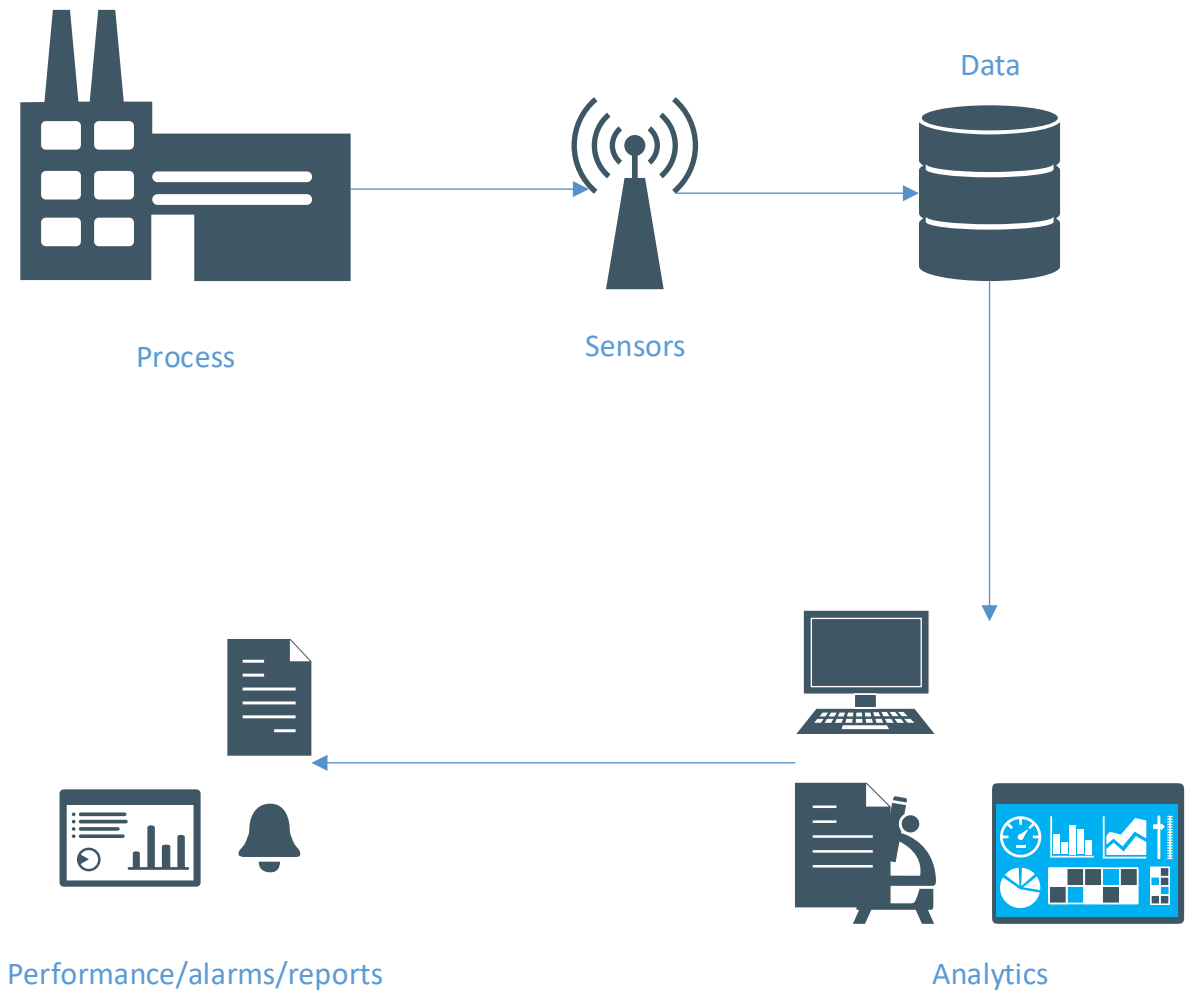

FIGURE 2.1: *Basic components of process monitoring.*

2.3 Connectivity and causality in processes

Elements in mineral processes are connected to each other through material, energy and information flow. Knowledge of these connections in processes can be useful for engineers for monitoring, analysis, and optimisation of the process. Connectivity and causality analysis techniques can be used to infer these connections. For further discussion purposes, connectivity and causality are defined as:

Definition 1. Connectivity: Links between elements in a process, so that changes in one variable influences the other. However, connectivity only describes the existence of influence between elements, without describing the direction of influence.

Definition 2. Causality: Links between elements in a process, so that a change in one element cause a change in another, and the direction of the influence is known. Causality from x to y means that changes in x cause changes in y.

From Definitions 1 and 2 it can be reasoned that connectivity is a necessary, but not sufficient, criteria to establish causality. Therefore, causality is characterised by two components: an observable connection between elements; and an observable direction of influence of that connection.

A definition of causality was put forward by the philosopher, David Hume, in 1748 [Hume, 2008]:

> we may define a cause to be an object followed by another, and where all the objects, similar to the first, are followed by objects similar to the second. Or, in other words, where, if the first object had not been, the second never had existed.

Derivatives of Hume's first definition, that a causal succession is supposed to be a succession that instantiates a regularity, remain prolific in the philosophy of causation[Lewis, 1973]. A formal description of causality in a statistical context was proposed by Wiener [1956]:

> X could be said to 'cause' Y when predictability of Y is improved by incorporating information about X

However, the existence of a connection does not provide sufficient information to infer that a causal link exists. The direction of influence also needs to be established. When X causes Y, a change in X results in a change in Y after some time has passed. Causality needs to incorporate a temporal element as well.

Elements in Definitions 1 and 2 can represent units or variables in a process. The flow of the material between units means that there will be a causal connection between the units. For example, the feed mass flow to a milling circuit will have a causal influence on the mill load. The causal influence is observable, e.g. increased feed mass flow will cause an increase in the mill loading. The direction of the causal influence is also observable by considering the temporal aspect of the influence. The increase in mill loading will be observed after the increase in the feed mass flow. The time delay between the increase in the feed mass flow and the mill loading may be due to transport delay, from where the feed mass flow is measured on a weightometer to the load cells measuring the load on the mill. The time delay may also be due to residence time in units with significant volume. For example, the mill discharge sump's residence time will means that deviations in slurry density before the sump will not instantaneously be observed if measured after the sump.

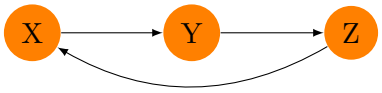

FIGURE 2.2: *Example of causal map for a system of three variables. Nodes represent variables, edges represent causal influence from one variable to another.*

2.4 Representing causality and connectivity

Graph theory can be used for the analysis and visualisation of connectivity and causality. In this section some basic graph theory that will be used for causality analysis in this dissertation are presented.

A *graph* is a mathematical model of pairwise relationships between elements[Bang-Jensen, 2010]. A graph is made up of *nodes* (sometimes called vertices), representing the elements, and *edges* (sometimes called arcs), representing the relationship between the elements. For connectivity analysis, the nodes represent variables or units within the process, and the edges represent a connection between them. A graph can be *directed* or *undirected*. In a directed graph, edges in the graph specify the directionality of the influence between nodes[Bang-Jensen, 2010]. When there is an edge between a pair of nodes, the node from which the edge originates is is the *source* node and the node to which the edge points is the *sink* node. Directed graphs are sometimes abbreviated to *digraphs*. In an undirected graph, there is no directionality assigned to edges between nodes[Bang-Jensen, 2010].

Many implementations of of causality and connectivity analysis exploit the advantages of visualisation of the connectivity. A graph can be represented visually. An example for a system of three variables, X, Y, and Z, is shown in 2.2.

A graph can be represented by an adjacency matrix[Bang-Jensen, 2010]. An adjacency matrix is a square matrix whose rows and columns correspond to nodes, and binary entries represent the edges. An entry of 1 in row i, column j, indicates that the node represented by row i has a causal influence on the node represented by column j. An entry of 0 indicates no connection exists. By convention the row represents the *source* element, and the column represents the *sink* element. Equation 2.1 provides an example of an adjacency matrix for the graph in Figure 2.2. The 1 in row 1, column 2 represents the edge that indicates that variable X has a causal influence on Y.

$$\mathbf{A} = \begin{matrix} 0 & 1 & 0 \\ 0 & 0 & 1 \\ 1 & 0 & 0 \end{matrix} \tag{2.1}$$

2.5 Uses for causality and connectivity analysis for process engineers

Connectivity and causality information in large-scale processes provide a number of potential applications for design and analysis of processes. These applications are briefly discussed here to illustrate the usefulness of these techniques.

2.5.1 Topology modelling and system identification

Chemical and mineral processes are complex. Understanding the interactions between elements in the process can be difficult, requiring scrutiny of disparate information sources. These information sources include process data from different types of sensors, engineering diagrams, process models, and design documents. The volumes of data available to engineers is increasing with advancements in Industry 4.0 solutions to process engineering problems[Reis & Gins, 2017]. Visual analytics can be used to provide engineers with more tangible tools for understanding this information [Keim *et al.*, 2010]. Knowledge of connectivity and causality of a process can be used to build a topology model of the process and visualise it. Romero & Graven [2013] developed a user-centered design methodology to visualise connectivity information to support engineers responsible for operation and maintenance of an oil and gas facility.

Parameter estimation for system identification can also be performed with a known system structure[Yang *et al.*, 2014]. Fixing the system structure in advance can streamline the system identification procedure, so that not every possible combination of inputs and outputs needs to be evaluated.

2.5.2 Process monitoring

Causality analysis can be used as a tool for process monitoring. One use for causality analysis is for fault diagnosis fault diagnosis. A fault may be defined as follows:

Definition 3. Fault: Abnormal event that causes that causes measured variables or key performance indicators (KPIs) to deviate from desired values, possibly causing performance or safety degradation.[Isermann, 2006]

Identifying the location of the fault is often termed root cause analysis (RCA). Modern chemical and mineral processes are highly interconnected through units, equipment, energy flow and material flow and information flow through control loops. This interaction is further complicated through recycle streams, complex control strategies, and control interaction. This interconnectivity means that a fault originating in one part of a process propagates to different parts of the process. This causes numerous measured variables to show effects of the fault, obscuring the root cause. The effect of the fault spreading through the process is often referred to as the 'smearing effect'[Van den Kerkhof *et al.*, 2013].

Since the faults propagate along connected paths in a process, knowledge of these connections may be utilised to trace the fault back to its root cause[Reis & Gins, 2017]. This connectivity information is often available from process knowledge. Fundamental process knowledge, acquired by engineers through education, training, or experience, can reveal the connections between variables[Yang *et al.*, 2014]. Another resource for this connectivity information is historical process data, which can be used to model the causality[Yang *et al.*, 2014].

Another way to look a the process monitoring problem is that engineers want to know the cause for a change in the process. In the cause of fault diagnosis, the change has detrimental effect, and the engineer wants to find the root cause of the change so that it can be corrected. However, change with a positive effect may also occur. For example if the recovery of a process increased, it would be useful to know what conditions caused the positive change so that the scenario can be repeated, or the process moved to an optimum by obtaining these conditions again.

Engineers can leverage data analysis techniques to analyse large time spans of data and classify operations of good and bad performance. The difference in performance may be due to specific

process conditions. Causality analysis can be used to identify the contributing variables to those conditions, and how they are influenced by, and influence other variables in the process.

2.5.3 Consequential alarm identification

Industrial processes have numerous alarms to indicate to an operator when an abnormal situation has occurred. Alarms are usually triggered when a KPI or measured variable deviates significantly from a desired value. Ideally only one alarm should be triggered during an abnormal event. However, as a result of interconnectivity and redundancy, an abnormal event which has propagated through a process may triggers a multitude of alarms[Wang *et al.*, 2016]. This abnormal event propagating through the process will trigger the alarms in sequential order. Causality analysis could then be used to determine the root cause alarm. This application can be seen as a type of fault diagnosis, with specific focus on alarm propagation.

The online consequential alarm identification results could be used to identify typical alarm patterns. These patterns could be saved offline. When a new alarm sequence matches one of the saved patterns, a single alarm for the known root cause can be triggered, instead of triggering all the alarms in the pattern. In this way alarm flooding can be reduced[Yang *et al.*, 2014].

By taking into account time lags between alarm variables, Yang *et al.* [2012] generated a correlation colour map of the alarm data to show clusters of alarms strongly correlated with each other. They found that this was useful to identify redundancy in the alarm network and alarm settings could be improved. The application was demonstrated on an industrial case study of a hydro-treater process in a refinery. Zhang *et al.* [2018] demonstrate the use of causality analysis for consequential alarm identification. This application was to analyse alarms of high central processing unit (CPU) utilisation in a computing network, as opposed to alarms from an industrial process. However, the application can be extended to different types of alarms. Hu *et al.* [2017] investigated the use of causality analysis techniques to determine cause-effect in alarm data. the application was demonstrated on data from an industrial oil plant.

2.5.4 Risk analysis

Risk analysis and hazard and operability (HAZOP) studies can be performed using connectivity and causality analysis. The possible fault propagation path can be identified using these techniques, so that the effects of a fault can be predicted in advance. This can be seen as a type of prognosis application of these techniques. The connectivity structure can be used to automate the inference using forward propagation[Yang *et al.*, 2014].

Risk analysis and HAZOP studies are typically done during design and commissioning of processes[Sinnott, 2009]. In scenarios where the connectivity was obtained from knowledge-based methods, once the process has been designed the connectivity can be extracted. Data-based causality techniques can only be applied on an existing process that is already running. So unless the risk and HAZOP are being re-evaluated, the data-based techniques would not be useful in this context. Re-evaluation of risk may be necessary if units are replaced or process operation is altered significantly.

Venkatasubramanian *et al.* [2000] reviewed how intelligent HAZOP techniques based on signed digraph (SDG) approach (see Section 2.8 for more information) can be used to aid traditional manual HAZOP methodologies. They demonstrated how these SDG based systems can reduce the engineering time and effort, and improve the reliability of the analysis by limiting the room for subjective human error[Venkatasubramanian *et al.*, 2000].

Cui *et al.* [2010] investigated an approach where automated connectivity extraction from piping and instrumentation diagrams (P&IDS) was integrated with HAZOP expert systems. They found that the integration aided the HAZOP procedure by sparing time and effort required for process specification.

Wang *et al.* [2012] developed a support system for HAZOP studies. The system first classifies typical accidents (or faults) and describes of their causes. A connectivity model, or 'influence relationship model' as it is referred to in the paper, is then constructed using the SDG approach. This connectivity model is then used to identify spread paths (propagation paths) of the fault through the system. this program, a number of influence relationship models, which can be utilized to present the relationship structure of the whole system, can be established, and a variety of spread paths, which can be employed to describe the occurrence of the accidents, can be identified. These models and paths can help analyzers to understand the analysis process of different chemical processes and to verify the analysis results. The system suggested helped to capture and formalise knowledge from process experience typically passed on from engineer to engineer. This experience knowledge includes the connectivity structure of the process, classification of typical faults, reasons for typical faults, and their effects.

This was suggested as a possible future research direction for the field of connectivity and causality analysis in the paper by Romero & Thornhill [2014], where the integration, navigation, and exploration of plant connectivity was discussed.

2.5.5 Control structure design

Connectivity and causality represent the basic causal nature of the process. Understanding the interactions of variables can aid design of the control structure of the process. This information can be used to determine the best locations for control loops and for sensors in the process [Yang *et al.*, 2014]. This application only makes sense for an existing process, with existing control structures. It could be used to improve control structure in an existing process. For example, complex interactions that are not apparent from traditional process modelling techniques may be revealed using causality analysis.

Birk *et al.* [2014] presented application software to support engineers in the selection of control configuration in interconnected processes. The software combines a graphical representation of the physical process layout, a directed graph that represents the process dynamics and controllers, and control configuration analysis tools, in one unified user interface. The control configuration analysis tool utilised most extensively was the relative gain array [Skogestad, 2010].

2.6 Causality analysis in the context of fault diagnosis

Figure 2.3 gives an overview of the process monitoring procedure. Fault detection is applied to data measured in the process. When no abnormal behaviour is detected, the fault detection loop continues. When an abnormality is detected, further investigation into the fault is performed with fault identification. When the root cause of the fault has been identified then the operator may decide what corrective action is necessary and the operator can then perform process recovery to return the process to its desired operation.

The focus of the mining industry on process optimisation and process monitoring[Deloitte, 2018, Hodouin, 2011], means that the fault diagnosis application of causality analysis is highly relevant.

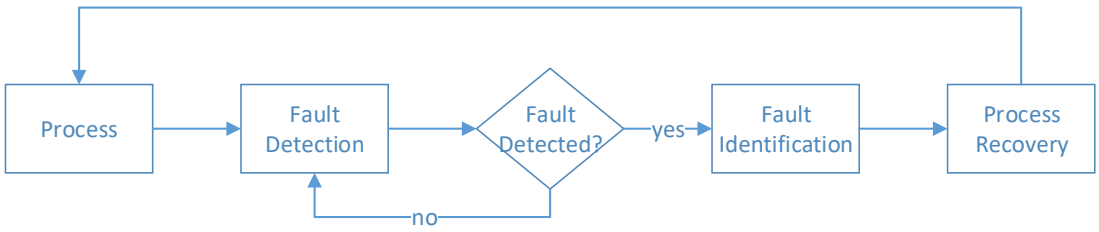

FIGURE 2.3: *Illustration of process monitoring loop.*

Therefore, this dissertation focuses on the use of causality analysis for fault diagnosis. This section therefore introduces fault diagnosis and places causality analysis within that context.

2.6.1 Fault detection

According to the the survey on industrial process monitoring and diagnosis by Qin [2012], two different approaches are followed in fault detection. One approach is to construct a model of the process based on observed normal operating conditions (NOC), and when new data deviates from this normal model, the presence of a fault is inferred. The other approach is to build models for all relevant fault cases, and determine whether new data matches any of these fault models. In this approach, fault detection and identification may happen simultaneously. Clearly the latter approach requires more modelling effort, and an extensive fault library that is difficult to construct. Therefore most process monitoring methods use the approach modelling NOC [Qin, 2012].

Principal component analysis (PCA) and partial least squares (PLS) have been the predominant techniques used for fault detection [Qin, 2012]. These multivariate projection methods allow for feature extraction of data from a large number of variables to effectively model process data [MacGregor & Kourti, 1995]. Principal component analysis (PCA) has been used by numerous authors. [Ge & Song, 2013, Kourti & MacGregor, 1995, MacGregor & Kourti, 1995, Westerhuis *et al.*, 1998, Xiao & He, 2011]. PLS has also been widely applied[Dong & Qin, 2017, MacGregor *et al.*, 1994, Westerhuis *et al.*, 1998, Wold *et al.*, 1996, Zhang *et al.*, 2012]. Independent component analysis (ICA) is another way to extract factors from data when significant non-Gaussian distributions make up the process data [Qin, 2012]. This approach was used by Liu *et al.* [2013], Odiowei & Yi Cao [2010], Yingwang & Ying [2013], Zhang & Ma [2012]. Using Fisher discriminant analysis (FDA), data collected from the plant during specific faults is categorized into classes. FDA is a dimensionality reduction technique in terms that maximise separation between these classes[Chiang *et al.*, 2000].

Some issues arise when considering the approach of modelling the NOC. The question of how to define and identify NOC does not have a straightforward answer. Another issue that is tied both to the problem of identifying NOC and with the implementation of fault detection, is that processes are dynamic and operating conditions vary over time[Li *et al.*, 2000]. The feed conditions may be different, set-points may be altered according to different performance priorities, control strategies may be altered. All these may cause an observed deviation from the observed NOC, but are not necessarily faults. To mitigate this measures can be employed to

ensure that the NOC data used covers a wide range of process conditions. Another mitigation strategy is to perform adaptive monitoring, where the model is updated recursively whenever a 'plant-model mismatch' is found. Li *et al.* [2000] discuss the use of a recursive PCA methodology, for example.

Spectral techniques for the purposes of oscillation detection are available. Jiang *et al.* [2007] presented the spectral envelope technique to detect and diagnose oscillations. The spectral envelope is calculated from the eigenvalues of the power spectral density matrix. When a peak in the spectral envelop is observed, it indicates the presence of an oscillation.

2.6.2 Fault identification

Detecting a fault is not sufficient on its own. Once it has been detected it is imperative to know more information, such as where the fault originated, what type of fault it was, and what was the magnitude of the fault. This additional information is useful to determine the corrective action needed to bring the process back to its desired state.

The application of causality analysis for fault identification was discussed in Section 2.5.2.

Fault identification methods are often paired with specific fault detection methods. For example, when PCA is used for fault detection, the contribution of each variable to the metric quantifying the deviation of the new data from NOC data can be analysed[Qin, 2003]. When a variable is shown to have a large contribution to the fault it is taken as an indication of the root cause. However, due to the smearing effect [Van den Kerkhof *et al.*, 2013], a large number of variables may show significant contributions, and therefore no single variable can be taken as an indication of the root cause. Adaptations of traditional contribution plots have been developed that improve fault identification. For example, the reconstruction based contribution method presented in Alcala & Qin [2009].

For oscillations diagnosis, the spectral envelope technique[Jiang *et al.*, 2007] allows for a hypothesis test to determine which variables contribute to the oscillation detected. An oscillation contribution index can also be calculated, which gives an indication of the relative contributions of each variable to the oscillation [Jiang *et al.*, 2007]. The ability to identify which variables are contributing to the oscillation, as well as the oscillation contribution index, give useful fault identification capabilities to this technique. However, the oscillation contribution index gives no indication of the order in which the oscillation propagated through the system.

Another oscillation diagnosis technique, the nonlinearity index, developed by Thornhill [2005], ranks variables according to the nonlinearity of their time series. The central concept of this approach is to exploit the fact that a process can act as a mechanical low pass filter [Thornhill, 2005] as the oscillation propagates to different variables. The low-pass process dynamics remove the higher harmonics in the trends and destroy the phase-coupling. This makes the waveforms more sinusoidal and more linear the further away from the root cause the variable is. Therefore the variables with the highest nonlinearity index are assumed to be closest to the root cause. The basis of the nonlinearity test is comparison of the predictability of the time series trend to that of generated surrogate trends [Thornhill, 2005]. Although this assumption, that the degree of nonlinearity indicates the order in which the oscillation propagated through the process, is generally reliable, there may be other causes for nonlinearity in the time series trends that mean that nonlinearity may be higher further away from the root cause. Chapter 4 presents an example of this.

As mentioned in Section 2.5.2, faults propagate along connected paths in a process, knowledge of these connections may be utilised to trace the fault back to its root cause. Causality analysis can

be used to analyse the propagation paths of faults through a process [Yang & Xiao, 2012]. This addresses the limitations of fault identification using traditional fault detection methods. Section 2.9 presents various causality analysis techniques and their application for fault diagnosis.

The performance of a fault detection methodology is often defined in terms of the detection delay; the time between the fault occurrence and the fault detection. Rapid fault detection is desired because the sooner a fault is detected the sooner it can be diagnosed and corrected for. Due to extensive research into numerous applications and techniques detection delay can be in the order of seconds or minutes in many applications, as reported by Reis & Gins [2017]. However, the diagnosis step can often take hours or days, with ad-hoc analyses that are note well formalised. This means that the limiting factor in the process monitoring loop is the diagnosis step [Reis & Gins, 2017]. Therefore improvements in this step presents the most potential benefit to industry. One of reasons for the slow progress of fault diagnosis techniques is that the techniques available often require significant input from engineers to apply the methods and interpret their results. This limitation is addressed in Section 5.3, by defining the desired performance of these methods.

2.6.3 Process recovery

The previous steps of the process monitoring loop are aimed at determining whether a fault has occurred, and when it has occurred, what the cause was. These steps are performed so that the corrective action needed to return the process to its desired state can be determined. At this point the automated, or data-based approaches typically end, and a process engineer can interpret the results of the fault diagnosis techniques and intervene in the process. Corrective action is dependent on the fault, but it may include direct intervention, such as replacement of faulty equipment. Corrective action could also be more indirect intervention, such as changes in control strategy, controller tuning, or set-point changes.

Olivier & Craig [2017] presented a strategy to determine the need for shutdown of a plant during fault conditions to take corrective action. When a fault has been identified and diagnosed an adaptive hypothesis test is used to determine whether to maintain plant operation. An economic operability analysis is then performed to determine whether the faults adversely affect economic performance enough to justify shutdown to repair the faults.

2.7 Resources for causality and connectivity information

Connectivity can be modelled either from knowledge of the process or from statistical methods applied to historical process data.

Process knowledge refers to the fundamental characteristics of the process that are understood by process experts. This information is either stored in mathematical models of the process, in process schematics that describe the connections between units, or fundamental process knowledge[Yang *et al.*, 2014]. This process knowledge is acquired by engineers through education, training, and experience.

Causal information may also be extracted from process data. The connections between measured variables are reflected in the data, since an event observed in one variable will be propagated through to the variable it is connected to.

The extraction of causality from process knowledge is discussed further in Section 2.8, while extraction of causality from process data is discussed further in Section 2.9.

2.8 Capturing connectivity from process knowledge

Process knowledge is a valuable source for determining process connectivity. Process knowledge is encoded in a variety of forms: equations/models describing the process from first principles; stored in human minds; process schematics, such as piping and instrumentation diagrams (P&IDs); and rule-based models[Arroyo *et al.*, 2014]. Topology captured from process knowledge is typically qualitative in nature[Yang *et al.*, 2014, Yang & Xiao, 2012]. This means that the existence of a connection can be inferred, but the strength of the connection cannot.

2.8.1 Connectivity from first principles and empirical mathematical models

For some processes, models have been developed expressing the dynamic system as a set of differential and algebraic equations[Maurya *et al.*, 2003]. In other instances, empirical or semi-empirical models can be used to describe the processes. These equations describe the relationships between variables in the process. In the case of differential equations, these relationships are causal, while with algebraic equations the relationships are non-causal[Maurya *et al.*, 2003]. Non-causal means only connectivity information can be obtained, not causality information. A connectivity map can be constructed systematically by analysing these equations. The drawback of this method is that these types of models are not available for all processes. Mineral processes tend to be characterised by a large degree of uncertainty and complexity. This uncertainty an complexity is a result of a number of factors, including: complex physical and chemical processes; varying ore compositions; complex multiphase characteristics; and varying distributions of solid particle sizes[Wills, 2007]. These factors make accurate models of mineral processes scarce. In some cases the accuracy of the available models, although adequate for the purposes of simulation or prediction, may be insufficient for accurate modelling of the process causality structure [Maurya *et al.*, 2003].

2.8.2 Manual construction of connectivity maps from human knowledge

Process experts have extensive knowledge of the interactions in a process, and this knowledge can be drawn upon to manually construct topology. Formalised procedures to perform this encoding of process knowledge into topology maps exist [Maurya *et al.*, 2003], known as signed directed graph (SDG) modelling. SDGs are connectivity maps where nodes process variables and edges between nodes indicate the directed connections between nodes. Each edge is assigned either a positive or negative sign, to indicate a positive or negative influence of one node on another. For a positive edge, an increase or decrease in one variable would cause a change in the same direction for the other variable. For a negative edge, a change in one variable would cause a change in the opposite direction for the other variable[Iri *et al.*, 1979]. The topology maps generated from human knowledge encapsulate a lot of information accurately, and propagation paths can be confidently identified. However, the procedures for generating these maps are extremely time-consuming and complicated [Yang *et al.*, 2014, Yang & Xiao, 2012].

Jiang *et al.* [2009] presented a methodology where a plant expert manually constructs an adjacency matrix that describes the connections between control loops. While it also requires process knowledge, this method is simpler than SDG construction from process knowledge, since only basic knowledge of the control loops is required. Despite its simplicity, it was shown to accurately identify fault propagation paths, since the faults would propagate through the control structure [Duan *et al.*, 2014, Jiang *et al.*, 2009, Yang *et al.*, 2014, Yang & Xiao, 2012].

2.8.3 Extraction of topology from process schematics

Models of the process based on the physical layout of units are referred to as topology-based models[Di Geronimo Gil *et al.*, 2011]. Plant diagrams, such as piping and instrumentation diagrams (P&IDs), can be considered formal descriptions of process knowledge. The connections between units, sensors and controllers are displayed visually. When an extensible mark-up language (XML) description of the diagram is available, the visual representation of connections is encoded in a programmatic format that can be exploited to automatically determine the connectivity[Thambirajah *et al.*, 2009]. Significant research has been performed to automate this procedure [Arroyo Esquivel, 2017, Thambirajah *et al.*, 2009, Yang *et al.*, 2014, Yang & Xiao, 2012, Yim *et al.*, 2006]. In a series of papers by Romero & Graven [2013], Romero *et al.* [2014] and Romero & Thornhill [2014], work on commercial software for extracting and visualising connectivity from XML schematics has been presented. The software allows for simple construction of an XML-based P&ID. This series of papers focuses on developing easy to use software for connectivity extraction and providing visual aids for various connectivity applications.

Although connectivity extraction from schematics may be automated, it requires that an accurate and up-to-date P&ID is available, and that this P&ID is available in XML description. Process schematics in digital formats are not always readily available or up-to-date. Often industrial companies only have these schematics in hard copy printouts. XML models can be constructed manually from these printouts, but this requires significant effort, especially if the schematic had to be updated. To address this challenge, [Arroyo Esquivel, 2017] developed a tool for capturing connectivity from hard copies of process schematics using computer vision techniques. The process schematics may be scanned into a PDF format and the connectivity information is automatically generated.

2.9 Capturing causality from historical process data

Sensors in processing plants measure process variables, generating a set of time series of the variables. These time series measurement can be recorded on a data historian. The relationship between variables' time series gives an indication of whether a causal connection between the variables exists. A number of techniques are available for analysing these relationships to capture causality information from process data [Yang *et al.*, 2014].

A formal description of causality inferred from process data was proposed by Wiener [1956]:

> X could be said to 'cause' Y when predictability of Y is improved by incorporating information about X

However, this does not provide sufficient information to infer that a causal link exists. If X causes Y, a change in X results in a change in Y after some time has passed. Therefore, causal dependency between variables is characterised by a temporal element as well[Pearl, 2003].

A number of methods exist, including: Granger causality; transfer entropy; cross-correlation; partial directed coherence; convergent cross-mapping; and k-Nearest neighbours. Calculations for each of these techniques are presented briefly to establish the core concepts for causality analysis.

2.9.1 Granger causality

Granger [1969] developed a formalisation of Wiener's causality definition in the context of regression models, called 'Granger causality':

> when inclusion of past measurements of X in a regression model of Y results in an improvement on the prediction of the autoregressive model of Y, then X is said to have a causal influence on Y

This definition incorporates some quantifiable measure of predictability improvement, but also incorporates temporal information, by including past measurements of the input. Consider the time series of two variables, $\mathbf{x_i}(t)$ and $\mathbf{x_j}(t)$. $\mathbf{x_j}(t)$ can be modelled as an autoregressive (AR) model [Madsen, 2008], as shown in Equation 2.2, referred to as the *restricted* model.

$$\mathbf{x}_j(t) = \sum_{r=1}^{k} B_j x_j(t-r) + \epsilon_j(t) \tag{2.2}$$

In this case only past values of x_j are incorporated to predict future values of itself. In Equation 2.2: k is the model order defining the time lag; B is the AR coefficient; and ϵ_j is the prediction error. $\mathbf{x}_j(t)$ can also be modelled incorporating past values of both $\mathbf{x}_i(t)$ and $\mathbf{x}_j(t)$, known as the *full* model as shown in Equation 2.3.

$$\mathbf{x}_j(t) = \sum_{r=1}^{k} [A_{ji,r} x_i(t-r) + A_{jj,r} x_j(t-r)] + \epsilon_{j|i}(t) \tag{2.3}$$

In Equation 2.3: A_{ji} and A_{jj} represent the regression coefficients. A_{ji}, A_{jj} and B_j can be determined using the least squares approach[Hill, 2011]. The model order, k, can be determined using the Akaike Information Criterion (AIC)[Akaike, 1974]. When the variance of $\epsilon_{j|i}(t)$ is less than the variance of $\epsilon_j(t)$, it implies that the prediction of Y is improved by including past values of x_i. x_i is then said to Granger cause x_j[Bressler & Seth, 2011]. The Granger causality can be quantified as shown in Equation 2.4.

$$F_{x_i \to x_j} = \ln \frac{var(\epsilon_j(t))}{var(\epsilon_{j|i(t)})} \tag{2.4}$$

When the prediction of x_j is not improved by including x_i, $var(\epsilon_{j|i}(t)) = var(\epsilon_j(t))$ and $F_{x_i \to x_j} = 0$. When the prediction of x_j is improved by including x_i, $var(\epsilon_{i|j}(t)) < var(\epsilon_i(t))$ and $F_{x_i \to x_j} > 0$ [Bressler & Seth, 2011].

Granger causality provides a causality measure with simple calculations that are computationally inexpensive. The linear regression concept from which the measure is derived is easy to understand and the results are easy to interpret, since regression is well understood.

A drawback of Granger causality is that the causality measure is dependent on the accuracy of the AR models. Granger causality relies on linear models of time series interaction that need to be fit to the data[Bressler & Seth, 2011], therefore nonlinear interactions in processes may cause Granger causality to be inaccurate.

Granger causality was initially developed for financial data analysis[Granger, 1969], but researchers have since found it to be useful for a number of applications. This includes extensive application in neuroscience[Bressler & Seth, 2011]. Granger causality has been applied for fault diagnosis in chemical processes[Yang & Xiao, 2012].

Yuan & Qin [2014] applied Granger causality for oscillation diagnosis. Their approach employed Principal Component Analysis (PCA) to first isolate the variables contributing to the oscillation. Since the first few PCs would have the most variation, and therefore would contain the variations caused by the oscillations. Therefore, the variables that contributed most according to the contribution plots were taken as oscillation source candidates. They also employed a spectral variation of Granger causality. They tested their methods on a simulated case study as well as industrial application on a case study from a plant of the Eastman Chemical Company. The time domain Granger causality analysis effectively identified the controlled variable (CV) and manipulated variable (MV) from one of the level control loops in the process, since these variables showed connections to many other variables in the system, but no connections from other variables in the system. The spectral Granger causality was also applied. As described in Section 2.9.4, the results of the spectral Granger causality were presented in a matrix of plots indicating the spectral GC magnitude as a function of the frequency. A peak at the oscillation frequency indicates the connection strength for the oscillation. They found that the time-domain Granger causality was good at identifying the propagation path, while the spectral GC provides more in-depth analysis of the individual connections strengths at the oscillation frequency [Yuan & Qin, 2014].

Kuhnert & Beyerer [2014] investigated a combined analysis with Granger causality, transfer entropy, and cross-correlation. The methods were tested on a simulated case study of a continuous stirred tank reactor (CSTR). The authors found that combining the results of all the causality analysis methods aided in root cause analysis. The reasoning for this combined approach was that the existence of a causal connection is a hypothesis that needs to be tested. The confidence in rejectingthe null hypothesis, that no connection exists, is improved when more evidence for its rejection is provided from different methods. The authors did indicate that this combination is *ad-hoc*, and lacks systematic guidelines for how the results should be combined.

Landman *et al.* [2014] applied Granger causality and PDC for diagnosis of oscillations in a large scale board machine. This is similar to the approach of [Yuan & Qin, 2014], since spectral Granger causality and PDC are equivalent. Landman's approach combined process knowledge-based connectivity with the data-based methods by limiting the data-based search for causal connections to those already confirmed by the plant connectivity. This was applied to reduce the large amount of spurious causal connections found by Granger causality. Even with this refinement procedure, Granger causality still found multiple propagation paths. Therefore PDC was used to refine the causality map even further, by exploiting the fact that it is able to find direct causal connections more effectively. This use of PDC by Landman *et al.* [2014] is discussed in Section 2.9.4.

Wakefield *et al.* [2018] applied Granger causality and transfer entropy for disturbance diagnosis in a simulation of a milling circuit in a minerals processing plant. The Granger causality results did show useful information for root cause analysis of the simulated faults. However, it was found that the results were difficult to interpret, with a large number of spurious causal connections. Additionally, the lack of clear systematic procedures for applying the techniques, such as guidelines for data selection and parametrisation, made the application difficult and interpretation of the results uncertain.

2.9.2 Transfer entropy

Another way to formulate Wiener's causality description is in an information-theoretic context. Consider two variables, X and Y. In this discussion the symbols X and Y are used in place of x_i and x_j to avoid confusing variable indices with time step indices. Transfer entropy is a measure

of the reduction in uncertainty of Y when incorporating past values of X[Schreiber, 2000]. The transfer entropy from X to Y can be calculated as shown in Equation 2.5.

$$T_{y|x} = \sum p(y_{i+h}, \mathbf{y}_i^{(K)}, \mathbf{x}_i^{(L)}) \log \frac{p(y_{i+h}|\mathbf{y}_i^{(K)}, \mathbf{x}_i^{(L)})}{p(y_{i+h}|\mathbf{y}_i^{(K)})} \tag{2.5}$$

In Equation 2.5: i represents the time step index; $p(a, b)$ represents the joint probability distribution function (PDF) between a and b; $p(a|b)$ represents the conditional PDF of a given b; h is the prediction horizon; $\mathbf{x}_i^{(L)} = [x_i, x_{i-\tau}, ..., x_{i-(L-1)\tau}]$ and $\mathbf{y}_i^{(K)} = [y_i, y_{i-\tau}, ..., y_{i-(K-1)\tau}]$ are the embedded vectors of X and Y with embedding dimensions, L and K respectively, and time interval, τ.

For example, an embedded matrix with $K = 3$ and $\tau = 4$, is shown in Equation 2.6.

$$\mathbf{X}^{(K)} = \begin{pmatrix} x_9 & x_5 & x_1 \\ x_{10} & x_6 & x_2 \\ x_{11} & x_7 & x_3 \\ \vdots & \vdots & \vdots \\ x_N & x_{N-4} & x_{N-8} \end{pmatrix} \tag{2.6}$$

The numerator of the logarithmic term in Equation 2.5 represents the probability that Y has a certain value (y_{i+h}), h samples in the future, when past values of both Y and X are known. The denominator of the logarithmic term in Equation 2.5 represents the probability that Y has a certain value (y_{i+h}), h samples in the future, when past values of only Y are known. When Y is independent of X, the numerator and denominator are equal, and the logarithm reduces to $\log(1) = 0$, giving $T_{y\to x} = 0$. When prediction of Y is improved by inclusion of X, the numerator is greater than the denominator and $T_{x\to y} > 0$. The PDFs can be calculated using kernel density estimation [Silverman, 1986]. The kernel density estimation approach used in this dissertation is discussed in a subsection at the end of this section.

A causality measure comparing the influence of X on Y with the influence of Y on X can be calculated according to Equation 2.7 [Bauer *et al.*, 2007a].

$$T_{x\to y} = T_{y|x} - T_{x|y} \tag{2.7}$$

The practice of subtracting the forward and reverse causal influence to obtain a net causal influence is common in causality analysis [Barnett & Seth, 2014].

The transfer entropy measure shown in Equation 2.5 can be unpacked to express it in terms of conditional Shannon entropies [Kantz & Schreiber, 1997], as shown in Equation 2.8.

$$\begin{aligned} T_{y|x} =& \sum p(y_{i+h}, \mathbf{y}_i^{(K)}, \mathbf{x}_i^{(L)}) \log \frac{p(y_{i+h}, \mathbf{y}_i^{(K)}, \mathbf{x}_i^{(L)})}{p(\mathbf{y}_i^{(K)}, \mathbf{x}_i^{(L)})} \\ &- \sum p(y_{i+h}, \mathbf{y}_i^{(K)}) \log \frac{p(y_{i+h}, \mathbf{y}_i^{(K)})}{p(\mathbf{y}_i^{(K)})} \\ =& H(y_{i+h}|\mathbf{y}_i^{(K)}) - H(y_{i+h}|\mathbf{y}_i^{(K)}, \mathbf{x}_i^{(L)}) \end{aligned} \tag{2.8}$$

where

$$H(y_{i+h}|\mathbf{y}_i^{(K)}) = -\sum p(y_{i+h}, \mathbf{y}_i^{(K)}) \log(y_{i+h}|\mathbf{y}_i^{(K)}) \tag{2.9}$$

is the Shannon entropy for Y conditioned on past values of itself, and

$$H(y_{i+h}|\mathbf{y}_i^{(K)}, \mathbf{x}_i^{(L)}) = -\sum p(y_{i+h}, \mathbf{y}_i^{(K)}, \mathbf{X}_i^{(L)}) \log p(y_{i+h}|\mathbf{y}_i^{(K)}, \mathbf{X}_i^{(L)}) \tag{2.10}$$

is the Shannon entropy for Y conditioned on past values of itself and X.

The similarity between transfer entropy and Granger causality is apparent. Where Granger causality focuses on predictability improvement when including past values of another variable, transfer entropy focuses on uncertainty reduction when including past values of another variable. In fact, Barnett *et al.* [2009] and Hlavackov-Schindler [2011] have demonstrated that Granger causality and transfer entropy are equivalent when applied to Gaussian variables.

Transfer entropy is not limited by the linearity assumption[Schreiber, 2000], therefore it may be more suited for application to systems showing nonlinear behaviour. Transfer entropy is restricted by the stationarity assumption[Schreiber, 2000]. This means that the dynamic properties of the system must not change over the set of data used[Box, 2008].

Transfer entropy has as many as four different parameters to select, namely: the embedding dimension for the source k; the embedding dimension for the destination L; the time interval τ; and the prediction horizon h. This makes automation of the procedure complicated. This is discussed further in Section 2.12.2.

Estimation of the PDF using kernel density estimation can make transfer entropy extremely computationally expensive. The size of PDF that has to be estimated is determined by the embedding dimensions. The largest PDF to be calculated would be $K + L + 1$ dimensions. This computational burden makes transfer entropy less appealing. The computational burden is increased when the optimal embedding dimensions need to be determined, since this also requires PDF estimation[Bauer *et al.*, 2007a]. Additionally, when the surrogate time series method is used to determine the significance threshold (explained in Section 2.12.3), the transfer entropy calculation is repeated a large number of times, further exasperating the computational complexity.

Bauer *et al.* [2007a] introduced the use of transfer entropy for fault diagnosis in chemical processes. The calculation procedures were presented, including a description of KDE for probability distribution estimation. Some parameter optimisation was investigated. The authors determined the minimum number of samples required for a significant transfer entropy to be calculated for a known causal connection. The optimal prediction horizon (h) and time interval (tau) were determined for the causal connections in the case study. This parametrisation is discussed further in Section 2.12.2 The techniques were applied to two case studies. The first was a reaction process at the Eastman Chemical Company, where an oscillatory disturbance entered the process through the reactor feed. The second was a distillation process at the Eastman Chemical Company, where sharp, repeating spikes were observed affecting multiple variables. Transfer entropy was able to effectively point to the pressure of an inert gas valve as the first variable in the causal map. Therefore the techniques were shown to be effective at isolating the root cause.

Shu & Zhao [2012] developed a modified transfer entropy to more accurately identify the time delay between variables. In Equation 2.5, the reference for the decrease in uncertainty is $x_i^{(K)}$. This means that as the prediction horizon, h, varies, the reference varies. In Shu's modification, $x_i^{(K)}$ is replaced with $x_{i+h-1}^{(K)}$, so that as h varies, the reference is fixed.

Naghoosi *et al.* [2013] applied transfer entropy, while using the mutual dependency and differential dependency curves for transfer entropy. The mutual dependency between all pairs of variables is used as a screening process, so that only variables that show significant mutual dependency are analysed further to calculate the transfer entropy. The mutual dependency curves

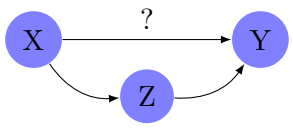

FIGURE 2.4: *Example of causal map showing indirect connection observed from $X \rightarrow Y$.*

are also used for parameter selection for transfer entropy. This parametrisation is discussed further in Section 2.12.2. They tested the ability of their method to identify accurate causal connections between variables in an industrial oil sands separation process used for bitumen extraction. They found that these techniques provided useful information for detecting causality between a number of process variables. This case study did not investigate any specific fault condition, but was rather concerned with individual causal connections.

Duan *et al.* [2013] demonstrated the use of direct causality detection using transfer entropy. Direct transfer entropy is used to calculate the transfer entropy between two variables while conditioning on the effect of confounding variables. Figure 2.4 illustrates this scenario. When X is connected to Z, and Z is connected to Y, it may appear that X is connected to Y. This indirect connection may be spurious. One way to determine whether this connection is a true connection is to condition on the intermediate variable, Z. In this way the effect of X on Y without the effect of Z is determined. By only considering direct transfer entropy, spurious causal connections can be minimised. A possible drawback of this technique is that the embedding dimensions of additional variables (not just K and L) also have to be selected, further complicating the parametrisation. This also requires estimation of additional conditional PDFs, so the computational expense is increased[Duan *et al.*, 2013]. The direct transfer entropy was tested on a case study of a flue gas desulfurization process at an oil company. The technique was shown to identify causal connections accurately, with minimal spurious connections identified.

Another complication is with the hypothesis test for significance (see Section 2.12.3). Surrogate time series are typically generated for this hypothesis test [Schreiber & Schmitz, 2000], where the causal connection from X to Y are destroyed. However, for direct transfer entropy the surrogate data has to satisfy the conditions that there is no connection from X to Y, but the indirect connection through Z still exists[Duan *et al.*, 2013].

Hajihosseini *et al.* [2014] applied transfer entropy to the Tennessee Eastman benchmark dataset. The novelty of their approach was that they used transfer entropy to generate causal maps to determine the patterns of information flow for different faults. These patterns could then be used to isolate different faults more effectively by matching them to previously identified patterns. This approach directly addresses the fact that processes often exhibit multimodality, where different process behaviour arises from operational changes, switching between control strategies, and from fault conditions[Yu, 2012]. Other applications of causality analysis apply causality measures to the data generated by the fault conditions under consideration.

As mentioned in Section 2.9.1, Kuhnert & Beyerer [2014] investigated a combined analysis with Granger causality, transfer entropy, and cross-correlation. The methods were tested on a simulated case study of a continuous stirred tank reactor (CSTR). The authors found that combining the results of all the causality analysis methods aided in root cause analysis.

Duan *et al.* [2015] developed an adaptation of transfer entropy that didn't involve estimation of the PDFs, called transfer 0-entropy ($T0E$). The motivation for the development of this technique was that measured variables in processes do not always follow a well-defined probability distribution. The probability distribution is typically estimated empirically, using KDE, for example. However, when a variable has a known range, but an unknown distribution, its uncer-

tainty can be quantified by the Lebesgue measure of the support of this random variable[Renyi, 1961]. Duan *et al.* [2015] exploited this idea to develop an analogous transfer entropy measure that utilises this uncertainty quantification, and applied this T0E for fault diagnosis. The $T0E$ method was shown to be effective for fault diagnosis on the benchmark industrial process data set of the Eastman Chemical Company. One identified limitation of this approach was that it was found t be conservative at detecting causal connections. This means that expected causal connections were missed using this approach. The authors stated that a possible reason for the conservativeness is that the information transfer measure calculates the least amount of information transferred from one variable to another.

Analogous to their previous work with Granger causality and process knowledge-based connectivity, Landman & Jamsa-Jounela [2016] applied the direct transfer entropy method[Duan *et al.*, 2013] for oscillation diagnosis in the large scale board machine. In this approach, transfer entropy was first calculated for all the pairs of candidate variables. A search algorithm was then employed to identify connections that were considered to be direct connections from a plant connectivity derived from process knowledge. The direct transfer entropy was then applied to exclude indirect connections. This approach reduces the computational load, so that direct transfer entropy does not have to be applied to every possible pair of candidate variables. The authors found that, although this hybrid method reduced the number of spurious connections, several spurious and indirect connections were still detected.

Rashidi *et al.* [2018] developed a modification of transfer entropy, the symbolic dynamic-based normalised transfer entropy (SDNTE), to address the computational burden of transfer entropy. The developed SDNTE is based on principles of time-series symbolization, xD-Markov machine, and Shannon entropy. The proposed approach was shown to work for the Tennessee Eastman simulation, as well as for an industrial case study of a large scale centrifuge.

As mentioned in Section 2.9.1, Wakefield *et al.* [2018] applied Granger causality and transfer entropy for disturbance diagnosis in a simulation of a milling circuit in a minerals processing plant.

Previous work by the author of this dissertation [Lindner & Auret, 2014] used principal component analysis (PCA) for fault detection, combined with transfer entropy and cross correlation for root cause analysis of disturbances in a simulated two-tank with heat exchange system. The same approach was then used for root cause analysis of disturbances in a base metals refinery simulation [Lindner *et al.*, 2014]. Finally, the approach was validated on an industrial case study of a fault in a platinum concentrator plant [Lindner & Auret, 2015]. These studies showed that the techniques were useful for fault diagnosis, but the interpretation of the causality analysis results was time consuming and fraught with possible errors due to human intervention. The need for a more automated approach to reduce ambiguity and uncertainty in the results was identified.

Kernel density estimation

The transfer entropy calculation shown in Equation 2.5 relies on calculation of probability density functions (PDFs). These PDFs can be estimated using non-parametric kernel density estimation (KDE) [Schreiber, 2000].

Kernel density methods can be understood in relation to histograms. Given some input data, $\mathbf{x}(t)$, a histogram can be constructed, where the range of the data is divided into equal sized bins. The number of values, x_i, that fall into each bin is counted. Figure 2.5 illustrates the estimation of a distribution using histograms. This is equivalent to placing a rectangular box

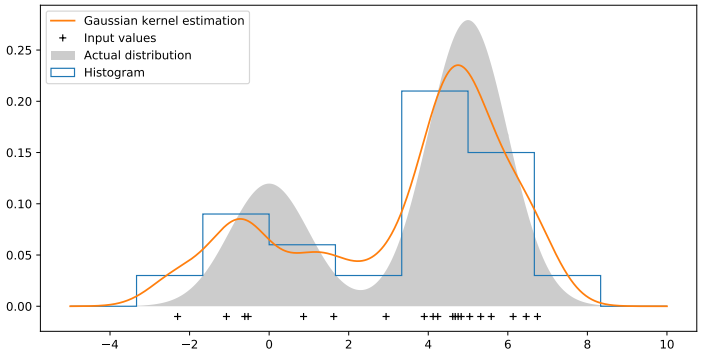

FIGURE 2.5: *Comparison of density estimation using histograms and Gaussian kernels.*

over the bin for every point that falls within it, and stacking these boxes on top of one another. However, the resulting distribution is sensitive to the width and placement of the bins.

Kernel density estimation provides a more accurate approach for estimation of the distribution [Silverman, 1986]. Kernel density estimation places a kernel function, $\mathbf{K}(x)$, centered over every point, x_i, and the kernel functions are summed to give an estimated of the probability density:

$$p(x) = \frac{1}{N}\sum_{i=1}^{N} K(x - x_i) \tag{2.11}$$

A Gaussian kernel function can be used, where:

$$K(x - x_i) = \frac{1}{\sqrt{(2\pi)}\theta}\exp\left(-\frac{(x - x_i)^2}{2\theta^2}\right) \tag{2.12}$$

θ is the bandwidth of the kernel. The bandwidth suggested by Li & Racine [2011] can be used as a rule of thumb $\theta = 1.06N^{-0.2}\sigma_x$, where σ_x is the standard deviation of the input data.

Figure 2.5 shows the histogram and Gaussian kernel estimations with the actual distribution. Since the kernel function placed over each point is smooth, the estimated distribution is smooth. In contrast, the rectangular boxes used in the histogram approach gives a very discrete looking distribution.

2.9.3 Cross-correlation

Cross-correlation[Govindan *et al.*, 2005] takes a slightly different approach to that of Granger causality and transfer entropy. Consider the two criteria that a relationship between the time series of X and Y must exist and that this relationship takes time to manifest. Cross-correlation analysis adjusts the time series of X and Y so that there is a lag between them. The correlation coefficient between the adjusted time series can be calculated, and this procedure can be repeated for a range of assumed lags. The correlation, ρ, for an specified lag, k, is calculated as shown in Equation 2.13.

$$\rho_k = \frac{1}{N-k}\sum_{i=1}^{N-k}\frac{(x_i - \mu_x)(y_{i+k} - \mu_y)}{\sigma_x\sigma_y} \tag{2.13}$$

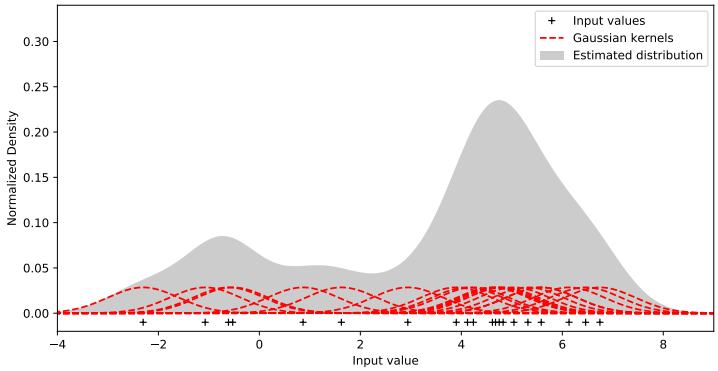

FIGURE 2.6: *Gaussian kernel density estimation illustration.*

In 2.13, N represents the number of samples and μ and σ represent the mean and standard deviation respectively of the time series. The maximum correlation found, ρ_{max}, is assumed to be the actual correlation between the time series. The lag that yields this maximum correlation value, k_{max} is assumed to be an estimate of the time delay between the variables.

The advantage of cross-correlation lies mostly in its simplicity and its computationally inexpensive calculation. It is easy to implement and to interpret the results.

However, cross-correlation can only detect linear interaction between time series. In processes where nonlinear behaviour is present, the linear correlation between the two time series may not be an accurate representation of the interaction between them[Bauer & Thornhill, 2008].

The trend in a time series is ignored in the linear correlation calculated for each lag. The time series is treated as ergodic, where every sample is representative of the entire time series. Values at different time instants are regarded as samples of the same random event [Yang *et al.*, 2014]. In other words, when the correlation between X and Y at a specific lag, k, is calculated, the values of the time series of X and Y are considered to be repeated measurements of the same event, instead of being seen as measurements of different events over time.

Bauer & Thornhill [2008] applied cross-correlation as a causality analysis measure for fault diagnosis for two industrial case studies. The cross-correlation value, ρ, was calculated, as well as the estimate fo the time delay, k_{max}. The time delay values were then used for a consistency check, to determine whether the time delays along the propagation paths were consistent. The first case study was a part of the Eastman Chemical Company process, where an oscillatory disturbance affected a number of measured variables. The second case study was a section of a large petroleum plant containing a recycle stream, where an oscillatory disturbance affected a large number of variables. For both case studies, the developed techniques accurately identified the propagation paths of the faults through the process.

As mentioned in Section 2.9.2, previous work by the author of this dissertation [Lindner & Auret, 2014] used principal component analysis (PCA) for fault detection, combined with transfer entropy and cross correlation for root cause analysis of disturbances in a simulated two-tank with heat exchange system. The same approach was then used for root cause analysis of disturbances in a base metals refinery simulation [Lindner *et al.*, 2014]. Finally, the approach was validated on an industrial case study of a fault in a platinum concentrator plant [Lindner & Auret, 2015].

As mentioned in Section 2.9.1, Kuhnert & Beyerer [2014] investigated a combined analysis with Granger causality, transfer entropy, and cross-correlation. The methods were tested on

a simulated case study of a continuous stirred tank reactor (CSTR). The authors found that combining the results of all the causality analysis methods aided in root cause analysis.

2.9.4 Partial directed coherence

Frequency domain methods for analysis of time series are often used to explore the periodic nature of time series [Jiang *et al.*, 2007]. This is especially useful when the application is analysis of oscillations in the process. Frequency domain methods for causality analysis represent the energy transfer between pairs of time series at each frequency[Baccal & Sameshima, 2001]. Partial directed coherence was developed to provide a frequency domain description of Granger causality [Baccal & Sameshima, 2001]. The time series system can be modelled according an M-dimensional autoregressive model, as shown in Equation 2.2.

$$\begin{bmatrix} x_1(t) \\ \vdots \\ x_M(t) \end{bmatrix} = \sum_{r=1}^{k} \mathbf{A}_r \begin{bmatrix} x_1(t-r) \\ \vdots \\ x_M(t-r) \end{bmatrix} + \begin{bmatrix} \epsilon_1(t) \\ \vdots \\ \epsilon_M(t) \end{bmatrix} \tag{2.14}$$

The frequency response of the process can be obtained by application of the Z transform (discrete version of Laplace transform) and setting $z^{-1} = e^{-\iota\omega}$, where ι represents the imaginary unit. This gives Equation 2.15.

$$\mathbf{A}(\omega)\mathbf{X}(\omega) = \mathbf{E}(\omega) \tag{2.15}$$

where $\mathbf{A}$ is a coefficient matrix whose entries are the coefficients between variable i and j are:

$$\mathbf{A}_{ij}(\omega) = -\sum_{r=1}^{k} a_{ij}(r) e^{-\iota\omega r} \tag{2.16}$$

$$\mathbf{X}(\omega) = x_1(\omega)x_2(\omega)\cdots x_N(\omega) \tag{2.17}$$

$$\mathbf{E}(\omega) = \epsilon_1(\omega)\epsilon_2(\omega)\cdots\epsilon_N(\omega) \tag{2.18}$$

When $a_{ij}(r) = 0$ for all values of r, there is statistical evidence that there is no causality from x_i to x_j . Building on this concept, the PDC from x_i to x_j is defined by Equation 2.19.

$$|\hat{\pi}_{ij}(\omega)| = \frac{|A_{ij}(\omega)|}{\sqrt{\sum_{i=1}^{M} |A_{ij}(\omega)|^2}} \tag{2.19}$$

As with Granger causality, the regression coefficients for PDC can be calculated using AIC[Zhang *et al.*, 2015].

Since the PDC is based on frequency domain calculations, it may be particularly useful for applications where the process experiences oscillatory behaviour[Yang *et al.*, 2014]. One drawback of this technique is that it does not provide a single value to quantify the causal connection between two variables. A matrix plot representation of the responses of each pair of variables is employed [Yang *et al.*, 2014]. Interpretation of frequency domain methods can be more obscure than interpretation of time series methods, which means that the physical meaning of the results of PDC is more difficult to grasp.

Landman *et al.* [2014] applied Granger causality for diagnosis of oscillations due to valve stiction in a drying process. They found that the high level of connectivity in the system made interpretation of the propagation paths difficult. Therefore, they used PDC to refine the causality map

further, due to its ability to capture direct causal connections[Faes *et al.*, 2010]. The ability to capture direct causal connections is attributed to the fact that PDC incorporates conditioning to exclude the influence of confounding variables[Gigi & Tangirala, 2010]. Landman *et al.* [2014] found that the PDC complemented the ability of Granger causality to find the propagation path of the oscillations.

As mentioned in Section 2.9.1, Yuan & Qin [2014] applied Granger causality for oscillation diagnosis, and investigated a spectral Granger causality approach, which is analogous to PDC. They tested their methods on a simulated case study as well as industrial application on a case study from a plant of the Eastman Chemical Company. The time domain Granger causality analysis effectively identified the controlled variable (CV) and manipulated variable (MV) from one of the level control loops in the process, since these variables showed connections to many other variables in the system, but no connections from other variables in the system. The spectral Granger causality was also applied. The results of the spectral Granger causality were presented in a matrix of plots indicating the spectral GC magnitude as a function of the frequency. A peak at the oscillation frequency indicates the connection strength for the oscillation. They found that the time-domain Granger causality was good at identifying the propagation path, while the spectral GC provides more in-depth analysis of the individual connections strengths at the oscillation frequency [Yuan & Qin, 2014].

Zhang *et al.* [2015] used PDC for oscillation diagnosis in a simulated process, as well as the Tennessee Eastman benchmark dataset. Independent component analysis (ICA) was used to isolate the candidate variables, and then PDC was applied to these variables. The PDC values at the dominant oscillation frequency were calculated, and used to construct a causal map. They demonstrated that PDC was effective at root cause analysis in both case studies

2.9.5 Convergent cross-mapping

Convergent cross-mapping (CCM) was proposed to detect causality for coupled variables in strong nonlinear variables in ecosystems [Sugihara *et al.*, 2012]. CCM compares the mutual prediction ability of embedding manifolds. Takens theorem [Takens, 1981] states that when two variables are causally linked, their shadow manifolds, $\mathbf{M}_x$ and $\mathbf{M}_y$, are diffeomorphic to the manifold of the original system. Diffeomorphism is an isomorphism of smooth manifolds. $\mathbf{M}_x$ and $\mathbf{M}_y$ are reconstructed using embedded vectors of the series for X and Y:

$$\mathbf{M}_{x,i} = [x_i, x_{i-\tau}, ..., x_{i-(L-1)\tau}] \tag{2.20}$$

$$\mathbf{M}_{y,i} = [y_i, y_{i-\tau}, ..., y_{i-(L-1)\tau}] \tag{2.21}$$

where L represents the embedding dimension, and x_i and y_i represent the values of x and y at time t_i. When x_i converges to a specific point x_{i-1}, y_i will converge to the corresponding point y_{i-1}. CCM predicts the point, y_i, using the nearest points for each, x_i, in $\mathbf{M}_x$ and their corresponding mapped points $\mathbf{M}_y$. The prediction is denoted as $\hat{y}_i$. The cross mapping between x and y is then the correlation between $\mathbf{y}_t$ and $\hat{\mathbf{y}}_t$.

$\mathbf{M}_x$ is used to predict $\mathbf{M}_x$ and evaluate the influence of y on x. When $\mathbf{M}_x$ and $\mathbf{M}_y$ are diffeomorphic to original system manifold, there is a one to one mapping between the points in $\mathbf{M}_x$ and $\mathbf{M}_y$:

$$\lim_{\mathbf{M}_{x,i} \to \mathbf{M}_{x,k0}} \mathbf{M}_{y,i} \to \mathbf{M}_{y,k0} = 0 \tag{2.22}$$

With $L + 1$ points in the manifold $\mathbf{M}_x$:

$$\mathbf{M}_{x,ki} = [\mathbf{M}_{x,k1}, \mathbf{M}_{x,k2}, \ldots, \mathbf{M}_{x,k(L+1)}] \tag{2.23}$$

When we determine these $K+1$ points which are close to $\mathbf{M}_{x,k0}$. The value of $\mathbf{M}_{y,k0}$ can be estimated using $\mathbf{M}_{y,ki}$:

$$d(\mathbf{M}_{x,ki}, \mathbf{M}_{x,k0}) = exp(-\frac{\mathbf{M}_{x,t_i} - \mathbf{M}_{x,t_0}}{\mathbf{M}_{x,k1} - \mathbf{M}_{x,k0}}) \tag{2.24}$$

$$\hat{\mathbf{M}}_{y,k0}|\mathbf{M}_x = \sum_{i=1}^{L+1} \frac{d(\mathbf{M}_{x,ki}, \mathbf{M}_{x,k0})}{\sum_{j=1}^{L+1} d(\mathbf{M}_{x,kj}, \mathbf{M}_{x,k0}))} \mathbf{M}_{y,ki} \tag{2.25}$$

The correlation between y and the prediction of y given x is the calculated as:

$$\rho_{x \to y} = \lim_{N \to \infty} cov(\mathbf{M}_y, \hat{\mathbf{M}}_y|\mathbf{M}_x) \tag{2.26}$$

Similar to transfer entropy, the computational complexity of CCM can get large very quickly as the embedding dimension, K, is increased. However, it is not as computationally expensive as transfer entropy, where the PDFs have to be estimated. An advantage of CCM is that it has been reported to work well for short time series [Clark *et al.*, 2015, Sugihara *et al.*, 2012]. This means that it may be preferable in cases where the number of samples is limited. CCM is also attractive due to its applicability to nonlinear systems [Luo *et al.*, 2017].

According to Ye *et al.* [2015], CCM works better for systems with weaker causal strengths, since strong causal dependencies will make CCM unable to distinguish between unidirectional and bidirectional connections.

Luo *et al.* [2017] applied CCM for detection of causal connections in the Tennessee Eastman simulated process. No specific fault conditions were analysed in this investigation. The focus was rather on detection of individual causal connections. The authors found that CCM was able to detect causal connections that were missed using transfer entropy, especially some loops in the system. Some known causal connections were, however, missed due to excessive noise.

Aftab *et al.* [2017] also demonstrated the use of CCM for oscillation diagnosis in industrial data from a South East Asian refinery. The authors presented an automated embedding dimension selection procedure that ensures optimal parametrisation. The case study data set was limited to only 512 samples, confirming that CCM can be useful for short time series. The authors found the procedure provided accurate information for root cause analysis.

2.9.6 k-Nearest neighbours

Again building on the idea of causality being quantified by predictability improvement, a causality measure can be derived from k-Nearest Neighbours (kNN) estimation.

Given two variables x, and y, embedded matrices are constructed. The Euclidean norm representing the distance between two embedded vectors, $\mathbf{x}_i$ and $\mathbf{x}_j$ is given by Equation 2.27.

$$d_{i,j} = ||\mathbf{x}_i - \mathbf{x}_j|| \tag{2.27}$$

where

$$\mathbf{x}_i = [x_i, x_{i-\tau}, \ldots, x_{i-(L-1)\tau}] \tag{2.28}$$

$$\mathbf{x}_j = [x_j, x_{j-\tau}, \ldots, x_{j-(L-1)\tau}] \tag{2.29}$$

In Equation 2.28, τ represents the sampling constant, and L represents the embedding dimension. The nearest neighbours of an embedded vector, $\mathbf{x}_i$, are the embedded vectors, $\mathbf{x}_j$, that have the

smallest value of $d_{i,j}$. A total of κ nearest neighbours are found, and $r_{i,j}$ represents the indices of the nearest neighbours for i from $j = 1 : \kappa$. A future value, x_{i+h} is assigned to each embedded vector. x_{i+h} is called the prediction value, and h represents the prediction horizon . The prediction value obtained from the nearest neighbours are denoted by $x_{r_{i,j}+h}$. This formulation is repeated for y, giving the indices of the nearest neighbours, $s_{i,j}$, and the prediction value y_{i+h}. The self-predictability factor can be calculated by Equation 2.30.

$$D_i(x) = \frac{1}{\kappa} \sum_{j=1}^{\kappa} |x_{i+h} - x_{r_{i,j}+h}| \tag{2.30}$$

The prediction value x_{i+h} is assigned to $\mathbf{y}_i$. When x_{i+h} is close to the predicted values of all the nearest neighbours, $x_{s_{i,j}+h}$, it can be inferred that y is a good predictor of x.

The predictability factor of x given y can be calculated using Equation 2.31

$$D_i(x|y) = \frac{1}{\kappa} \sum_{j=1}^{\kappa} |x_{i+h} - x_{s_{i,j}+h}| \tag{2.31}$$

The dependence measure can then be calculated by Equation 2.32.

$$\eta(X|Y) = \frac{1}{\tilde{N} \sum_{i=1}^{\tilde{N}} \frac{D_i(x|y)}{D_i(x)}} \tag{2.32}$$

The prediction ability of x to y is then determined using the reverse. When there is an asymmetric prediction ability, the existence of a directional causal relationship can be inferred. The causality measure can be calculated using Equation 2.33:

$$\eta_{x \to y} = \eta(x|y) - \eta(y|x) \tag{2.33}$$

As with transfer entropy and CCM, the kNN approach's computational complexity will be influenced by the choice of the embedding dimension. The approach is simple to follow, and the mechanisms easier to understand than transfer entropy. However, the intuitive regression-based approach of Granger causality is still more straightforward than kNN.

Bauer *et al.* [2007b] used the kNN approach for fault diagnosis of a distillation unit in the Eastman Chemical Company. In the first case study, a periodic disturbance affected multiple measured variables. In the second case study, a repeating spiky disturbances affected the process. The results showed that kNN was able to accurately identify the propagation paths of the faults in both case studies. The authors also developed default parameters for the calculation of kNN, so that industrial implementation could be simplified.

Stockmann *et al.* [2012] also applied the kNN approach for causality analysis for diagnosis of oscillations in a hydrocracking plant. The authors showed that the root cause was successfully identified using this technique. The authors indicated that the method could be used even in the difficult cases of nonlinear multi-input single-output systems.

2.10 Combining knowledge and data-based connectivity and causality

Knowledge-based resources and data-based resources for connectivity and causality each have advantageous and disadvantageous characteristics. The characteristics of knowledge-based and

data-based methods are discussed here, and also summarised in Table 2.1 to illustrate the comparison between them.

Knowledge-based methods are typically static. The schematics or models used do not take into account changing process conditions. For example, changes in feed ore composition common in mineral processing plants [Wills, 2007] can significantly alter process operation. Models can be constructed that depend on the operating conditions, but that requires that these changing conditions are observable. In some cases, feed ore compositions are not measured, for example.

Data-based methods can be dynamic, since the most up-to-date data can be used to generate the causality models. The presence of a fault can also change the causal structure of the process. For example, faulty actuator behaviour could mean that the link between a controlled variable and the manipulated variable associated with the actuator is broken. Data-based causality can be used to analyse the data in the presence of a fault, to ensure that the propagation paths observed are representative of the causality in the process.

Not all of the knowledge-based methods can be automated. Using the automated XML cause-and-effect analyser discussed in Thambirajah *et al.* [2009], and the vision-based techniques of Arroyo Esquivel [2017]. The procedure for manual generation of topology from process knowledge can be time consuming[Yang & Xiao, 2012]. Approaches where the topology generation can be automated once the information has been updated are therefore more useful.

The computational complexity of data-based causality techniques can be a hindrance to application for engineers[Duan *et al.*, 2015]. Computational complexity of the automated knowledge based techniques is not as severe[Arroyo Esquivel, 2017].

Provided that the source of the topology information is accurate and up-to-date, knowledge-based connectivity extraction provides reliable topology. One can be confident that the connections derived are true connections in the process, and there will be no spurious connection. Data-based causality can find spurious connections (see Section 2.12.3). However, some interactions within a process are very complex, and may be missed by knowledge-based methods. For example, the interaction between multiple control loops may cause connections between variables that are far removed from each other physically.

Process knowledge-based techniques are qualitative in nature [Thambirajah *et al.*, 2009]. This means that relative strengths of connections cannot be inferred. Connection strength can aid interpretation of the propagation paths of faults. Data-based causality analysis measures can provide relative strengths of the connections.

From Table 2.1 it can be seen that data-based and knowledge-based techniques may be complementary. Therefore, some researchers have incorporated a hybrid approach that combines both. Different approaches may include validating the knowledge-based connections using the data-based connections, or vice-versa.

An approach used frequently is to first establish knowledge-based connections, and validate them with data-based connections. This approach reduces the amount of variable pairs which are tested for causality, thereby reducing the computation burden of the data-based techniques. This approach was used by Landman *et al.* [2014] to combine Granger causality with connectivity obtained from XML schematics and Landman & Jamsa-Jounela [2016] to do the same with transfer entropy. Both these papers found that incorporating the knowledge-based information reduced the number of spurious connections.

Yang *et al.* [2010] constructed signed digraphs (SDGs) from process knowledge, and used transfer entropy to validate the edges in the graph. In Thambirajah *et al.* [2009] transfer entropy was used to determine possible root causes. Process connectivity extracted from XML descriptions of

TABLE 2.1: *Summary of comparisons of the characteristics for knowledge and data-based causality.*

Criteria	Knowledge-Based	Data-based
Dynamic	Sometimes	✓
Non-intuitive connections		✓
Automation	✓	✓
Computationally conservative	✓	
No possible spurious connections	✓	
Possible missed connections	✓	✓
Quantitative		✓
High resolution		✓

the process was then used to determine which of the propagation paths was physically possible.

Yang *et al.* [2014] presented a technique in their textbook that used both cross-correlation and transfer entropy to validate a SDG generated from process knowledge. They also presented the opposite approach, using process knowledge to validate data-based connectivity. They generated a connectivity matrix from cross-correlation, and then validated each edge with the reachability matrix in the SDG.

Two approaches to combining process connectivity with data-based causality exist: specifying the connectivity structure in advance and only considering those connections; or calculating the causality and then using the process connectivity for validation. The former approach allows reduction of the computational burden of the causality analysis methods. It may also ensure that indirect and shortcut connections are ignored, since only direct connections are specified in advance. However, it may be that assuming this structure in advance may miss non-intuitive connections that may be present in the process. Consider a case where the control structure is broken due to saturation of a valve.

2.11 Summary of causality analysis literature

Now that the concepts of causality analysis have been introduced, a broad overview of the published literature can be discussed. This section presents a summary of causality analysis applications for fault diagnosis in published literature. Table 2.2 provides a summary of the data-based causality analysis applications. The table provides an overview of the method used, the type of disturbance it was used for, and the type of process it was used for. The entries are also sorted according to publication date, which gives an overview of how the method popularity changed over time. This serves as an overview of the relevant literature.

TABLE 2.2: *Overview of literature on causality analysis for fault diagnosis in industrial processes. The methods are abbreviated as follows: TE = Transfer Entropy; GC = Granger Causality; PDC = Partial Directed Coherence; CC = Cross-Correlation; CCM = Convergent Cross Mapping; KNN = K-Nearest Neighbours.*

Reference	**Method**	**Fault type**	**Process**
Bauer *et al.* [2007a]	TE	Oscillation	Chemical Process
Bauer *et al.* [2007b]	kNN	Oscillation and irregular spiky deviation	Chemical Process

Table 2.2: *Overview of literature on causality analysis for fault diagnosis in industrial processes. The methods are abbreviated as follows: TE = Transfer Entropy; GC = Granger Causality; PDC = Partial Directed Coherence; CC = Cross-Correlation; CCM = Convergent Cross Mapping; KNN = K-Nearest Neighbours.*

Reference	Method	Fault type	Process
Bauer & Thornhill [2008]	CC	Oscillation	Chemical Process & Section of Petrochemical Plant
Thambirajah *et al.* [2009]	TE	Oscillation and irregular spiky deviations	Chemical process
Yang *et al.* [2010]	TE & CC	Oscillation	Final Tailings Pumphouse
Shu & Zhao [2012]	TE	Oscillation	Water mixing process & Tennessee Eastman
Stockmann *et al.* [2012]	kNN	Oscillation	Hydrocracking plant
Yang & Xiao [2012]	TE, GC, CC, & PDC	NA	Literature review
Duan *et al.* [2013]	TE	Oscillation	Flue gas desulphurisation process (Oil and gas)
Naghoosi *et al.* [2013]	TE	Normal operating conditions	Final Tailings Pumphouse
Duan *et al.* [2014]	TE & GC	Oscillation	Tennessee Eastman dataset
Kuhnert & Beyerer [2014]	TE, GC, & CC	White noise addition&Periodic valve malfunction	Simulated CSTR &Laboratory scale level control system
Lindner & Auret [2014]	TE & CC	Step input disturbance	Two-tank simulation
Lindner *et al.* [2014]	TE & CC	Abrupt valve failure	Base metals refinery simulation
Landman *et al.* [2014]	GC & PDC	Oscillation	Large Scale board machine
Yuan & Qin [2014]	GC	Oscillation	Chemical process
Yang *et al.* [2014]	TE, GC, PDC, & CC	Oscillations	Tennessee Eastman
Hajihosseini *et al.* [2014]	TE	Oscillations	Tennessee Eastman
Duan *et al.* [2015]	TE	Oscillation	Tennessee Eastman dataset
Lindner & Auret [2015]	TE & CC	Gradual change in feed conditions	Platinum concentrator plant
Zhang *et al.* [2015]	PDC	Oscillations	Tennessee Eastman
Landman & Jamsa-Jounela [2016]	TE	Oscillations	Large scale board machine
Aftab *et al.* [2017]	CCM	Oscillation	Refinery
Luo *et al.* [2017]	CCM	Oscillation	Tennessee Eastman Simulation

TABLE 2.2: *Overview of literature on causality analysis for fault diagnosis in industrial processes. The methods are abbreviated as follows: TE = Transfer Entropy; GC = Granger Causality; PDC = Partial Directed Coherence; CC = Cross-Correlation; CCM = Convergent Cross Mapping; KNN = K-Nearest Neighbours.*

Reference	Method	Fault type	Process
Lindner *et al.* [2018b]	TE	Oscillations	Platinum concentrator plant
Rashidi *et al.* [2018]	TE	Oscillations	Tennessee Eastman Simulation & large scale centrifuge
Wakefield *et al.* [2018]	TE & GC	Abrupt change in ore hardness	Milling circuit simulation

2.11.1 Applications by industry

Many of the applications listed in Table 2.2 have considered the Tennessee Eastman benchmark dataset. The variety of real processes to which these techniques have been applied is limited. This gives an indication of the reluctance of industry to accept these techniques as viable fault diagnosis approaches. The reason for this reluctance may be attributed to the difficulty of applying these methods in an automated and robust fashion to diverse process conditions and trends in process data.

Figure 2.7 presents a pie chart summarising the causality analysis applications by industry. The majority of the applications are in the chemical processing industry or simulations of chemical process, and most of these consider the Tenessee Eastman benchmark dataset.

In previous works by this author, transfer entropy and cross-correlation were used for causality analysis in mineral processing plants [Lindner *et al.*, 2014]. Another work from the same research lab, on which this author was co-author, applied transfer entropy and Granger causality to a simulation of a milling circuit in a concentrator plant [Wakefield *et al.*, 2018]. To the best of the author's knowledge no other examples of application to the minerals processing industry exist in published literature. The nature of mineral processes provide significant opportunities for improving performance in mineral processes using fault diagnosis. However, it also poses unique challenges for application of causality analysis in these processes.

Minerals processing involves a large amount of uncertainty. Measuring techniques for many important variables are often unavailable due to cost or process constraints. Important properties of processing streams cannot be measured without intrusive or time consuming sampling methods. For example, the grade of processing streams is often calculated offline using X-ray fluorescence (XRF) analyses, or mineral assays on a shiftly basis. The grade is one of the most important product quality variables, so being unable to measure it frequently means that control and operational set-points have to rely on other measurements.

Input conditions, such as feed grade and ore hardness, vary significantly, since the feed originates from underground ores with varying properties. The difficulty of measuring important feed, operational, and quality variables means that datasets are often information-sparse.

For some properties, measurements are available, but the measurement techniques are prone to inaccuracy, often due to environmental influences. This means that the measurements can be unreliable or noisy. The accuracy of any data-based analysis will be affected by the noisy and inaccurate measurements.

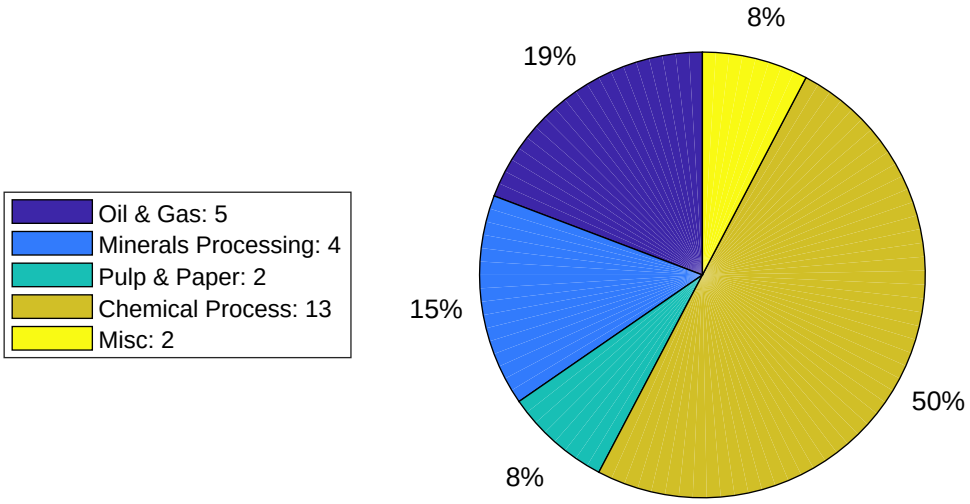

Figure 2.7: *Percentage of works cited in Table 2.2 grouped by industry application.*

2.11.2 Application by technique

Of the 27 works cited in Table 2.2 (aside from the literature review [Yang & Xiao, 2012] and textbook [Yang *et al.*, 2014]), 19 of them use transfer entropy, 6 use Granger causality, 4 use PDC, 9 use cross-correlation, 2 use convergent cross-mapping, and 2 use kNN. Figure 2.8 presents a pie chart of the works cited, showing the percentages of each method used. The popularity of a technique can be seen as an indication of its maturity. If more researchers have investigated its use, the strengths and weaknesses are well known and may have been addressed already.

Transfer entropy is overwhelmingly the most popular technique. The entries in Table 2.2 are sorted by date, so it also shows that transfer entropy has remained popular in recent times. This also indicates that, despite the numerous examples of transfer entropy accurately identifying root causes, the challenges of applying transfer entropy are still being addressed. More recent applications focus on avoiding the computational burden [Naghoosi *et al.*, 2013] or extending the approach for direct transfer entropy calculations [Duan *et al.*, 2013, Landman & Jamsa-Jounela, 2016]. Cross-correlation is also popular technique, although its use has diminished in recent applications. The cross-correlation technique is simple and easy to interpret, which may account for its popularity. Granger causality has been gaining traction in the fault diagnosis literature. The regression concepts of Granger causality are easy to understand and interpret, and the computational burden is low. The simple extension to multivariate calculations and conditional Granger causality [Yuan & Qin, 2014] makes it appealing for many engineers.

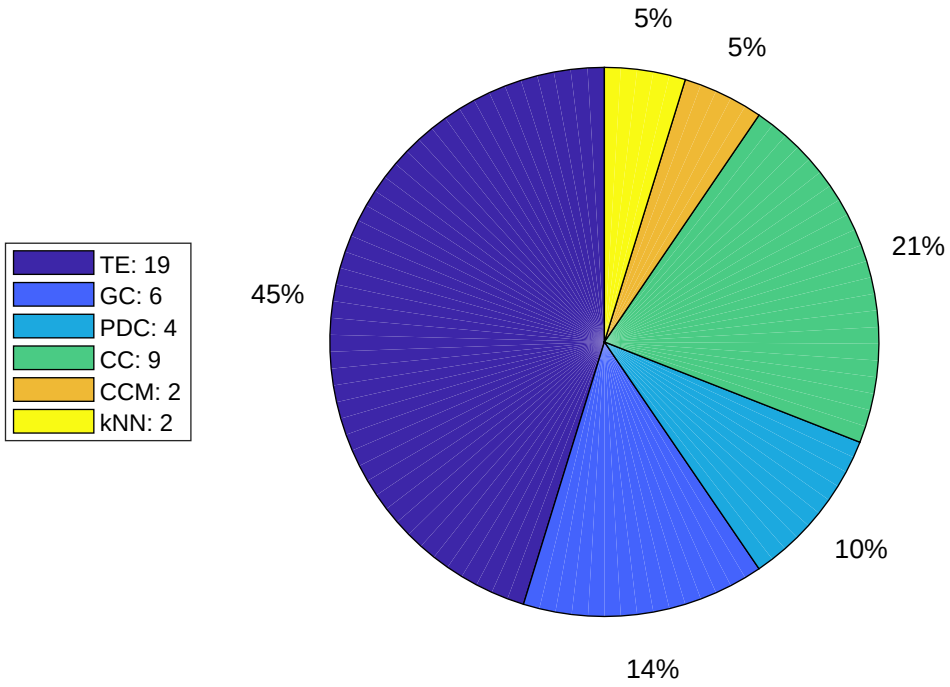

FIGURE 2.8: *Percentage of works cited in Table 2.2 grouped by causality analysis method. The percentages are calculated from the total number of applications of individual methods, since some works apply more than one technique.*

2.11.3 Applications by fault type

The 'Fault Type' column in Table 2.2 indicates what type of fault was being diagnosed in the case study. The vast majority of the case studies considered oscillations affecting the process. Chemical process often exhibit oscillatory behaviour, as a result of poorly tuned feedback controllers, faulty valves, or external disturbances [Thornhill & Horch, 2007]. Oscillations propagate through causal connections in a process with unique trends that tend to be persistent. Causality analysis techniques are well suited to analysing this kind of problem. The fluctuation in measurements caused by oscillations also means that the data-based techniques are able to capture a wide range of variation in values, making their modelling (for example for kernel density estimation) more accurate.

Step changes can occur in chemical processes, such as abrupt changes in feed compositions, temperatures or flow rates. Such abrupt changes may be caused, for example, by changing operator shifts, switching control strategies or changing feedstocks. Another type of non-oscillatory faults is a ramp change that may occur in some processes; where a persistent increasing or decreasing trend may be observed. Ramp trends can occur as a result of drifting sensors or valve malfunctions.

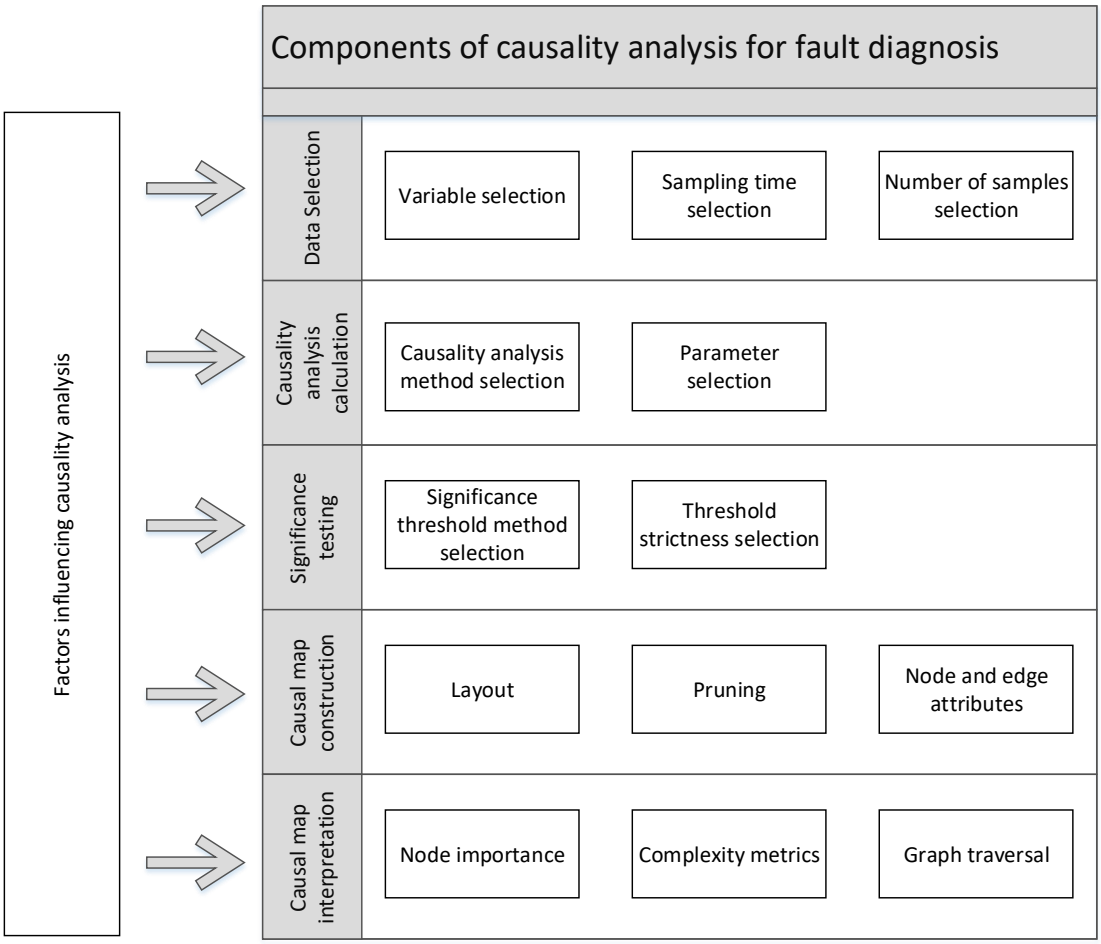

Figure 2.9: *Overview of components of causality analysis based fault diagnosis.*

2.12 Critical literature review of components of causality analysis based fault diagnosis

Now that the concepts of causality analysis have been introduced, and a broad overview of the published literature has been discussed, the important components of causality analysis can be discussed.

The application of causality analysis for fault diagnosis consists of a large number of components. Successful application of causality analysis requires that all these components work together harmoniously and effectively. Figure 2.9 provides an overview of all the components required for application of causality analysis. The components are subdivided into five overall steps: data selection, causality analysis calculation, significance testing, causal map construction, and causal map interpretation. This section discusses how these components have been addressed in literature, and highlights the areas that still require improvement. This discussion is limited to Granger causality and transfer entropy, which were identified in Section 2.11 as being the most popular and industrially mature of the techniques considered in this chapter.

2.12.1 Data selection

The first step in the causal analysis is to select the data that will be analysed.

Variable selection

Selecting variables to include in the causality analysis is important. It can greatly reduce the computational load, and can simplify interpretation of the results. Most of the applications identify oscillations in the time series and determine which variables oscillate at this common frequency. Only these variables are then included in further analysis. Landman *et al.* [2014] and Landman & Jamsa-Jounela [2016] identified variables with a common oscillation by observing their power spectra. Only these variables were included in the analysis. Duan *et al.* [2014] used the spectral envelope method [Jiang *et al.*, 2007] to automatically identify the variables oscillating at a the same frequency. Yuan & Qin [2014] used principal component analysis (PCA) to identify which variables contributed to the oscillation.

Sampling time selection

As part of the data selection, the sampling time of the data used in the analysis needs to be selected.

Barnett & Seth [2017] investigated the impact of subsampling on the causal detection ability of Granger causality in neurophysical processes. They found that the causal delay between the variables had a significant effect on the appropriate sampling time. They observed that the detection ability decays exponentially as the sampling time increases beyond the causal delay. Although their study focused on Granger causality, the same result can be inferred for other causality analysis techniques, such as transfer entropy.

To the best of this author's knowledge, none of the other applications of causality analysis for fault diagnosis have specified the sampling time required for causality analysis.

Number of samples selection

The number of samples to include in the analysis needs to be selected.

Bauer *et al.* [2007a] performed a sensitivity analysis on the number of samples. The minimum number of samples required to obtain a significant transfer entropy value for known causal connections was determined. The results indicated that the minimum number of samples should be set to 2000 samples if possible, but could be as low as 400 samples. This investigation considered known causal connections from an industrial case study. Therefore it is uncertain whether these results are representative for different case studies. The impact of different process dynamics, and different process characteristics was therefore not considered. Additionally, the interaction between the optimal number of samples and other parameters, such as the sampling time, or prediction horizon, have not been considered.

2.12.2 Causality analysis calculation

In the published literature focusing on the use of transfer entropy for fault diagnosis in industrial processes, few authors discuss the workflow applied for data selection, variable selection, and

optimal parametrisation. The results of the transfer entropy analysis are extremely sensitive to selection of these properties.

Horch *et al.* [2007] presented a workflow for the application of transfer entropy. Although the workflow involved many of the same general steps as presented in this section, key application details were omitted. Specific parametrisation guidelines were omitted, and the default parameters for transfer entropy suggested by Bauer *et al.* [2007a] were used. The number of samples to include, sampling time selected, and which variables to include were not discussed either. Transfer entropy results are very sensitive to parameter selection, as noted by Duan *et al.* [2014].

Table 2.3 summarises the parameter selection approaches for transfer entropy used by other authors. In some cases the selection procedures were not described, but the values used were given. In other cases neither were described.

TABLE 2.3: *Summary of decisions and parameter selection methods used for transfer entropy in literature. In cases where no guidelines were given, the value used for the specific case study is reported. In cases where neither guidelines nor the actual values used are provided, 'not given' is reported.*

Reference	Bauer *et al.* [2007a]	Naghoosi *et al.* [2013]	Shu & Zhao [2012]	Duan *et al.* [2013]	Duan *et al.* [2015]	Hajihosseini *et al.* [2014]	Landman & Jamsa-Jounela [2016]
Variables	Common oscillations	Not given	Not given	Not given	Spectral envelope to determine common oscillations	Not given	Common oscillations
$\mathbf{N_S}$	Preferably minimum of 2000 , possibly as low as 400	15000	200	3544	No less than 2000	Sliding window of 400	3000
$\mathbf{T_S}$	10s	60s	1.8s	60s		3 min	10s
τ	Vary until $\Delta T_{x\to y} = 0$	Differential dependency method	1	Initialise τ =1	Initialise τ =1	1	Initialise τ =1
h	$h = \tau$	Differential dependency method	Vary h and find maximum	Initialise $h = 1$	Initialise $h = 1$	1	Initialise $h = 1$
K	0	Differential dependency method	1	Vary until $\Delta H_{yy} = 0$	Vary until $\Delta H_{yy} = 0$	1	Vary until $\Delta H_{yy} = 0$
L	2	Differential dependency method	1	Vary until $\Delta T_{x\to y} = 0$	Vary until $\Delta T_{x\to y} = 0$	2	Vary until $\Delta T_{x\to y} = 0$

Causality analysis method selection

Duan *et al.* [2014] demonstrated and compared different techniques for root cause diagnosis of plant wide oscillations. Granger causality and transfer entropy were the data-based causality analysis techniques they compared, and some of their advantages and disadvantages were listed. They found that Granger causality is easier to implement, robust to data selection, has low computational burden, and its application techniques are well developed. However, it is only suitable for linear relationships between variables, and may be prone to model misspecification. They also found that transfer entropy is robust to data selection, suitable for both linear and nonlinear relationships. However, it is sensitive to calculation parameter selection, difficult to implement, and the computational burden is large.

Kuhnert [2013] presented guidelines for technique selection based on process characteristics. These guidelines were developed based on simulated experiments to determine which technique gave the most accurate results for different process characteristics. They found that transfer entropy was applicable for both linear and nonlinear systems, and applicable for systems with long dead time and short dead time between variables. They also found that Granger causality was only applicable for linear systems with short dead time between variables. Although these guidelines are useful, they were were based on simulated experiments and not on real case studies. Also, only the accuracy of the techniques was considered. Investigation of other factors, as discussed in Chapter 5 is also important.

Parameter selection

For Granger causality, parameter selection is limited to choosing the model order, k. Selection of this parameter is straightforward, and accurate using the AIC.

The parametrisation of transfer is complex, requiring four important parameters to be set. The hyper-parameters for transfer entropy are: the prediction horizon, h; the sampling parameter, τ; the embedding dimension for the output variable, K; and the embedding dimension for the input variable, L.

The kernel density estimation step itself, discussed in Section 2.9.2, has a bandwidth parameter that has to be selected. The accuracy of the estimated distribution will be sensitive to this parameter. This means that the accuracy of the calculated transfer entropy may also be sensitive to this parameter. Optimal selection of this bandwidth was not included in the scope of this dissertation, since many robust guidelines for the selection of the bandwidth have been developed. For example, the rule of thumb suggested by Li & Racine [2011].

Bauer *et al.* [2007a] addressed some aspects of parametrisation. The optimal prediction horizon (h) and time interval (tau) were determined for the causal connections in an industrial case study, where existing causal connections were known from process knowledge. They chose default values of $K = 0$ and $L = 2$. The transfer entropy between all the known causal connections was calculated over a range of tau , to find the τ that gave the largest significant transfer entropy value. The same was then applied to determine the optimal h values. The results indicated that default values of $\tau = h = 4$ provided robust transfer entropy results for a wide range of process conditions. Subsequently, many implementations of transfer entropy have used these default values. These optimal parameters were based on a specific case study, however. The impact of different process dynamics, and different types of processes was not considered in this investigation.

Many parametrisation techniques approach the problem by calculating transfer entropy over

a range of embedding dimensions (e.g. K) to find the embedding where there is no longer a difference in information captured between K and $K+1$. K is an optimal embedding dimensions if points in the K-dimensional space remain close in the $(K+1)$-dimensional space [Cao, 1997]. Default values of $K = 0$ and $L = 2$ are chosen. The time interval, τ, was then varied until the difference in $T_{x\to y}$ no longer varied significantly with changing τ. If this plateau of τ is not observed over the range of values, then the prediction horizon, H, is increased until Algorithm 2.1 shows the procedure.

Algorithm 2.1: Parameter selection method 1: Finding optimal τ and H

Input : $\mathbf{X}, \mathbf{Y}$
Output: K, L

$K = 1$;
$L = 2$;
while $\Delta T_{x\to y} > 0$ **do**
  $\mathbf{X}_i^{(K)} = [\mathbf{x}_i, \mathbf{x}_{i-\tau}, ..., \mathbf{x}_{i-(K-1)\tau}]$;
  $\mathbf{Y}_i^{(L)} = [\mathbf{y}_i, \mathbf{y}_{i-\tau}, ..., \mathbf{y}_{i-(L-1)\tau}]$;
  $T_{x\to y} =$;
  $\Delta T_{x\to y} = T_{x\to y}(k) - T_{x\to y}(k-1)$;
  $\tau = H = \tau + 1$;

Another method, applied by Duan [2014], first selects a default value of $h = \tau = 1$, then varies K until the Shannon entropy for Y (see Equation 2.9) no longer changes with changing K. Then L is varied until $T_{x\to y}$ no longer changes significantly with changing L. However, when K or L becomes too large a larger τ is chosen and the procedure is repeated. Algorithm 2.2 details the procedure.

Algorithm 2.2: Parameter selection method 2: Finding optimal K and L

Input : $\mathbf{X}, \mathbf{Y}$
Output: K, L

$\tau = H = 4$;
while $\Delta H_{yy} > 0$ **do**
  $\mathbf{X}_i^{(K)} = [\mathbf{x}_i, \mathbf{x}_{i-\tau}, ..., \mathbf{x}_{i-(K-1)\tau}]$;
  $\mathbf{Y}_i^{(L)} = [\mathbf{y}_i, \mathbf{y}_{i-\tau}, ..., \mathbf{y}_{i-(L-1)\tau}]$;
  $H_{yy} =$;
  $\Delta H(y_{i+h}|\mathbf{y}_i^{(K)}) = H(y_{i+h}|\mathbf{y}_i^{(k)}) - H(y_{i+h}|\mathbf{y}_i^{(k-1)})$;
  $k = k + 1$;
while $\Delta T_{x\to y} > 0$ **do**
  $\mathbf{X}_i^{(K)} = [\mathbf{x}_i, \mathbf{x}_{i-\tau}, ..., \mathbf{x}_{i-(K-1)\tau}]$;
  $T_{x\to y} =$;
  $\Delta T_{x\to y} = T_{x\to y}(k) - T_{x\to y}(k-1)$;
  $l = l + 1$;

The second method can be computationally expensive, which is why the first method is preferred.

Naghoosi *et al.* [2013] approached parametrisation from the viewpoint of mutual dependency. The authors used time lagged dependency and differential dependency curves to determine the most important time lags in the variables and use this information to parametrise transfer

entropy. The additional steps for determining these time lags are computationally expensive, although not as expensive as the previous methods. The method does consider the time delay between variables. However, other dynamics, such as the residence time and oscillation period, are not considered.

Approaching the problem from the other direction, identifying the dynamics and using them to specify the parameters, may make the application procedure more robust and remove the computational burden of searching for optimal parameters over a range of values. Chapter 7 therefore introduces a novel parametrisation procedure that selects the optimal h an τ based on the interaction of these parameters with the process and fault dynamics.

2.12.3 Significance testing

Uncertainty inherent in process measurement means that non-zero transfer entropy values will be calculated even when there is no causal relationship. These spurious connections make analysis of fault propagation paths difficult. Spurious connections give a false representation of the propagation path of the fault. Therefore, a hypothesis test is needed to determine the statistical significance of the causality measure. However, this significance test is not infallible, and spurious connections may still be found. A causal connection means that variation in one variable will cause similar variation in another variable, after some time. Variation caused by sensor noise would mean that variation in the output variable is not caused by variation in the input variable, therefore the causal connection would be obscured. Process noise, caused by common cause variation (for example slight variation in feed compositions) may show a strong trend between the variation in the input and output variables, meaning that the causal connection may be detected. However, high frequency variations can cause the value of the input variable to change too quickly for a response to be seen in the output variable, which would obscure the causal connection. Mitigation of the impact of noise can be achieved through proper significance testing.

The hypothesis tests for transfer entropy and Granger causality have been discussed extensively in the fault diagnosis literature. The methods for determining statistical significance are well developed and robust. The methods used in this dissertation are discussed in detail in the following subsections.

Significance threshold method selection

Hypothesis tests to determine the statistical significance of the values obtained need to be employed. For Granger causality the hypothesis test can take the form of an F-statistical test [Bressler & Seth, 2011], as shown in Equation 2.34. N_s represents the sample size of the time series used. RSS_r and RSS_f represent the sum of the square of the residuals in the restricted and full models respectively, as shown in Equation 2.35.

$$\frac{\frac{RSS_r - RSS_f}{k}}{\frac{RSS_f}{N_s - 2k - 1}} \sim F_{k, N-2k-1} \tag{2.34}$$

where the numerator degrees of freedom are k, and the denominator degrees of freedom are $N - 2k - 1$, and

$$RSS_r = \sum_{t=k+1}^{N_s} \epsilon_j^2(t) \tag{2.35}$$

$$RSS_f = \sum_{t=k+1}^{N_s} \epsilon_{j|i}^2(t) \tag{2.36}$$

When the F-test calculated from Equation 2.34 is larger than the value of the F-distribution at a chosen α value, the null hypothesis that there is no causal connection between the two variables can be rejected[Bressler & Seth, 2011].

Unlike Granger causality, the distribution of the causal statistic for transfer entropy is not known[Bressler & Seth, 2011]. This means that computationally expensive resampling techniques must be used for the hypothesis test. A significance threshold for the transfer entropy can be calculated using a method suggested by Kantz & Schreiber [1997], Schreiber & Schmitz [2000], where Monte Carlo simulations are used to generate a distribution for a hypothesis test using multiple (N_{surr}) surrogate time series for each variable. The null hypothesis is that there is no causal connection between the pair of variables. Therefore, the surrogate data sets are designed have the same statistical properties as the original data, but with any potential causal link destroyed[Vicente *et al.*, 2010].

To generate surrogates with these criteria, the iteratively Adjusted Amplitude Fourier Transform (iAAFT) approach is used. The iAFFT works by Gaussian rescaling of the time series, a Fourier transform with randomised phases is applied to the scaled time series, and then the inverse of the first scaling step is applied. These steps are repeated until deviation of autocorrelation from that of original time series is satisfactorily small or until there is no change in amplitudes[Schreiber & Schmitz, 2000].

The first step in iAAFT surrogate data generation is Gaussian rescaling of the time series. Let $\mathbf{g}(t)$ be a sequence drawn from a Gaussian distribution and sorted in ascending order. $rank(\mathbf{x}(t))$ denotes the ascending rank of $\mathbf{x}(t)$. The rescaled sequence is then given by:

$$\mathbf{s}(t) = \mathbf{g}(rank(\mathbf{x}(t))) \tag{2.37}$$

A Fourier transform can be applied to this scaled series:

$$|S(\omega)| = \left| \frac{1}{\sqrt{N}} \sum_{t=0}^{N-1} r(t) \exp\left(\frac{\iota 2\pi t\omega}{N}\right) \right| \tag{2.38}$$

The Amplitude Adjusted Fourier Transform (AAFT) surrogate can then be calculated by multiplying the Fourier transform by random phases and then performing the inverse Fourier transform:

$$\bar{\mathbf{s}}(t) = \frac{1}{\sqrt{N}} \sum_{\omega=0}^{N-1} |S(\omega)| \exp\left(-\frac{\iota 2\pi t\omega}{N}\right) e^{\iota\alpha_k} \tag{2.39}$$

where α_k is uniformly random sampled between $0 < \alpha_k < 2\pi$. $e^{\iota\alpha_k}$ in Equation 2.39 is the phase randomisation term.

The iAAFT applies the AAFT procedure iteratively. The initial $\bar{\mathbf{r}}^{(0)}(t)$ is an AAFT of the original data $\mathbf{x}(t)$. The Fourier transform is applied to $\bar{\mathbf{r}}^{(i)}(t)$

$$\bar{\mathbf{R}}^{(i)}(\omega) = \frac{1}{\sqrt{N}} \sum_{t=0}^{N-1} \bar{r}^{(i)}(t) \exp\left(\frac{\iota 2\pi t\omega}{N}\right) \tag{2.40}$$

The surrogate data for this iteration is then obtained by applying the inverse Fourier transform. In this inversion, the actual amplitudes are replaced by $|S(\omega)|$, but keeping the phase from Equation 2.40, $e^{\iota\omega^{(i)}} = \bar{\mathbf{R}}^{(i)}(\omega)/|\bar{\mathbf{R}}^{(i)}(\omega)|$:

$$\bar{\mathbf{s}}^{(i)}(t) = \frac{1}{\sqrt{N}} \sum_{\omega=0}^{N-1} |S(\omega)| \exp\left(-\frac{\iota 2\pi t\omega}{N}\right) e^{\iota\omega^{(i)}} \tag{2.41}$$

The next $\bar{\mathbf{r}}^{(i+1)}(t)$ is then assigned by rank ordering the original data:

$$\bar{\mathbf{r}}^{(i+1)}(t) = \mathbf{c}(rank(\bar{\mathbf{s}}^{(i)}(t))) \tag{2.42}$$

where $\mathbf{c}(t)$ is a copy of $\mathbf{x}(t)$ in ascending order. This process is repeated until deviation of autocorrelation from that of original time series is satisfactorily small or until there is no change in amplitudes. The final $\bar{\mathbf{r}}(t)$ is then taken as the final surrogate time series, $\bar{\mathbf{s}}(t)$.

The transfer entropy between the surrogates for each pair of variables, $T^{surr}_{x\to y}$, is then calculated, and an $a \times \sigma$ threshold is set. This threshold, $S_{x\to y}$, is calculated as shown in Equation 2.43.

$$S_{x\to y} = \mu_{T^{surr}_{x\to y}} + a \times \sigma_{T^{surr}_{x\to y}} \tag{2.43}$$

where $\mu_{T^{surr}_{x\to y}}$ and $\sigma_{T^{surr}_{x\to y}}$ represent the mean and standard deviation of the N_{surr} surrogate transfer entropies respectively, and a represents the number of standard deviations from the mean. When $T_{x\to y} > S_{x\to y}$, then the null hypothesis that there is no causal connection between the two variables can be rejected[Wibral *et al.*, 2014].

Threshold strictness selection

The hypothesis test described in the previous section are not infallible, an spurious causal connections will still be observed. Strict threshold for the hypothesis will ensure that less spurious causal connections are identified. On the other hand, too strict thresholds will cause true connections to be missed. There is a trade-off between the number of true connections and the number of missing connections.

For the hypothesis test for statistical significance for Granger causality, show in Equation 2.34, the α value can be chosen according to how strict the threshold should be. An α value of 0.05, for example, means that the null hypothesis is accepted or rejected with a 95% significance level. An α value of 0.01 was used by Landman *et al.* [2014]. In Duan *et al.* [2014], an α value of 0.05 was chosen. Yuan & Qin [2014] stated that the α value was typically 0.01 or 0.05.

For transfer entropy, the strictness of the significance threshold can be altered by choosing the number of standard deviations from the mean, a. However, since the transfer entropy does not strictly follow a Gaussian distribution, it is not valid to assign a confidence level to a specific a value. [Bauer *et al.*, 2007a], Hajihosseini *et al.* [2014], and Duan *et al.* [2014] all reported using a $6-\sigma$ significance threshold, as opposed to a $2-$ or $3-\sigma$ threshold, to have more robust results.

2.12.4 Causal map construction

Once the causality analysis has been performed, an adjacency matrix is populated from the results. A causal map is then constructed to visualise the causality between the measured variables. This causal map can represent the propagation path of the fault through the process. The construction of the causal map has not been discussed much in the literature of causality analysis for fault diagnosis. The reason for this is that most authors have focussed on improving the accuracy and reliability of techniques to extract causality from process data, and have not focussed on the visualisation of the results.

Layout

Visual interpretation of causality maps can be aided by the layout of the nodes. The layout methods can be simple. For example, Bauer *et al.* [2007a] presented the causal map with all the nodes in a straight line, ordered so that source nodes are first, and sink nodes are last. This layout is useful for quickly identifying the root cause variable. However, for dense graphs this layout may be very confusing. Landman *et al.* [2014] used a grid layout. This layout is neat, but makes it difficult to visualise the direction of propagation. Forcing a structured grid layout may be useful to mirror the plant layout, e.g. it can be used to mimic the process flow diagram, showing how the data-based causal structure compares to the flow of the process.

In many scenarios a layout that reveals hierarchical structure may be desired. A layered layout reveals such a hierarchical structure [Sugiyama *et al.*, 1981]. In the layered algorithm the nodes are arranged in a set of layers, so that each edge joins two nodes belonging to different layers. In the layered structure, the sequence of nodes on the propagation path may be visualised in sequential order. Figure 2.10 shows an example of causality map using the layered layout.

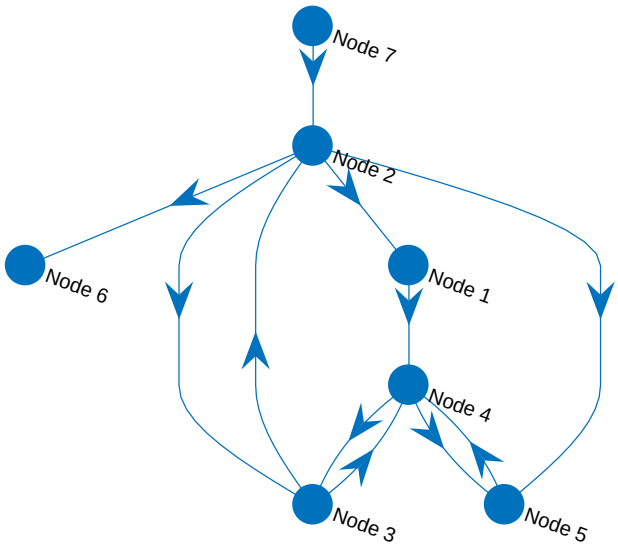

FIGURE 2.10: *Example of layered layout of causality maps*

Another layout is the circle layout. In the circle layout, the nodes are placed in a circle centred around the origin. This layout is useful for visualising the importance of each node, by visualising the amount of edges entering or leaving the node. This may reveal which node is a source node that influences many other nodes, or which is a sink node that is influenced by many other nodes. Figure 2.11 shows a causality map with the circle layout. This layout can be especially useful in scenarios where there is no clear start and end node, i.e. in a cyclical graph. In such a graph it is useful to see which nodes are most important relative to the others. The circle layout reveals this readily. A drawback of this layout is that it does not reveal anything about the structure of the underlying process. This layout was used by Yuan & Qin [2014], Zhang *et al.* [2015]. Duan *et al.* [2015] first used the circular layout to present the results, and then constructed a layered map to better visualise the propagation paths.

The force layout assigns attractive forces to the endpoints of edges, and repulsive forces to nodes. The balance of repulsive and attractive forces means that nodes that two nodes that are not connected by edges are pushed away from each other, since there is no attractive force between

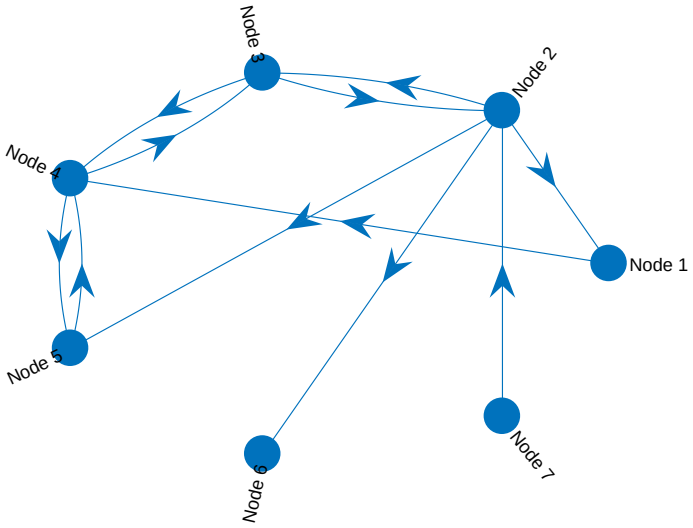

FIGURE 2.11: *Example of circle layout of causality maps*

them. This structure is useful for revealing the importance of nods, as with the circular layout. A node with many edges associated will attract the nodes that it connected to, making them cluster together. These clusters can also reveal hierarchical structure, as with the layered layout. A causality map with the force layout is shown in Figure 2.12.

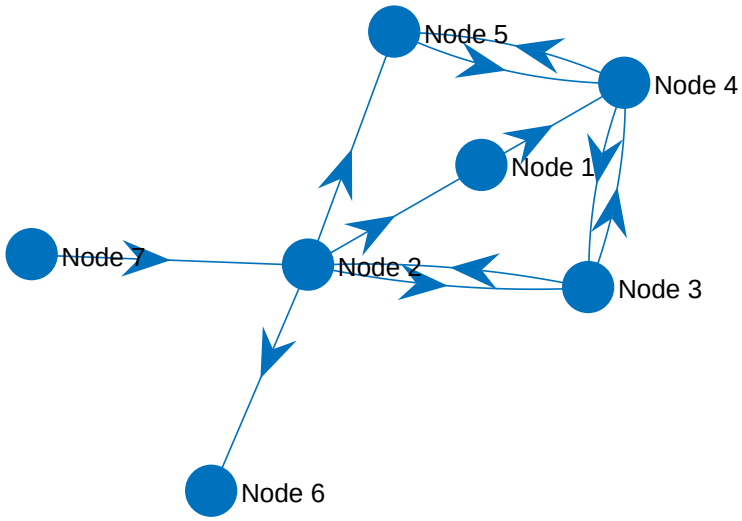

FIGURE 2.12: *Example of force layout of causality maps*

Although the authors mentioned in the paragraphs above utilised different layouts, none provided specific motivation for the use. Therefore, this component of causality analysis requires improvement.

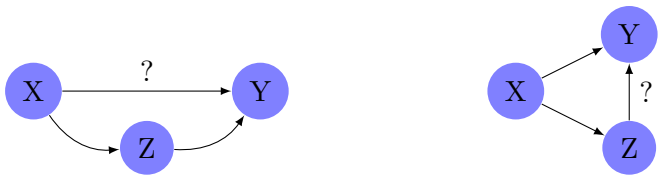

(a) *Shortcut scenario* (b) *Common variable scenario*

FIGURE 2.13: *Example of causal map showing indirect connection observed from $X \rightarrow Y$.*

Pruning

Causality maps may often show indirect connections, where a causal connection is identified due to the influence of an intermediate variable. Figure 2.13a illustrates this scenario. When X is connected to Z, and Z is connected to Y, it may appear that X is connected to Y. This indirect connection may be spurious. One way to determine whether this connection is a true connection, is to condition on the intermediate variable, for example, using the direct transfer entropy approach in Duan *et al.* [2013]. In this way the effect of X on Y without the effect of Z is determined. However, in the case of transfer entropy, this conditioning increases the computational load[Duan *et al.*, 2013]. Additionally, shortcut connections may still be true connections. However, the more dense a graph i,s the more difficult it is to interpret the propagation path. Therefore, a practical way of dealing with these shortcut connections is to use 'pruning' algorithms, that remove all shortcut edges. A version of this approach was used by Bauer *et al.* [2007a] to simplify the causal map obtained from transfer entropy. However, this approach can be improved using graph theoretic tools for graph pruning.

The transitive reduction algorithm is a formalised algorithm for removing shortcut edges. The transitive reduction of a graph G, is another graph, $G_{reduction}$, with the same number of nodes, but the fewest edges, so that $G_{reduction}$ has the same reachability as G [Aho *et al.*, 1972]. This is achieved by iterating through the graph using a depth-first search. For each combination of three nodes found, x, y, and z, if there are edges $x \rightarrow y$, $y \rightarrow z$, and $x \rightarrow z$, then $x \rightarrow z$ is removed [Aho *et al.*, 1972].

Figure 2.14 illustrates the transitive reduction. The original graph, G, is shown in Figure 2.14a, and the transitive reduction, $G_{reduction}$ is shown in Figure 2.14b. The shortcut edges from $A \rightarrow$ and $D \rightarrow E$ were removed.

The transitive reduction for an acyclic graph, G, will always be a unique subgraph of of G with the same nodes as G. A subgraph is a graph made of a subset of the nodes and edges of G. For a graph with cycles, however, the transitive reduction is not unique, and will not necessarily be a subgraph of the original. Consider the graph, G, in Figure 2.15a. The graph has a cycle between nodes A,B, C, and D. The transitive reduction of G is obtained by finding all the strongly connected components (SCCs) of G. An SCC is a subgraph of G, where all the nodes in the subgraph are mutually reachable. The cycle between nodes A,B, C, and D is an SCC. Nodes E and F each form their own SCC. A directed cycle is constructed for each SCC, connecting all the nodes in the SCC. An edge is constructed between each individual SCC. Because the transitive reduction in this case is not unique, edges may be constructed that did not exist in the original graph. For example, the edges from $A \rightarrow F$ and from $A \rightarrow E$. This artificial construction of edges may be misleading when interpreting causal maps. However, the presence of the cycles means that there was a path from $A \rightarrow F$ in the original graph. Despite

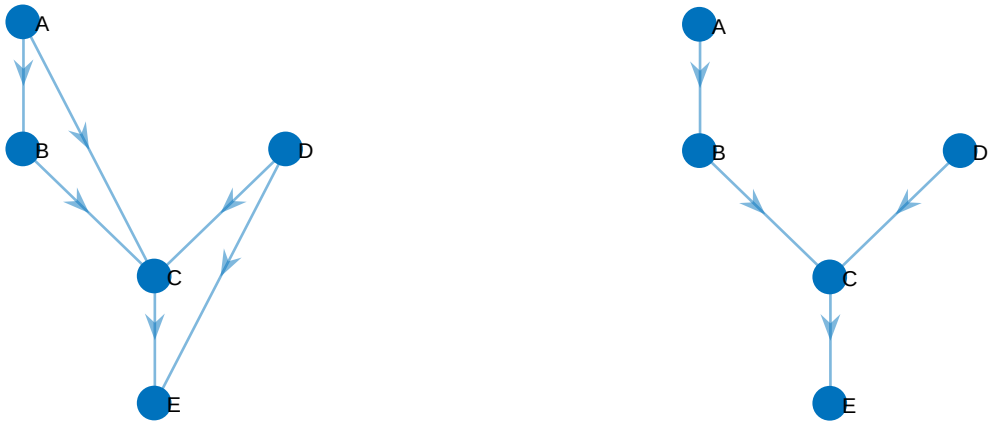

(a) *Original graph, G* (b) *Transitive reduction , $G_{reduction}$*

FIGURE 2.14: *Transitive reduction illustration. Shortcuts from $A \rightarrow C$ and $D \rightarrow E$ were removed.*

the possible confusion caused by these artificial edges, the transitive reduction can be used as a visualisation tool, to succinctly capture the information about the propagation path of the fault.

Assigning node and edge attributes

In addition to visualising the pairwise connections between measured variables, causality maps can be augmented with additional attributes that can aid interpretation.

Nodes can be coloured differently according to specifics attributes, such as variable categories, or sensor location. To do this the appropriate meta-data must be available for the engineer applying this technique. This is one way of incorporating process knowledge to aid fault diagnosis using causality maps. In many cases the data historian may already contain this meta-data for each variable. This structure can be exploited automatically to augment causal maps.

The strength of the connections in a causality map gives an indication of the relative importance of the connections. In scenarios where there are multiple possible propagation paths, the relative connection strengths can give an indication of which propagation path is more likely to reveal the true root cause. The connection strengths can be visualised by assigning them as edge weights, and adjusting the line thickness of the edges to represent these edge weights.

To the best of this author's knowledge, this component of causality analysis has not been exploited to aid interpretation of causal maps.

2.12.5 Causal map interpretation

Causality maps provide powerful visualisation tools for fault diagnosis. The connections in the map may represent the propagation path. This interpretation can be subjective in many cases.

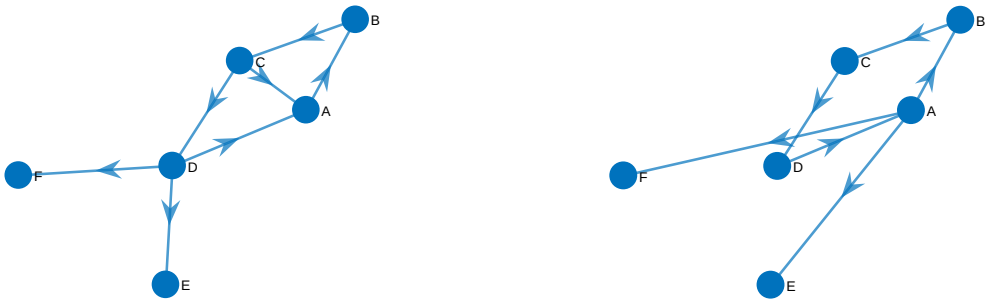

(a) *Original graph with cycle* (b) *Transitive reduction of graph with cycle*

FIGURE 2.15: *Transitive reduction of graph with a cycle.*

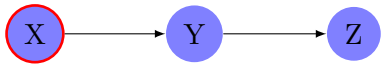

FIGURE 2.16: *Causality map showing straightforward root cause interpretation. In this scenario x is considered the root cause.*

For example, what if multiple propagation paths appear? What if multiple root causes appear? This ambiguity complicates the decision making process. For the causality analysis procedure to meet the desired characteristics described in Section 5.3, the interpretation procedure needs to be as automated and systematic as possible.

The simplest approach assumes that the root cause is found at the start of the causality map and that that the causality map presents the variables in sequence as the fault propagated through the process. This approach was used by Bauer *et al.* [2007a], Landman & Jamsa-Jounela [2016], Landman *et al.* [2014]. In Figure 2.16, for example, variable x would be considered the root cause. However, there are scenarios where this interpretation is more ambiguous. For example in more complex causality maps, where multiple propagation paths point to different root nodes.

Causal maps can be augmented with further interpretation tools to deal with cases where the causality map is more complex.

Node importance

Yuan & Qin [2014] assigned a 'maximum flow' (maxflow) attribute to each node in the causal

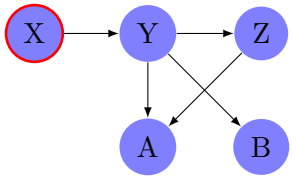

FIGURE 2.17: *Causality map demonstrating maximum flow attribute. Maximum flow is defined as number of edges exiting node minus the number of edges entering the node. MaxFlow for each node:* $X_{MaxFlow} = 1, Y_{MaxFlow} = 2, Z_{MaxFlow} = 0, A_{MaxFlow} = -2, B_{MaxFlow} = -1$.

map. The maximum flow was taken as difference between 'outflow' and 'inflow' for each node. Inflow is defined as the number of edges entering the node, and outflow is defined as the number of edges exiting the node. The variables were then ranked according their maximum flow. The variable ranked first was considered the root cause variable. The logic behind this approach is that variables with higher maximum flow have a larger net influence on subsequent nodes, and this influence is due to that variable being a driver of the fault. The maxflow is illustrated further in Section9.6. The concept of the maxflow of a node is illustrated in Figure 2.17. In this example the maximum flows for each node are shown in Equation 2.44.

$$\begin{aligned} X_{MaxFlow} &= 1 - 0 = 1 \\ Y_{MaxFlow} &= 3 - 1 = 2 \\ Z_{MaxFlow} &= 1 - 1 = 0 \\ A_{MaxFlow} &= 0 - 2 = -2 \\ B_{MaxFlow} &= 0 - 1 = -1 \end{aligned} \tag{2.44}$$

Therefore Y would be considered the root cause, since it ranked highest according to maximum flow. This method provides a more systematic approach to interpreting causality maps. In this example, however, the node with the higher maximum flow, Y, still has a preceding node, X. The maximum flow application is more useful in scenarios where the causal map is dense, as with the case study in [Yuan & Qin, 2014]

Kuhnert & Beyerer [2014] generated a root cause priority list, summing the causal influence of one variable on all the other variables in the system, as shown in Equation 2.45.

$$RC_j = \sum_{i=1}^{i \neq j} q_{x_j \to x_i} \tag{2.45}$$

where $q_{x_j \to x_i}$ is the causal strength from x_j to x_i. In the paper by Kuhnert & Beyerer [2014], causal strength, scaled from 0 to 1, is assigned to each node. In addition to this method for assigning node importance, Kuhnert & Beyerer [2014] also presented visualisation adaptations on traditional causal maps. These adaptations allowed visualisation of the causal strengths obtained from multiple causality analysis techniques, namely the cross-correlation, transfer entropy, Granger causality, and a support vector machine method. These visualisations are useful when multiple techniques are to be compared.

Another approach used for ranking nodes in the graph is one using the PageRank[Bryan & Leise, 2006] algorithm. Streicher *et al.* [2014] used this approach. The algorithm assigns a score to each node based on its influence on the rest of the causal network. This is similar to the maximum flow approach. However it considers the effect of each node in the context of the entire network, whereas the maximum flow approach only considers the effect of the node directly before and after the node under consideration.x

Complexity metrics

Complex causality maps are difficult to interpret. A metric describing the complexity of causal maps can give an indication of how easy it is to identify the root cause and the propagation path of the fault. To the best of this author's knowledge, none of the applications of causality analysis for fault diagnosis has discussed the use of any complexity metric.

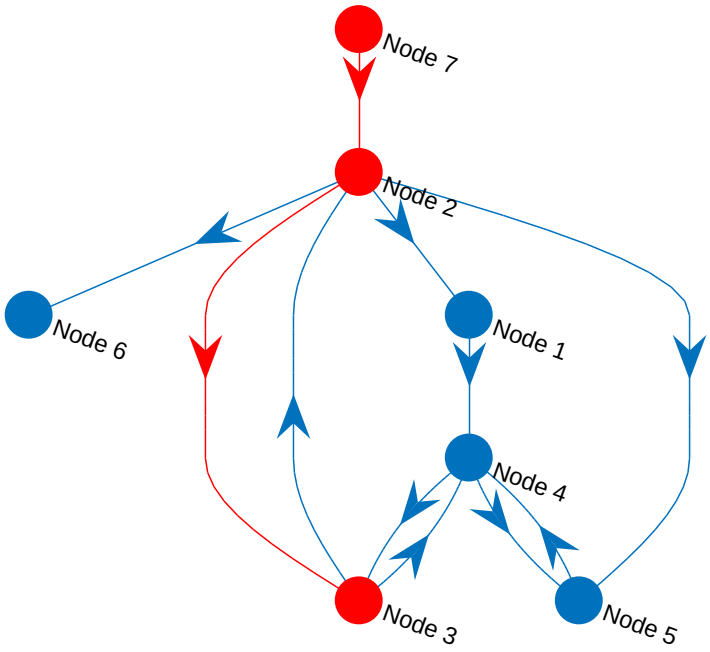

FIGURE 2.18: *Example of shortest path found between Node7 and Node3*

Graph traversal

The causal map provides a model for how process elements are connected to each other. In the fault diagnosis use case, this model gives a representation of how the fault propagated through the process. Tools for graph traversal, where the paths between different nodes can be identified in the graph, can be used to analyse propagation paths of faults[Yang & Xiao, 2012]. This can be useful to understand the propagation of the fault, to compare multiple propagation paths to determine which is most plausible, and to verify results of the causality analysis.

In the SDG-based fault propagation analysis, the most common algorithm for graph traversal is depth-first search[Yang & Xiao, 2012]. A depth-first search algorithm of Tarjan [1972] constructs paths in the causal map by beginning at a start node (specified by the user), and discovers adjacent nodes sequentially. This continues until the algorithm encounters a node where all the adjacent nodes have already been visited. At this point, the search backtracks along the discovered path to the closest previously discovered node without a discovered neighbour. This is implemented recursively until all nodes reachable from the start node have been visited. This can then be used to determine all propagation paths from a single node in a causal map.

Iri *et al.* [1979] used the depth-first search algorithm to find the maximum strongly connected component in a SDG, and used this maximum strongly connected component as an indication of the fault origin.

Graph traversal can be used to highlight the shortest path between two nodes. This can be used to analyse propagation paths between a possible root cause node in a causality map, and a symptom node. For example, in the graph shown in Figure 2.10, one can determine the shortest path between $Node7$, which appears as a root node, and $Node3$, which appears as the final sink node. The resulting shortest path is shown in Figure 2.18.

To the best of this author's knowledge, this kind of fault propagation inference based on graph

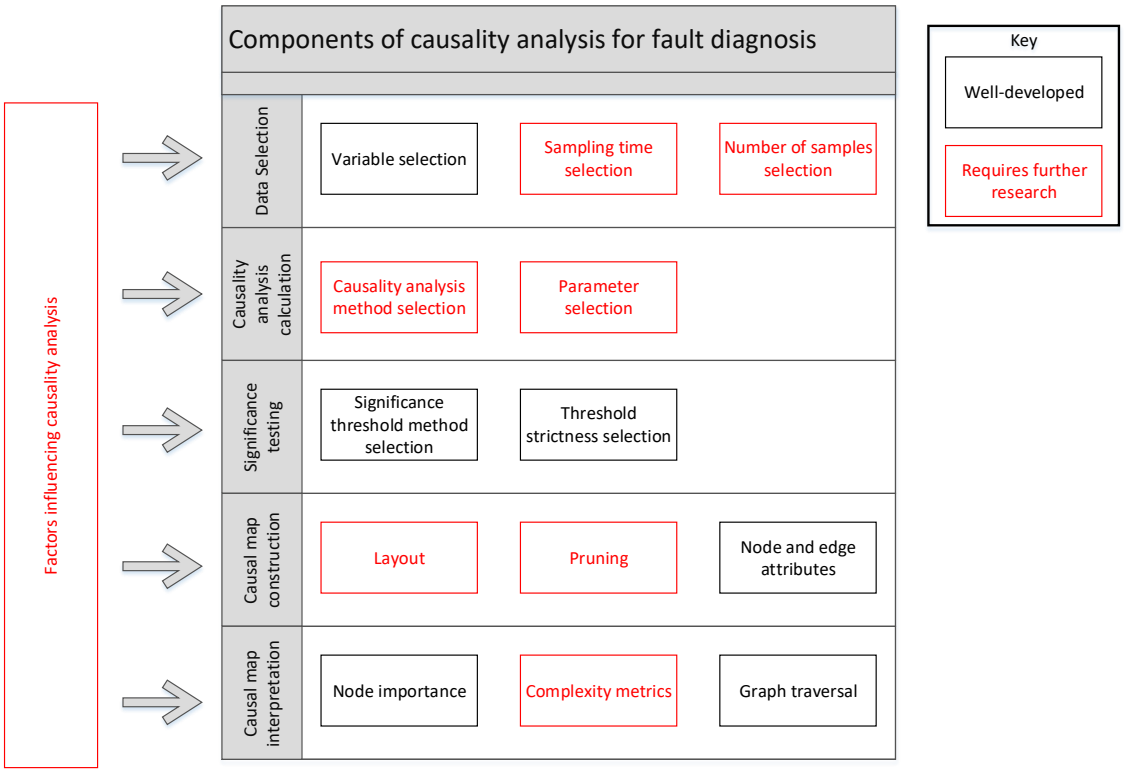

FIGURE 2.19: *Overview of components of causality analysis based fault diagnosis that require improvement.*

traversal has not been applied directly to causality maps obtained from data-based causality analysis. As mentioned in Section 2.12.4, the reason for this is that most authors have focussed on improving the accuracy and reliability of techniques to extract causality from process data, and have not focussed on the interpretation of the results from the techniques.

2.13 Components of causality analysis based fault diagnosis that require improvement

Section 2.12 showed that the application of causality analysis for fault diagnosis consists of a large number of components. Successful application of causality analysis requires that all these components work together harmoniously and effectively. Figure 2.19 provides an overview of all the components required for application of causality analysis, which components this dissertation aims to contribute to.

2.14 Chapter conclusions

The objectives of this chapter were: to conduct a critical review of the relevant literature on causality analysis for fault diagnosis, to identify areas that require improvement to aid industrial implementation; and to present the relevant background information of causality analysis technique.

This chapter introduced the concepts and calculations required for causality analysis. This chapter also provided a critical literature review of causality analysis for fault diagnosis. This literature review showed that transfer entropy and Granger causality were the most popular, and therefore the most mature, techniques. For this reason the rest of this dissertation focuses on these two techniques.

The literature review identified components necessary for causality analysis that require further research to aid industrial implementation of the techniques. These components are discussed in Section 2.12. The components are subdivided into five overall steps: data selection, causality analysis calculation, significance testing, causal map construction, and causal map interpretation. The first component that requires improvement is that there is no systematic workflow for data selection and causality analysis calculation. Specifically, the selection of the sampling time, the number of samples, and the parameters (such as the embedding dimensions, time interval, and prediction horizon). For this reason Objective II was defined.

Another component of causality analysis that requires further research is the decision of which causality analysis method to use in a specific scenario. Some researchers have investigated this, but not all the performance criteria of causality analysis techniques were investigated. Objective III was defined to address this.

Causality analysis for fault diagnosis relies on the interpretation of the results to provide useful information to users. This requires construction of a causal map, and interpretation of that map. This chapter identified that construction and interpretation of causality analysis techniques has been neglected in the published literature, with most applications employing an *ad-hoc* interpretation of results. Specifically, the layout of causal maps, techniques for pruning causal maps, and metrics to describe the complexity of causal map need further research. Objective IV was defined to address this shortcoming.

Chapter 3 gives an overview of the research methodology to address these objectives in this dissertation.

CHAPTER 3

Overview of dissertation methodology

Contents

3.1 Chapter introduction 55
3.2 Demonstrating the effectiveness of causality analysis for fault diagnosis 57
3.3 Investigating the factors that affect causality analysis 57
3.4 Developing a workflow for the application of causality analysis 57
3.5 Comparative analysis of Granger causality and transfer entropy 57
3.6 Tools for interpretation of causality analysis 58

3.1 Chapter introduction

Chapter 2 discussed the literature pertaining to the use of causality analysis for fault diagnosis in industrial processes. The discussion revealed that the literature is rich with examples of application of causality analysis for fault diagnosis, but industrial adoption of the techniques is still limited. This is due to the limitations of the techniques for automated application, unclear decisions on which techniques to use, and the difficulty of interpreting the results of the techniques.

The objectives outlined in Chapter 1 will be used to address these shortcomings. These objectives are repeated here:

Objective I. To *investigate* the factors that affect performance of causality analysis techniques.

Objective II. To *design* a systematic workflow for application of causality analysis for fault diagnosis.

Objective III. To *design* a tool to aid the decision of which causality analysis method to select.

Objective IV. To *present* tools for interpretation of causal maps for root cause analysis.

Section 2.12 showed that the application of causality analysis for fault diagnosis consists of a large number of components. Successful application of causality analysis requires that all these components work together harmoniously and effectively. Figure 3.1 provides an overview of all the components required for application of causality analysis, which components this dissertation aims to contribute to, and in which chapter that contribution is presented. The components are subdivided into five overall steps: data selection, causality analysis calculation, significance testing, causal map construction, and causal map interpretation.

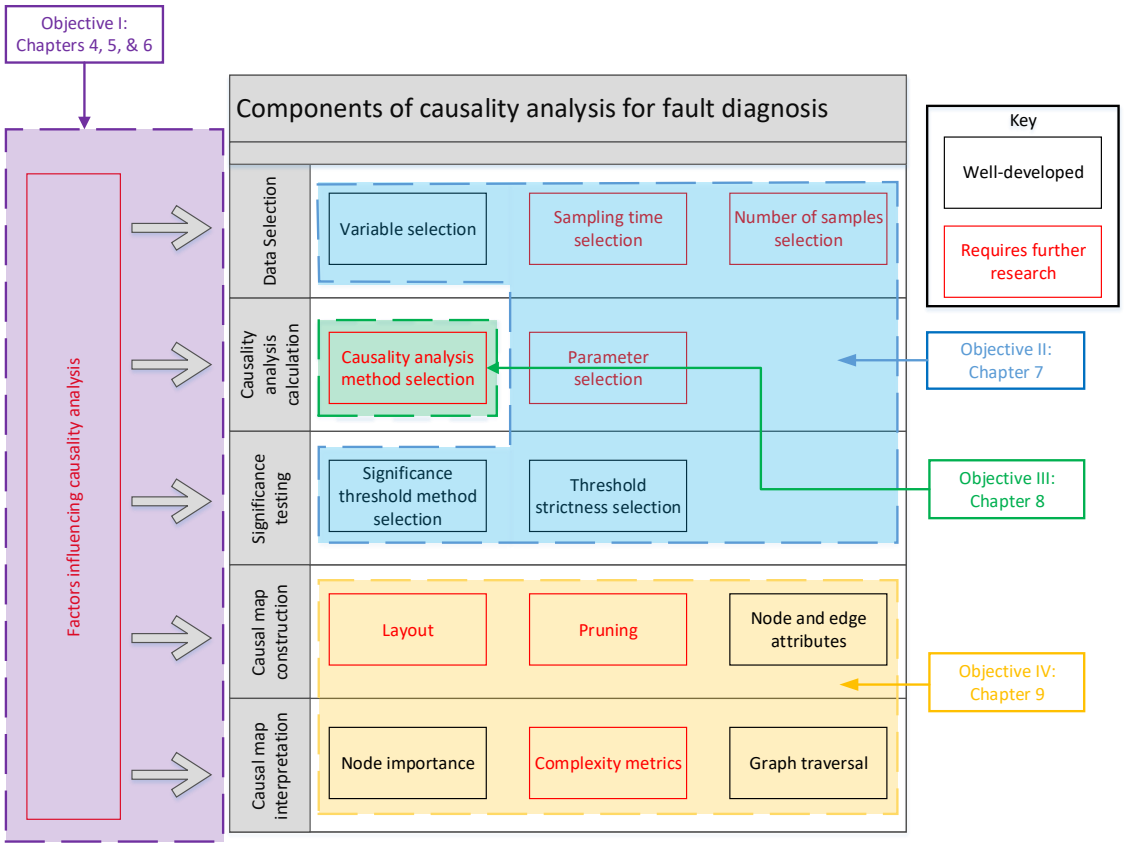

FIGURE 3.1: *Overview of chapters addressing components of causality analysis based fault diagnosis.*

An overview of the research methodology followed to address these objectives is presented in this chapter.

3.2 Demonstrating the effectiveness of causality analysis for fault diagnosis

Before any of the objectives are directly addressed, Chapter 4 demonstrates the usefulness of causality analysis for fault diagnosis. Transfer entropy and the nonlinearity index are used to diagnose an oscillation propagating through multiple control loops in a mineral process plant. The nonlinearity index was chosen because it is a well established oscillation diagnosis technique [Thornhill & Horch, 2007]. Transfer entropy was chosen because it is a popular causality analysis technique, as discussed in Chapter 2. Their validity for oscillation diagnosis is compared, highlighting the benefits and pitfalls when applied to a real industrial case study.

3.3 Investigating the factors that affect causality analysis

Objective I addresses the need for understanding the factors that affect causality analysis so that they can be successfully applied for fault diagnosis in industrial processes. To understand the factors that impact causality analysis, performance criteria for the techniques have to be established. Chapter 5 discusses the desired performance of causality analysis techniques. Chapter 6 investigates some of the factors that impact causality analysis, namely: controller interaction; disturbance type; and process noise. Additionally, in Section 7.4, the relationships between process dynamics and calculation parameters are determined using an ANalysis Of Variance (ANOVA). The results of this analysis are also used to provide guidelines for parameter selection, as part of the fulfilment of Objective II, discussed in the following section.

3.4 Developing a workflow for the application of causality analysis

Once the performance criteria and the factors affecting them have been investigated, Objective II can be addressed. This objective addresses the need for a systematic workflow to remove uncertainty and ambiguity in application of causality analysis techniques. Chapter 7 presents a systematic workflow for the application of transfer entropy for oscillation diagnosis. The workflow addresses the selection of each important parameter required and provides guidelines for selecting the optimal parameters based on the process conditions. The workflow is then demonstrated on an industrial case study of oscillations affected a mineral processing plant.

3.5 Comparative analysis of Granger causality and transfer entropy

Objective III addresses the need to provide guidelines for which of the numerous available causality analysis techniques to select. Chapter 8 present a comparative analysis of This chapter compares transfer entropy and Granger causality based on the performance criteria established in Chapter 5. The accuracy and precision of Granger causality and transfer entropy are tested and

compared using a simulated case study. Based on this comparison, a decision flow is presented, to aid engineers in deciding which technique to use and how to interpret the results. Finally, the features and the presented decision flow are illustrated on an industrial case study of a plant-wide oscillation.

3.6 Tools for interpretation of causality analysis

The final step in the causality analysis procedure is the root cause analysis once the results have been obtained. This root cause analysis requires interpretation of the causal maps generated from causality analysis. Objective IV addresses the need for tools to aid interpretation of the causal maps. In Chapter 9 visualisation and algorithmic tools to aid graph interpretation are developed and demonstrated.

CHAPTER 4

Demonstrating the use of transfer entropy for oscillation diagnosis

Contents

4.1 Chapter introduction 59
4.2 Chapter objectives 60
4.3 Methods 60
4.3.1 Transfer entropy *60*
4.3.2 Nonlinearity index *61*
4.4 Description of case study 62
4.4.1 Flotation circuit operation and control *62*
4.4.2 Oscillations in the flotation circuit *63*
4.5 Results and discussion 64
4.5.1 Transfer entropy results *64*
4.5.2 Nonlinearity index results *66*
4.5.3 Discrepancy of different methods and further analysis *66*
4.5.4 Shortcomings of causality analysis approach *69*
4.6 Chapter conclusion 69

4.1 Chapter introduction

A version of this chapter was published as a peer-reviewed conference paper: Lindner B, Chioua M, Groenewald J, Auret L & Bauer M, 2018b, Diagnosis of Oscillations in an Industrial Mineral Process Using Transfer Entropy and Nonlinearity Index, IFAC-PapersOnLine, 51(24), pp. 1409-1416.[Lindner *et al.*, 2018b]

Data-based causality analysis methods have been discussed in Chapter 2. In this chapter, the usefulness of causality analysis for fault diagnosis is demonstrated. The transfer entropy analysis, as well as the discussion of the results and formulation of the paper was primarily performed by this author. The nonlinearity index analysis was performed by the co-author of the paper. The results are discussed here to compare the nonlinearity index, which is a well established oscillation diagnosis technique, with transfer entropy, which is a causality analysis technique.

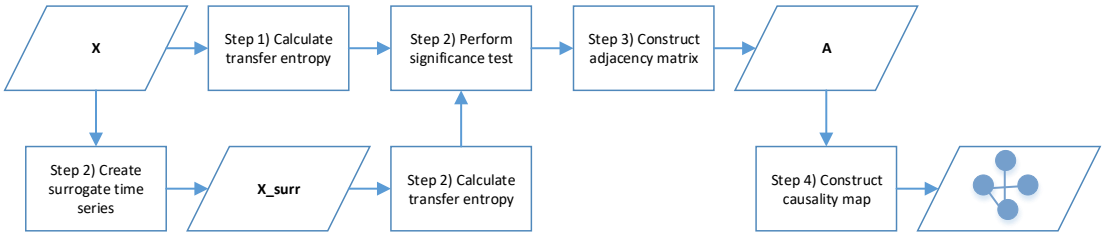

FIGURE 4.1: *Basic methodology for transfer entropy application.*

This is used to highlight the usefulness of causality analysis techniques for fault diagnosis, but also to demonstrate the shortcomings of these techniques that this dissertation aims to improve.

Mineral processes employ advanced control strategies to operate multiple units at desired conditions for optimisation of production rate and grade. Hundreds of control loops are typically used in such a control strategy. Satisfactory operation of these loops is essential to ensure optimal process conditions are maintained. Oscillations in these processes can cause fluctuations in the controlled variables of multiple units as the oscillation propagates through the process. Swift diagnosis and corrective action of such oscillations is essential to ensure efficient mineral beneficiation.

This chapter is structured as follows: Section 4.2 outlines the objectives of this chapter; Section 4.3 describes the application of transfer entropy and the nonlinearity index; Section 4.4 describes the case study of the oscillation in a flotation circuit; Section 4.5 presents the results of application of transfer entropy and nonlinearity index for oscillation diagnosis; and finally Section 4.6 presents the conclusions and some some further recommendations.

4.2 Chapter objectives

The objectives of this chapter are:

I To *investigate* the root cause of an oscillation in a flotation circuit of a mineral process.

II To *demonstrate* the effectiveness of causality analysis for fault diagnosis.

4.3 Methods

The application of transfer entropy and the nonlinearity index are described here.

4.3.1 Transfer entropy

Transfer entropy was discussed in Chapter 2.9.2

Application of transfer entropy for oscillation diagnosis is achieved by the following steps in Figure 4.1. These steps are described here:

Step 1) Calculate $T_{x\rightarrow y}$, using Equations 2.7 and 2.5, for every pair of variables.

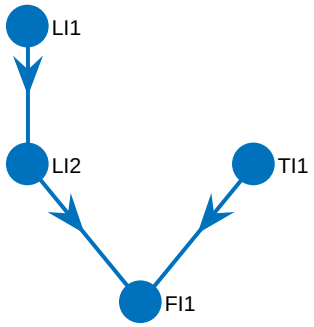

FIGURE 4.2: *Example of causal map of adjacency matrix in Equation 2.1.*

Step 2) Create N_{surr} surrogate time series for each variable. Calculate transfer entropy between the surrogates of pairs of variables. The significance threshold for each pair is then calculated with Equation 2.43. When $T_{i\to j} < S_{i\to j}$, the value is set to 0.

Step 3) Construct an adjacency matrix, $\mathbf{A}$. This is a square matrix whose rows and columns represent process variables, and binary entries represent the edges. By convention the row represents the *source* element, and the column represents the *sink* element. An example of an adjacency matrix is presented here:

$$\mathbf{A} = \begin{array}{c|cccc} & LI1 & LI2 & FI1 & TI1 \\ \hline LI1 & 0 & 1 & 0 & 0 \\ LI2 & 0 & 0 & 1 & 0 \\ FI1 & 0 & 0 & 0 & 0 \\ TI1 & 0 & 0 & 1 & 0 \end{array} \tag{4.1}$$

An entry of 1 in row i, column j, indicates $T_{i\to j} > S_{i\to j}$, which means that the node represented by row i has a causal influence on the node represented by column j. An entry of 0 indicates $T_{i\to j} < S_{i\to j}$, and therefore no connection exists.

Step 4) Construct a causality map from $\mathbf{A}$, where nodes represent the variables, and edges represent connections between them. Figure 4.2 shows the causal map constructed from the adjacency matrix in Equation 4.1 This map illustrates the propagation path of the oscillation. The first variable in this propagation path is closest to the root cause of the oscillation.

4.3.2 Nonlinearity index

Thornhill [2005] developed a nonlinearity index that ranks variables according to the nonlinearity of their time series. See Section 5.4.4 for a description of nonlinearity in processes. Details of the application can be found in Thornhill [2005]. A plant acts as a mechanical low pass filter [Thornhill, 2005] as the oscillation propagates to different variables. The low-pass process dynamics remove the higher harmonics in the trends and destroy the phase-coupling. This makes the waveforms more sinusoidal and more linear the further away from the root cause the variable is. The basis of the nonlinearity index is comparison of the predictability of the time series trend to that of generated surrogate trends [Thornhill, 2005]. A higher nonlinearity index value indicates a more nonlinear time series. Values below 1 indicate no significantly linear behaviour. Therefore the variables with the highest nonlinearity index are assumed to be closest to the root cause.

Horch *et al.* [2007] presented a solution for plant-wide disturbance analysis that incorporates both the nonlinearity index and transfer entropy. In their approach, the two analyses are performed in parallel. Both results combined are taken into consideration to determine the root cause.

4.4 Description of case study

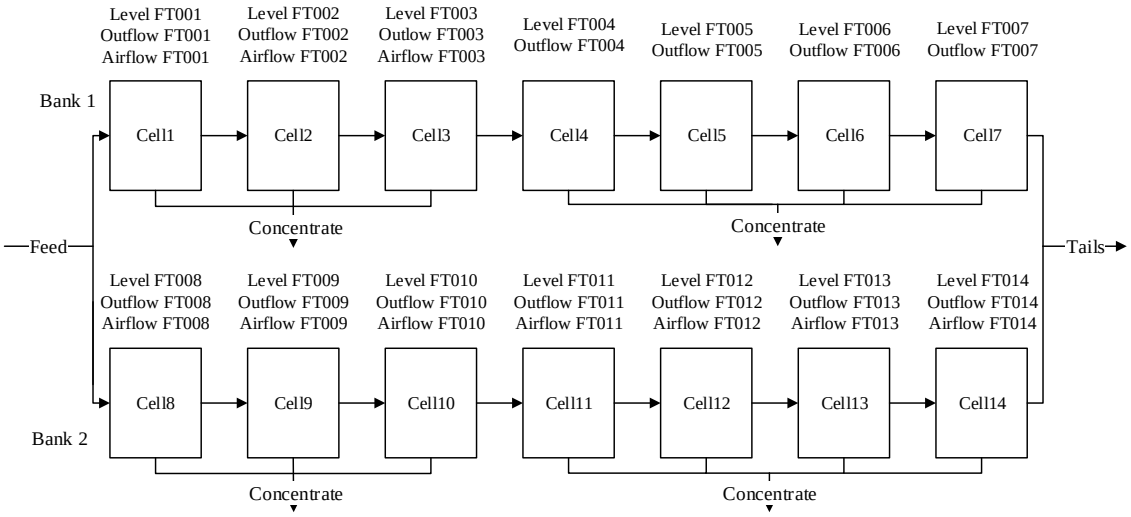

FIGURE 4.3: *Simplified process flow diagram of flotation circuit under consideration. Two banks of seven flotation cells in series make up the circuit. Each cell's outflow flows into the subsequent cell.*

Oscillations in a flotation circuit of a mineral concentrator plant were observed. To provide sufficient context for diagnosis of the oscillations, the operation and control of the circuit is described, and the trends of the variables showing oscillations are presented.

4.4.1 Flotation circuit operation and control

Flotation is used to separate valuable mineral particles from gangue particles in a concentrator process. Separation is achieved by selectively imposing hydrophobicity on the valuable mineral particles, so that they will attach to air bubbles and float to the top of the cell [Wills, 2007]. A flotation circuit is a series of flotation cells. A simplified process flow diagram of the flotation circuit under consideration is shown in Figure 4.3. This flotation circuit consists two parallel banks, each with seven flotation cells in series. The concentrate from the first three cells of each bank are combined, and the concentrate from the last four cells are combined. The outflow (tails) from each cell flows into the following cell. Finally the combined tails are combined and processed further in downstream units.

A flotation circuit control strategy to stabilise the mass pull and optimise the final concentrate grade of the circuit is implemented in a layered approach [Muller *et al.*, 2010]. The first layer utilises PID feedback loops for regulatory control of the cell levels and air addition rate. The cell outflows are used to control cell levels using a multivariable level controller that considers interaction of upstream cells on downstream cells to compensate for disturbances that could propagate down a series of cells. This multivariable level controller allows all control valves in

the circuit to act simultaneously. The second layer is a supervisory control layer to stabilise the individual cell and overall circuit mass pulls by manipulating reagent addition, froth depth (by manipulating cell level set points) and air addition rate. This control layer implements a fuzzy logic rules-based expert controller. The third layer is an optimisation layer that optimises the final concentrate grade by manipulating the set-points of the mass pulls. A model predictive control strategy is implemented to achieve this.

4.4.2 Oscillations in the flotation circuit

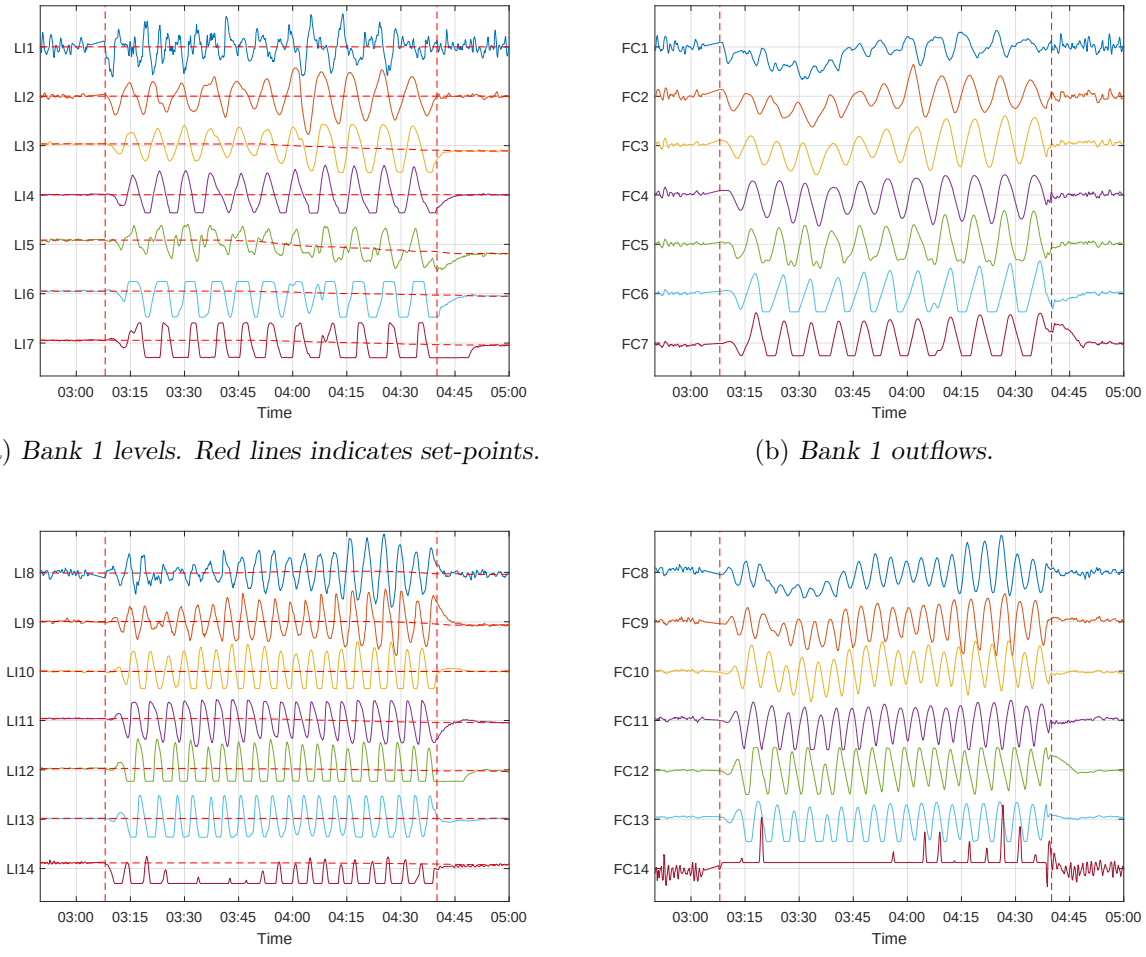

(a) *Bank 1 levels. Red lines indicates set-points.*

(b) *Bank 1 outflows.*

(c) *Bank 2 levels. Red lines indicates set-points.*

(d) *Bank 2 outflows.*

FIGURE 4.4: *Flotation circuit variables showing oscillatory behaviour. Vertical dashed lines indicate onset and end of oscillations.*

Oscillations were observed in the levels of the cells in the flotation circuit. The oscillations were present in both flotation banks. This section of the plant is responsible for extracting the majority of the valuable minerals in the plant [Muller *et al.*, 2010], therefore poor control performance in this section has significant adverse effects on the recovery of valuable minerals.

The oscillations propagated through the circuit, affecting both the controlled variables (CVs), the levels, and manipulated variables (MVs), the outflows. Figure 4.4 plots the levels and outflows in the flotation circuit. Processing units directly upstream and downstream of this flotation circuit

did not show any effect of the oscillation, so this oscillation was localised to this flotation circuit. The oscillation was detected from manual inspection of the plant data. Automated oscillation detection techniques are available, see Thornhill & Horch [2007] for examples. However, the oscillations in this case study were clearly observable and localised to one section of the plant, and the focus of this chapter is root cause diagnosis. Therefore oscillation detection techniques were not employed or discussed in this work.

It was noted that the multivariable level control layer, and the optimisation layer were off during this oscillatory period. Therefore, the only control affecting this section during this time was the base layer regulatory control between the levels and the outflows.

The root cause analysis was limited to variables that displayed oscillations. These 28 variables are shown in Figure 4.4. The oscillation is transient, persisting for 1h 30 min. The start and end times of the oscillations are clear, since the CVs are stable and well controlled at their set-points before and after the oscillations. The sampling time is 10s, and the number of samples is 560. Variables from the processing unit directly upstream of this flotation circuit did not show effects of the oscillations.

This is a useful case study for testing of analysis techniques. The oscillations are clearly present in a large number of variables, with clear start and end times. To encourage the development and testing of different control performance monitoring methods on real industrial data, the data for this case study has been made available on the industrial data repository on the website for the South African Council for Automation and Control. The case study can be found at: 'sacac.org.za/resources/' under 'PID Data/Plantwide data/plantwide-minerals-lindner-2018.csv'.

Using the fast-Fourier transform (FFT) to find the peak oscillation frequencies [Shumway & Stoffer, 2014] it was observed that the oscillations in Bank 1 (Cells 1 to 7) were at a lower frequency than Bank 2 (Cells 8 to 14). The CVs and MVs in Bank 1 all displayed a common oscillation period of 465 s. The CVs and MVs in Bank 2 all displayed a common oscillation period of 266 s.

4.5 Results and discussion

Transfer entropy and the nonlinearity index were both applied to the dataset for oscillation diagnosis in order to compare the advantages and pitfalls of each method for industrial oscillation diagnosis. The nonlinearity index analysis was performed by the co-author of the conference paper where a version of this chapter was previously published [Lindner *et al.*, 2018b].

The variables displaying the oscillation were grouped according to their common oscillation frequencies, as described in Section 4.4.2, so Bank 1 and Bank 2's variables were analysed separately.

4.5.1 Transfer entropy results

Transfer entropy was applied to the data from the flotation circuit. Default calculation parameters suggested by Bauer *et al.* [2007a] were used. The CVs and MVs were separated, and the transfer entropy analysis was performed separately for each group, since the oscillation could propagate through both the CVs and MVs due to the control and material flow in the circuit. This grouping of variables according to their categories is discussed further in Section 9.5. The

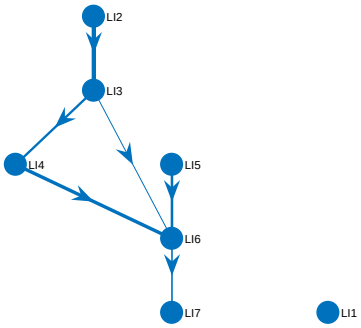

(a) *Propagation path for Bank 1 levels*

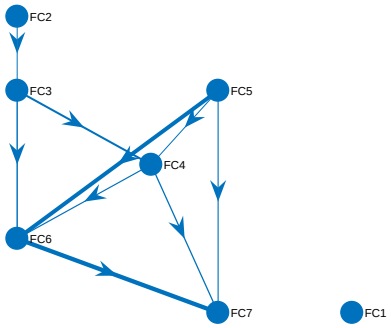

(b) *Propagation path for Bank 1 outflows*

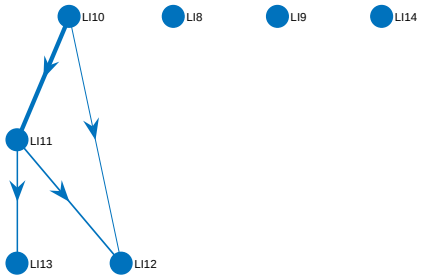

(c) *Propagation path for Bank 2 levels*

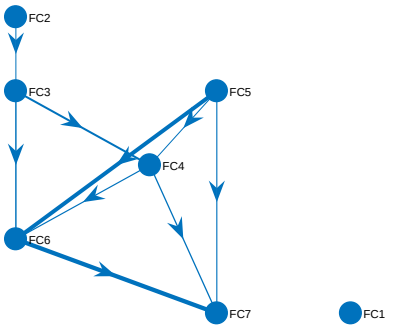

(d) *Propagation path for Bank 2 outflows*

FIGURE 4.5: *Propagation paths derived from transfer entropy for oscillations in the flotation circuit.*

results for each group were then compared to determine whether the propagation paths were consistent with each other.

The propagation paths obtained from transfer entropy applied to Bank 1's levels and outflows are shown in Figures 4.5a and 4.5b respectively. Both show a propagation path from Cell 2 to Cell 7. Neither causal map shows a causal flow from Cell 1 to Cell 2. Observing the trends for LI1 and LI2 in Figure 4.4, the oscillation in LI1 appears less pronounced than in other trends. This indicates that process noise may have obscured the causal connections. Figure 4.5b shows a connection from Cell 5 to Cell 4, which is contradicts the physical flow of the process. From the inspection of the trends for Cells 4 and 5 in Figure 4.4 it can be seen that Cell 4 showed some saturation at its lower limit. The trends for LI5 show jagged peaks, where there are multiple peaks for each cycle. These irregular trends may have caused transfer entropy to fail at detecting a causal connection from Cell 4 to Cell 5.

Figure 4.5b also shows both FC2 and FC5 as possible root nodes. This result is confusing, making it unclear what the actual root cause is. Considering that LI2 is the root node for the level variables' causal map, there is more evidence to support the hypothesis that Cell 2 is the root node.

The propagation paths obtained from transfer entropy applied to Bank 2's levels and outflows are shown in Figures 4.5c and 4.5d. Fig 4.5c shows a propagation path from Cell 10 to Cell 13. Fig 4.5d shows a propagation path from Cell 8 to Cell 13. Notably, no connection is observed from LI8 to LI9 or LI9 to LI10. Figure 4.4c shows that the trend of LI8 displays a less pronounced oscillation and a bit of noise, which may have obscured the causal connection. Cell 14's level and outflow show no causal connection with other variables. Figures 4.4c and 4.4d show severe saturation for Cell 14's level and outflow. This means that the causal connection between these variables and the other variables may have been obscured.

Transfer entropy applied to Bank 1 and Bank 2's variables both indicate the oscillations originating in the first cells and propagating down the banks to the last cells. Bank 1's causal map shows Cell 2 as the root node, while Bank 2's causal map for the outflows shows Cell 8 as the root node. Both Banks' results can be considered in context of one another. Since these two banks are in parallel, when an oscillation appears to propagate from the first cell of Bank 2, it is likely that this oscillation originated simultaneously in the first cell of Bank 1. The transfer entropy results are compared with those of the nonlinearity index and their accuracy when considering additional process knowledge context is discussed in Section 4.5.3.

4.5.2 Nonlinearity index results

The nonlinearity index approach was applied to rank the variables according to the degree of nonlinearity. This analysis was performed by the co-author of the conference paper, where a version of this chapter was previously published [Lindner *et al.*, 2018b].

The results of the nonlinearity index are presented in Table 4.1. The results for Bank 1 indicate strong nonlinearity in a number of the flotation circuit variables. LI5 displayed strong nonlinearity. In Figures 4.4a and 4.4b the severe nonlinear trends for Cell 5 can be seen. The oscillations appear jagged, with a smaller peak present in each repeating peak. In contrast, Cells 1 and 2 show oscillations with a smoother sine wave form. These observations confirm the nonlinearity rankings obtained using the nonlinearity index.

For Bank 2, Cell 13 showed the highest nonlinearity index value, indicating that this cell's level was closest to the oscillation root cause. Cells 8 and 9 showed linear results, indicating they were furthest from the oscillation root cause. The trends in Figures 4.4c and 4.4d show smoother sine oscillations for Cells 8 and 9, with more jagged trends for Cells 11 and 13. Bank 1 and Bank 2 showed similar results, where the first cells showed linear oscillatory trends, and the later cells showed nonlinear behaviour. Cells 5 and 13 may be considered closest to the root cause of the oscillation in each bank according to this technique, since they displayed the largest nonlinearity indices.

4.5.3 Discrepancy of different methods and further analysis

The transfer entropy results indicated that the oscillation propagated from the first cells through the circuit to the last cells, for both banks. The nonlinearity index gave contradictory results, indicating that LI5 and LI13 were closest to the sources of the oscillation for each Bank. To determine which of the methods gave the correct root cause, some additional context is necessary.

An oscillation takes time to propagate through the process, due to the residence time of the cells and the transport delay between cells. The sequence of the oscillation propagation may give further insight into the propagation path. The trends for the levels were inspected to determine when the first peak of the oscillations appeared. The locations of these peaks establishes the

TABLE 4.1: *Nonlinearity index results for Bank 1 and Bank 2.*

Bank 1		**Bank 2**	
Variable	**Nonlinearity Index**	**Variable**	**Nonlinearity Index**
LI5	2.48	LI13	2.88
LI7	1.97	LI11	2.86
FC5	1.92	LI12	2.71
FC7	1.88	LI14	2.49
LI4	1.7	LI10	2.36
LI6	1.57	FC11	2.01
LI3	1.35	FC13	1.87
FC6	1.33	FC12	1.38
FC3	1.19	FC10	1.22
FC4	1.09	LI9	Linear
FC1	Linear	FC8	Linear
FC2	Linear	LI8	Linear
LI2	Linear	FC9	Linear
LI1	Linear		

TABLE 4.2: *Start times of oscillations, indicating sequence of oscillation propagation.*

Bank 1		Bank 2	
Variable	**Start time [hh:mm:ss]**	**Variable**	**Start time [hh:mm:ss]**
LI1	03:10:00	LI8	03:10:10
LI2	03:11:00	LI9	03:10:40
LI3	03:11:50	LI10	03:11:50
LI4	03:12:10	LI11	03:11:40
LI5	03:12:20	LI12	03:12:20
LI6	03:13:10	LI13	03:12:20
LI7	03:13:00	LI14	03:10:50

sequence in which the oscillations appear in the cells. The start times are shown in Table 4.2. Most of the start times are in sequential order, from the first cell to the last cell for each bank. One exception is that the start time for LI14 is earlier than for LI10, LI11, LI12, and LI13. However, in Figure 4.4c it can be seen that the signal for LI14 displays saturation, making it difficult to accurately determine the start of the oscillation. LI7 appears to precede LI6, and LI11 appears to precede LI10. However, since the difference is only one sample (with the sampling time at 10 seconds), it is difficult to determine which was first.

The sequential order of the oscillations confirms the propagation path obtained from the transfer entropy results. This indicates that the nonlinearity index failed to correctly identify the root cause. The nonlinearity index approach assumes that a nonlinearity occurs, causing an oscillation, and as that oscillation propagates through the process it becomes less nonlinear. In this case however, the oscillation caused nonlinear trends to arise downstream of the root cause of the fault. Taking the trend of LI5 as an example, Figure 4.4a shows double peaks at each cycle.

Data-based diagnosis techniques have an inherent limitation in that they can only point to variables associated with the root cause of the fault. Further analysis is needed to determine

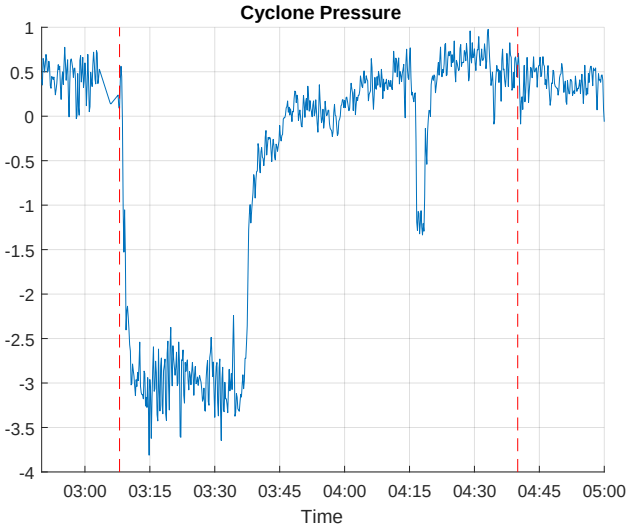

FIGURE 4.6: *Cyclone pressure just upstream of flotation circuit showing sharp dip at oscillation start at time 03:08:00.*

what caused the oscillation to manifest in that variable. Considering the unit just upstream of this flotation circuit, it was observed that the cyclone pressure decreased sharply just before the onset of the oscillation, as shown in Figure 4.6. This pressure is measured for a bank of cyclones where the number of cyclones in operation can be varied. This drop in pressure occurred when an additional cyclone was brought online. This sudden drop caused as flow disruption to the flotation banks, which caused the levels of the first cells in each bank (LI1 and LI8) to deviate from their set-points.

Further inspection also revealed that both the supervisory and optimisation advanced process control (APC) and the multivariable level controller were switched off for the duration of the oscillation. Only the base layer PID control, regulating the cell levels using the outflows from the cells, was enabled. This indicates that the regulatory control was unable to correct for the deviations in LI1 and LI8. Poor controller tuning may have caused the levels to become unstable and the absence of the multivariable controller allowed the resulting oscillations to propagate throughout the circuit. This may indicate that the base layer PID tuning had not been updated for a long time, and the corrective action suggested by this analysis was to retune the base layer control. Each bank was tuned with different PID parameters, which explains why the oscillation periods for each bank was different.

After the oscillations persisted for some time, the supervisory control level is switched back on to compensate for the oscillations by gradually changing the set points of the levels. This compensation is ineffective at first, but when the multivariable level controller is turned on again, the circuit quickly stabilises. This indicates that the multivariable controller is very effective at rejecting oscillations.

To summarise the findings of this analysis: transfer entropy indicated that the oscillation originated in Cells 1 and 8. This was confirmed by observing the sequence in which the oscillations appeared in each cell. A cyclone immediately upstream of the cells where the oscillation originated showed a sudden decrease in pressure, causing deviation of LI1 and LI8 from their set points. Suboptimal controller tuning may have resulted in the inability of the control to correct for these deviations, allowing the oscillation to propagate through the circuit. The corrective action suggested by this analysis was to retune the base layer control.

4.5.4 Shortcomings of causality analysis approach

Although transfer entropy was used to successfully diagnose the fault conditions in this case study, numerous difficulties in the implementation were encountered.

In the applications of causality analysis for fault diagnosis in literature, no clear, systematic guidelines have been presented for the numerous steps required for implementation of transfer entropy. The variables selected for analysis were those that showed oscillations from visual inspection. The length of the data set used was limited to the data under fault conditions. These decisions were made based on process knowledge and intuition, and from past experience with causality analysis. More systematic guidelines for these decisions can aid engineers who are not experts in causality analysis to implement these techniques successfully. This limitation is therefore addressed in Chapter 7.

For parameter selection, the approach followed in this case study was to use the basic procedure of transfer entropy, with the default parameters suggested in Bauer *et al.* [2007a]. A trial-and-error approach was implemented before settling on this, where different values of K, L, τ and h were tested. The results of transfer entropy are sensitive to optimal parameters [Duan *et al.*, 2014]. Therefore more systematic procedures for parametrisation can ensure confidence that the results obtained are representative of the propagation paths in the process. This limitation is therefore addressed in Chapter 7.

Some difficulties were also observed in the interpretation of the results once the causality analysis calculations had been performed. The decision to separate the variables based on the different banks was a logical decision since the two flotation banks are parallel processing streams. The decision to separate the variables according to their categories as either CVs or MVs was made since the causal map with all the variables was complex and difficult to interpret. This decision was made based on process knowledge and experience with causality analysis techniques.

Figure 4.5b also showed both FC2 and FC5 as possible root nodes. This result is confusing, making it unclear what the actual root cause is. The causal maps need to be considered with careful attention to all the information available to the practitioner.

Clear guidelines of how to construct the causal maps, and augment them with process knowledge, could aid engineers who are not causality analysis experts to interpret the causal maps. The difficulties associated with interpreting causal maps are addressed in Chapter 9.

Causality analysis can, in most cases, point to variables closely associated associated with the fault. This analysis is limited to measured variables. The fault to be corrected was poor controller tuning. The causal map could not point directly to this, but could point to the sequence of events related to this.

4.6 Chapter conclusion

An oscillation propagating through a flotation circuit was diagnosed using transfer entropy and the nonlinearity index. The two methods gave contradictory results. Considering knowledge of the material and control flow in the process, and the sequence of the oscillations in the system, it was concluded that the propagation path obtained using transfer entropy was accurate. The oscillation originated in, or just upstream of the first cells (Cells 1 and 8), in the flotation circuit. The nonlinearity index indicated that LI5 was closest to the sources of the oscillation. The nonlinearity index assumes that as an oscillation propagates through a process, appearing in different variables' time series, the trends become less nonlinear. In this case however, the

oscillation caused nonlinear trends to arise downstream of the root cause of the fault.

The discrepancy in the results obtained for the two methods demonstrates the need to fully consider the assumptions of data-based techniques when interpreting their results. A universally applicable method for oscillation diagnosis is unlikely, with different techniques working for different scenarios. Understanding the limitations of techniques can lead to more successful and reliable applications of oscillation diagnosis strategies in industrial processes.

Once the correct propagation path had been identified, further analysis was needed to determine what caused the oscillations in Cells 1 and 8. A cyclone immediately upstream of the cells where the oscillation originated showed a sudden decrease in pressure. This drop in pressure caused a flow disruption to the flotation banks. This may have initiated the deviation of LI1 and LI8 from their set points. Suboptimal base layer controller tuning may have resulted in the inability of the control to correct for the fluctuations, allowing the oscillation to propagate through the circuit. The corrective action suggested by this analysis was to retune the base layer control.

These results indicate that careful consideration of process knowledge is paramount to meaningful interpretation of the results from otherwise automated techniques.

This chapter demonstrated that transfer entropy can effectively be used to aid diagnosis of oscillations in an industrial process. However, the approach followed in this case study was based on previous experience with causality analysis techniques. No clear guidelines exist in literature for many of the steps required to successfully implement causality analysis for fault diagnosis. For this reason the factors affecting performance of causality analysis techniques need to be investigated, so that such guidelines can be developed. Chapter 5 defines the desired performance and then discusses the factors affecting the performance. Subsequent chapters then address these factors and develop guidelines for the implementation of the techniques for fault diagnosis.

CHAPTER 5

Defining desired performance of causality analysis techniques

Contents

5.1 Chapter introduction 71
5.2 Chapter objectives 72
5.3 Performance criteria for causality analysis 72
5.3.1 Accuracy and precision of causality analysis *72*
5.3.2 Automatability of causality analysis *73*
5.3.3 Interpretability of causality analysis *74*
5.3.4 Computational complexity of causality analysis *75*
5.3.5 Applicability for different process characteristics *75*
5.4 Factors affecting performance of causality analysis 76
5.4.1 Noise and significance testing *76*
5.4.2 Fault type *76*
5.4.3 Process interactions *77*
5.4.4 Time series characteristics *78*
5.4.5 Time frame and parameter selection *79*
5.5 Chapter conclusion 80

5.1 Chapter introduction

Parts of this chapter were published in a peer-review conference paper: Lindner B, Auret L & Bauer M, 2017a, Investigating the Impact of Perturbations in Chemical Processes on Data-Based Causality Analysis. Part 1: Defining Desired Performance of Causality Analysis Techniques, IFAC-PapersOnLine, 50(1), pp. 3269-3274.[Lindner *et al.*, 2017a]

The summary of the literature provided in Chapter 2.11 demonstrated that many authors have proven the effectiveness of causality analysis techniques. Additionally, Chapter 4 in this dissertation demonstrated the effectiveness of causality analysis for fault diagnosis. However, the techniques have not been widely adopted in industry. The aim of this dissertation is to improve on existing causality analysis techniques to make them more accessible to industry experts. To achieve this, Objective I was defined: to investigate the factors affecting performance of causality

analysis techniques. To address the objective, the desired performance of causality analysis techniques are defined in this chapter, so that their usefulness and shortcomings for fault diagnosis can be evaluated. The factors affecting the performance of the techniques are then discussed.

This chapter is structured as follows: Section 5.3 formulates the desired characteristics and performance criteria of causality analysis methods; Section 5.4 identifies the factors that affect the characteristics and performance of causality analysis. Finally, Section 5.5 presents some conclusions drawn.

5.2 Chapter objectives

The objectives of this chapter are:

I To *define* the desired characteristics of causality analysis techniques.

II To *identify* the factors that impact the characteristics of the techniques.

5.3 Performance criteria for causality analysis

In this section, the desired performance criteria for causality analysis techniques are defined. The desired performance criteria discussed here are: accuracy and precision; automatability; interpretability; computational complexity; applicability for different process characteristics. Automatability, interpretability and applicability for process characteristics are subjective performance criteria. Accuracy, precision, and computational complexity are quantifiable metrics. Although some of these performance criteria are subjective, this chapter aims to address them as thoroughly as possible, to provide a basis for comparing techniques.

5.3.1 Accuracy and precision of causality analysis

Causality analysis is considered accurate when the method was able to identify the correct root cause of the fault. The diagnosis procedure can be considered useful when the corrective action suggested by the root cause analysis successfully removes the fault. This view of the accuracy considers how accurately overall causality analysis procedure was able to point out the propagation path of the fault. This procedure includes calculation of the causal statistic for individual pairs of measured variables, as well as interpretation of the causal map for the entire system of pairwise causal connections. However, this accuracy can only be evaluated for individual case studies.

Uncertainty in process measurements means that non-zero transfer entropy and Granger causality values will be calculated even when there is no causal relationship. As mentioned in Section 2.12.3, a hypothesis test is needed to determine the statistical significance of the causal statistic calculated between a pair of measured variables. However, this significance test is not infallible, and spurious connections may still be found[Bressler & Seth, 2011]. These spurious connections make analysis of fault propagation paths difficult. Spurious connections give a false representation of the propagation path of the fault. The reverse is also true, real causal connections might be missed because of this uncertainty.

Spurious and missing connections may also occur due to the limiting assumptions discussed in Section 5.3.5. For example, if Granger causality was used to calculate causality in a process

with nonlinear behaviour, the linear regression model may not be able to capture the nonlinear process dynamics and the causal connection may be missed. Non-stationarity in the time series could cause spurious connections for both techniques. The factors affecting the accuracy are discussed further in Section 5.4.

The validity of individual causal connections can be scrutinised to evaluate the method's accuracy. When the ground truth causality is known, one can quantify the missed connection rate, true connection rate, and the false (or spurious) connection rate:

Definition 4. True connection rate (TCR): the fraction of causal connections in the true propagation path in the true propagation path that were detected using the data-based technique:

$$TCR = \frac{C_{detected,true}}{C_{knowledge}} \tag{5.1}$$

where $C_{detected,true}$ is the number of true causal connections found using the data-based technique, and $C_{knowledge}$ is the number of connections in the true propagation path. This is the opposite of the missing connection rate (MCR): $MCR = 1 - TCR$.

Definition 5. Relative true connection rate (RTCR): the fraction of total edges in the causality map that are true connections:

$$RTCR = \frac{C_{detetcted,true}}{C_{detected}} \tag{5.2}$$

where $C_{detected,true}$ is the number of true causal connections found, and $C_{detected}$ is the total number of detected connections. This is the opposite of the relative false connection rate (FCR): $FCR = 1 - RTCR$.

Accuracy is defined by a high true connection rate and low false and missed connection rates. Precision can be defined by how consistently the method detects the connections under similar conditions. Section 8.4 utilises these accuracy and precision metrics in a simulated case study where the true causal structure is known.

5.3.2 Automatability of causality analysis

Section 2.12, and the case study in Chapter 4, illustrated that application of causality analysis for fault diagnosis is complex. Numerous steps are required, including data selection, parameter selection, causality analysis calculation,and interpretation of results. Each of these steps introduces possible entrance points for errors in subjective human reasoning. Often engineers will have to resort to time consuming trial-and-error approaches until useful causality maps are generated.

Automated procedures for each of these steps, and for their integration into an overall fault diagnosis methodology, can limit the need for human intervention. In the steps where full automation is not possible, systematic procedures and detailed guidelines for the steps can also limit the need for trial-and error approaches. Improved automatability will therefore improve accuracy and precision of the techniques, in turn improving the robustness. This means that an engineer applying the techniques can be more confident in the validity of the reasoning applied to the results of causality analysis. Additionally, improving automatibililty can also save time and effort for engineers, so that their reasoning skills can rather be applied to determining what corrective action to take after root cause analysis.

The following definition is used to test whether a calculation procedure is automatable:

Definition 6. A calculation procedure is *automatable* when all hyper-parameters can be defined without human intervention.

5.3.3 Interpretability of causality analysis

Fault diagnosis techniques are used by engineers to gain insight into abnormal behaviour occurring within a process. When applying causality analysis for fault diagnosis, the engineer has to interpret the causal map to see whether a clear propagation path is identified. It is important that the engineer can understand the information presented simply, and understand the implications. For example, when a spurious connection passes the significance test because of excessive noise in the signal, and is displayed on the causal map, the engineer will need to use process knowledge and understanding of the causal statistic to understand why that spurious connection was found.

This interpretation has two components: mathematical interpretation of the underlying causal statistic; and visual interpretation of the causality maps.

When the underlying causal statistic is based on mathematical concepts that are easy to understand, the implementation is more accessible for an engineer to implement themselves. As illustrated further in Chapter 7, the accuracy of the causality analysis calculations are sensitive to parameter selection, such as the model order in Granger causality, or the time interval for transfer entropy. Successful application of the techniques can be improved when the engineer understands the importance of the parameters. Therefore, in simpler mathematical calculations for causality, it may be easier to grasp the importance of the parameters. Additionally, once the causal analysis has been implemented, understanding the underlying mathematics aids successful interpretation of the results.

On the other hand, the reason complex mathematical techniques are developed is to accurately capture complex interactions in time series. Therefore, relying on only simple techniques may in some scenarios produce inaccurate results. The scenarios where different methods are applicable is investigate further in Chapter 8.

This criteria is subjective, since it depends on the familiarity and personal experience of an engineer with different mathematical concepts. However, it is still useful to keep this criteria in mind when evaluating techniques.

The end result of the causality analysis is a causality map. When this causality map gives a clear indication of the propagation path that is logically consistent with process knowledge, then the variables at the start of the propagation path can be further investigated. When the suggested propagation path is ambiguous, it may be uncertain what the root cause was. There may be more than one suggested propagation path in the causal map pointing to different root cause variables. In the case where these different root cause variables are associated with the same unit in the plant, or the same controller, then it can be inferred that the root cause is closely associated with that unit and can be investigated.

When there are multiple root causes all associated with different units, or sections of the plant, then the root cause is more ambiguous. In this scenario it is possible that multiple faults are occurring simultaneously[Chiang *et al.*, 2015]. However, a simplifying assumption that is typically applied is that only one fault occurs at any time is applied, since the probability of occurrence of simultaneous independent faults is small, as suggested by [Shiozaki *et al.*, 1985].

All causal effects in a system are identifiable when the causal map is acyclic [Pearl, 2009]. Cyclical causal maps, where each node is reachable from any other node[Bang-Jensen, 2010], show no clear start or end nodes, and therefore give no clear indication of the possible root cause of the fault. Figure 5.1 gives an example of a cyclical graph. In such a scenario, there is no clear indication of which variable is the driving force for the system.

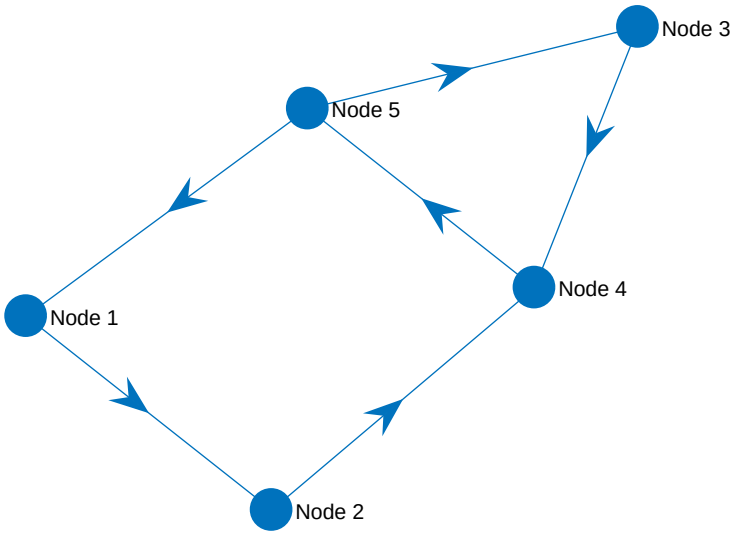

FIGURE 5.1: *Example of a cyclical causal map.*

The complexity of a causal can give an indication of how difficult it is to interpret. For example, in a dense causal map, with many edges, it may be difficult to follow the paths between nodes in the map. This would make it difficult to identify the propagation path of the fault through the system. Section 9.7 presents some graph complexity metrics.

5.3.4 Computational complexity of causality analysis

Ideally, computational complexity of causality analysis techniques should be as low as possible. This makes the implementation accessible to engineers in an industrial setting. Solutions for reducing the computational time for complex calculations exist. Cloud computing utilities are readily accessible. Graphics processing units can also be used. However, if the need for these advanced computing solutions can be avoided, implementation can be more accessible.

What amount of time is considered excessive depends on the situation. Online, automated fault diagnosis would require a solution within minutes. If the plant is experiencing an ongoing fault the engineer needs to isolate the root cause as fast as possible to return the plant to normal operation. On the other hand, if the analysis is being performed offline to gain more information about fault conditions that happened some time in the past, the engineer may not mind waiting a few hours for results.

5.3.5 Applicability for different process characteristics

The applicability of a causality analysis technique may be limited by the underlying assumptions of the calculations it is based on. These limitations include linearity and stationarity (see Section 5.4.4), A technique that is applicable for a wider range of process characteristics is desirable, so that the technique can be used with confidence in different scenarios.

Kuhnert [2013] presented guidelines for technique selection based on process characteristics. These guidelines were developed based on simulated experiments to determine which technique

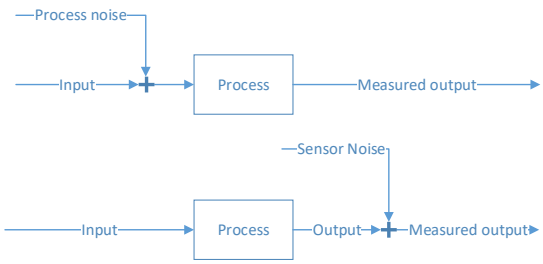

FIGURE 5.2: *Illustration of sensor and process noise.*

gave the most accurate results for different process characteristics. The characteristics investigated included linearity, as well as the dead time between variables. This is investigated further in Chapter 8.

5.4 Factors affecting performance of causality analysis

Section 5.3 outlined the criteria to evaluate the performance of causality analysis techniques for fault diagnosis. This defines a basis for discussion of the factors that may affect this performance in this section. This section provides a discussion of these factors, and the impact of these factors investigated in detail in subsequent chapters of this dissertation.

5.4.1 Noise and significance testing

Sensor noise and common process noise can add uncertainty to the causality analysis calculations. Figure 5.2 illustrates the distinction between sensor noise and process noise. Process noise refers to common cause variation in a process. An example of common cause variation may be variations in mineral compositions of ore fed to a concentrator process. Sensor noise is noise that arises due to the uncertainty in measurement of a property.

A causal connection means that variation in one variable will cause similar variation in another variable, after some time. Variation caused by sensor noise would mean that variation in the output variable is not caused by variation in the input variable, therefore the causal connection would be obscured. Variation caused by process noise may show a strong trend between the variation in the input and output variables, meaning that the causal connection may be detected. However, high frequency variations can cause the value of the input variable to change too quickly for a response to be seen in the output variable, which would obscure the causal connection. Proper significance testing can mitigate the impact of noise on the performance of causality analysis methods. See Section 2.12.3 for a discussion of significance testing methods.

The impact of noise on the accuracy of causality analysis measures is investigated in Chapter 6.

5.4.2 Fault type

The type of fault affecting the process may affect the results of the causality analysis. Section 2.11 showed that the majority of the research into causality analysis for root cause analysis has

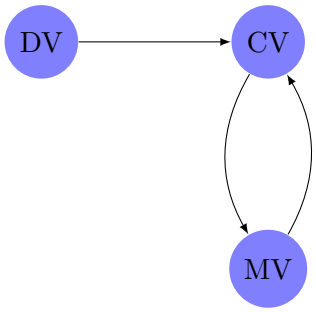

FIGURE 5.3: *Example of causal map for control loop. DV = disturbance variable, CV = controlled variable, MV = manipulated variable.*

been applied for diagnosis of plant-wide oscillations. Chemical processes often exhibit oscillatory behaviour, often as a result of poorly tuned feedback controllers[Thornhill & Horch, 2007]. Oscillations propagate through causal connections in a process with a unique trend that tends to be persistent, and causing enough excitation in one variable that it manifests in another variable. The causal effect from one variable to another is therefore pronounced, and persistent, meaning that long data-sets are available for analysis. Causality analysis is therefore well suited for diagnosis of oscillations.

However, oscillations are not the only fault trend of interest when diagnosing fault conditions. Step changes can occur in chemical processes, such as abrupt changes in feed compositions, temperatures or flow rates. Such abrupt changes may be caused, for example, by changing operator shifts, switching control strategies or changing feedstocks. Another type of non-oscillatory fault is a slow drift that may occur in some processes; where a persistent increasing or decreasing trend may be observed. Ramp trends can occur as a result of drifting sensors or valve malfunctions.

Applications to non-oscillatory data conditions have been researched. Duan *et al.* [2013], Kuhnert [2013], and Yang *et al.* [2014] all demonstrated the use of transfer entropy to capture causality in a non-oscillating process. However, these applications investigated the ability of the techniques to identify individual causal connections. They did not investigate the diagnosis of non-oscillatory faults. Therefore, the strengths and weaknesses of different causality analysis techniques to accurately detect causality between two variables influenced by such faults have not been investigated. In Chapter 6, oscillatory and step perturbations of varying amplitudes and dynamics are input into a simulation to observed their effect on the ability of causal analysis techniques to detect a causal connection.

5.4.3 Process interactions

Causality analysis should detect all types of causal connections in a process. For chemical processes these include: mass flow; energy flow; and information flow. Information flow, or controller influence, presents interesting interactions.

Consider a case where there is some disturbance variable (DV) that influences the controlled variable (CV). Without control, a change in the DV would cause a change in the CV. However, when control is applied, a change in the DV would cause a change in the manipulated variable (MV) as well. A causal connection therefore exists between X and the MV, and another causal connection may exist between the MV and CV. Figure 5.3

A confounding variable may result in spurious causality between two variables being detected. For example, a disturbance in a utility, such as steam supply, may affect a large number of

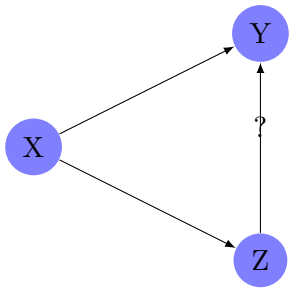

FIGURE 5.4: *Example of causal map showing possible confounding from variable X, where X is an unmeasured variable.*

measured variables, which in turn affect each other. The causal influence of the utility on two variables may be misinterpreted as an apparent causal influence between the variables themselves. Figure 5.4 illustrates this scenario. This is particularly relevant, considering that in Chapter 4, one of the limitations of causality analysis that was identified was that only the measured variables can be analysed. Therefore, a fault can be due to an unmeasured, confounding variable.

5.4.4 Time series characteristics

As mentioned in Section 5.3.5, causality analysis techniques may have limitations for detecting causality with certain time series characteristics, such as linearity of the data, and stationarity of the data. The time series characteristics may therefore affect how generally applicable the causality analysis measure is, and how accurately the measure identifies causal connections in specific scenarios.

Granger causality incorporates linear regression models of time series', and may therefore be limited in its ability to capture nonlinear features of the time series trends[Bressler & Seth, 2011]. Consider a differential equation describing the relationship between variables x and y in its continuous and discrete forms:

$$\begin{aligned} \frac{dy}{dt} &= a_1 y + b_1 x \\ y(t+1) &= a_2 y(t) + b_2 x(t) \end{aligned} \tag{5.3}$$

The differential equation describing y in Equation 5.3 is linearly separable, containing no nonlinear terms. The discrete part of Equation 5.3 is similar to the AR models presented for Granger causality in Equations 2.2 and 2.3. The differential equation describing y in Equation 5.3. Therefore the past observations of x and y can be used to predict y using the linear regression model shown in Equation 2.3. Equation 5.3 is an example of a description of a process where there is linear interaction between the two variables. For example, the change in a tank's level is linearly proportional to a change in the flow rate into the tank.

Consider another differential equation:

$$\begin{aligned} \frac{dy}{dt} &= a_1 yx \\ y(t+1) &= a_2 y(t)x(t) \end{aligned} \tag{5.4}$$

The differential equation describing the relationship between y and x in Equation 5.4 contains a nonlinear term. Even when the parameters in Equation 5.4 are stationary, the system is

nonlinear. Therefore a linear regression model would not be able to fit the past observations of y and x to y. Equation 5.4 is an example of a description of a process where the interaction between the variables is nonlinear. For example, where a reaction rate is some nonlinear function of a species concentration.

Although transfer entropy is not limited to linear time series, the joint PDFs need to be calculated for stationary time series[Lizier, 2014]. This means that the autocorrelation, mean, and variance of the time series are not a function of time [Girod, 2001]. Granger causality also assumes stationarity to calculate the regression coefficients[Bressler & Seth, 2011].

The impact of time series characteristics on the general applicability of causality analysis techniques is investigated further in Chapter 8.

5.4.5 Time frame and parameter selection

The dynamics of the system under consideration has a profound impact on the calculated causality. The causality analysis techniques considered in this dissertation, Granger causality and transfer entropy, are lag-based techniques [Yang *et al.*, 2014]. The influence of X on Y is only felt after that time delay, so that predictability improvement of Y occurs when incorporating past information about X at a time delay.

The residence time of the process being analysed is also important. When the process dynamics are very slow, and the causality analysis technique is only considering a small portion of the data, the influence of the input variable on the output variable will not be detectable.

The time frame of the data included in the analysis should therefore be long enough to include sufficient information to incorporate the process dynamics. The process dynamics includes the time delay and the residence time of the process.

This temporal information is included in parameters in the calculations of the techniques. For Granger causality the parameter that includes temporal information is the model order, k. For transfer entropy it is the embedding dimensions (K and L), the prediction horizon (h), and the time interval (τ). Additionally, the sampling time of the data (T_s) will affect how long a time frame is included in the analysis. Optimal selection of these parameters is important to ensure that they correspond to the physical dynamics between the pairs of variables. There is some interaction between these parameters. For example, a larger sampling time will mean that a larger time frame is covered. However, it will also mean that the data included is of lower resolution, and may therefore negatively affect the ability to detect the causal connection.

Figure 5.5 illustrates the time frame covered by the causality analysis, and how the parameters relate to this time frame. For Granger causality, the total time frame is the sampling time multiplied by the model order. For transfer entropy, the total time frame is determined by the largest embedding dimension. In the example in Figure 5.5b, $K = 3$, $L = 4$, $h = 3$, and $\tau = 2$. Therefore the overall time frame is $T_s(L\tau + h)$.

To determine whether the fault dynamics do have a significant impact on the causality analysis methods, Section 6.4 investigates the impact of changing oscillation frequency on the causal connection calculated between two variables. More importantly, Section 7.4 investigates the impact of process dynamics, such as the time delay, residence time, and again the oscillation frequency, on the optimal parameter selection.

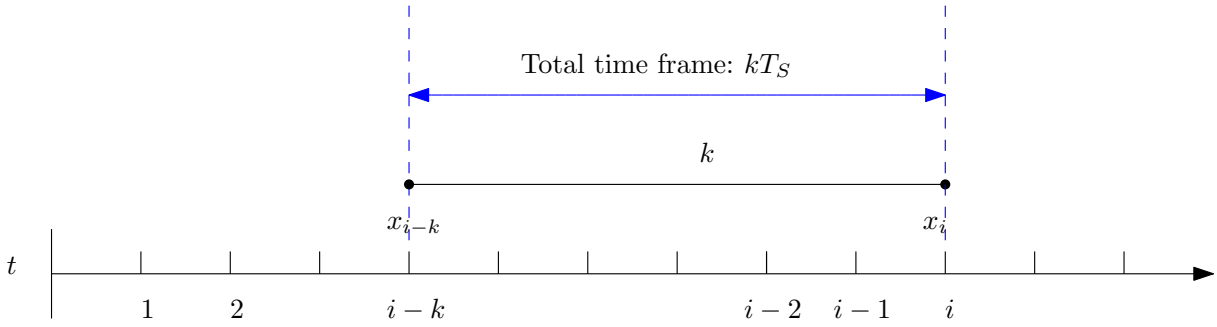

(a) *Time frame for Granger causality calculations.*

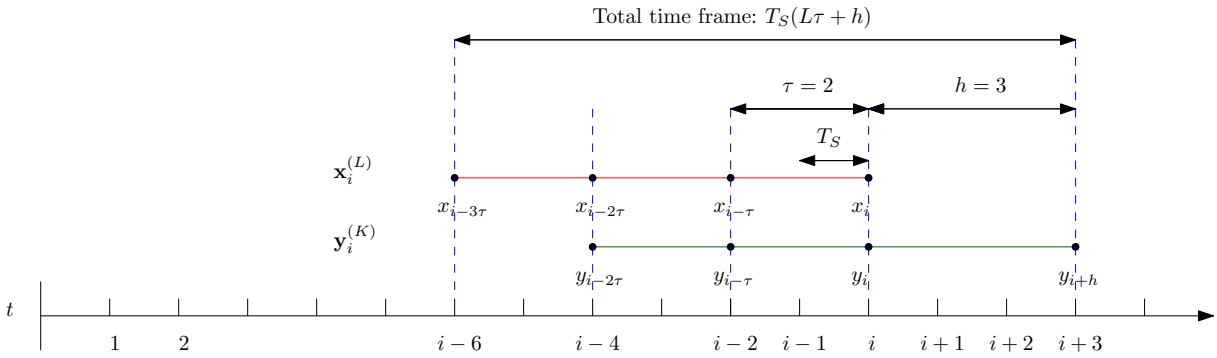

(b) *Time frame for transfer entropy calculations.In this example, $K=3$, $L=4$, $h=3$, and $\tau=2$.*

FIGURE 5.5: *Illustration of the parameters influencing time frame for Granger causality and transfer entropy calculations.*

5.5 Chapter conclusion

Development of accurate and automated causality analysis techniques requires an improved understanding of the strengths and limitations of the available techniques to detect causality under a wide range of typical process conditions.

In this chapter, the desired performance of causality analysis techniques is defined. The desired performance criteria was defined in terms of: general applicability; automatability; interpretability; accuracy; precision; and computational complexity.

The factors affecting the performance of causality analysis techniques were discussed. Factors affecting the performance include: noise; fault types; process interactions; time series characteristics; and parameter selection.

Now that the desired performance has been defined, and factors affecting the desired performance have been identified and discussed, subsequent chapters will further investigate the impact of these factors. Chapter 6 investigates the impact of noise, controller interaction, and different fault types on the performance of causality analysis techniques. Parts of Chapter 7 investigates the impact of process dynamics on the accuracy of causality analysis techniques, as well as the interaction of process dynamics with the optimal parameter selection.

CHAPTER 6

Investigating the impact of perturbations on causality analysis measures

Contents

6.1 Chapter introduction 81
6.2 Chapter objectives 82
6.3 Methodology 82
6.3.1 Two-tank simulation used to generate experimental time series data . . 83
6.3.2 Expected performance of causality analysis 84
6.4 Results for system under influence of oscillatory perturbations 85
6.5 Results for system under influence of step perturbations 89
6.6 Chapter conclusions 89

6.1 Chapter introduction

A version of this chapter was published as a peer-reviewed conference paper: Lindner B, Auret L & Bauer M, 2017b, Investigating the Impact of Perturbations in Chemical Processes on Data-Based Causality Analysis. Part 2: Testing Granger Causality and Transfer Entropy, IFAC-PapersOnLine, 50(1), pp. 3275-3280.[Lindner *et al.*, 2017b]

The discussion in Chapter 5 established that important desired performance criteria for causality-based fault diagnosis are: accuracy and precision; automatability; interpretability; computational complexity; and applicability for different process characteristics. The factors affecting performance of causality analysis techniques were also discussed. Among those factors discussed was the impact of noise, process interaction, and types of faults. This chapter investigates the impact of those factors on the accuracy of Granger causality and transfer entropy. Specifically, the impact of process noise and sensor noise, the impact of controller interaction, and the impact of step perturbations and oscillatory perturbations are investigated.

This chapter is structured as follows: Section 6.2 outlines the objectives of this chapter; Section 6.3 presents the methodology followed to address these objectives; Section 6.4 presents the results for the system under the influence of oscillatory perturbations; Section 6.5 presents the results for the system under the influence of step perturbations; and finally, Section 6.6 summarises the conclusions of this chapter.

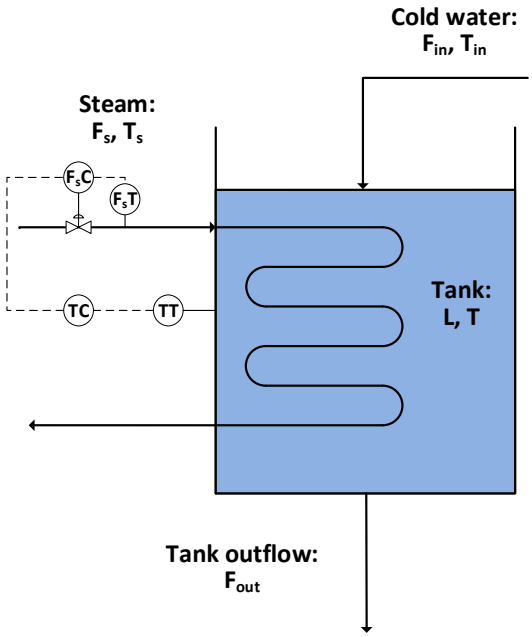

FIGURE 6.1: *Diagram of simulated tank with heat exchange system.*

6.2 Chapter objectives

The objectives of this chapter are:

1. To *investigate* the impact of different perturbations on the causality analysis between variables.
2. To *investigate* the impact of noise on the performance of causality analysis techniques.
3. To *investigate* the impact of controller interaction on the performance of causality analysis techniques.

6.3 Methodology

In this chapter, the impact of some of the factors affecting the accuracy of causality analysis techniques are to be investigated. The impact of process noise and sensor noise, the impact of controller interaction, and the impact of step perturbations and oscillatory perturbations are investigated. Step and oscillatory perturbations will be simulated for a simple system with a clear, direct cause-effect relationship between a pair of variables. The Granger causality and transfer entropy between this pair of variables will be calculated, and the results analysed in the context of the desired performance outlined in Chapter 5.

For Granger causality the Akaike Information Criterion (AIC) was used to select the model order, k. The same model order was used for the reduced and full model.

For transfer entropy the embedding dimensions had to be selected. First, the prediction horison and time interval were assumed to be the same as the transport delay between T_{in} and T:

TABLE 6.1: *Tank simulation model parameters.*

Parameter	Description	Value/Initial value	Units
A	Cross-sectional area of tank	1	$[m^2]$
C_p	Specific heat capacity of water	4186	$[\frac{J}{kgK}]$
$C_{p,s}$	Specific heat capacity of steam	1996	$[\frac{J}{kgK}]$
ρ	Density of water	1000	$[\frac{kg}{m^3}]$
ρ_s	Density of steam	0.6	$[\frac{kg}{m^3}]$
K_L	Level proportionality constant	0.128	$[\frac{m^3}{m^{0.5}min}]$
L	Tank level	2	$[m]$
T	Tank temperature	50	$[°C]$
T_D	Time delay	2	$[min]$
T_{ref}	Reference temperature	25	$[°C]$
T_{in}	Inlet temperature	25	$[°C]$
F_{in}	Inlet flowrate	0.181	$[\frac{m^3}{min}]$
T_s	Inlet steam temperature	100	$[°C]$
F_s	Inlet steam flowrate	0.5	$[\frac{m^3}{min}]$

$h = \tau = 2$. The embedding dimensions $K = 1$ and $L = 2$ were selected.

Parametrisation of transfer entropy is complex, so for this study the parameters chosen may not have been optimal. However, the objectives of this chapter are not to compare optimal implementations of the two techniques, but rather to gain an understanding of how the techniques are affected by the factors outlined in Chapter 5. Chapter 7 addresses optimal parametrisation methods.

6.3.1 Two-tank simulation used to generate experimental time series data

A SIMULINK simulation of a water tank with a heat exchange coil, as shown in Figure 6.1, was used to generate the time series data. A cold water stream enters the tank with a flow rate F_{in} and temperature T_{in}. The flow rate out of the tank is proportional to the square root of the tank level, L. Steam coils run through the tank at a measured flow rate of F_s. When control is implemented, the tank temperature is controlled by varying F_s using a PID controller. The mass balance is given by:

$$A\frac{dL(t)}{dt} = F_{in} - k_L\sqrt{L(t)} \tag{6.1}$$

where F_{in} is kept constant. The energy balance is given by:

$$\begin{aligned}\rho C_p A\frac{dL(t)T(t)}{dt} =& \rho C_p F_{in}(T_{in}(t-T_D) - T_{ref}) - \rho C_p k_L\sqrt{L(t)}(T_{out}(t) - T_{ref}) \\ &+ \rho_s C_{p,s} F_s(T_{s,in}(t) - T_{s,out}(t))\end{aligned} \tag{6.2}$$

where T_D is the time delay between the measurement point for T_{in} and T.

To simulate process noise and sensor noise, Gaussian noise is added to the measured variables (T_{in} and T) using a random number generator in Simulink. An illustration of the distinction between process noise and sensor noise is shown in Figure 5.2.

TABLE 6.3: *Ranges of perturbations used for sensitivity analysis (δ = fault size).*

Perturbation	δ	**Period**
Oscillatory	$0°C \rightarrow 25°C$	$1min \rightarrow 50min$
Step	$0°C \rightarrow 25°C$	-

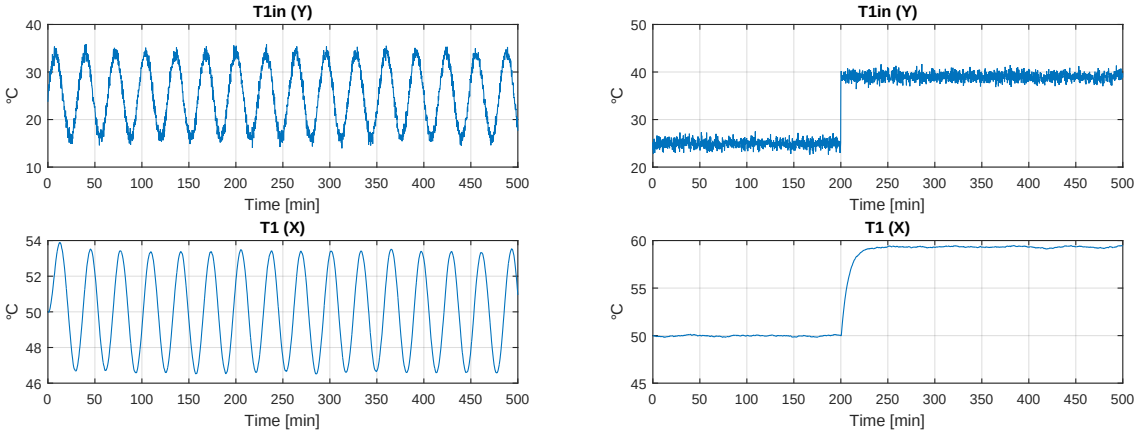

(a) *Response of T_1 to oscillating T_{1in}.* (b) *Response of T_1 to step change in T_{1in}.*

FIGURE 6.2: *Response of T_1 to perturbations in T_{1in}.*

It can be argued that time series generated from simulations may not accurately represent the real-world response of processes. However, the benefit of being able to simulate different perturbations to the process and examine their effect on the causality makes a simulated case study ideal for the purposes of this work.

A sensitivity analysis on the effect of oscillating perturbations and step perturbations on the causality from T_{in} to T was performed. Oscillations in T_{in} and step changes in T_{in} were introduced. Three different simulated scenarios were generated:

- Base case: Gaussian sensor noise added to $T_{in}$and T signals.
- Process noise case: Gaussian noise is introduced to T_{in} signal before numerical integration, in addition to sensor noise added to both measured variables (T_{in} and T). The effect of extra excitation introduced by process noise on the causality is to be investigated.
- Closed loop case: a controller is added that varies F_s to control T. The effect of controller action on the causality is to be investigated.

Examples of the time series for oscillating inputs and step inputs are shown in Figures 6.2a and 6.2b respectively.

6.3.2 Expected performance of causality analysis

To investigate the impact of the factors considered in this chapter, step and oscillatory perturbations are introduced into a simulated process. Figure 6.3 illustrates the expected response

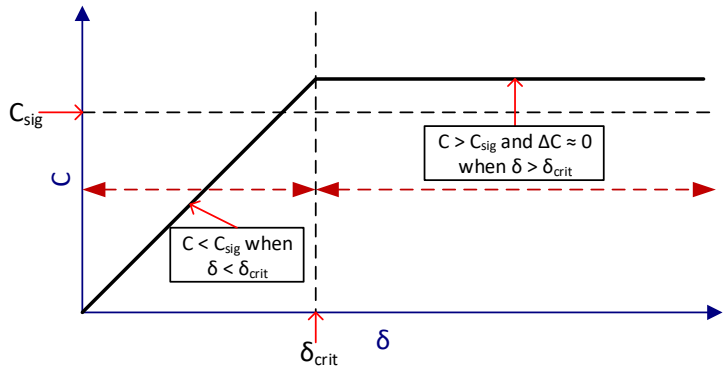

FIGURE 6.3: *Expected response of causality measures to perturbations. δ = fault size. C = causality measure*

of the causality measures to increasing size of perturbations. The ideal responses of the topology methods is a flat response, where the causality measure remains significant and constant (allowing for some variation due to stochasticity) regardless of the perturbations experienced; $\Delta C \cong 0$ and $C > C_{sig}$. This flat response would indicate that the causality measure is accurate at identifying the known causal connection, and precise, since it identifies the causal connection consistently. The actual responses may deviate from this ideal.

The expected trend is that large amplitude oscillations or large step changes would cause strong causal connections between variables, since a large change in the input would cause a pronounced change in the output. It is expected that this effect would only be noticeable once the amplitude of the perturbation exceeded some signal to noise ratio threshold, since noise would obfuscate the causal connection. This means that there would be some critical value of the perturbation amplitude, δ_{crit}, where $C < C_{sig}$ for $\delta < \delta_{crit}$.

For oscillatory perturbations, medium frequency oscillations would result in strong causal connections, since the response of the output variable to changes in the input is gradual enough that a clear trend would appear. Very low frequency oscillations, however, would cause such gradual changes that the effect would be obscured by the more rapid dynamics of the noise in the process. Very high frequencies would appear similar to noise, where insufficient time is allowed for a trend to develop between the input and output.

6.4 Results for system under influence of oscillatory perturbations

Figure 6.4 displays the causality measures between T_{in} and T obtained for oscillatory perturbations. Table 6.4 shows the mean and standard deviations of the Granger causalities and transfer entropies for each contour plot.

High frequency, large amplitude oscillations result in larger values for Granger causality and transfer entropy. Observing the response as the process conditions move from high frequency to low frequency, a steep slope in the causality measure is observed at very high frequencies. At very high frequencies the oscillations appear as fluctuations similar to noise, obscuring the

TABLE 6.4: *Means and standard deviations of Granger causality and transfer entropies shown in Figure 6.4.*

	Granger causality	Transfer entropy
Open loop oscillation	$\mu = 0.100, \sigma = 0.015$	$\mu = 1.38, \sigma = 0.99$
Open loop with process noise	$\mu = 0.087, \sigma = 0.016$	$\mu = 0.798, \sigma = 0.695$
Closed loop oscillation	$\mu = 0.074, \sigma = 0.016$	$\mu = 0.802, \sigma = 0.477$

causal relationship. As the frequency decreases the more gradual slope in T_{in} results in a more pronounced oscillatory trend in T. This means that values of T are easier to predict using past values of T_{in}, resulting in larger causality values.

As the process conditions move towards even lower frequencies the causality measures decrease slightly. The perturbation in the input propagating to the output is so gradual that the effect is dominated by the more rapid dynamics of the noise in the process. The decrease in causality measure at lower frequencies is more gradual for Granger causality than it is for transfer entropy. This is due to the fact that the transfer entropy parameters were kept constant. The window over which the transfer entropy observe the responses becomes too small to capture the longer dynamics. With Granger causality, the model order selected with the AIC compensates for the longer dynamics.

An increase in the causality measure is also seen as process conditions move from low amplitude to high amplitudes. As the amplitude increases the excitation in the system increases, meaning that oscillations in T_{in} cause more pronounced oscillations in T. The signal to noise ratio increases, meaning that the perturbation dominates the noise. This pronounced effect means that the noise has less of an impact on the accuracy of the PDFs calculated for transfer entropy. The information transferred from T_{in} to T is not contaminated by the uncertainty added by the noise. This pronounced effect means that information contained in past values of T_{in} provides information for predicting values of T. This response corresponds to the expected response demonstrated in Figure 6.3.

By comparing Figure 6.4b with 6.4d, and considering the mean transfer entropies shown in Table 6.4 are 1.38 and 0.708 respectively, it can be seen that the calculated transfer entropy values are lower when process noise is added. This indicates that the process noise adds stochasticity, meaning that the information contained in past values of T_{in} is unrelated to information in T. This means that the causal connection is obscured by adding information that is not transferred from one variable to another. The signals, T_{in} and T, are now influenced by both the input noise and the oscillatory perturbations. The PDFs calculated for the signals may be more inaccurate, since the true distributions are now a mix between the distributions for the input noise and the distributions for the perturbations. Kernel density estimation may overfit to the noise in the process, resulting in a fit with high variance. By comparing Figure 6.4a with 6.4c, there is no observable effect of the noise, as there is for transfer entropy. Granger causality fits linear regression models to the data, which assumes that the errors follow a Gaussian distribution. This means that the while the model fit may have a large bias, it would have a low variance. The possibility that the KDEs for transfer entropy may have overfit the noise in the data could account for its sensitivity to noise when compared to Granger causality.

Figures 6.4e and 6.4f show the response during closed loop operation. There is still a peak at high amplitudes and high frequencies, but at low frequencies the causality values are lower than the open loop case. Low frequency oscillations are more successfully attenuated by the controller, so the impact of these oscillations on the temperature would be less pronounced, obscuring the causal relationship.

The significance thresholds for transfer entropy are shown as red contours on the plots. For Granger causality, where each calculated value is subjected to the F-test, all the calculated values were significant. This indicates that Granger causality is able to detect the causal connection even when there is little excitation caused by perturbations. Despite the extreme cases, for a large range of conditions the responses are flat, indicating that the causality measures are effective for calculating causality in oscillatory conditions. Comparing the left side of Figure 6.4 with the right side, Granger causality appears to provide a flatter response surface than transfer entropy. This indicates that Granger causality is more reliable at detecting causality for the ranges of oscillations considered.

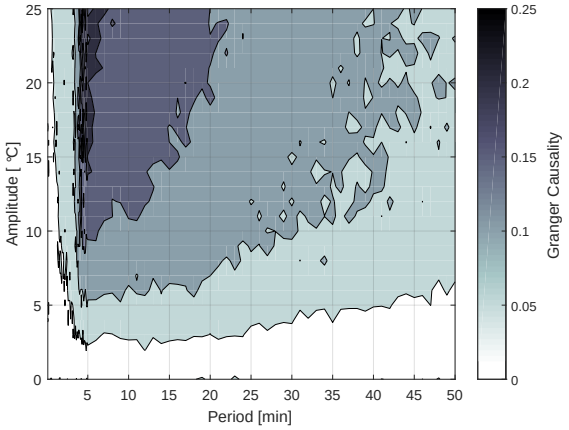

(a) *Granger causality for open loop oscillations*

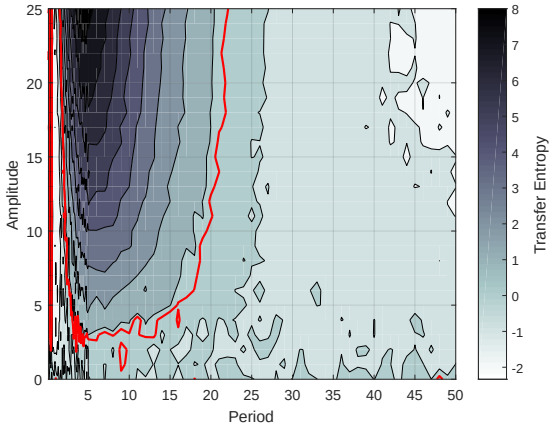

(b) *Transfer entropy for open loop oscillations*

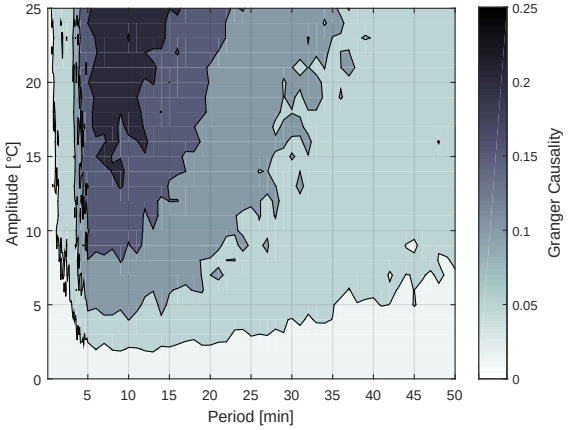

(c) *Granger causality for oscillations with process noise.*

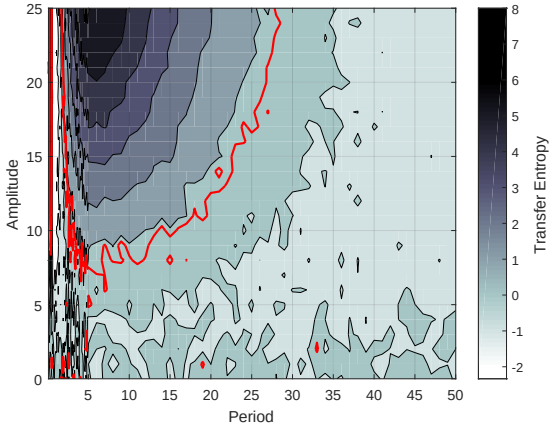

(d) *Transfer entropy for oscillations with process noise*

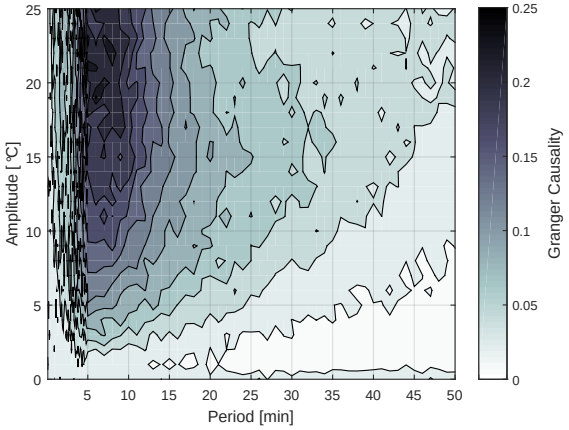

(e) *Granger Causality for closed loop oscillations*

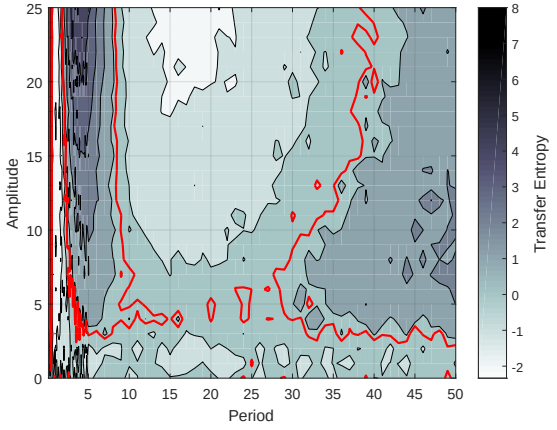

(f) *Transfer entropy for closed loop oscillations*

FIGURE 6.4: *Impact of oscillatory perturbations on Granger Causality and transfer entropy. Red line on transfer entropy graphs represent the significance value. For Granger causality, the F-test determined that all calculated values were significant.*

6.5 Results for system under influence of step perturbations

Figure 6.5 shows the resulting $T_{in} \rightarrow T$ causality measure for the step perturbations. For the open loop cases, increasing step size results in larger causality measures. As the step size increases, the excitation in the system becomes more pronounced. This means that the changes in T_{in} cause more pronounced changes in T and the causal relationship is easier to detect. The signal to noise ratio increases, and the effect of the noise is reduced.

For the Granger causality, all the values were significant according to the F-test, indicating that Granger causality was reliable for causality detection for all the step inputs. The significance thresholds for transfer entropy are shown as the red line on the figures. Transfer entropy showed small values below the threshold initially, and gradually increasing to significant values as the step size increased. This indicates that when the excitation in the system is small, the transfer entropy fails to detect the causal relationship. When the amplitude is larger, the signal to noise ratio increases, and the effect of the perturbation dominates the effect of the noise. The results of both Granger causality and transfer entropy were consistent with the expected response show in Figure 6.3. Increasing amplitudes of the step perturbations showed increasing causality strengths.

For Granger causality, no difference is observed with the introduction of process noise, indicating robustness to the extra noise in the step input conditions. For transfer entropy the introduction of process noise caused a dramatic decrease in the calculated values, indicating that transfer entropy is very sensitive to the extra stochasticity added by the introduction of process noise. This effect was observed in Section 6.4, and the discussion is repeated here for clarity. The signals, T_{in} and T, are now influenced by both the input noise and the oscillatory perturbations. The PDFs calculated for the signals may be more inaccurate, since the true distributions are now a mix between the distributions for the input noise and the distributions for the perturbations. Since Granger causality is not trying to fit any distributions, but rather just linear models, it may be more robust to the noise.

Figures 6.5a and 6.5b show the response during closed loop operation. For Granger causality the response is flat, since the controller successfully attenuates the disturbance caused by the step change, obscuring the causal relationship. For transfer entropy, the calculated causality is only slightly lower, indicating that for step disturbances transfer entropy can still detect the causal relationship even with the effect of the controller. The Granger causalities calculated were still significant, even though they were slightly lower, indicating that both techniques reliably detected the causal relationship.

6.6 Chapter conclusions

The impact of noise, controller interaction, and fault types on causality analysis performance were investigated in this chapter. Overall, both techniques displayed robustness by accurately detection known causal connections for all the process conditions investigated. There were some logically consistent exceptions. For oscillatory conditions, high frequencies resemble noise, where the variation in the input variable does not propagate to the output variable. Therefore lower causality measures were obtained at high frequencies. The effect of low frequency oscillations is so gradual that the observed window used by the causality measures are too small to detect a causal relationship. Closed loop operation attenuates slow acting oscillations and step perturbations, disguising causal relationships.

Although the purpose of this chapter is not to provide a comparative analysis of Granger causal-

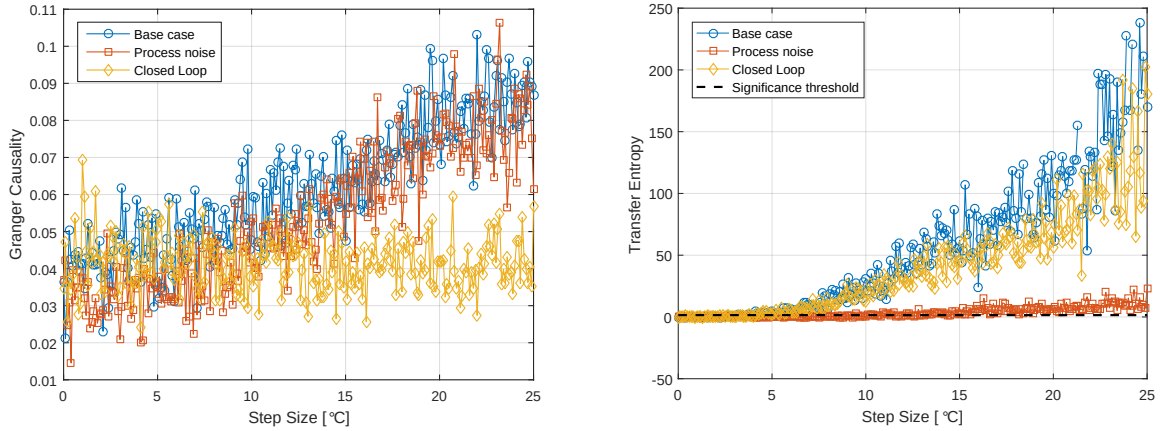

(a) *Granger causality for step perturbations* (b) *Transfer entropy for step perturbations*

Figure 6.5: *Impact of step perturbations on Granger causality and transfer entropy. All calculated Granger causality values were significant according to the F-test.*

ity and transfer entropy (Chapter 8 addresses this), some points of comparison are useful to discuss the strengths and weaknesses of each. Granger causality gave flatter responses than transfer entropy for a wide range of oscillatory conditions, indicating reliability. Transfer entropy was less affected by the influence of the controller in detecting the causal connection. Transfer entropy was more sensitive to the influence of additional process noise.

This chapter investigated the impact of some process conditions on the accuracy of causality analysis measures. Now that this investigation has provided some insight into the strengths and weaknesses of these techniques, pragmatic guidelines for their implementation can be addressed. Chapter 7 provides an investigation of how different process dynamics affect the ability of these techniques to accurately identify causal connections between variables, and how these dynamics are related to the optimal parameters to calculate the causality between variables. Guidelines for data selection, parameter selection, and the overall implementation procedure are introduced in the framework of a systematic workflow. It may be noted that this section already investigated the impact of the dynamics of oscillatory disturbances, however, Chapter 7 also investigates the interaction between these dynamics and the optimal parameters for causality analysis.

CHAPTER 7

Developing guidelines for selection of parameters in causality analysis

Contents

7.1 Chapter introduction . . . 91
7.2 Chapter objectives . . . 92
7.3 Workflow for application of transfer entropy for oscillation diagnosis . . . 93
7.3.1 Detect fault . . . *95*
7.3.2 Perform spectral analysis (optional) . . . *95*
7.3.3 Select data for transfer entropy analysis . . . *95*
7.3.4 Determine process dynamics (optional) . . . *96*
7.3.5 Select parameters for transfer entropy analysis . . . *96*
7.3.6 Perform transfer entropy analysis . . . *96*
7.4 Establishing guidelines for transfer entropy application . . . 97
7.4.1 Selecting the number of samples . . . *97*
7.4.2 Selecting the sampling time . . . *98*
7.4.3 Selecting embedding parameters . . . *99*
7.4.4 Selecting prediction horizon and time interval . . . *100*
7.4.5 Final guidelines for parametrisation . . . *101*
7.5 Demonstrating workflow on real case study . . . 103
7.5.1 Detect fault . . . *103*
7.5.2 Perform spectral analysis (optional) . . . *104*
7.5.3 Select data for transfer entropy . . . *104*
7.5.4 Determine process dynamics (optional) . . . *105*
7.5.5 Select parameters for transfer entropy . . . *106*
7.5.6 Perform transfer entropy analysis . . . *106*
7.6 Chapter conclusion . . . 110

7.1 Chapter introduction

A version of this chapter has been submitted for publication: Lindner B, Auret L & Bauer M, 2018, A systematic workflow for oscillation diagnosis using transfer entropy, Manuscript

accepted for final submission by IEEE Transactions on Control Systems Technology. [Lindner *et al.*, 2018a].

As discussed in Chapter 2.11, transfer entropy is a popular causality analysis technique that has been proven effective at fault diagnosis in a variety of applications [Bauer *et al.*, 2007a, Duan *et al.*, 2013, 2015, Hajihosseini *et al.*, 2014, Landman *et al.*, 2014, Naghoosi *et al.*, 2013, Shu & Zhao, 2012, Wakefield *et al.*, 2018]. Despite the evidence of successful fault diagnosis applications, transfer entropy has not been widely adopted for fault diagnosis in processing industries. Chapter 5 presented the desired characteristics of causality analysis techniques and identified automated application and reliability of the results as crucial for feasible implementation.

Application of transfer entropy is a complicated procedure, with numerous parameters to be selected. Many of the academic applications of transfer entropy use default parameters, or often don't specify what values of parameters were used or how they were selected. Horch *et al.* [2007] presented a workflow for the application of transfer entropy. However, specific parametrisation guidelines were omitted, and the default parameters for transfer entropy suggested by Bauer *et al.* [2007a] were used. Lack of systematic guidelines for application of transfer entropy means that results are often unreliable or too time consuming to implement. Naghoosi *et al.* [2013] and Duan *et al.* [2013] presented systematic parametrisation approaches. However, these approaches require information theory calculations to be performed at multiple embedding dimensions, and are therefore time consuming and computationally expensive. Additionally, these parametrisation procedures were not integrated into a complete workflow with all the application steps required.

Development of systematic workflow for application of transfer entropy can provide a meaningful contribution to this technique. This chapter presents a systematic workflow for the application of transfer entropy for oscillation diagnosis. The workflow addresses the selection of each important parameter required and provides guidelines for selecting the optimal parameters based on the process conditions. Transfer entropy is applied to time series generated from process measurements. It exploits lagged information between pairs of variables. This means that process dynamics will have a significant influence on the optimal parameter selection. Identifying and understanding the relationships between process dynamics and transfer entropy parameters will allow for more robust, systematic procedure of parametrisation.

The outline of this chapter is as follows: in Section 7.3 the workflow for calculation of transfer entropy is presented; in Section 7.4 the relationships between process dynamics and calculation parameters are determined to provide guidelines for parameter selection; in Section 7.5 the workflow is demonstrated and tested on an industrial case study; in Section 7.6 the conclusions of the investigation are presented.

7.2 Chapter objectives

The objectives of this chapter are:

I To *develop* a systematic workflow for the application of transfer entropy for oscillation diagnosis. This workflow must address:

(a) robust parametrisation of transfer entropy

(b) variable selection

(c) data selection

II To *test* the systematic workflow for diagnosis of an oscillation in a case study of oscillations in the flotation section of a platinum concentrator plant.

7.3 Workflow for application of transfer entropy for oscillation diagnosis

Oscillations in industrial processes can propagate to multiple units and possibly degrade performance [Thornhill, 2005]. Swift and accurate diagnosis of the oscillation is necessary to ensure that corrective action can be taken as soon as possible. Transfer entropy can be used to diagnose such a plant-wide oscillation by inferring its propagation path. However, application of transfer entropy for oscillation diagnosis is a complex task with multiple steps. Many of these steps require the user to specify parameters which significantly affect the accuracy of the results. A systematic workflow for application of transfer entropy is presented in Figure 7.1. Each step of the workflow is described in detail in this section.

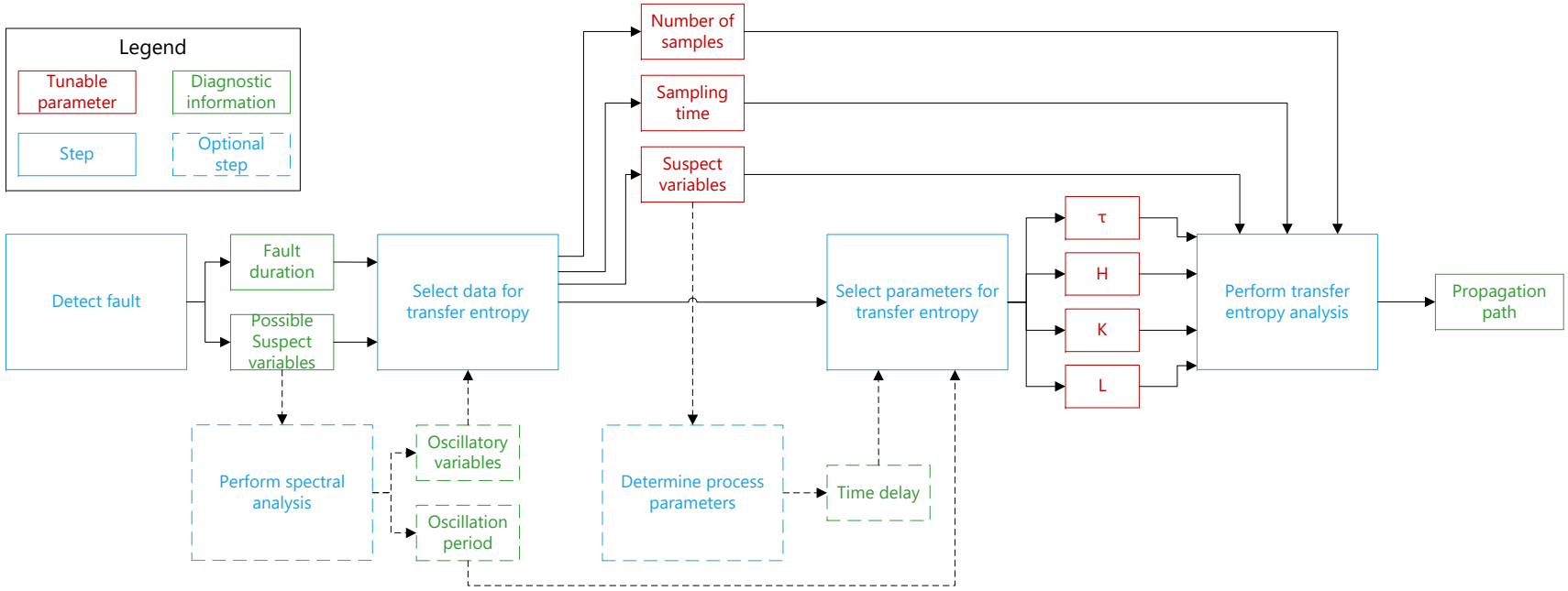

FIGURE 7.1: *Workflow for application of transfer entropy for oscillation diagnosis. Dashed outlines indicate optional steps.*

7.3.1 Detect fault

The first step in the workflow is to detect the fault. This is either by visual inspection, alarms indicating deviation of measured variables or KPIs from their acceptable ranges, or an automated fault detection strategy, such as the spectral envelope method [Jiang *et al.*, 2007]. The duration of the fault can be found by determining when the oscillation's effects first appeared, and when it disappeared, either due to corrective action, or disappearance of the disturbance. In an online setting, the fault may be ongoing, and it is up to an engineer to apply the diagnosis procedure and take corrective action. The general location of the fault can be determined, by identifying which process units are affected. Visual inspection of the time series data can indicate which variables show symptoms of the fault. This initial step can narrow the suspect variables down to a unit or section of the plant.

This workflow is focused on oscillation diagnosis. Indeed, the majority of applications of transfer entropy in chemical or mineral processes has been for oscillation diagnosis. Oscillations often occur in processes and there is therefore a need for automated diagnosis procedures. In the presence of an oscillatory disturbance, there is enough excitation in the signals that a wide range of values are observed. This means that the PDF estimation is more accurate, since the distributions of the signals are smoother. This workflow could be adapted to be used for other types of disturbances, such a step changes in feed conditions. However, the impact on the optimal parameters would have to be investigated.

7.3.2 Perform spectral analysis (optional)

Spectral analysis may then be performed on this reduced set of variables to determine the oscillation period. A fast Fourier transform can be used to find the frequency that gives the peak power spectrum [Shumway & Stoffer, 2014]. This dominant frequency may represent the frequency of the oscillation. The oscillation period may later be used for parameter selection. Each of the variables that show this common oscillation period may possibly be an indication of where the oscillation originated, or they may be showing symptoms of the oscillation after it has propagated through the process. The suspect variables can then be narrowed down even further to those with this common oscillation period.

This is an optional step. This variable selection is commonly used when applying transfer entropy for oscillation diagnosis [Bauer *et al.*, 2007a, Duan *et al.*, 2013, 2015, Landman & Jamsa-Jounela, 2016]. If the dominant frequency is not identified, the causality analysis can be performed on the suspect variables identified in the fault detection step. However, this means that the transfer entropy will have to be calculated for a large number of candidate variables. This will increase the computation time dramatically.

In this workflow the oscillation period can be used to select optimal parameters for transfer entropy. If this information is not available other parametrisation techniques (discussed further in Section 7.3.5) may be used. However, Section 7.4 shows that the optimal parameters are sensitive to the oscillation period. Therefore using different parametrisation techniques that do not take into account the oscillation period may result in suboptimal parameter selection.

7.3.3 Select data for transfer entropy analysis

The next step is to select the data to be included in further analysis. Namely, selecting the number of samples to include (N_s), the sampling time of the data used (T_s), and the variables

to include. The duration of the fault and the sampling time of the data available may dictate the selection of N_s and T_s. However, it may be desired to include a smaller number of samples to reduce the computational burden. This can either be done by simply selecting a smaller subset of data, or by subsampling the data. The variables identified as possible suspect variables in the fault detection step can be used for subsequent analysis. Alternatively, if the spectral analysis step has been performed then only the variables showing oscillations at a common frequency can be selected.

7.3.4 Determine process dynamics (optional)

In this workflow the process dynamics, specifically the time delays of the process, are used to inform the parameter selection. System identification techniques can be used to estimate the time delay between each of the suspect variables.

This step is optional, if this information is not available other parametrisation techniques (discussed further in Section 7.3.5) may be used. However, Section 7.4 shows that the optimal parameters are sensitive to the process dynamics. This is confirmed by [Duan *et al.*, 2014]. Therefore using different parametrisation techniques that do not take into account the process dynamics may result in suboptimal parameter selection.

7.3.5 Select parameters for transfer entropy analysis

The next step is to select the parameters for calculation of the transfer entropy. Knowledge of the process and fault dynamics will allow robust selection of these parameters. This selection has been addressed by other researchers. Section 2.12.2 discusses these in detail. Bauer *et al.* [2007a] suggested choosing default values of $K = 0$ and $L = 2$. The sampling time τ is then varied until the difference in $T_{x\to y}$ no longer changes significantly with changing τ. Duan *et al.* [2013] suggested a slightly different approach, where initial values of $H = \tau = 1$ are selected. The embedding dimension, K, is varied until the Shannon entropy for y no longer changes. Then the embedding dimension, L, is varied until $T_{x\to y}$ no longer changes significantly. If K or L becomes too large, a larger τ is chosen and the procedure is repeated. Naghoosi *et al.* [2013] used time lagged dependency and differential dependency curves to determine the most important time lags and used this information to parametrise transfer entropy. This approach is more systematic, and does consider the underlying process dynamics indirectly. However, these procedures are computationally expensive, since they require calculating PDFs for a range of parameter values.

This chapter proposes a novel parameter selection methodology that incorporates process dynamics. In Section 7.4 relationships between process dynamics and the tunable parameters are investigated in order to provide guidelines for their selection in the context of this workflow. These guidelines are an important contribution of this work. The suggested guidelines related the optimal H and τ to the oscillation period (obtained from the 'Perform spectral analysis' step) and the time delay (obtained from the 'Determine process dynamics' step).

7.3.6 Perform transfer entropy analysis

With the parameters selected in the previous step, the transfer entropy calculations between each pair of variables can then be calculated using Equation 2.5. The PDFs can be calculated using kernel density estimation [Bauer *et al.*, 2007a]. The kernel density estimation step itself

has a bandwidth parameter that has to be selected. Optimal selection of this bandwidth was not included in the scope of this parametrisation investigation. This is discussed in Section 2.9.2. The focus of this investigation was on the parameters most sensitive to the process dynamics. The bandwidth suggested by Li & Racine [2011] can be used as a rule of thumb $\theta = 1.06N^{-0.2}\sigma_x$.

Because transfer entropy is calculated for data generated from a process influenced by stochasticity, non-zero values for transfer entropy will be calculated even when there is no causal relationship. Hypothesis tests are needed to determine the statistical significance of the calculated values. A significance threshold can be calculated using Equation 2.43. A causal map can then be constructed. The nodes in the causal map represent the measured variables, and the edges represent significant causal connections between the variables. From this causal map, the propagation path of the oscillation can be inferred. Further analysis can then be performed to establish the sequence of events that lead to the oscillation occurring in the process.

7.4 Establishing guidelines for transfer entropy application

The workflow presented in Section 7.3 involves selection of multiple parameters, namely: the number of samples (N_S); the sampling time (T_S); the time interval (τ); the prediction horizon (h); the output embedding dimension (K); and the input embedding dimension (L). The optimal values for these tunable parameters may be influenced by the process conditions. Therefore the relationships between process and fault dynamics and the parameters required for calculation of transfer entropy are investigated.

A simple tank process was simulated, where an oscillation was introduced in the temperature of the tank's inlet stream. This simulation was described in Section 6.3.1. There is a known causal connection between this inlet temperature and the outlet temperature of the tank. Therefore this oscillation would propagate from T_{in} to T_{out}. The process dynamics that could affect the calculated transfer entropy between T_{in} and T_{out} are the time delay between them (T_D), the time constant between them (τ_p), and the period of the introduced oscillation (P).

The calculation parameters that may influence the transfer entropy result are: the number of samples (N_S); sampling time (T_S); prediction horizon (h); time interval (τ); embedding dimension (K and L). The relationship between the process dynamics and each individual calculation parameter can be determined by simulating the process for a range of values for T_D, τ_p, and P. The transfer entropy can then be calculated for each combination of process dynamics for a range of values of the calculated parameters. In this way the response of the transfer entropy to each process condition and calculated parameters can be analysed. An analysis of variance (ANOVA) is performed to establish which factors have a significant effect on the transfer entropy. Further analysis can then be performed for each significant factor. The ANOVA results are presented in Appendix A.

7.4.1 Selecting the number of samples

The ANOVA presented in Appendix A showed that the number of samples (N_S) was a significant factor for accurate transfer entropy calculations. Limited interaction between N_S and the other factors was observed. Therefore the influence of N_S on the transfer entropy alone can be investigated. The general trend in Figure 7.2 was that higher levels of N_S gave higher transfer entropy values. This indicates that a larger N_S gave more accurate transfer entropy results. To confirm this the transfer entropy was calculated for a range of values of P, T_D, τ_p, and N_S with more levels than the 4 levels included in the ANOVA. Figure 7.2 plots the mean transfer

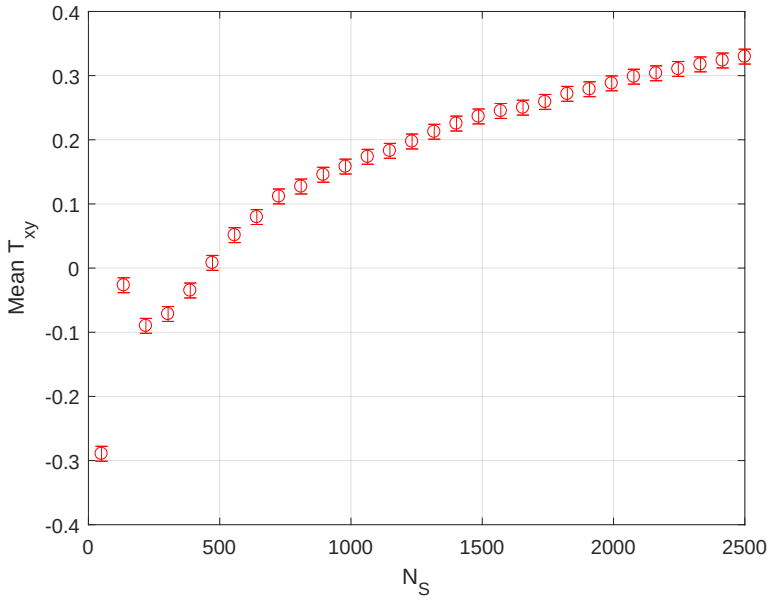

FIGURE 7.2: *Mean transfer entropy for known connection ($T_{in} \rightarrow T_{out}$) plotted against number of samples. The optimal number of samples is the largest available.*

entropy value for each N_S level. The increasing trend indicates that the larger N_S is the larger the transfer entropy is. This indicates that a larger number of samples provides more accurate transfer entropy values, since more samples will be included in the estimation of the PDFs. This also illustrates how sensitive transfer entropy is to the optimal number of samples, with some values below 500 samples showing negative transfer entropy.

A guideline for the minimum number of samples is useful, especially in an online context, where it is necessary to know how many samples need to be collected for the analysis. In a scenario where the oscillation did not persist for long enough to collect more than the minimum number of samples, the analysis can still be performed. However, the results will then have to be analysed with caution, and careful consideration must be given to any corrective action taken from the results of this analysis. In an offline context the maximum number of samples available for the analysis is limited to the number of samples that the oscillation persists for. Additionally, transfer entropy is computationally expensive, therefore selecting a smaller number of samples can reduce the analysis time. Figure 7.2 indicates a steeper drop in the mean transfer entropy value when N_S is below 500 samples.

Bauer *et al.* [2007a] investigated the minimum number of samples required to obtain a significant transfer entropy value. The results indicated that the minimum number of samples should be set to 2000 samples if possible, but could be as low as 400 samples. These results are consistent with those observed in this investigation.

7.4.2 Selecting the sampling time

The ANOVA did not indicate that the sampling time (T_S) significantly impacted the transfer entropy. This is unexpected, since changing the sampling time changes the time scales of each of the parameters. Additionally, altering the sampling time alters the shape of the reconstructed oscillation trend. However, the general trend in Figure A.1a indicated that lower T_S levels gave higher transfer entropy values. To confirm this the transfer entropy was calculated for a range

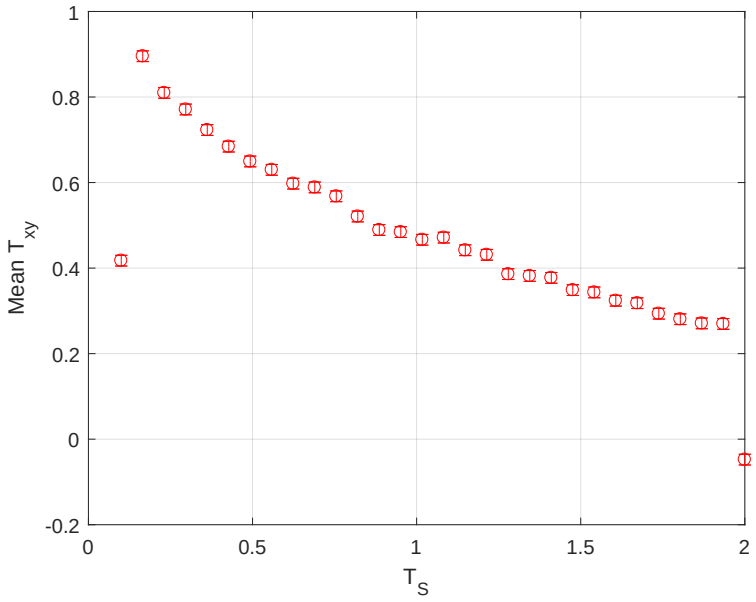

FIGURE 7.3: *Mean transfer entropy for known connection ($T_{in} \rightarrow T_{out}$) plotted against sampling time. The optimal sampling time is the smallest available.*

of values of P, T_D, τ_p, and T_S with more levels than the 4 levels included in the ANOVA. Figure 7.3 plots the mean transfer entropy value for each T_S level. The decreasing trend indicates that the smallest sampling time results in the most accurate transfer entropy value. This result is logically consistent, since the smallest sampling time provides the highest resolution for the data. The sensitivity of transfer entropy to the sampling time is evident from this plot.

In some cases it may be desirable to increase the sampling time in order to reduce the number of samples while still covering the same time span. There is no clear evidence of an inflection point where the transfer entropy value became significantly lower in Figure 7.3. However, Shannon's sampling theorem [Shannon, 1948] can provide a guideline for the maximum allowable sampling time. According to this theorem, the maximum sampling time before the reconstructed trend no longer captures the oscillation is $0.5P$. Barnett & Seth [2017] showed that the detection ability of a causality analysis method decays exponentially as the sampling time increases beyond the causal delay. Therefore the sampling time should ideally also be less than the time delay between variables.

7.4.3 Selecting embedding parameters

The ANOVA results indicate that the embedding dimensions (K and L) significantly affected the transfer entropy results, and have significant interaction with τ. The results are less sensitive to the chosen K parameter. Since increasing these parameters greatly contributes to the computational cost of transfer entropy, the range of values that can be implemented practically is limited. Equation 2.5 requires estimation of joint PDFs. The dimensions of the PDFs that need to be calculated are a function of K and L. Bauer *et al.* [2007a] suggested limiting the embedding dimension to $K = 0$ and $L = 2$. This is a pragmatic solution to reducing the complexity of the transfer entropy workflow. It is therefore suggested that K and L be fixed, and τ and H can be used to capture the process dynamics accurately. Figure A.1b in the appendix shows the mean transfer entropy values for the interaction of K and L. $K = 1, L = 2$ gives

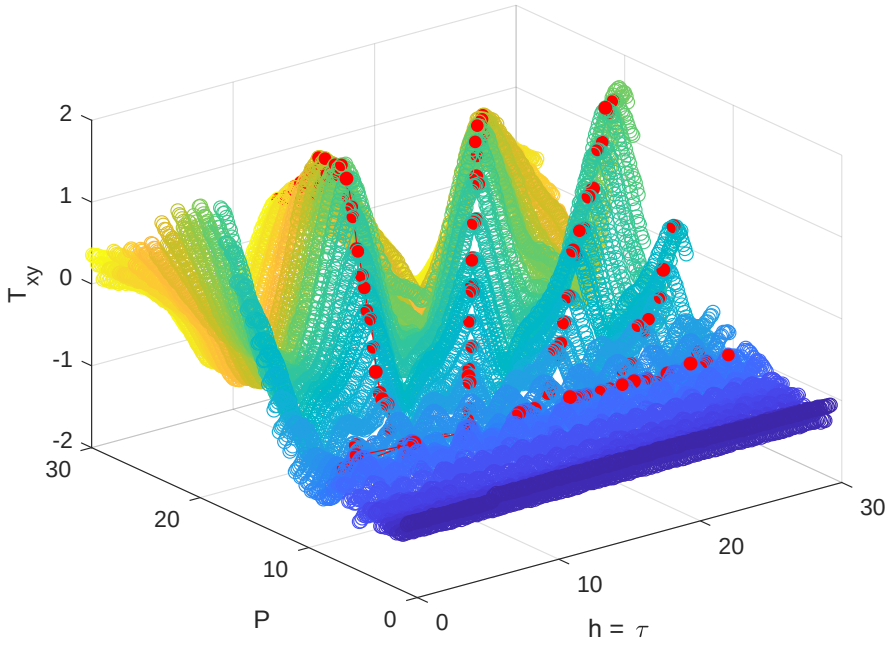

Figure 7.4: *Effect of τ and P on transfer entropy for known connection ($T_{in} \rightarrow T_{out}$), indicating relationship between P and the optimal τ. Locations of the peaks are indicated by the red markers.*

larger transfer entropy values than $K = 0, L = 2$. The largest PDF that needs to be calculated is $p(y_{i+H}, \mathbf{Y}_i^{(K)}, \mathbf{X}_i^{(L)})$, which has a dimension of $K + L + 1$. This means that for $K = 1, L = 2$, a four-dimensional PDF is the largest that has to be constructed. Therefore $K = 1, L = 2$ can be taken as the default values without impractically costly computations.

7.4.4 Selecting prediction horizon and time interval

Bauer *et al.* [2007a] suggested that the time interval (τ) and prediction horizon (h) should be equal to each other, since they would give similar responses to the process dynamics. Therefore in this study these parameters were kept equal. ANOVA results indicated that selection of τ may be influenced by P, τ_p, and T_D, since their interactions gave lower P-values.

Figure 7.4 displays transfer entropy plotted against P and τ. The dimensions of both x and y axes are in minutes. The transfer entropy response surface shows repeating peaks whose position is dependant on the value of P and τ. The shape of this surface reveals how sensitive transfer entropy is to the selection of τ for different oscillation periods, and therefore illustrates the need for considering these dynamics for optimal parameter selection. These repeating peaks indicate aliasing, where the oscillatory trend is obscured at certain values of τ. The optimal time interval value, τ_{max}, can be taken as the location of the first peak. I.e. the first τ value that resulted in a peak for each oscillation period.

Figure 7.5 plots τ_{max} against P, for a single T_D and τ_p. A strong linear relationship between P on τ_{max} is evident. A similar linear relationship was observed between T_D and τ_{max}. No relationship was observed between τ_p and τ. Therefore τ_p was excluded from further analysis.

A three dimensional plot of the optimal time interval (τ_{max}) against oscillation period (P) and time delay (T_D) is displayed in Figure 7.6. The figure confirms the linear relationship between

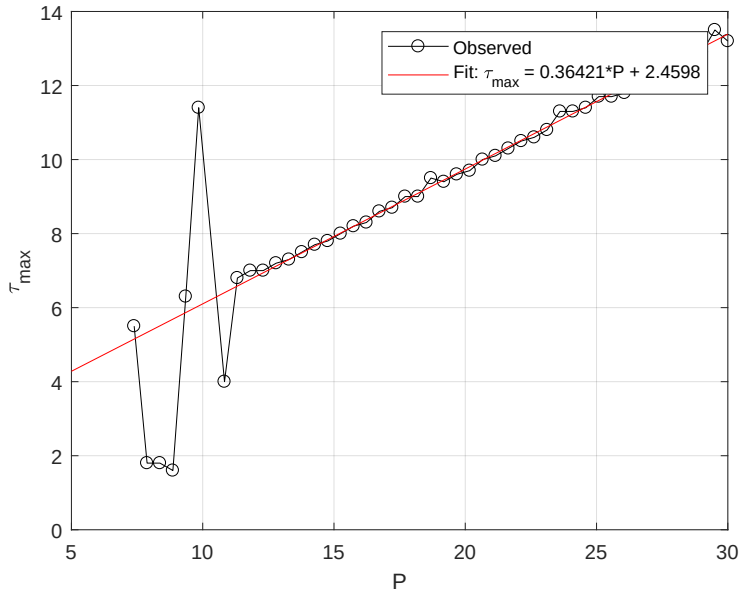

FIGURE 7.5: *Linear relationship between optimal time interval (τ_{max} in min) and oscillation period (P in min). $R^2 = 0.82$*

TABLE 7.1: *Guidelines for parameter selection for transfer entropy using fault and process conditions.*

Parameter	**Suggested value**	**Suggested range**
Number of samples (N_S)	Maximum	$[500 - N_{S,max}]$
Sampling time (T_S)	Minimum	$[T_{s,min} - 0.5P]$
Output embedding dimension (K)	1	$[0 - 3]$
Input embedding dimension (L)	2	$[1 - 3]$
Time interval (τ)	$(0.33P + 0.53T_D + 0.66)/T_s$	$[0 - P/T_S]$
Prediction horizon (h)	$h = \tau$	$h = \tau$

T_D and τ_{max}, and between P and τ_{max}. The linear relationship fit to the curve is shown in Equation 7.1, and plotted in Figure 7.6.

$$T_s * \hat{\tau}_{max} = 0.33P + 0.53T_D + 0.66 \tag{7.1}$$

Note that in Figure 7.6, the dimensions of all three axes are in minutes, with a constant sampling time of 0.1 minutes. Therefore the left hand side of the equation incorporates the sampling time so that the dimension of $\hat{\tau}_{max}$ is number of samples. This provides an empirical formula for selection the time interval (τ) and prediction horizon (h) based on the time delay and oscillation period of the trends being analysed using transfer entropy. The R^2 value for this fit was 0.56. Although this is a low value, the fit is adequate to provide guidelines for the selection of the parameters. This will be tested in Section 7.5, where this formula will be used for parameter selection.

The distance between the repeating peaks of the time interval in Figure 7.4 varied according to the value of the oscillation period. Figure 7.7 plots the peak distance against oscillation period (P). The linear model fit to this response had a slope of 0.5. This suggests aliasing that can be explained by Shannon's sampling theorem. When the time interval (τ) is shifted by half a period, the reconstruction of the data represents an oscillatory trend once again. If it was desired to search multiple values for the optimal τ, this result can be used to limit the search space for the optimal τ to one whole period, $[0 - P]$, since the optimum τ_{max} would be in that range. To make this generalisable to any sampling time, this can be adjusted to make τ's dimensions in

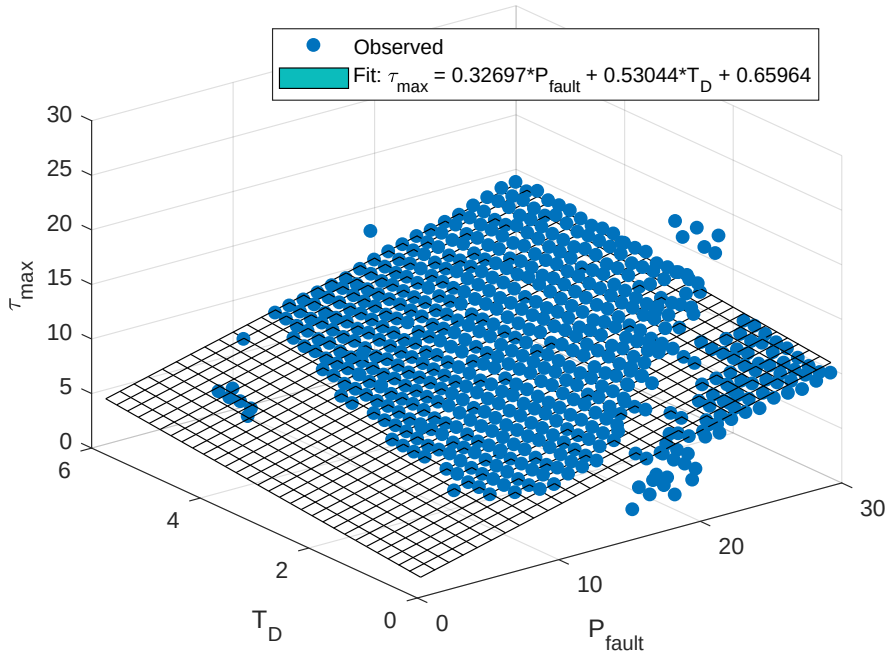

FIGURE 7.6: *Linear relationship between oscillation period (P) and time delay (T_D), and optimal time interval (τ_{max}). $R^2 = 0.56$*

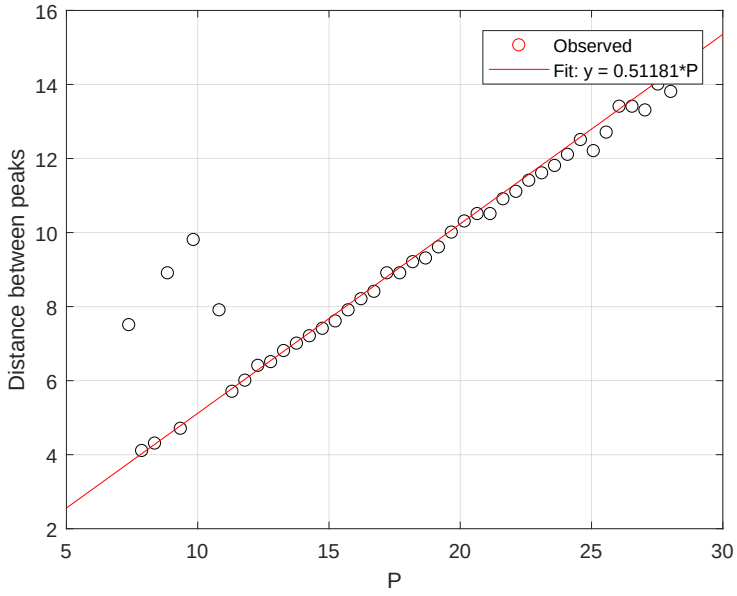

FIGURE 7.7: *Linear relationship between P and distance between τ peaks. $R^2 = 0.82$*

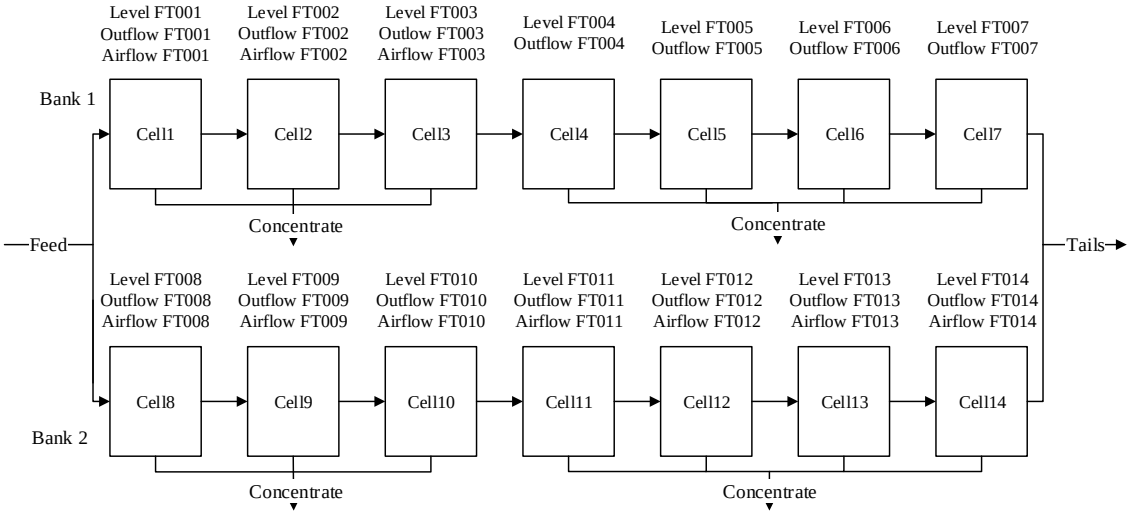

FIGURE 7.8: *Simplified process flow diagram of flotation circuit under consideration. Two banks of seven flotation cells in series make up the circuit.*

7.5 Demonstrating workflow on real case study

The workflow outlined in Figure 7.1, implemented with the guidelines for parametrisation outlined in Table 7.1, was applied to an industrial case study of a plant-wide oscillation in a mineral concentrator plant flotation circuit. This case study was used in Chapter 4.

To provide context for this case study the flotation circuit operation and control is described here. Flotation is used to separate valuable mineral particles from gangue particles in a concentrator process. This is achieved by selectively imposing hydrophobicity on the valuable mineral particles, causing the valuable particles to attach to air bubbles and float to the top of the cell [Wills, 2007] A simplified process flow diagram of the flotation circuit under consideration is shown in Figure 7.8. This flotation circuit consists two parallel banks, each with seven flotation cells in series. The concentrate from the first three cells of each bank are combined, and the concentrate from the last four cells are combined. The outflow (tails) from each cell flows into the subsequent cell. The final tails are combined and processed further in downstream units.

The following sections demonstrate the application of the developed workflow with the suggested parametrisation strategy.

7.5.1 Detect fault

In this case study the oscillation was observed during a post-hoc inspection of plant data. Oscillatory behaviour affecting a number of control loops were observed. The fault may also have been detected online using conventional oscillation detection strategies, such as the spectral envelope technique. This article focusses on the parametrisation of the diagnosis techniques employed after the fault has been detected. Therefore automated fault detection strategies are not discussed in further detail.

Figure 7.9 plots the levels (LI1 to LI7) and outflows (FC1 to FC7) from Bank 1 in the flotation circuit, which all showed the oscillatory trends. From inspection it was observed that the oscilla-

tion was transient. Before the oscillations appeared at 03:09:00 AM, and after they disappeared at 04:40:00 AM, the levels were stable well controlled around their set-points. The oscillation persisted for roughly 1H30MIN. All the measured variables showing oscillatory trends were localised to the flotation section of the plant. Therefore all measured variables in this section were selected for further analysis. This included all level, outflow, and airflow measurements. This amounted to 38 variables.

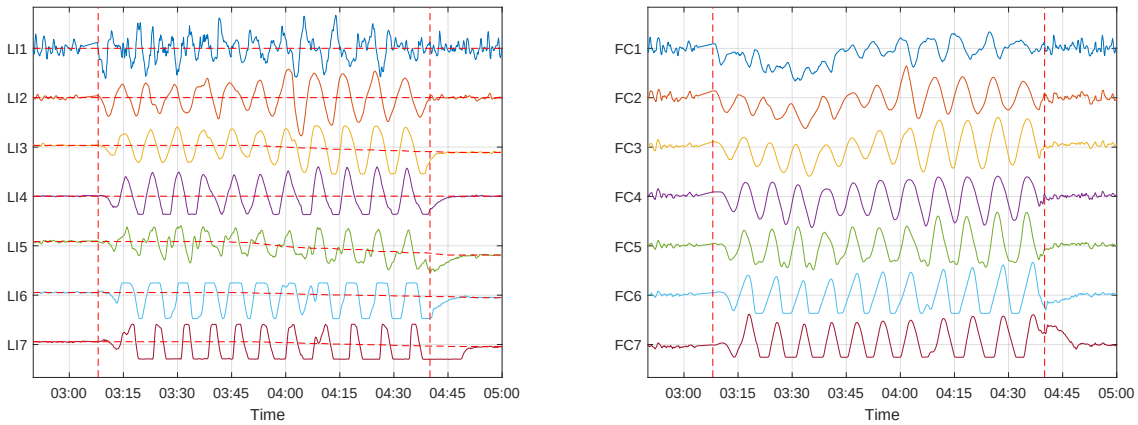

(a) *Bank 1 levels. Red lines indicates set-points.*

(b) *Bank 1 outflows.*

Figure 7.9: *Circuit variables showing oscillatory behaviour. Vertical dashed lines indicate onset and end of oscillations.*

- **Fault duration:** 03:09:00 AM to 04:40:00 AM, duration of 1H30MIN
- **Possible suspect variables:** All level, outflow, and airflow measurements in the flotation circuit.

7.5.2 Perform spectral analysis (optional)

Once the oscillation has been detected, additional information on the nature of the oscillation may be discerned using spectral analysis. Using the fast-Fourier transform to find the peak oscillation frequencies it was observed that a number of the selected trends displayed a common oscillation frequency of 0.00215 Hz (a period of 465 s).To illustrate this, the power spectrum for LI2 is plotted in Figure 7.10.

The variables that shared this oscillation period were the levels and outflows in the first bank of the flotation circuit.

- **Oscillatory variables:** Variables with common oscillation period were all levels and outflows in bank 1.
- **Oscillation period:** $P = 465s$.

7.5.3 Select data for transfer entropy

The suspect variables were identified in Section 7.5.2 as all the outflow and level variables in Bank 1. The outflows are the manipulated variables (MVs) for the levels, which are the controlled

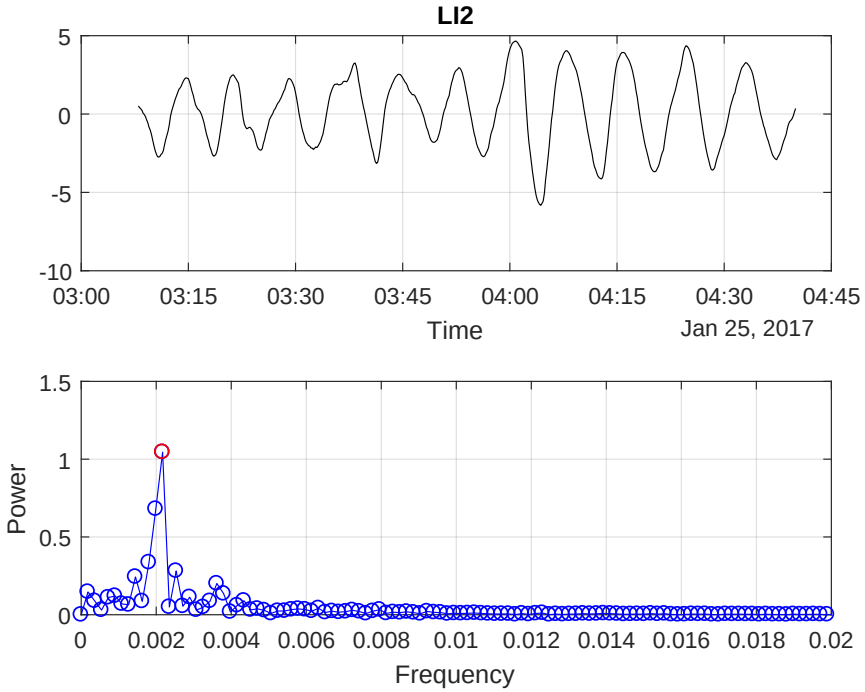

FIGURE 7.10: *Oscillatory trend for LI2 with power spectra showing peak frequency corresponding to oscillation.*

variables (CVs). The oscillation should propagate in the same way through the MVs and CVs. Therefore it was decided to analyse the outflows and levels separately to see if they showed similar propagation paths through the flotation circuit. The sampling time of the data obtained from the data historian was $10s$. In Section 7.5.1 the duration of the oscillation was found to be 1H30MIN, which is equal to 540 samples. This is very close to the minimum number of samples suggested. Subsampling to decrease the number of samples is unnecessary. Therefore the sampling time and the number of samples is kept the same.

- **Sampling time:** $T_S = 10s$.
- **Number of samples:** $N_S = 540 samples$.
- **Suspect variables:** Levels and outflows in Bank 1.

7.5.4 Determine process dynamics (optional)

Suspect variables were narrowed down during the spectral analysis. For each pair of these variables system identification was performed to fit a first order plus time delay model. This basic model gave a rough estimate of the time constants of the time delays between the variables. The *System Identification Toolbox* in MATLAB was used to determine the time delay estimates for each pair of candidate variables. The function used evaluates an autoregressive exogenous (ARX) model structure for the input and output variables specified[Sderstrm, 1989]. The function the finds the time delay that provides the best fit for this model. The presence of a time delay itself might indicate a causal connection. However, as discussed in Section 2.9, inference of a causal connection requires both some indication of causal strength (e.g. in terms of uncertainty reduction for transfer entropy) and the presence of a time delay.

TABLE 7.3: *The time delay (T_D, in seconds) between level variables.*

	$LI1$	$LI2$	$LI3$	$LI4$	$LI5$	$LI6$	$LI7$
$LI1$	0	0	10	80	330	200	400
$LI2$	0	0	40	140	190	380	350
$LI3$	220	230	0	40	20	40	120
$LI4$	160	160	130	0	20	40	150
$LI5$	10	130	20	330	0	10	70
$LI6$	400	170	300	110	280	0	70
$LI7$	400	10	250	260	320	390	0

TABLE 7.4: *The time delay (T_D, in seconds) between outflow variables*

	$FC1$	$FC2$	$FC3$	$FC4$	$FC5$	$FC6$	$FC7$
$FC1$	0	0	10	180	240	10	320
$FC2$	400	0	0	20	10	190	10
$FC3$	240	240	0	50	40	10	20
$FC4$	140	250	0	0	0	10	120
$FC5$	120	130	270	50	0	0	50
$FC6$	300	200	90	0	230	0	330
$FC7$	320	30	120	0	260	290	0

- **Time delay for levels:** The time delay (T_D, in seconds) between each pair of level variables is shown in Table 7.3.
- **Time delay for outflow:** The time delay (T_D, in seconds) between each pair of outflow variables is shown in Table 7.4.

7.5.5 Select parameters for transfer entropy

The time delay and the oscillation period can be used to get parameters for transfer entropy, using the relations obtained in Section 7.4, and presented in Table 7.1.

- **Embedding dimension for input:** $K = 1$.
- **Embedding dimension for output:** $L = 2$.
- **Time interval:** The time interval can be calculated from T_D and P using Equation 7.1. The time interval (τ, in number of samples) for each pair of level variables is shown in Table 7.5. The time interval for each pair of outflow variables is shown in Table 7.6.
- **Prediction horizon:** $H = \tau$.

7.5.6 Perform transfer entropy analysis

Once all the parameters have been selected for each pair of variables the transfer entropy analysis can be performed. The propagation paths shown in Figure 7.11 were obtained. The propagation

TABLE 7.5: *The time interval (τ, in number of samples) between level variables*

	$LI1$	$LI2$	$LI3$	$LI4$	$LI5$	$LI6$	$LI7$
$LI1$	–	15	15	19	32	25	36
$LI2$	15	–	17	22	25	35	33
$LI3$	26	27	–	17	16	17	21
$LI4$	23	23	22	–	16	17	23
$LI5$	15	22	16	32	–	15	18
$LI6$	36	24	31	21	30	–	18
$LI7$	36	15	28	29	32	35	–

TABLE 7.6: *The selected time interval (τ, in number of samples) between outflow variables*

	$FC1$	$FC2$	$FC3$	$FC4$	$FC5$	$FC6$	$FC7$
$FC1$	–	15	15	24	27	15	32
$FC2$	36	–	15	16	15	25	15
$FC3$	27	27	–	17	17	15	16
$FC4$	22	28	15	–	15	15	21
$FC5$	21	22	29	17	–	15	17
$FC6$	31	25	20	15	27	–	32
$FC7$	32	16	21	15	29	30	–

path for the level variables (Figure 7.11a) shows the oscillation propagating from the first cells to the last cells in the circuit. The connection from Cell 5 to Cell 2 contradicts this flow path. Figure 7.9a shows that the trend for LI5 is highly nonlinear, which may have resulted in spurious connections. The connectivity obtained is sparse, with no connections to Cell 4 and Cell 7. The propagation path for the outflow variables (Figure 7.11b) shows more direct connections from Cell 1 to Cell 6 and Cell 7. The propagation paths do indicate an oscillation originating in the first cells and propagating through to the last cells in the circuit. The two propagation paths are consistent with each other. Some further analysis incorporating process knowledge may be used to validate the propagation paths obtained. Further analysis is also necessary to discern more details of the cause of the oscillation.

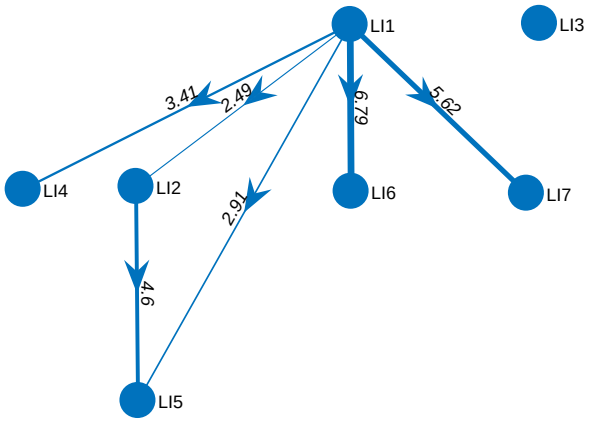

(a) *Propagation path for Bank 1 levels.*

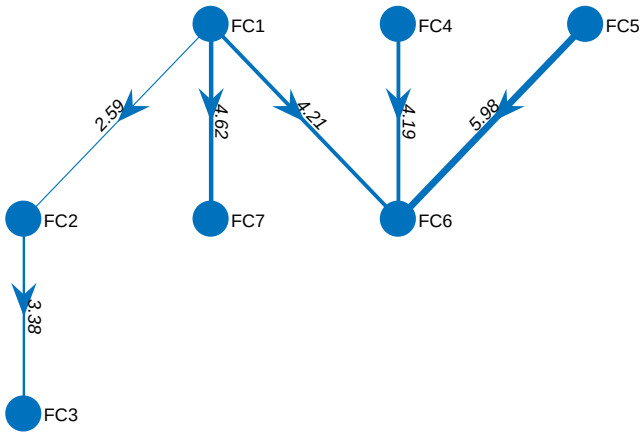

(b) *Propagation path for Bank 1 outflows*

Figure 7.11: *Propagation paths for oscillations in the flotation circuit. Values displayed on edges represent the transfer entropy value calculated.*

TABLE 7.7: *Start times of oscillations, indicating sequence of propagation.*

Variable	Start time [hh:mm:ss]
LI1	03:10:00
LI2	03:11:00
LI3	03:11:50
LI4	03:12:10
LI5	03:12:20
LI6	03:13:10
LI7	03:13:00

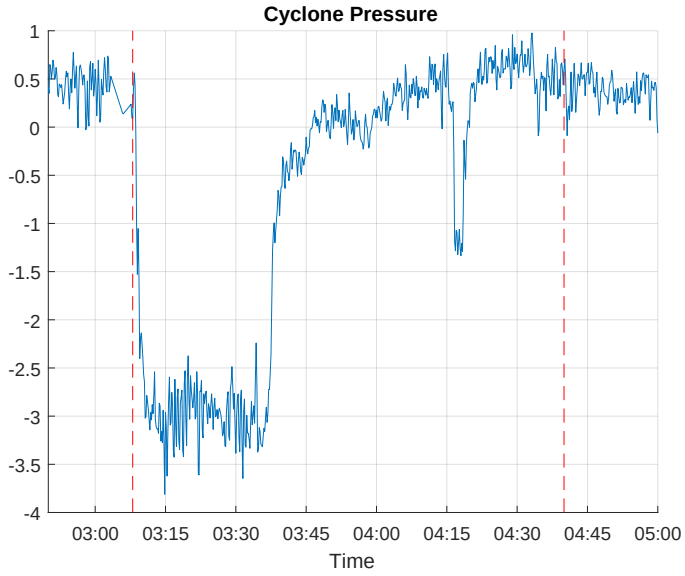

FIGURE 7.12: *Cyclone pressure just upstream of flotation circuit showing sharp dip at oscillation start at time 03:08:00.*

An oscillation takes time to propagate through the process, due to the dynamics of the process occurring in the cells. The sequence of the oscillation propagation may give further insight into the propagation path. To establish the sequence in which the oscillations appear in the cells, the trends for the levels were analysed to find local maxima corresponding to oscillation peaks. The locations of the first peak for each trend were used to establish the sequence of appearance of the oscillations. The first peak times are shown in Table 7.7. The first peaks are in mostly sequential order from the first cell to the last cell. One exception is that LI7 appears to precede LI6. However, since the difference is only one sample (with the sampling time at 10 seconds), it is difficult to determine which was first. The sequential order of the oscillations from the first cells to the last cells confirms the propagation path obtained from the transfer entropy results shown in Figure 4.5.

Data-based diagnosis techniques have an inherent limitation in that they can only point to variables associated with the root cause of the fault. Further analysis is needed to determine what caused the oscillation to manifest in that variable. Considering the unit just upstream of this flotation circuit, it was observed that the cyclone pressure decreased sharply just before the onset of the oscillation, as shown in Figure 7.12. This sudden upset may have caused the levels of the first cell (LI1) to deviate from their set-points.

Both the supervisory and optimisation advanced process control (APC) and the multivariable level controller usually present in the circuit [Muller *et al.*, 2010] were switched off for the duration of the oscillation. Only the base layer PID control, regulating the cell levels using the outflows from the cells, was operational. This indicates that the regulatory control was unable to correct for the deviation in LI1. Poor controller tuning may have caused the levels to become unstable. The absence of the multivariable controller allowed the resulting oscillations to propagate unhindered throughout the circuit. After the oscillations had persisted for some time, the supervisory control level was enabled again to compensate for the oscillations by gradually changing the set points of the levels. This compensation was ineffective at first, but when the multivariable level controller was turned on again, the circuit quickly returned to stable operation. This indicates that the multivariable controller is very effective at rejecting oscillations.

To summarise the findings of this oscillation diagnosis: transfer entropy indicated that the oscillation originated in Cell 1. This was confirmed by observing the sequence in which the oscillations appeared in each cell. A cyclone immediately upstream of the cells where the oscillation originated showed a sharp decrease in pressure. This pressure drop caused a flow disruption to the flotation banks, causing deviation of LI1 from its set points. Suboptimal controller tuning may have resulted in the inability of the control to correct for these deviations, allowing the oscillation to propagate through the circuit. Therefore the corrective action identified by this analysis was to retune the base layer control.

7.6 Chapter conclusion

A systematic workflow for the application of transfer entropy for oscillation diagnosis was developed. This workflow exploited the relationships between the underlying process dynamics and the parameters required for calculation of transfer entropy to establish guidelines for parameter selection. The guidelines obtained from this investigation are summarised in Table 7.1. A significant contribution from the investigation of these relationships was that a linear relationship could be fit to predict the optimal time interval given the oscillation period and time delay. This provides an empirical relationship for selecting the time interval based on process dynamics.

The workflow using the developed guidelines was applied to an oscillation diagnosis case study from a minerals concentrator plant. The workflow provided a systematic approach to accurately determining the fault propagation path. Although the workflow presented here focussed on transfer entropy, other causality analysis techniques can be substituted in transfer entropy's place. The only caveat is that the parametrisation procedure would be different. Substituting Granger causality, for example, would simply require that the AIC be used to select the model order.

Now that the workflow for application of causality analysis has been laid out, the next component required for application of causality analysis for fault diagnosis is to decide which method to use. Chapter 8 presents a comparative analysis of Granger causality and transfer entropy, based on the criteria outlined in Chapter 5. This comparison is used to provide guidelines for which technique to select.

CHAPTER 8

Comparative analysis between transfer entropy and Granger causality

Contents

8.1 Chapter introduction . . . 111
8.2 Chapter objectives . . . 112
8.3 Comparing the features of Granger causality and transfer entropy . . . 113
8.3.1 Accuracy and precision of causality analysis techniques . . . 113
8.3.2 Automatability of causality analysis techniques . . . 113
8.3.3 Interpretability of causality analysis techniques . . . 114
8.3.4 Computational complexity of causality analysis . . . 115
8.3.5 Applicability for different process characteristics . . . 116
8.4 Comparing the accuracy and precision of Granger causality and transfer entropy in a simulated system . . . 117
8.4.1 Description of simulated process case study . . . 117
8.4.2 Comparison of Granger causality and transfer entropy to ground truth in simulated case study . . . 118
8.4.3 Summary of simulated case study comparing Granger causality and transfer entropy . . . 122
8.5 Decision flow for application of Granger causality or transfer entropy . . . 122
8.6 Illustrating the features of Granger causality and transfer entropy on an industrial case study . . . 124
8.6.1 Case study description . . . 124
8.6.2 Transfer entropy results . . . 125
8.6.3 Granger causality results . . . 128
8.6.4 Summarising the difference between Granger causality and transfer entropy for the industrial case study . . . 129
8.7 Chapter conclusion . . . 130

8.1 Chapter introduction

A version of this chapter has been submitted for publication: Lindner B, Auret L, Bauer M & Groenewald JWD, Comparative analysis of Granger causality and transfer entropy to present

a decision flow for the application of oscillation diagnosis. Manuscript accepted pending major revisions for publication to Journal of Process Control.

Up to this point in the dissertation, a number of variations of causality analysis have been introduced. Chapter 5 highlighted the desired characteristics of causality analysis techniques, and pointed out that automated, or at least systematic application of the techniques can remove ambiguity in the results. Chapter 7 presented a workflow for the application of transfer entropy to address the need for a systematic application procedure. Although this workflow is catered for transfer entropy, Granger causality could be substituted in its place. However, the decision of which causality analysis technique to use has not been addressed.

Duan *et al.* [2014] demonstrated and compared different techniques for root cause diagnosis of plant wide oscillations. Granger causality and transfer entropy were the data-based causality analysis techniques they compared, and some of their advantages and disadvantages were listed. They found that Granger causality is easier to implement, robust to data selection, has low computational burden, and its application techniques are well developed. However, it is only suitable for linear relationships between variables, and may be prone to model misspecification. They also found that transfer entropy is robust to data selection, and suitable for both linear and nonlinear relationships. However, it is sensitive to calculation parameter selection, difficult to implement, and the computational burden is large.

Kuhnert [2013] provided guidelines for technique selection based on process characteristics. However, the guidelines were based on simulated experiments, and only the accuracy of the techniques was considered. Investigation of other factors is important. This study and the one by Duan *et al.* [2014] both show that the different methods have varying strengths and weaknesses, and each may be uniquely suited to different applications.

A comparative analysis of different techniques can be used to provide guidelines for which technique to select. The point of departure for this comparative analysis is can be to compare the two most popular techniques identified in Section 2.11, Granger causality and transfer entropy. Their wide-spread application in literature means that these transfer entropy and Granger causality are mature techniques. This chapter compares transfer entropy and Granger causality based on their accuracy, precision, automatability, interpretability, computational complexity, and applicability for different process characteristics. Based on this comparison, a decision flow is presented, to aid engineers in deciding which technique to use and how to interpret the results.

The outline of this Chapter is as follows: in Section 8.2 the objectives of this chapter are presented; in Section 8.3, the features of Granger causality and transfer entropy are compared; in Section 8.4, the accuracy and precision of Granger causality and transfer entropy are tested and compared using a simulated case study; in Section 8.5 the decision flow for application of Granger causality or transfer entropy based on the findings of the paper are presented; in Section 8.6, the features and the presented decision flow are illustrated on an industrial case study of a plant-wide oscillation; finally, in Section 8.7, the conclusions of the paper are presented.

8.2 Chapter objectives

The objectives of this chapter are:

I To *compare* the features of Granger causality and transfer entropy.

II To *develop* a decision flow to aid engineers in choosing between transfer entropy and Granger causality.

III To *demonstrate* the features of Granger causality and transfer entropy in am industrial case study and illustrate the use of the decision flow.

8.3 Comparing the features of Granger causality and transfer entropy

Deciding between the numerous causality analysis approaches can be difficult. Different literature sources may advocate different techniques. Each technique has its own strengths and weaknesses, without clear guidelines for when they are appropriate. The desired characteristics of causality analysis techniques were discussed in Chapter 5. In this section, the features of Granger causality and transfer entropy are compared based on those characteristics, namely: accuracy and precision; automatability; interpretability; computational complexity; applicability for different process characteristics.

8.3.1 Accuracy and precision of causality analysis techniques

Causality analysis is considered accurate when the method was able to identify the correct root cause of the fault. The method can be deemed useful if the corrective action suggested by the root cause analysis successfully removes the fault.

Uncertainty in process measurements means that non-zero transfer entropy and Granger causality values will be calculated even when there is no causal relationship. As mentioned in Section 2.12.3, a hypothesis test is needed to determine the statistical significance of the values. However, this significance test is not infallible, and spurious connections may still be found. These spurious connections make analysis of fault propagation paths difficult. Spurious connections give a false representation of the propagation path of the fault. The reverse is also true, real causal connections might be missed because of this uncertainty.

The validity of individual causal connections can be scrutinised to evaluate the method's accuracy. Spurious and missing connections may also occur due to the limiting assumptions discussed in Section 5.3.5. For example, if Granger causality was used to calculate causality in a process with nonlinear behaviour, the linear regression model may not be able to capture the nonlinear process dynamics and the causal connection may be missed. Non-stationarity in the time series could cause spurious connections for both techniques. See Section 5.4.4 for a more detailed discussion of nonlinearity and stationarity.

When the ground truth causality is known, one can quantify the missed connection rate, true connection rate, and the false connection rate. Accuracy is defined by a high true connection rate and a low false and missed connection rates. Precision can be defined by how consistently the method finds the connections.

Section 8.4 evaluates the accuracy and precision of Granger causality and transfer entropy by testing them on a simulated system.

8.3.2 Automatability of causality analysis techniques

Application of causality analysis techniques is complex, with numerous parameters to select. The more automated the application procedure is, the less ambiguity there will be in the results. Reduced ambiguity will inspire confidence that the results of the causality analysis reflect the behaviour of the process.

Granger causality is an easily automatable technique. The model order, k, in Equation 2.4, and the α value for the F-test are the only hyper-parameters to select. The optimal k can be selected as the one that minimises the Akaike information criteria (AIC) [Bressler & Seth, 2011].

Parameter selection for transfer entropy is more complicated. Equation 2.7 shows that four parameters need to be selected, K, L, h, and τ. The transfer entropy results are sensitive to these parameters [Duan *et al.*, 2014]. This was confirmed in Chapter 7. Parameter search procedures are typically employed [Duan *et al.*, 2013, Naghoosi *et al.*, 2013], but are computationally expensive and therefore difficult to implement. Many researchers use the default parameters suggested by Bauer *et al.* [2007a]. Chapter 7 presented a systematic, automated workflow for application of transfer entropy for oscillation diagnosis. This workflow presents guidelines for calculation parameter selection based on process dynamics, namely the time delay between variables and the oscillation frequency. Additionally, clear guidelines were given for each step in the application procedure. This systematic workflow can also be modified to replace transfer entropy with Granger causality. The workflow allows automatic selection of all hyper-parameters, k for Granger causality, and τ, h, K, and L for transfer entropy. Therefore both Granger causality and transfer entropy are automatable according to the definition given in Section 5.3.2.

8.3.3 Interpretability of causality analysis techniques

Fault diagnosis techniques are used by engineers to gain insight into abnormal behaviour occurring within a process. This engineer has to interpret the causal map to see whether a clear propagation path is manifested. It is important that the engineer can understand the information presented simply, and understand the implications. For example, when a spurious connection passes the significance test because of excessive noise in the signal, and is displayed on the causal map, the engineer will need to use process knowledge and understanding of the causal statistic to understand why that spurious connection was found.

This interpretation has two components: mathematical interpretation of the underlying causal statistic; and visual interpretation of the causality maps.

Mathematical interpretation

For both Granger causality and transfer entropy, the causal statistics are not directly linked to any physical engineering quantity. However, it is easier to reason about the Granger causality since it is based on simple regression statistics. The significance test, the F-test, is also based on a known distribution. The information theory used for transfer entropy is more complicated, and interpretation of the values obtained is not straightforward. Furthermore, the significance test based on Monte Carlo simulations used for transfer entropy is more difficult to interpret than that based on a known distribution used for Granger causality.

Visual interpretation

The end result of the causality analysis is a causality map. When this causality map gives a clear indication of the propagation path that is logically consistent with process knowledge, then the variables at the start of the propagation path can be further investigated. When the suggested propagation path is ambiguous it may be uncertain what the root cause was. There may be more than one suggested propagation path in the causal map pointing to different root cause variables. In the case where these different root cause variables are associated with the same

unit in the plant, or the same controller, then it can be inferred that the root cause is closely associated with that unit and can be investigated. When there are multiple root causes all associated with different units, or sections of the plant, then the root cause is more ambiguous. In this scenario it is possible that multiple faults are occurring simultaneously[Chiang *et al.*, 2015]. However, a simplifying assumption that only one fault occurs at any time is applied, since the probability of occurrence of simultaneous independent faults is small, as suggested by [Shiozaki *et al.*, 1985].

All causal effects in a system are identifiable when the causal map is acyclic [Pearl, 2009]. Cyclical causal maps, where each node is reachable from any other node[Bang-Jensen, 2010], show no clear start or end nodes, and therefore give no clear indication of where to further investigate the fault.

Because this interpretation is complicated, the decision flow presented in Section 8.5 provides steps for dealing with ambiguous root causes.

The visual interpretability of the causality maps for either Granger causality or transfer entropy will be a function of the accuracy of the method. Large amounts of spurious connections will make it difficult to interpret the causal map. The visual interpretability will also be affected by the complexity of the system which the causal map represents. However, visualisation tools described in Chapter 9 can be applied to the causality maps from either technique to aid with visual interpretation.

8.3.4 Computational complexity of causality analysis

Transfer entropy is a computationally expensive technique. Duan [2014] derived the computational complexity for transfer entropy as $O(N^2(K+L)^2)$, where K and L represent the embedding dimensions chosen, and N represents the number of samples. In Chapter 7 the suggested values were $K = 1$ and $L = 2$ to limit the computational complexity. These calculations are repeated when the significance calculations are performed.

For Granger causality the core calculation is the least squares regression of the $N \times Mk$ matrix, where k is the model order, N is the number of samples, and M is the number of variables. This distils to a $O(M^3k^3N)$ problem for a specific model order, k. This is repeated for a range of model orders that cover the time spans common in processes. For most chemical and mineral processes, the unit residence times are at most of the order of a few minutes[Wills, 2007]. Therefore, at a sampling time of around 10s, which is common for data historians, the range of model orders is typically from $k = 1 : 30$. The typical values for M depend on the size of the plant being monitored and the problem being analysed. However, typical values are between 10 and 30 variables. The typical values for N range from a minimum of 500 samples [Bauer *et al.*, 2007a], to arbitrarily large numbers of samples. However, around 2000 samples is common.

To generalise the computational time required to perform the significance threshold calculations for transfer entropy, the time taken taken for a single pair of variables was calculated while varying the number of samples. The computational time as a function of the number of samples could then be obtained. It must be noted that it was not attempted to optimise the transfer entropy code used for this analysis, apart from the use of parallel computation. More mature toolboxes for transfer entropy, such as JIDT [Lizier, 2014], may provide faster computation time.

Figure 8.1 shows the computational time required to calculate the significance threshold for a single pair of variables, for 100 surrogates, as a function of the number of samples. The computational time was found to be a power law function of the number of samples, $CPU_{time} = 34 \times N^{0.5}$. The relative transfer entropy method method was used (Equation 2.5), which is

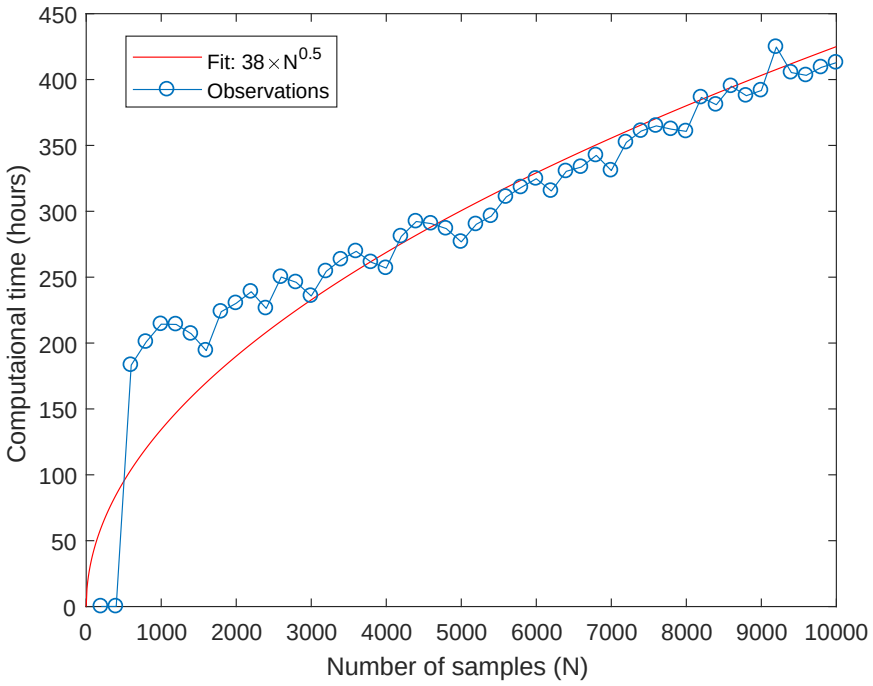

FIGURE 8.1: *Computational time required to calculate transfer entropy significance for one pair of variables as a function of number of samples. System used: 32 GB RAM, 3.33 GHz processor. The computational time was found to be well approximated by* $CPU_{time} = 34 \times N^{0.5}$

symmetrical, and self pairs are ignored, so this has to be repeated $(M^2 - M)/2$ times. The calculation of the PDFs is a very parallel problem, and therefore it can be assumed that doubling the amount of cores halves the computational time. This is a simplifying assumption that ignores some of the inefficiencies that are introduced by splitting iterations among parallel workers. Therefore, a rough estimate of the amount of time taken for the calculation of transfer entropy is given by Equation 8.1.

$$CPU_{time} = \frac{34 \times N^{0.5}(M^2 - M) \times N_{cores}}{2} \tag{8.1}$$

The computational complexity for transfer entropy is higher than that for Granger causality. The decision flow in Section 8.5 therefore incorporates a preliminary complexity analysis, to decide whether the time it will take to compute transfer entropy is excessive or not. What amount of time is considered excessive depends on the situation. Online, automated fault diagnosis would require a solution within minutes. When the plant is experiencing an ongoing fault the engineer needs to isolate the root cause as fast as possible to return the plant to normal operation. On the other hand, when the analysis is being performed offline to gain more information about fault conditions that happened some time in the past, the engineer may not mind waiting a few hours for results.

8.3.5 Applicability for different process characteristics

The applicability of a causality analysis technique may be limited by the underlying assumptions of the calculations it is based on.

Granger causality incorporates linear regression, and may therefore be limited in its ability to capture nonlinear behaviour in time series trends. See Section 5.4.4 for a more detailed discussion of nonlinearity and stationarity. Transfer entropy is not limited by this linear model assumption. Many chemical and mineral processes are known to contain nonlinear interactions. Applying a nonlinearity identification technique may help decide whether Granger causality or transfer entropy is appropriate for the system under consideration. However, nonlinear systems often behave linearly over large-scale interactions [Bressler & Seth, 2011].

In industrial processes, control systems maintain process variables close to a desired operating region where the system behaviour typically remains linear. The fault affecting the process may have originated from nonlinear phenomena, such as valve stiction. In such cases the process acts as a mechanical low pass filter as the oscillation propagates to different variables[Thornhill, 2005]. The low-pass process dynamics remove the higher harmonics in the trends and destroy phase-coupling. This means that nonlinear behaviour is unlikely to be sustained in the process.

Although transfer entropy is not limited to linear systems, the joint PDFs need to be calculated for stationary time series. This means that the autocorrelation, mean, and variance of the time series are not a function of time [Girod, 2001]. Granger causality also assumes stationarity to calculate the regression coefficients.

Kuhnert [2013] presented guidelines for technique selection based on process characteristics. These guidelines were developed based on simulated experiments to determine which technique gave the most accurate results for different process characteristics. They found that transfer entropy was applicable for both linear and nonlinear systems, and applicable for systems with long dead time and short dead time between variables. They also found that Granger causality was only applicable for linear systems with short dead time between variables.

The fact that transfer entropy is applicable for nonlinear and linear systems, and that it is applicable for systems with long and short dead time between variables indicates that transfer entropy is more generally applicable than Granger causality.

8.4 Comparing the accuracy and precision of Granger causality and transfer entropy in a simulated system

To compare the accuracy and precision of Granger causality and transfer entropy, their ability to find true connections in a simulated process was tested. The causal maps obtained from Granger causality and transfer entropy were compared to the true causal map to classify edges as true connections, false connections, or indirect connections. Since the simulation added random noise to the signals, repeated measurements could be taken. The repeated measurements allowed the precision of each technique to be evaluated.

8.4.1 Description of simulated process case study

A simple process of two tanks in series with heat exchangers was simulated. Figure 8.2 shows a diagram of the process. The tank levels are controlled by the flow of cold water into the tank using PID controllers. The tank temperatures are controlled by the steam flow rate through the heating coils using PID controllers. Random noise was added to the signals to simulate noise in the process.

An oscillation was introduced in the cold water input temperature, T_{1in}. Figure 8.3 shows the oscillations in the signals from one of the repeated simulations. This oscillation would propagate

through the process from T_{1in} by first affecting the first tank's temperature T_1. The temperature controller would then change the steam flow rate, F_3, to compensate. The controller is unable to fully reject the input disturbance, the second tank's temperature, T_2, would also be affected. The second tank's temperature controller would then change the steam flow rate, F_4, to compensate. The actual propagation path of the oscillation is known, and can therefore be used as ground truth to compare the causal maps obtained from Granger causality and transfer entropy. This true propagation path is shown in Figure 8.5a.

This simulation was repeated 1000 times. Only the random noise added to the signals was altered between simulations, so the oscillation affecting the process remained the same.

8.4.2 Comparison of Granger causality and transfer entropy to ground truth in simulated case study

Granger causality and transfer entropy were used to analyse the signals from the two tank simulation to identify the propagation path of the oscillation. The resulting causality maps were compared to the true propagation path derived from first principles knowledge of the process, shown in Figure 8.5a. The edges in the causality maps were classified as true connections, false connections, or indirect connections. Indirect connections are defined when a causal connection is identified due to the influence of an intermediate variable. Accuracy metrics are defined as follows:

Definition 7. True connection rate (TCR): the fraction of causal connections in the true propagation path in the true propagation path that were detected using the data-based technique:

$$TCR = \frac{C_{detected,true}}{C_{knowledge}} \tag{8.2}$$

where $C_{detected,true}$ is the number of true causal connections found using the data-based technique, and $C_{knowledge}$ is the number of connections in the true propagation path. This is the opposite of the missing connection rate (MCR): $MCR = 1 - TCR$.

Definition 8. Relative true connection rate (RTCR): the fraction of total edges in the causality map that are true connections:

$$RTCR = \frac{C_{detetcted,true}}{C_{detected}} \tag{8.3}$$

where $C_{detected,true}$ is the number of true causal connections found, and $C_{detected}$ is the total number of detected connections. This is the opposite of the relative false connection rate (FCR): $FCR = 1 - RTCR$.

Table 8.1: *Means and standard deviations of true connection rates and relative true connection rate shown in Figure 8.4.*

	Transfer entropy	Granger causality
TCR Mean	50%	62%
TCR Standard deviation	1%	14%
RTCR Mean	75%	70%
RTCR Standard deviation	16%	16%

Figure 8.4 plots the distributions of the true connection rate and relative true connection rate for both Granger causality and transfer entropy for the 1000 repetitions. Table 8.1 shows the means and standard deviations obtained.

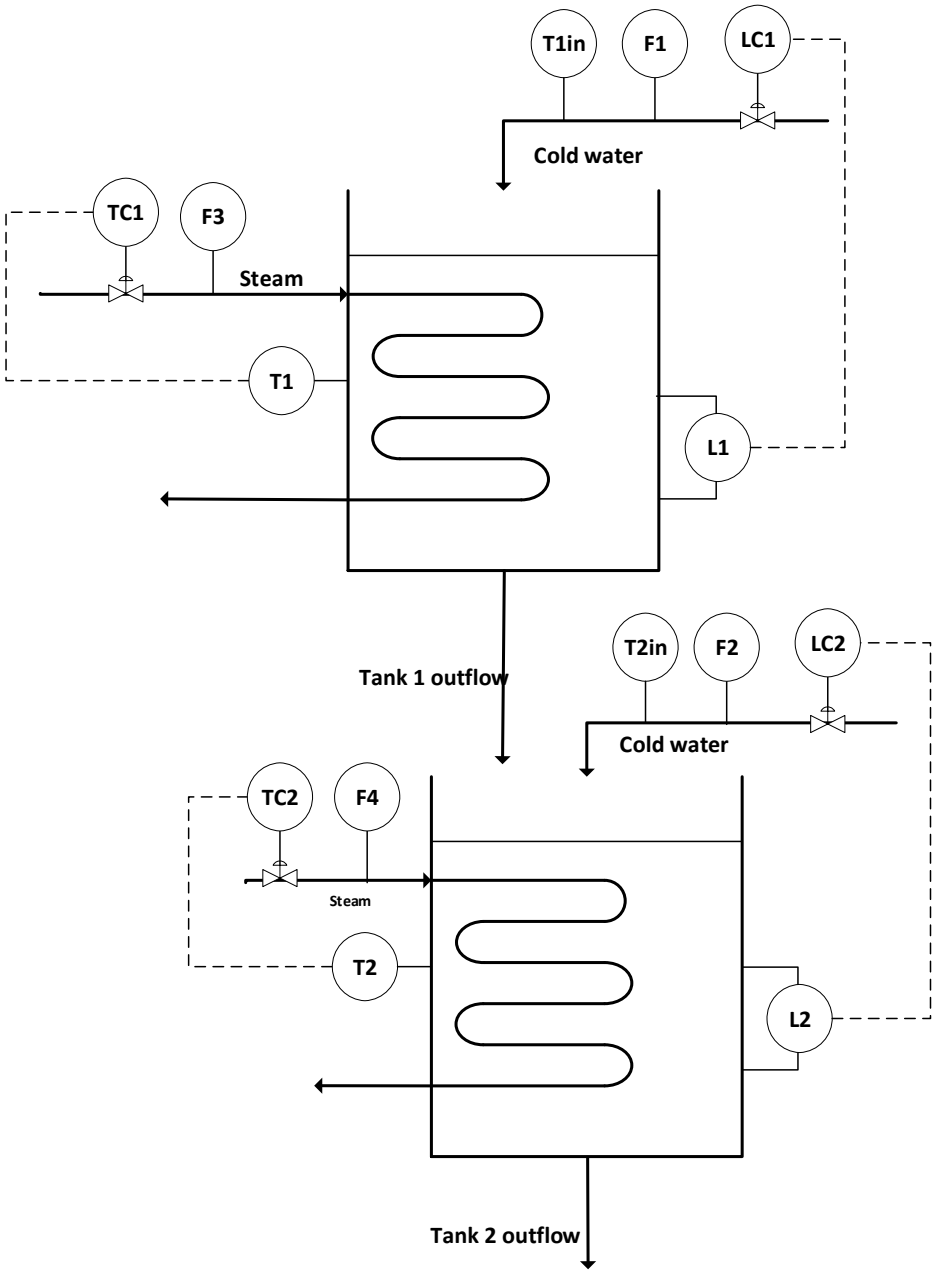

FIGURE 8.2: *Diagram of simulated two tank process. Two tanks in series with heat exchangers. Tank levels are controller by the flow of cold water into the tank, tank temperatures are controlled by the steam flow rate through the heating coils. Random noise was added to the signals.*

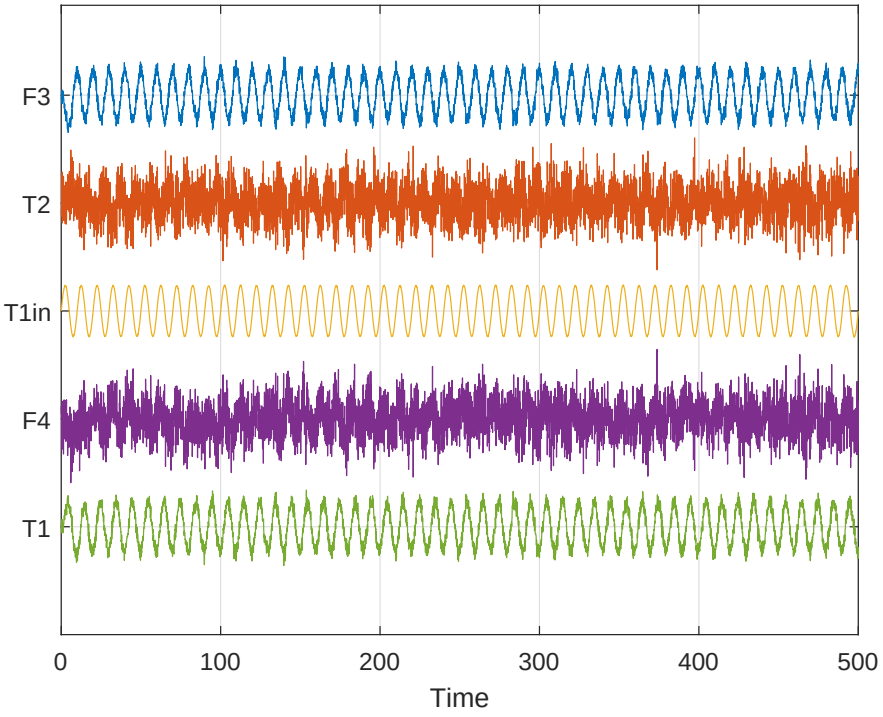

FIGURE 8.3: *Oscillations in signals in two tank process.*

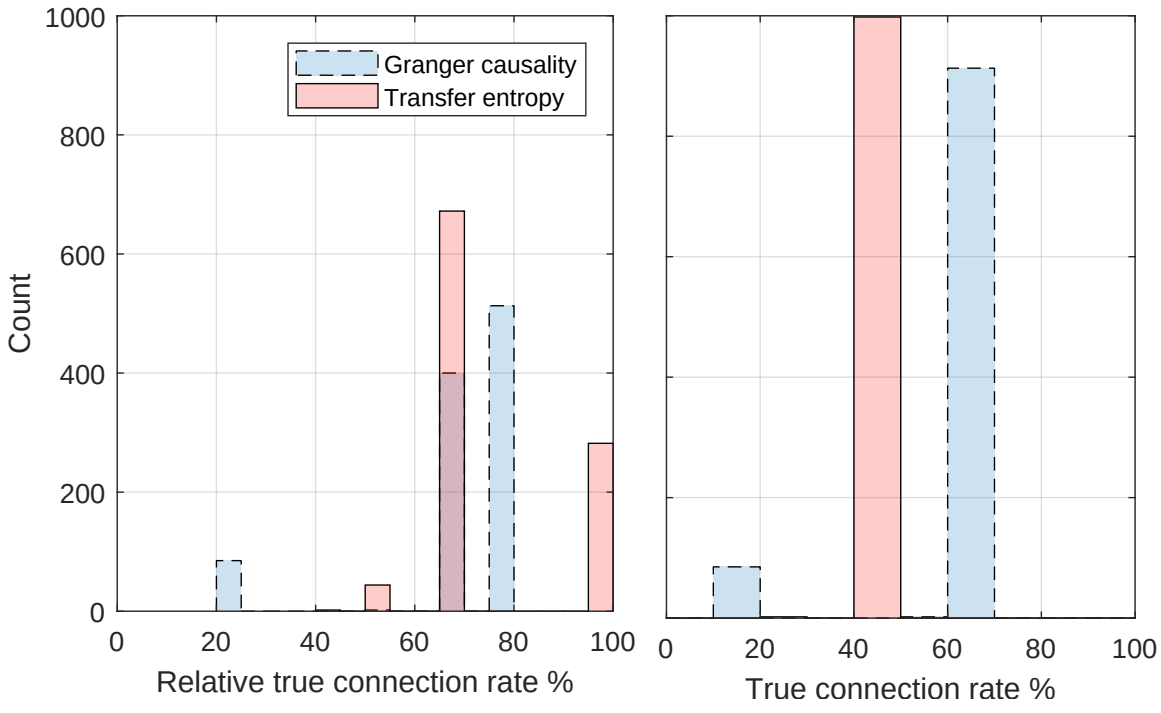

FIGURE 8.4: *Distributions of true connection rates and relative true connection rates for Granger causality and transfer entropy in the simulated two-tank process.*

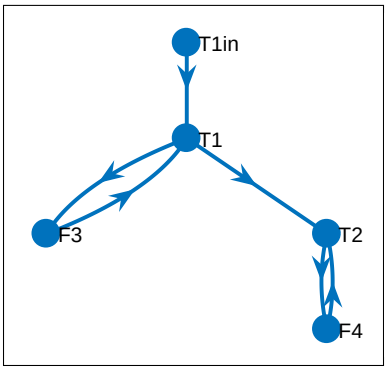

(a) *True propagation path*

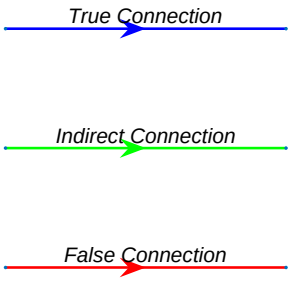

(b) *Legend*

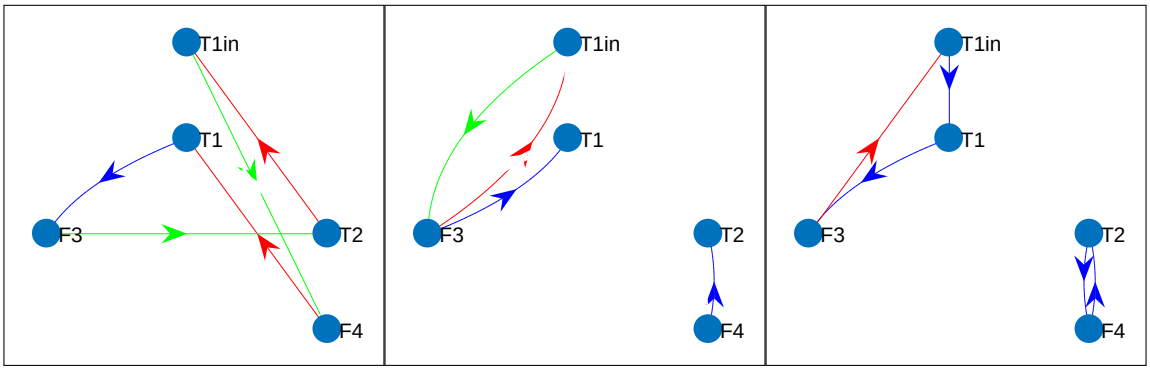

(c) *Granger causality minimum* (d) *Granger causality median* (e) *Granger causality maximum*

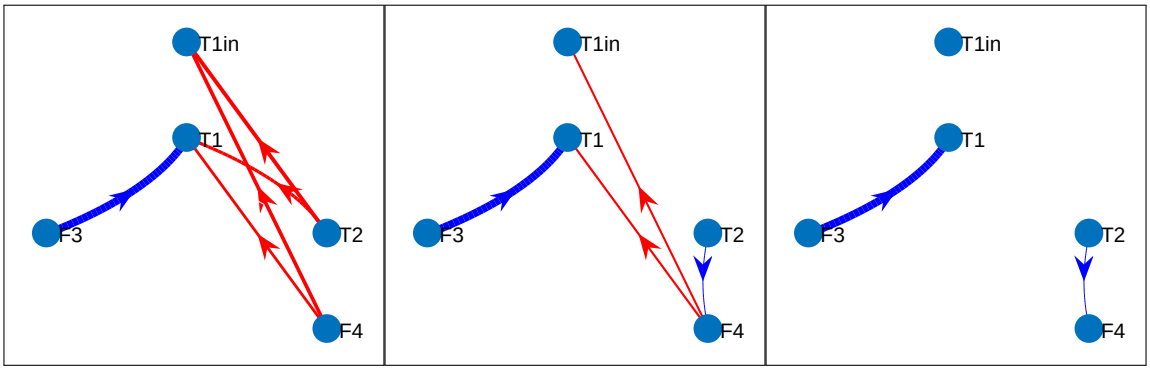

(f) *Transfer entropy minimum* (g) *Transfer entropy median* (h) *Transfer entropy maximum*

FIGURE 8.5: *Granger causality and transfer entropy results from repeated simulated experiments compared to true propagation path. Results shown from minimum, median, and maximum true connection rates.*

The means of the distributions indicate accuracy. Transfer entropy showed a higher mean RTCR, but a lower mean TCR. This indicates that although it doesn't find all the true connections, the connections that it does find are more likely to be true connections. The variance of the distributions give an indication of precision. The standard deviation for transfer entropy is very low for the TCR, and the standard deviations for the two techniques are almost identical for the RTCR. This indicates that transfer entropy is more precise than Granger causality.

Representative samples of the Granger causality and transfer entropy results are presented along with the true propagation path in Figure 8.5.

Granger causality consistently found strong connections related to the control connections between F_3 and T_1, and F_4 and T_2. In these control loop, T_1 and T_2 are the controlled variables (CV), and F_3 and F_4 are the manipulated variables (MV). This is because the introduction of the oscillation to the process causes excessive controller action, strengthening the causal relationship between its CV and MV. Transfer entropy also consistently found the control connection from F_4 to T_2. Transfer entropy consistently found the connection from $T_{1,in}$ to T_1. This connection shows the propagation from the input temperature.

Granger causality found indirect connections often. This means that some of the low RTCRs observed in Figure 8.4 are actually because indirect connections were not taken into account. For this system, transfer entropy did not find any indirect connections. Indirect connections may be considered to be misleading. Identifying all the direct connections along the propagation path of the oscillation will give insight into the symptoms and the root cause of the oscillation. However, indirect connections still provide this information at lower resolution, missing some connections along the way.

8.4.3 Summary of simulated case study comparing Granger causality and transfer entropy

Considering the relative true connection rates, transfer entropy was slightly more accurate. The standard deviations also indicated that transfer entropy was more precise. These results must be considered with caution. Simulated systems are useful for constructing controlled experiments and repeated experiments, but they can never fully replicate the common cause variation and complex interactions in real processes.

8.5 Decision flow for application of Granger causality or transfer entropy

Section 8.3 compared the features of Granger causality and transfer entropy. Section 8.4 then compared their accuracy and precision using simulated experiments. A decision flow was developed to aid users in deciding when to use Granger causality or transfer entropy, as well as to aid in the interpretation of the causality maps obtained from these techniques. This decision flow was developed from the comparisons in Sections 8.3 and 8.4, as well as from the experience of the authors using causality analysis for fault diagnosis. This decision flow is presented in Figure 8.6.

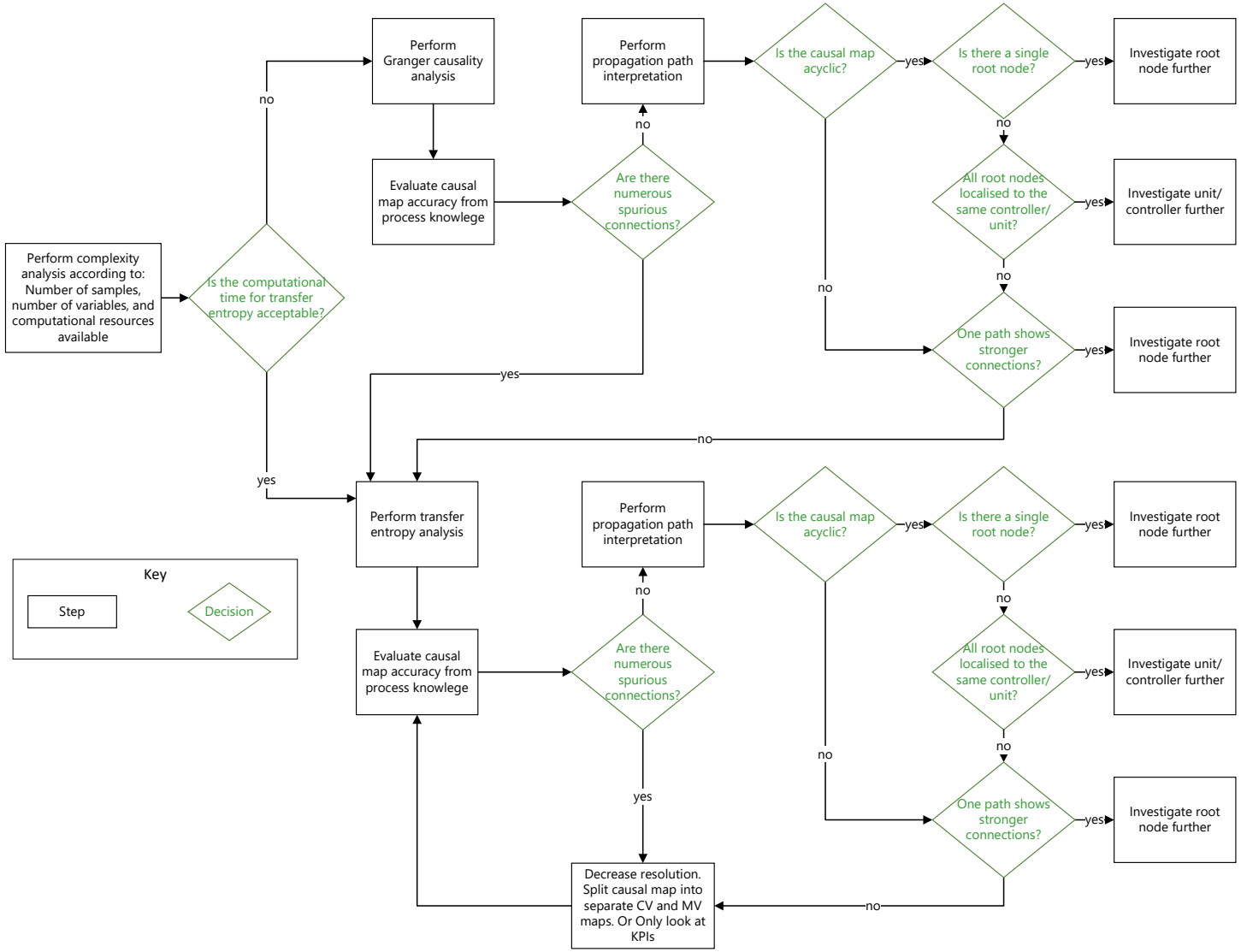

FIGURE 8.6: *Decision flow for application of Granger causality or transfer entropy for fault diagnosis.*

The first step is to perform a computational complexity analysis that takes into account the number of samples, the number of variables, and the computational resources available. Equation 8.1 can be used to estimate the calculation time required for transfer entropy. If the calculation time is acceptable, transfer entropy is preferred, since it has been found to be more accurate and precise and yields more visually interpretable causality maps, as demonstrated in Section 8.6. If the calculation time is unacceptably large, then Granger causality can be used. Granger causality analysis can be performed and the accuracy can be evaluated from process knowledge. If numerous spurious connections are observed then transfer entropy can be employed instead, since transfer entropy is more accurate. If not, the propagation path can be interpreted.

Interpretation of causal maps is complicated. The interpretation of the propagation path starts with determining whether the causal map is acyclic. An acyclic map has a definitive start node and end nodes, giving a clear suggestion of the sequence of nodes in the propagation path. When a cyclical map shows stronger connections for some of the edges it may still indicate important connections along the propagation path. When an acyclic map shows a single root node, this gives one possible root node that can be investigated further. Sometimes an acyclic map shows multiple root nodes. However, if all these nodes are localised to the same unit in the plant, or possibly to the same controller, this part of the plant can be investigated further. If there are multiple root nodes that are not related to a specific unit or controller in the plant, the strength of the connections may give an indication of which of the root nodes is most important. This node can then be investigated further.

If no definitive root cause is obtained from following the propagation path interpretation decision flow, then transfer entropy can be applied.

The same procedure is followed after performing the transfer entropy analysis. The causal map accuracy is evaluated from process knowledge. If numerous spurious connections are found, this time the resolution of the causal map can be decreased. This can be achieved separating the causal map into smaller groups of variables. For example, the map can be split to just contain controlled variables, or manipulated variables. This separation was applied in Chapter 4, and found to be effective. By reducing the resolution, the density of the graph, the number of edges per node, may be reduced and a propagation path may be more visible. After resolution reduction the evaluation can be performed again. If there are not numerous spurious connections, the propagation path interpretation can be performed. If no definitive root cause is obtained from following the propagation path interpretation decision flow, then the resolution reduction can be performed again.

8.6 Illustrating the features of Granger causality and transfer entropy on an industrial case study

To illustrate the features of Granger causality and transfer entropy discussed in Section 8.3, as well as to demonstrate the decision flow presented in Section 8.5, both techniques were used to analyse a plant wide oscillation in a mineral concentrator plant.

8.6.1 Case study description

A simplified flow diagram of the industrial process is shown in Figure 8.7. In the primary milling section, ore rocks are ground up to liberate the valuable minerals from the gangue (non-valuable) mineral. The ground up fines are sent to a sump, which is a surge tank where water is added to

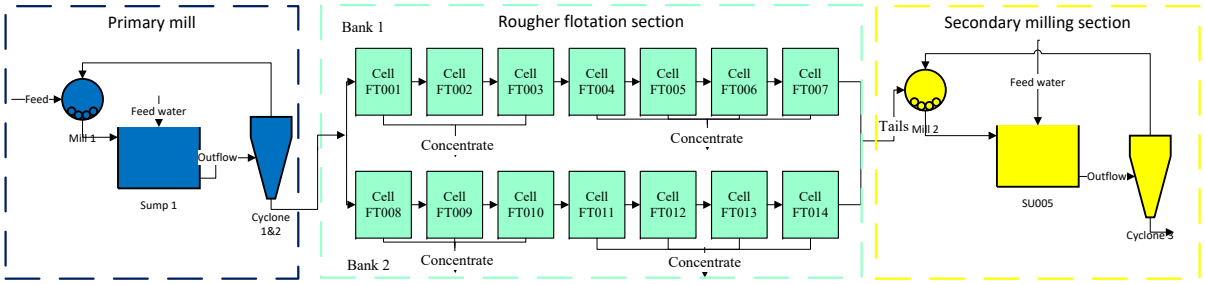

FIGURE 8.7: *Simplified process flow diagram showing the primary milling circuit, the rougher flotation section and the secondary milling section.*

control the level. The slurry is then sent to a hydrocyclone for separation. Oversized particles are recycled to the mill, while fine particles are sent to the flotation section. Flotation is used to separate the valuable and gangue particles, by selectively imposing hydrophobicity on the valuable mineral particles. This causes the valuable particles to attach to air bubbles and float to the top of the cell [Wills, 2007]. The final tails are combined and sent to the secondary milling circuit. The secondary milling circuit operates similarly to the primary milling circuit.

Oscillations were observed in the mass pull of the flotation circuit, which is an important key performance indicator (KPI), and is included in the advanced process control (APC) strategy of the flotation circuit. The mass pull is the proportion of the feed material reporting to the concentrate [Wills, 2007]. The oscillation persisted for 12h35min. The period of the oscillation in the mass pull signal was 69 min.

The root cause of the oscillation was uncertain from first inspection, because the variables used to control the mass pull, namely the flotation cell levels and the air addition to the cells, did not show abnormal trends. However, by analysing the frequency spectrum to find the peak oscillation frequencies, it was observed that 27 of the monitored variables displayed this shared oscillation frequency (see Appendix B). The time series trends of these variables are plotted in Figure 8.8. These variables are spread throughout three sections of the plant: the primary milling section; the flotation section; and the secondary milling section. Since the Primary Mill circuit is the first processing unit in the plant, it appears that the oscillation originated within that circuit. However, since the milling circuit contains a recycle stream, it is not apparent from first inspection which unit or controller was associated with the start off the oscillation. This makes it a useful case study for testing causality analysis techniques.

The workflow presented in Chapter 7 was followed to analyse this oscillation. This paper does not focus on the application procedure, but Appendix B presents the details.

8.6.2 Transfer entropy results

The causal map obtained from transfer entropy is shown in Figure 8.9.

Following the decision flow in Figure 8.6, the first step after performing transfer entropy is to evaluate the accuracy of the causal map by identifying whether there are spurious causal connections. This step requires knowledge of the process. To augment the causal map with process knowledge, the nodes in the causal map have been coloured according to which section of the plant they are located in. Blue indicates primary milling section, green indicates the flotation section, and yellow indicates the secondary milling section. The overall material flow of the plant, as shown in Figure 8.7, is from primary milling to flotation to secondary milling.

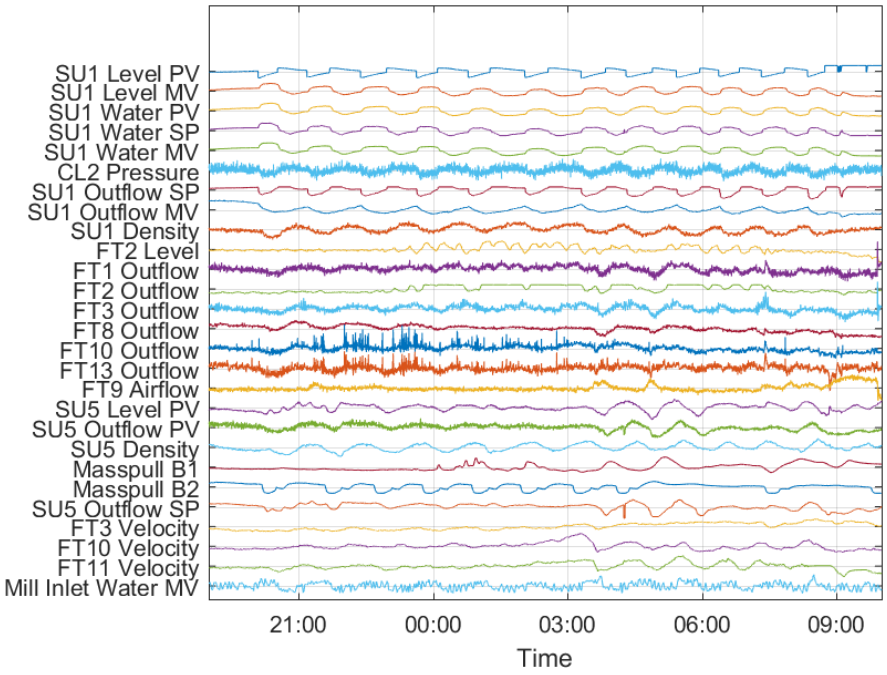

FIGURE 8.8: *Trends for all variables showing oscillation at period of 69 minutes. This includes variables from primary milling circuit, rougher flotation circuit, and secondary milling circuit.*

The causal map should generally reflect this flow, showing nodes going from blue to green to yellow, and not in the opposite direction. See 9.5 for a discussion about how to augment causal maps with node and edge attributes.

In the causal map shown in Figure 8.9, the only spurious connection is the causal connection from Cell 3's velocity ($FT3Velocity$) to Sump 1's outflow ($SU1OutflowMV$). The flotation cell, Cell 3, is downstream of Sump 1 in the process, and no controller interaction could account for this connection. This spurious connection is not on the propagation path from the other root nodes, Sump 1's water addition setpoint ($SU1WaterSP$) and Sump 1's level ($SU1LevelPV$). Therefore the spurious connection can be ignored without influencing the interpretation of the causal map.

The next step in the decision flow is to interpret the propagation paths in the causal map. The first question is, 'Is the graph acyclic?'. In this case the graph is acyclic, with visible start nodes, Sump 1's water addition setpoint ($SU1WaterSP$) and Sump 1's level ($SU1LevelPV$), and end node Sump 5's density ($SU5Density$). There is a cyclical section of the graph, between Sump 1's water addition MV ($SU1WaterMV$), Sump 1's outflow setpoint ($SU1OutflowSP$), and Sump 1's density ($DensitySU1$). However, this cycle does not interfere with the main propagation path between the root nodes Sump 1's water addition setpoint ($SU1WaterSP$) and Sump 1's level ($SU1LevelPV$) and the end node Sump 5's density ($SU5Density$).

The next question in the workflow is, 'Is there a single root cause variable?' The answer is no. The causal map suggests three possible root cause variables: Sump 1's water addition setpoint ($SU1WaterSP$), Cell 3's velocity ($FT3Velocity$), and Sump 1's level ($SU1LevelPV$). As described earlier, the connection from Cell 3's velocity to Sump 1's outflow is a spurious connection, and can be excluded from further analysis. This leaves two root cause variables The next question is, 'Are all the root nodes localised to the same controller/unit?' Sump 1's

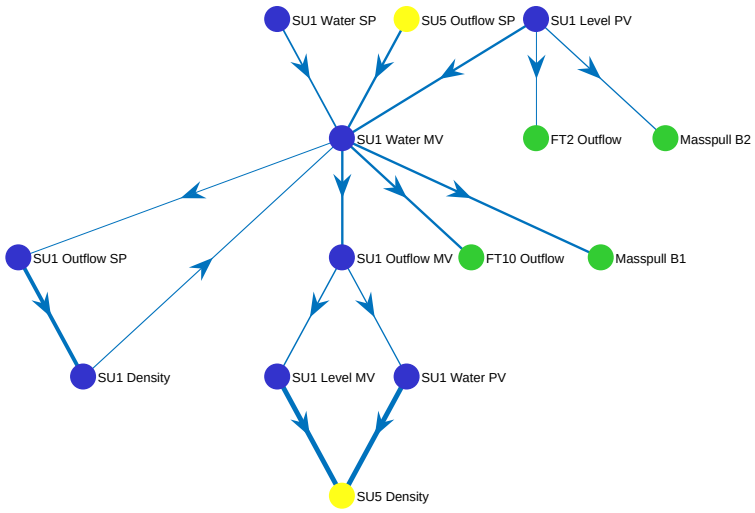

FIGURE 8.9: *Transfer entropy propagation paths for oscillations in the primary milling, flotation, and secondary milling circuits. Values displayed on edges and edge width represent the transfer entropy value calculated. Colours on nodes indicated the section of the plant where the variables are located.*

water addition setpoint ($SU1WaterSP$) and Sump 1's level ($SU1LevelPV$) are both associated with Sump 1's level controller. So the answer is yes. The decision flow suggests that Sump 1's variables should be investigate further as possible root cause variables.

Figure 8.10 shows the time series trends of the sump variables at the start of the oscillation. The trends indicate that the sudden drop in the sump level occurred first. This caused the sump level controller to compensate by varying the sump feed water. This sump water fluctuation resulted in fluctuations in the sump density. This density variation propagated through the flotation circuit to the secondary milling circuit. The causal map confirms this, showing Sump 5's density ($SU5Density$) to be the end node. The variation in density throughout the flotation circuit had a severe impact on flotation performance, since the hydrodynamic properties of the contents of the flotation cells had changed. This is what caused the mass pull to oscillate, event though most of the cell levels remained normal. The flotation circuit is equipped with a multivariable level control strategy. This means that the level oscillation in the sump was effectively rejected in the flotation section, and the cell levels did not oscillate. The cause of the oscillation in the mass pull was therefore not clear. This illustrates the need for a causal analysis tool such as transfer entropy to investigate such events.

In addition to the propagation paths from the primary milling section through to the secondary milling section, the direct causal connection from Sump 1's level to Bank 2's mass pull ($SU1LevelPV \rightarrow MasspullB2$) indicates that the oscillations in the sump level strongly contributed to the oscillations in the mass pull. This direct connection may seem misleading, since the actual propagation path would flow through a number of intermediate variables first before affecting the mass pull. However, the direct connection still displays useful information about where the oscillation originated.

Transfer entropy effectively isolated the root cause of a plant-wide oscillation to a single unit. The causal map generated using transfer entropy is a useful visual tool for root cause analysis. The causal map is easily interpretable, showing a clear propagation path with only one spurious connection.

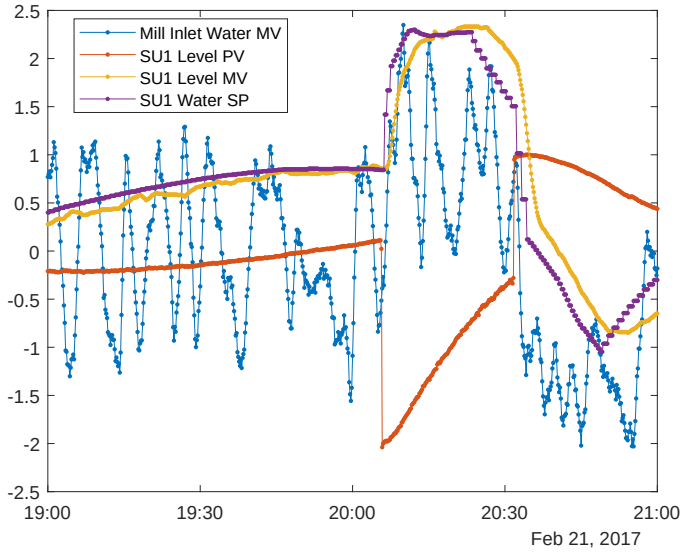

FIGURE 8.10: *Time series plots of sump variables at start of oscillation.*

8.6.3 Granger causality results

The propagation path obtained for Granger causality is shown in Figure 8.11. The same workflow used for transfer entropy, described in Appendix B, was used. The only difference in the application was that Granger causality was substituted in for transfer entropy for the causality analysis procedure.

Following the decision flow in Figure 8.6, the first step after performing Granger causality is to evaluate the accuracy of the causal map by identifying whether there are spurious causal connections. As done with the transfer entropy, the nodes were coloured to reflect the plant section. The cyclical nature of the graph does not reflect the material flow in the process.

In the causal map shown in Figure 8.11, there are multiple spurious connections. The connection from Sump 5's density to Bank 1's mass pull ($SU5Density \rightarrow MasspullB1$) and Sump 5's outflow setpoint to Cell 3's velocity ($SU5OutflowSP \rightarrow FT3Velocity$) are both spurious since the secondary milling section is downstream of the flotation section, and no material flow or control would create these causal connections. The connection from Cell 11's velocity to Sump 1's level ($FT11Velocity \rightarrow SU1LevelPV$) is spurious, since the flotation section is downstream of the primary milling section. The connection from Cell 3's outflow to Cell 8's outflow ($FT3Outflow \rightarrow FT8Outflow$) may be spurious, since these are variables from two separate flotation banks that could not affect each other. In general the causal map has one main propagation path, and all of these spurious connections are part of that path. this means that these connections cannot be ignored without affecting the interpretation of the propagation path. If the decision flow in Figure 8.6 were being followed, then the answer to the question 'Are there numerous spurious connections?', would be yes. The decision flow then suggests that the causality analysis be repeated with transfer entropy instead.

Although the decision flow suggests that Granger causality is no longer useful in this scenario, it is still worth examining the causal map to compare the features to the transfer entropy causal map. The next step in the decision flow is to interpret the propagation paths in the causal map. The first question is, 'Is the graph acyclic?'. In this case the graph is cyclic, there is no clear start node or end node. The next question is, 'Does one path show stronger

FIGURE 8.11: *Granger causality propagation paths for oscillations in the primary milling, flotation, and secondary milling circuits.*

connections?'. In this causal map there is a propagation path from Sump 1's level to Sump 1's outflow setpoint ($SU1LevelPV \rightarrow SU1WaterSP \rightarrow SU1WaterMV \rightarrow SU1OutflowSP$) with strongly weighted connections. This does indicate that Sump 1's level controller is closely associated with the root cause of the oscillation.

There is an interesting mutual causation loop between $SU1LevelMV$ and $SU1WaterPV$. The level MV is the flow out of the sump. A change in this MV would change the density within the sump, and the density controller would change the inlet water, $SU1WaterPV$. Therefore this loop is consistent with the process operation. This mutual causation would not be detected with the transfer entropy method as it is applied in this dissertation, since the net transfer entropy is calculated (see Equation 2.7). In some cases, this means that Granger causality may provide a more accurate representation of the propagation path than transfer entropy will.

Careful interpretation of the causal map revealed some of the same information that the transfer entropy analysis did. However, because of the numerous spurious connections and the cyclical nature of the causality map the results were much harder to interpret than the transfer entropy results.

8.6.4 Summarising the difference between Granger causality and transfer entropy for the industrial case study

Now that both Granger causality and transfer entropy have been tested on the industrial case study, the features discussed in Section 8.3 can be compared.

Accuracy

Both Granger causality and transfer entropy provided tools to accurately isolate the oscillation to the primary mill sump. Data-based techniques for root cause analysis are limited to measured variables. This means that both Granger causality and transfer entropy would not be able to point directly to the underlying cause of the fault, but can direct the attention to measured variables closely associated with it.

Granger causality resulted in three causal connections that could be confidently identified as spurious, and one that is probably spurious, based on process knowledge. Transfer entropy resulted in only one spurious connection. Therefore, on the basis of the number of false connections, transfer entropy was more accurate in this case study.

The Granger causality results demonstrated this method's ability to detect mutual causation between variables. This mutual causation would not be detected with the net transfer entropy used in this dissertation. In some cases, this means that Granger causality may provide a more accurate representation of the propagation path than transfer entropy will. However, in this case study, this limitation did not have an effect on transfer entropy's ability to show the overall propagation path.

Automatability

Using the workflow in Chapter 7, the application procedure for transfer entropy and Granger causality were both fully automated according to the automatability definition provided in 5.3.2.

Interpretability

Transfer entropy generated a causal map with a clear propagation path. Two possible root nodes were identified, but since both were related to the same controller the propagation path was still clear. Granger causality resulted in a cyclical causal map with no clear start and end nodes. By examining connection strengths some useful information about the oscillation propagation could be inferred. Therefore, transfer entropy gave a more visually interpretable causal map.

Computational complexity

The CPU time required for computation of each method was quantified. The computer used was a computational server with 32 GB RAM and 3.33 GHz processor. For transfer entropy, parallel computation was used in the computation of the PDFs, where 8 parallel workers were used. As expected, transfer entropy was much more computationally expensive than Granger causality. Granger causality only took 2.5 minutes. Transfer entropy took 27 hours. This is prohibitively long for rapid analysis of the root cause. Of that time, the transfer entropy calculation itself between all 27 variables only took 15 minutes. The significance testing using Monte Carlo simulations of surrogate time series took the rest of the time.

Applicability for different process characteristics

In this case study some of the oscillations, for example in $SU1LevelPV$, showed nonlinear behaviour. This may be why Granger causality showed more spurious connections than transfer entropy. The time series trends of all the variables included in the analysis were stationary for the period under observation, showing no change in the mean or autocorrelation over time.

8.7 Chapter conclusion

This paper presented a comparative analysis of Granger causality and transfer entropy used for fault diagnosis in an industrial processes. The comparison was based on the following features:

accuracy, precision, automatability, interpretability, computational complexity, and applicability for different process characteristics.

Transfer entropy was found to be more generalisable, and visually interpretable. However, Granger causality is much less computationally expensive, and easier to interpret the meaning of the values obtained. To directly address the the accuracy and precision of Granger causality and transfer entropy, their ability to find true connections in a simulated process was tested. The results indicated that transfer entropy showed higher accuracy and precision.

A decision flow was developed from these comparisons to aid users in deciding when to use Granger causality or transfer entropy, as well as to aid in the interpretation of the causality maps obtained from these techniques. This decision flow is presented in Figure 8.6.

The features of Granger causality and transfer entropy were illustrated on an industrial case study of oscillations in a mineral processing plant. In this case study, the causal map obtained from the transfer entropy analysis showed two root cause variables associated with the same unit in the process. The transfer entropy results were able to provide useful information for further analysis into the cause of the fault. Granger causality, on the other hand, showed a large number of spurious connections, and gave no clear indication of the root cause.

Although the causal map obtained from transfer entropy provided useful information for root cause analysis, the interpretation required careful reasoning. In scenarios where the causal map is more complex, this interpretation will be even harder and more time consuming. To aid engineers with the interpretation of causality maps for fault diagnosis, Chapter 9 presents guidelines for their construction and interpretation.

CHAPTER 9

Development of visual and algorithmic graph interpretation tools for fault diagnosis

Contents

9.1 Chapter introduction . . . 133
9.2 Chapter objectives . . . 134
9.3 Graph layouts . . . 134
9.4 Graph pruning using transitive reduction . . . 137
9.5 Assigning node and edge attributes . . . 139
9.5.1 Assigning edge weights based on connection strength . . . 139
9.5.2 Grouping nodes according to variable location . . . 140
9.5.3 Grouping nodes according to variable categories . . . 144
9.6 Assigning node importance . . . 146
9.7 Graph complexity metrics . . . 146
9.8 Graph traversal . . . 147
9.9 Recommended causal map interpretation procedure . . . 150
9.10 Chapter conclusion . . . 150

9.1 Chapter introduction

Chapter 7 presented a systematic workflow for the application of transfer entropy that addressed the numerous data selection and parameter selection steps required for fault diagnosis. Chapter 8 addressed the need to compare characteristics of different techniques and provide guidelines for selection of techniques. Between those two chapters, the decision of which technique to use, as well as the application procedure once a technique has been selected, are covered. The final step in the causality analysis procedure that has not been fully addressed is the root cause analysis once the results have been obtained. This root cause analysis requires interpretation of the causal maps generated from causality analysis. The construction and interpretation of these maps has been addressed superficially and demonstrated in previous chapters. However, it was not the main focus of those chapters. In this chapter visualisation and algorithmic tools to aid graph interpretation are developed and demonstrated.

This chapter is structured as follows: Section 9.2 presents the objective of this chapter; Section 9.3 investigates methods for setting the layout of causal maps; Section 9.4 presents the use of

transitive reduction to prune shortcut connections from causal maps; Section 9.5 presents tools for augmenting causal maps with node and edge attribute; Section 9.6 presents tools for assigning the importance of nodes in the causal map; Section 9.7 presents a metric to define the complexity of causal maps; Section 9.8 discusses tools to traverse causal maps to highlight propagation paths; Section 9.9 outlines the recommended procedure for constructing and interpreting causal maps based on the tools presented in this chapter; and finally, Section 9.10 presents the conclusions of this chapter.

9.2 Chapter objectives

The objective of this chapter is to *develop* and *demonstrate* visualisation and algorithmic tools to augment graph interpretation for fault diagnosis. This is to address Objective IV.

9.3 Graph layouts

Visual interpretation of causality maps can be aided by the layout of the nodes.

In many scenarios, a layout that reveals hierarchical structure may be desired. A layered layout reveals such a hierarchical structure [Sugiyama *et al.*, 1981]. In the layered algorithm the nodes are arranged in a set of layers, so that each edge joins two nodes belonging to different layers. In the layered structure the sequence of nodes on the propagation path may be visualised in sequential order. Figure 9.1a shows the causality map for the plant wide oscillation case study presented in Section 8.6 using the layered layout. In scenarios where the causality map has a clear start and end node, this layout reveals this propagation path effectively. This is the case in Figure 9.1a.

The force layout assigns attractive forces to the endpoints of edges, and repulsive forces to nodes. The balance of repulsive and attractive forces means that nodes that two nodes that are not connected by edges are pushed away from each other, since there is no attractive force between them. This structure is useful for revealing the importance of nods, as with the circular layout. A node with many edges associated will attract the nodes that it connected to, making them cluster. These clusters can also reveal hierarchical structure, as with the layered layout. The causality map for the plant-wide oscillation with the force layout is shown in Figure 9.1b. The causal map reveals $SU1WaterMV$ is an important node, with a large number of nodes clustered around it.

Another layout is the circle layout. In the circle layout, the nodes are placed in a circle centred around the origin. This layout is useful for visualising the importance of each node, by visualising the amount of edges entering or leaving the node. This may reveal which node is a source node that influences many other nodes, or which is a sink node that is influenced by many other nodes. Figure 9.1c shows the plant-wide oscillation causality map with the circle layout. This layout can be especially useful in scenarios where there is no clear start and end node, i.e. in a cyclical graph. In such a graph it is useful to see which nodes are most important relative to the others. The circle layout reveals this readily. A drawback of this layout is that it does not reveal anything about the structure of the underlying process. This layout was used by Yuan & Qin [2014], Zhang *et al.* [2015]. Duan *et al.* [2015] first used the circular layout to present the results, and then constructed a layered map to better visualise the propagation paths.

Selection of the appropriate layout is dependent on the situation and the type of information the engineer wants to glean from the causal map. The layout method is best for root cause

identification in sparse causal maps with minimal cyclical loops. The circle method is best for root cause identification in dense causal maps with cyclical connections. The force layout is useful for identifying important causal structures within the process. Not much attention has been paid to the layout of the causality maps in process fault diagnosis literature (see Section 2.12.4). The choice of layout is often seen as a matter of personal preference, or an ad-hoc choice for what gives the most visually intuitive map in the specific scenario. This author's personal experience with the case studies applied is that the layered layout provides the most robust and visually intuitive representation of the causal map.

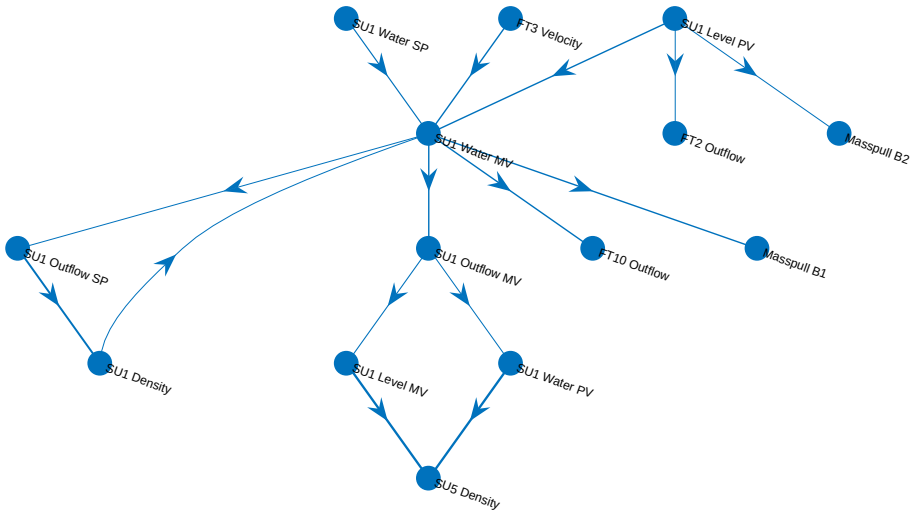

(a) *Layered layout.*

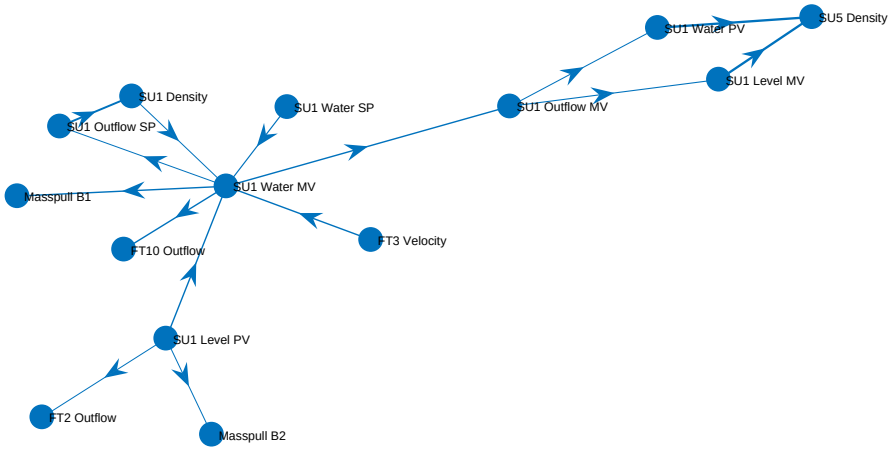

(b) *Force layout*

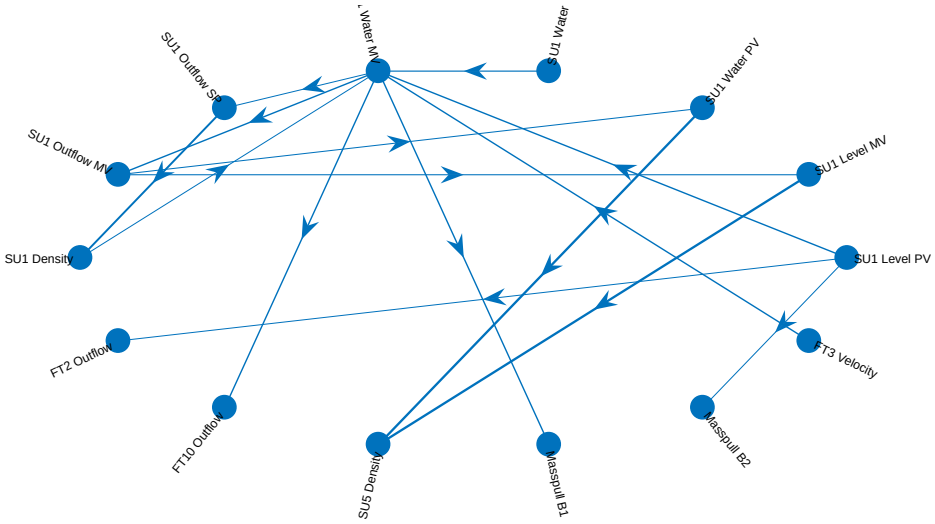

(c) *Circle layout*

Figure 9.1: *Different layouts of causality maps.*

9.4 Graph pruning using transitive reduction

Causality maps constructed from causality analysis results may be dense, and difficult to interpret. The maps may often show indirect connections, where a causal connection is identified due to the influence of an intermediate variable. Th presence of cycles in the graph can also make it difficult to follow paths between nodes to interpret the overall propagation path. Transitive reduction can be used as a visualisation tool to reduce the complexity of the graph and make it easier to interpret. Section 9.7 presents some graph complexity metrics that will be used in this section.

Figure 9.2a shows the original causality map obtained using transfer entropy. Figure 9.2 shows the transitive reduction of that causality map. Figure 9.2 is much easier to interpret, but still retains the important information about the oscillation propagation.

The graph density can be calculated using Equation 9.1. The graph density is discussed in more detail in Section 9.7. However, the concept is used here to illustrate the improvement in interpretability of the graph using transitive reduction. The original causality map has 14 nodes and 27 edges, so the graph density is $D = 0.148$. The reduced causality map has 14 nodes and 15 edges, so the graph density is $D = 0.082$. The reduced graph complexity indicates that the reduced graph is easier to interpret. The results of the causality analysis for this case study indicated that $SU1LevelPV$ was a plausible root node. From Figure 9.2a it is difficult to see the propagation path from $SU1LevelPV$ to $SU5Density$. Once the transitive reduction has been applied, in Figure 9.2, the propagation path of the oscillation is clear: from $SU1LevelPV \rightarrow SU1WaterMV \rightarrow SU1OutlfowMV \rightarrow SU1LevelMV \rightarrow SU5Density$.

The original graph contained a cycle between $SU1WaterMV$, $SU1OutflowSP$, and $SU1Density$. Because of this cycle the transitive reduction algorithm constructed new edges that were not present in the original graph (see Figure 2.15 For example, the edge from $FT3Velocity \rightarrow SU1WaterMV$. This artificial construction of edges may be misleading when interpreting causal maps. However, the presence of the cycles means that there was a path from $FT3Velocity \rightarrow SU1WaterMV$ in the original graph. Despite the possible confusion caused by these artificial edges, the transitive reduction can be used as a visualisation tool, to succinctly capture the information about the propagation path of the fault.

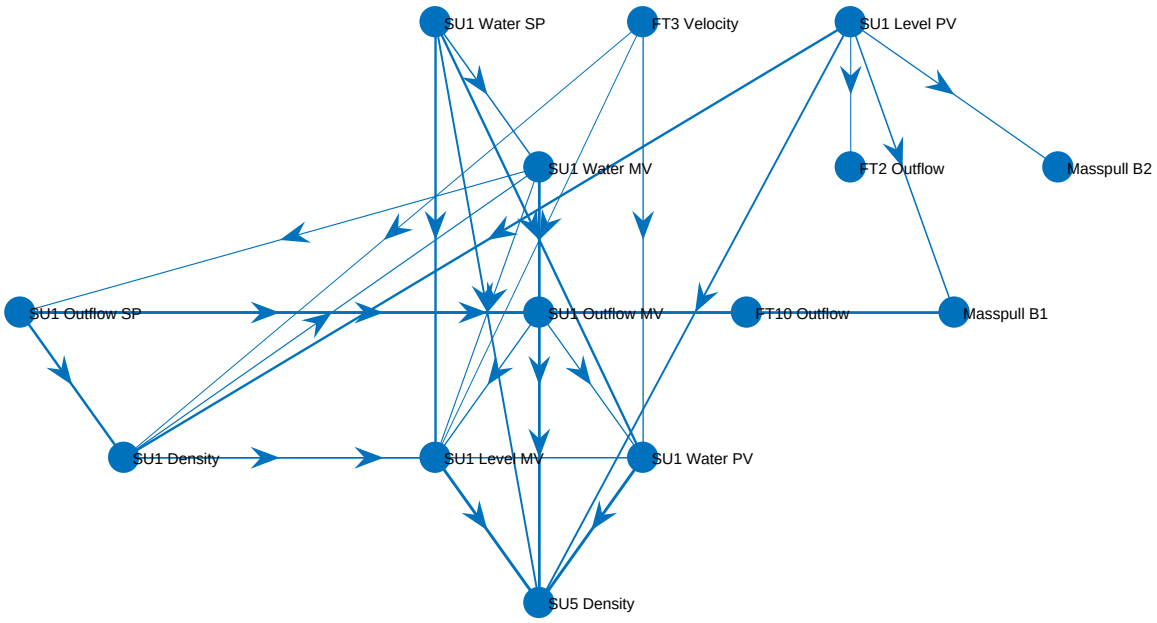

(a) *Original graph, G.* $D = 0.148$.

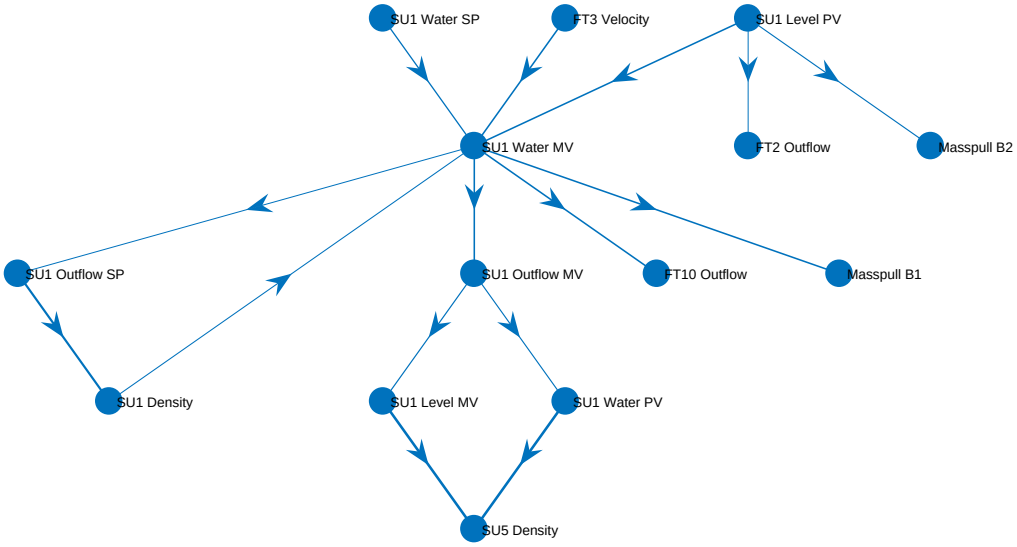

(b) *Transitive reduction , $G_{reduction}$.* $D = 0.082$

Figure 9.2: *Transitive reduction for the primary milling oscillation.*

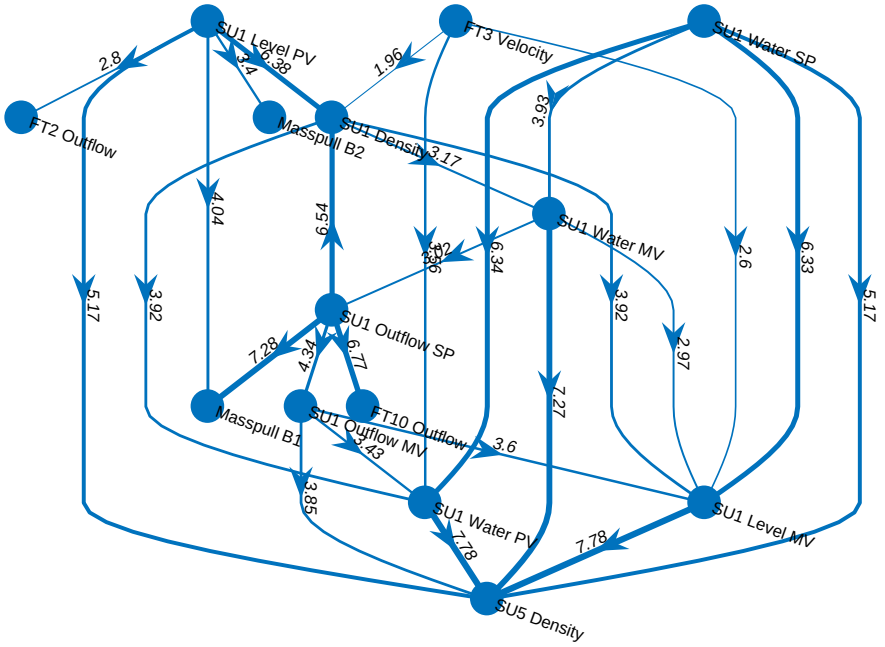

FIGURE 9.3: *Causality map for plant wide oscillation visualising connection strength using edge width. The edge widths used the connection strength (shown on the edge labels), scaled so that the strongest connection has the thickest line, while the weakest connection has the thinnest line.*

9.5 Assigning node and edge attributes

As discussed in Section 2.12.4, causality maps can be augmented by assigning additional attributes to nodes and edges.

9.5.1 Assigning edge weights based on connection strength

The strength of the connections in a causality map gives an indication of the relative importance of the connections. In scenarios where there are multiple possible propagation paths, the relative connection strengths can give an indication of which propagation path is more likely to reveal the true root cause. The connection strengths can be visualised by assigning them as edge weights, and adjusting the line thickness of the edges to represent these edge weights.

Figure 9.3 shows the causality map for plant wide oscillation visualising connection strength using edge width. The edge widths used the connection strength (shown on the edge labels), scaled so that the strongest connection has the thickest line, while the weakest connection has the thinnest line. The causality map shown is very dense and convoluted, but the edge widths show that many strong connections originate from the $SU1WaterSP$ node. This indicates that this node is strongly associated with the root cause of the oscillation. Since the oscillation originated in the Primary Milling Sump, this information is matches the root cause analysis results in Chapter 8.

9.5.2 Grouping nodes according to variable location

Process knowledge may also inform sensible groupings of variables so that causality analysis does not have to be calculated over the entire space. This can greatly reduce computational complexity. For example, in the case where two parallel streams exist, process knowledge would be able to group the two streams independent of each other, since there would be no connections between them. This means that the causalities don't have to be calculated between variables of different streams.

In the example presented in Chapter 4, transfer entropy was used to determine the propagation path of oscillations in the rougher flotation section. A flow diagram of the process is shown in Figure 4.3. This flotation circuit consists two parallel banks, each with seven flotation cells in series. The concentrate from the first three cells of each bank are combined, and the concentrate from the last four cells are combined. The outflow (tails) from each cell flows into the following cell. Finally, the tails are combined and processed further in downstream units. PID feedback loops are used for regulatory control of the cell levels and air addition rate [Muller *et al.*, 2010].

Figure 9.4 shows the causality map for all the levels and variables in the flotation circuit Nodes with cell numbers from 1 to 7 are from Bank 1, and those with cell numbers from 8 to 14 are from Bank 2. However, the two banks are operated in parallel, with no mass flow or control interaction between them. Therefore the causal connections from Bank 1's nodes to Bank 2's nodes are spurious. For example, $LevelFT001$ to $OutflowFT008$. To reduce the graph complexity and to reduce the number of spurious connections, the two banks can be treated separately. Figure 9.5 shows the causality map where each bank is treated separately. The separate graphs quickly show that for both banks, the oscillation propagates from the cells at the start of the bank to those at the end. This indicates a common cause just upstream of both banks. In Chapter 4, it was shown that the cyclone pressure immediately upstream of these cells dropped, causing the cell levels to fluctuate.

Separating the nodes also reduces the computational burden. Each bank has 14 measured variables showing oscillations. If the entire bank were treated at once the number of pairs of transfer entropy calculations required would be $28^2 = 784$. Treating each bank separately reduces that number to $2 \times 14^2 = 392$.

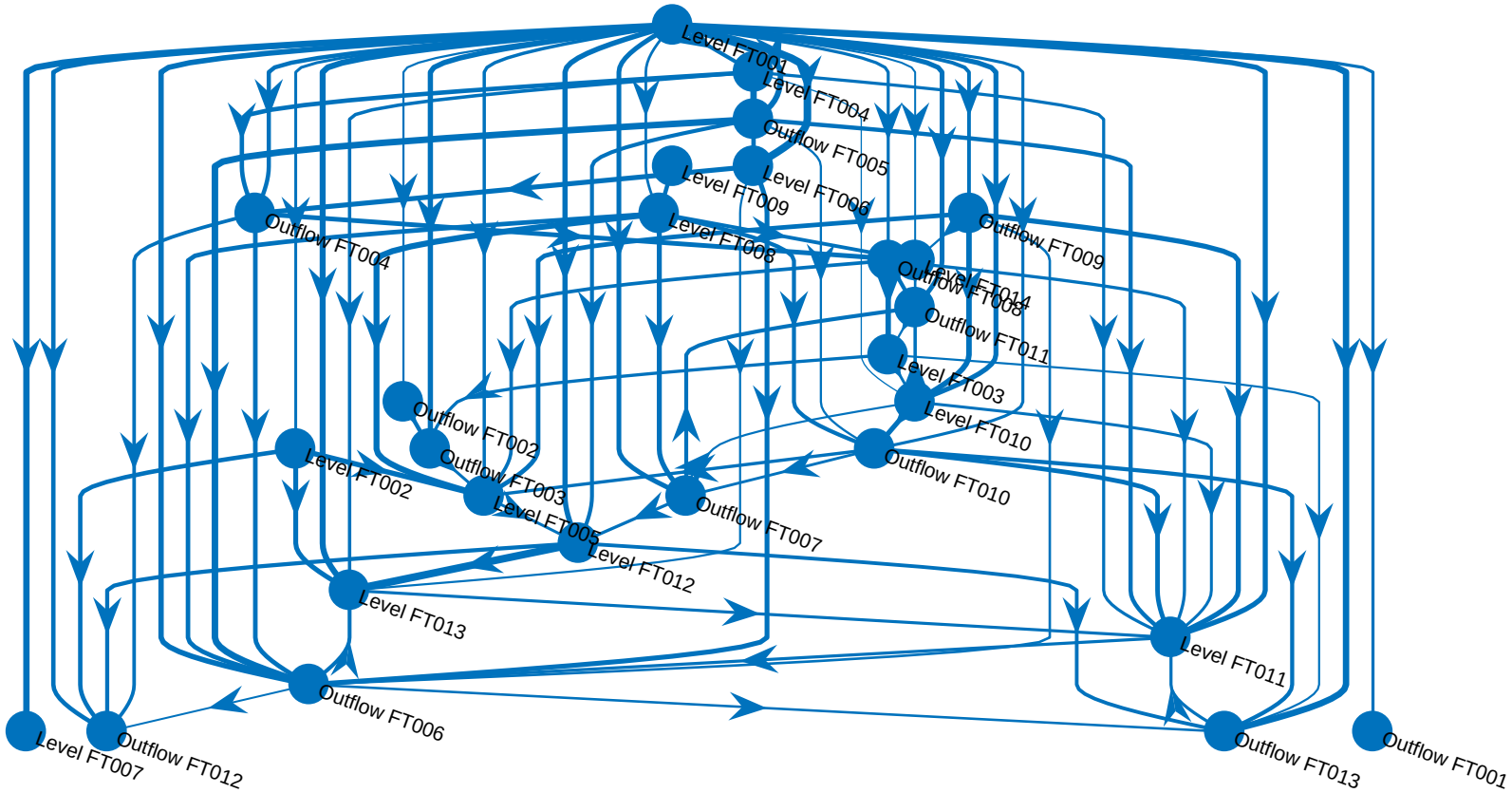

FIGURE 9.4: *Causality map for both banks in flotation circuit. Graph density,* $D = 0.134$.

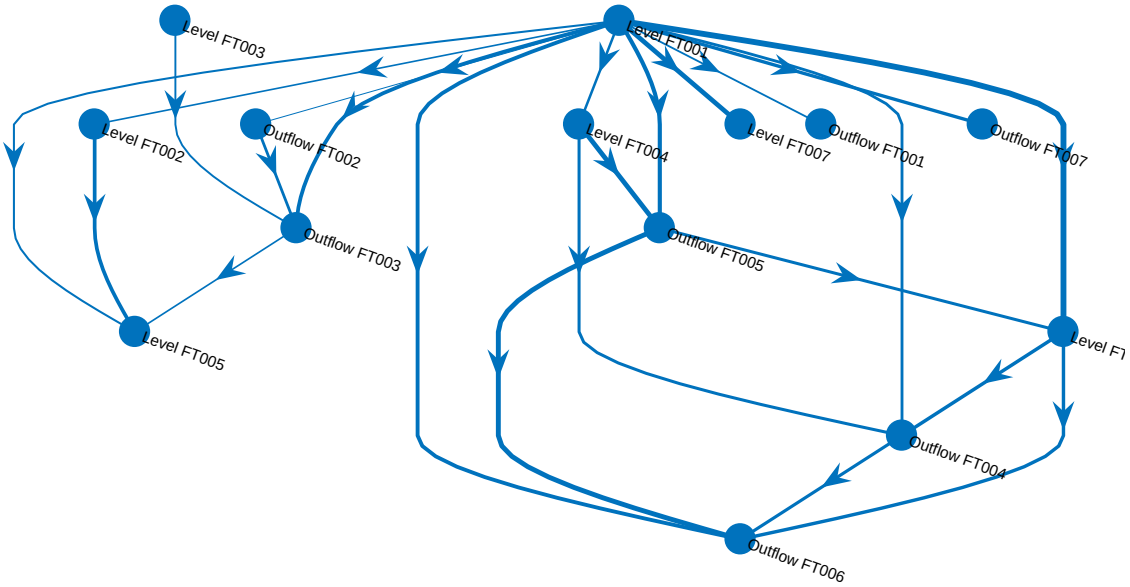

(a) *Propagation path for Bank 1. Graph density,* $D = 0.13$.

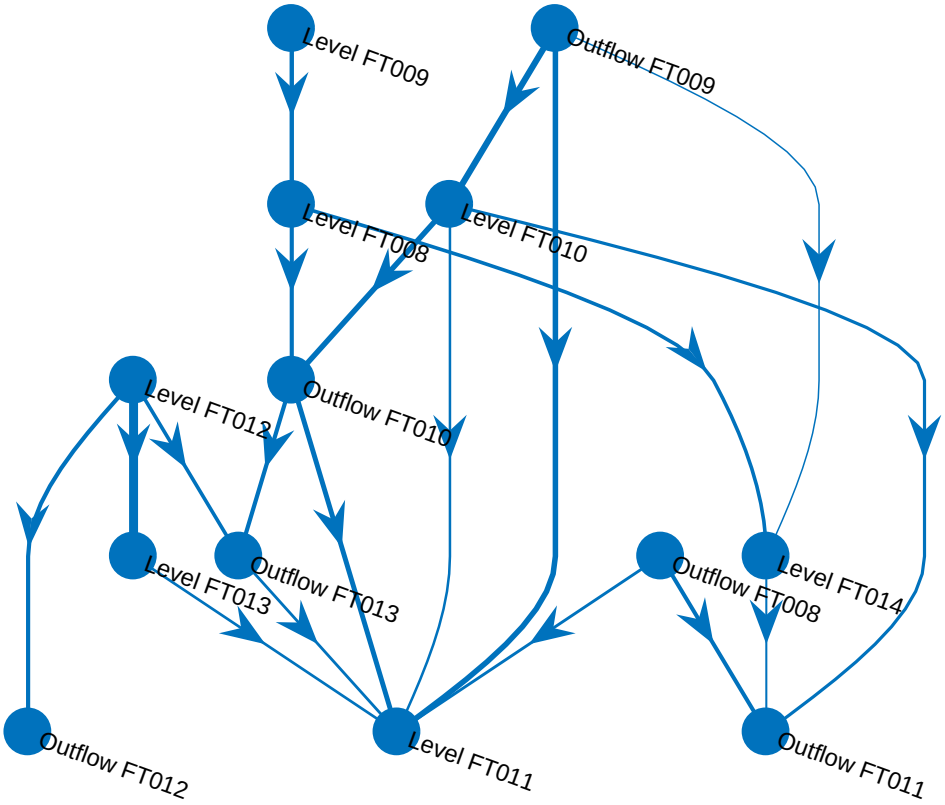

(b) *Propagation path for Bank 2. Graph density,* $D = 0.122$.

Figure 9.5: *Propagation paths for oscillations in the flotation circuit. Each bank treated separately*

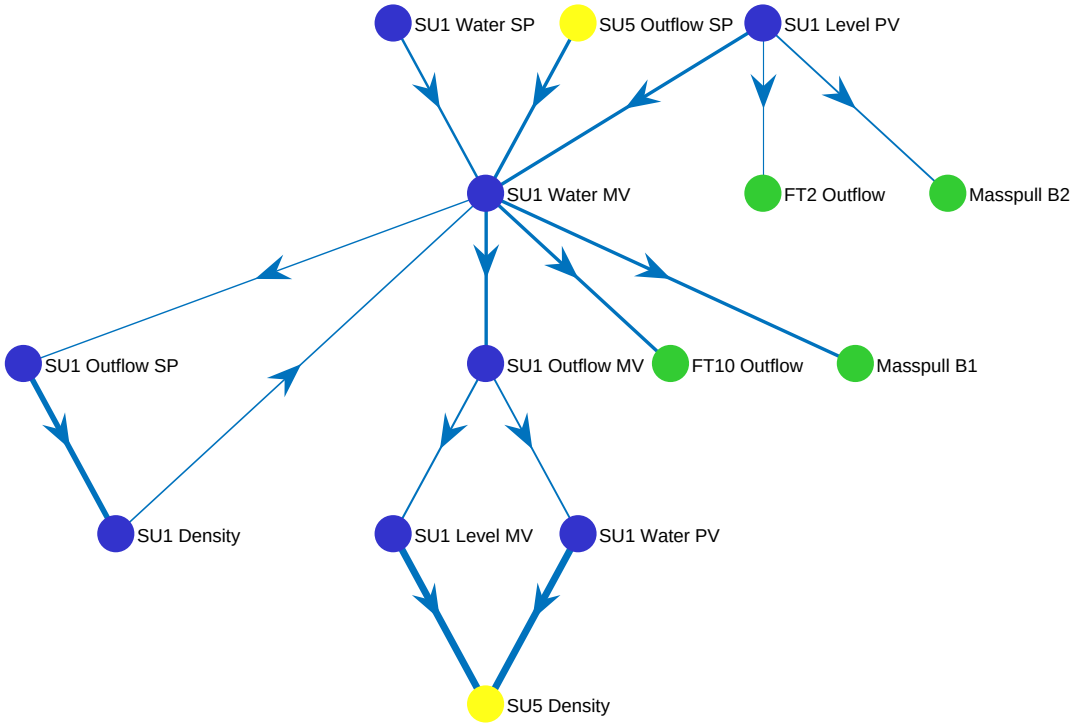

FIGURE 9.6: *Causality map coloured according to plant sections. Blue nodes represent variables in the primary milling section. Green nodes represent variables in the rougher flotation section. Yellow nodes indicate variables in the secondary milling section.*

Causality maps can be coloured according to the location of the variable in the plant. In this way the overall direction of the propagation path can be visualised, and sequential structure may be revealed. The resolution of the analysis may dictate which colouring is most appropriate. At a plant-wide resolution, different sections of the plant can be coloured differently. At a finer resolution, when the fault is not on a plant-wide scale, but rather localised to a single section, the nodes can be coloured according to different units. At the smallest resolution, the nodes can be coloured according to the controller they are associated with.

Figure 9.6 shows a causality map coloured according to plant sections. Blue nodes represent variables in the primary milling section. Green nodes represent variables in the rougher flotation section. Yellow nodes indicate variables in the secondary milling section. This colouring of nodes aids interpretation of the causality map. The colours demonstrate that the propagation path starts with blue nodes and progresses towards the yellow nodes. This indicates that the oscillation began in the primary milling section and propagated through to the secondary milling circuit. The colours also indicate that the oscillations propagate from the blue nodes to the green nodes, showing the propagation from the primary milling circuit to the rougher flotation section. This shows that, even though the process flows from the primary milling circuit to the rougher flotation section to the secondary milling circuit, the causality map doesn't show this sequential flow. Considering the type of variables in the rougher flotation section, the levels and masspulls are affected by the levels in the primary milling sumps. These variables do not show direct effects on the density in the secondary milling circuit. If density measurements were available

in the rougher flotation section, the causality map might show a more sequential propagation path that corresponded more directly to the process flow.

9.5.3 Grouping nodes according to variable categories

Nodes in the causality maps can also be grouped according to different variable categories. The nodes can be grouped according to sensor type, e.g. flow measurement, density measurement, or temperature measurement. In this way the effect of the fault propagation on the process may be revealed. For example, it may illustrate how a change in level in a sump affects the density of downstream units. Another possibility is to group nodes according to control categories, e.g. CV, MV, or SP. The effect of the fault propagation on the plant control may be revealed using this approach.

Consider again the causality map shown in Figure 9.5. The variables showing the oscillations are the CVs and MVs of the level controllers for each cell. Figure 9.7 shows the causality maps divided further into separate CV and MV causal maps. The resulting causality maps are much easier to interpret.

The causality map showing the CVs for Bank 1 indicates that the oscillation started in Cell 2 and propagated through the Bank to Cell 7. The causality map for the MVs for Bank 1 shows the same propagation path. Since the CV and MVs for each controller would clearly be linked, it makes sense to separate them. In this scenario, the controller link between the levels and outflows means that the oscillation will propagate through them in the same way.

There are other scenarios where the CVs and MVs may not display the same information. For example, if the controller were able to attenuate the disturbance propagating through the process, then the CVs would not necessarily show the propagation path clearly. This was the case in the plant-wide oscillation case study, where the Sump level in the primary milling circuit fluctuated, but this fluctuation did not propagate through to the flotation cell levels. In such a scenario only plotting the CVs would not necessarily add more information about the fault propagation path. A hierarchical approach, the entire process is considered first, and drilling down to lower levels, is the best approach.

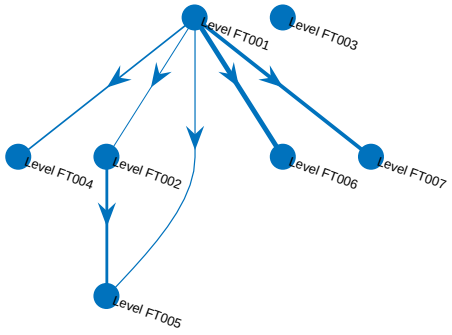

(a) *Propagation path for Bank 1 levels. Graph density,* $D = 0.143$.

(b) *Propagation path for Bank 1 outflows. Graph density,* $D = 0.071$.

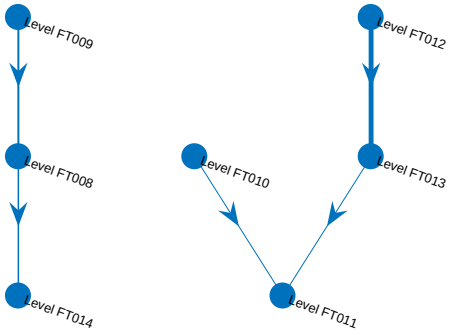

(c) *Propagation path for Bank 2 levels. Graph density,* $D = 0.12$.

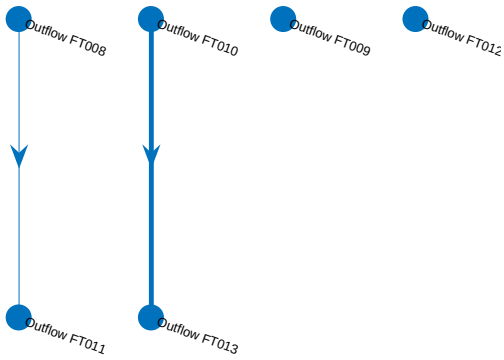

(d) *Propagation path for Bank 2 outflows. Graph density,* $D = 0.067$.

FIGURE 9.7: *Propagation paths for oscillations in the flotation circuit. CVs and MVs treated separately.*

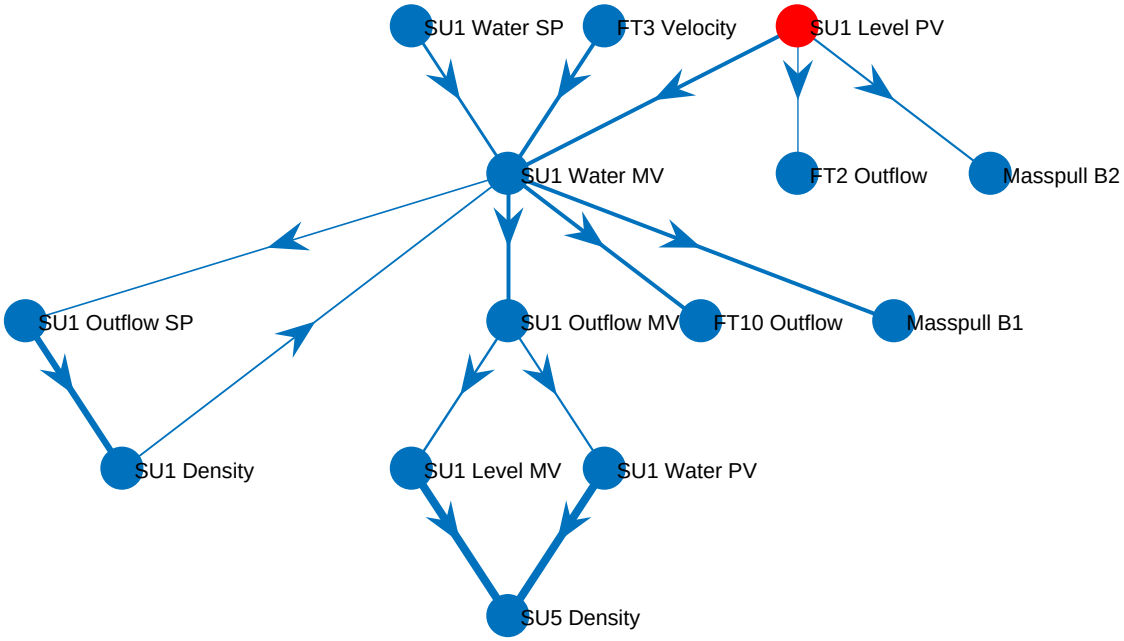

Figure 9.8: *Causality map for primary mill oscillation. The node showing the highest maxflow, $SU1LevelPV$ is highlighted to indicate the suggested root cause.*

9.6 Assigning node importance

Interpretation of causality maps may be improved by assigning importance to the nodes and edges. In this way the relative contributions of variables to the fault can be inferred.

Figure 9.8 shows the causality map for the milling oscillation case study from Chapter 8, and Table 9.1 shows the inflows, outflows, and maxflows for this causality map. The node $SU1LevelPV$ shows the highest maxflow, and is highlighted in red in Figure 9.8 and in Table 9.1. Highlighting this node augments the causal map so that the user's eye is immediately drawn to the node with the highest maxflow. In this case, the highlighted node corresponds to the results discussed in Chapter 8, where it was inferred that the Primary Mill Discharge Sump's level controller was responsible for the oscillations.

9.7 Graph complexity metrics

Some metrics can be calculated to give an indication of graph complexity. Very complex causality maps are difficult to interpret. Graph density can be used for this. A dense graph has a large number of edges per node, while a sparse graph has a small number of edges per node. A dense graph may be harder to interpret visually, since the large number of edges may be hard to follow. This may obscure the propagation path. The graph density, D, for a directed graph is can be calculated according to Equation 9.1[Gibbons, 1985].

$$D = \frac{E}{V(V-1)} \tag{9.1}$$

TABLE 9.1: *Inflow, outflow, and maxflow for the nodes in Figure 9.8. SU1LevelPV showed the highest maxflow.*

Node	Inflow	Outflow	Maxflow
SU1 Level PV	0	3	3
SU1 Level MV	1	1	0
SU1 Water PV	1	1	0
SU1 Water SP	0	1	1
SU1 Water MV	4	4	0
SU1 Outflow SP	1	1	0
SU1 Outflow MV	1	2	1
SU1 Density	1	1	0
FT2 Outflow	1	0	-1
FT10 Outflow	1	0	-1
SU5 Density	2	0	-2
Masspull B1	1	0	-1
Masspull B2	1	0	-1
FT3 Velocity	0	1	1

where E represents the number of edges in the graph, and V represents the number of nodes (or vertices) in the graph The maximum number of edges for a directed graph is $V(V-1)$, so $D = 1$ for a fully connected graph.

9.8 Graph traversal

As discussed in Section 2.12.5, graph traversal techniques can be used to analyse propagation paths of faults in causality maps. This can help in identification of the root cause of the fault, by analysing the path from a suspected root node to another node downstream in the system. For example, in the plant-wide oscillation case study, $SU1LevelPV$ was identified as a possible root cause. The maxflow also indicated that this was the most important root node. $SU5Density$ is the final node in the causality map. The shortest path from $SU1LevelPV$ to $SU5Density$ can be determined. This path is highlighted in Figure 9.9. Highlighting the path obtained using graph traversal quickly shows the propagation path from the Primary Mill through to the Secondary Mill.

The depth-first search algorithm can also be used to highlight the influence of a root node on the rest of the graph. Figure 9.10 shows the results of a depth-first search to determine all the nodes that are reachable from $SU1LevelPV$, and the edges between them.

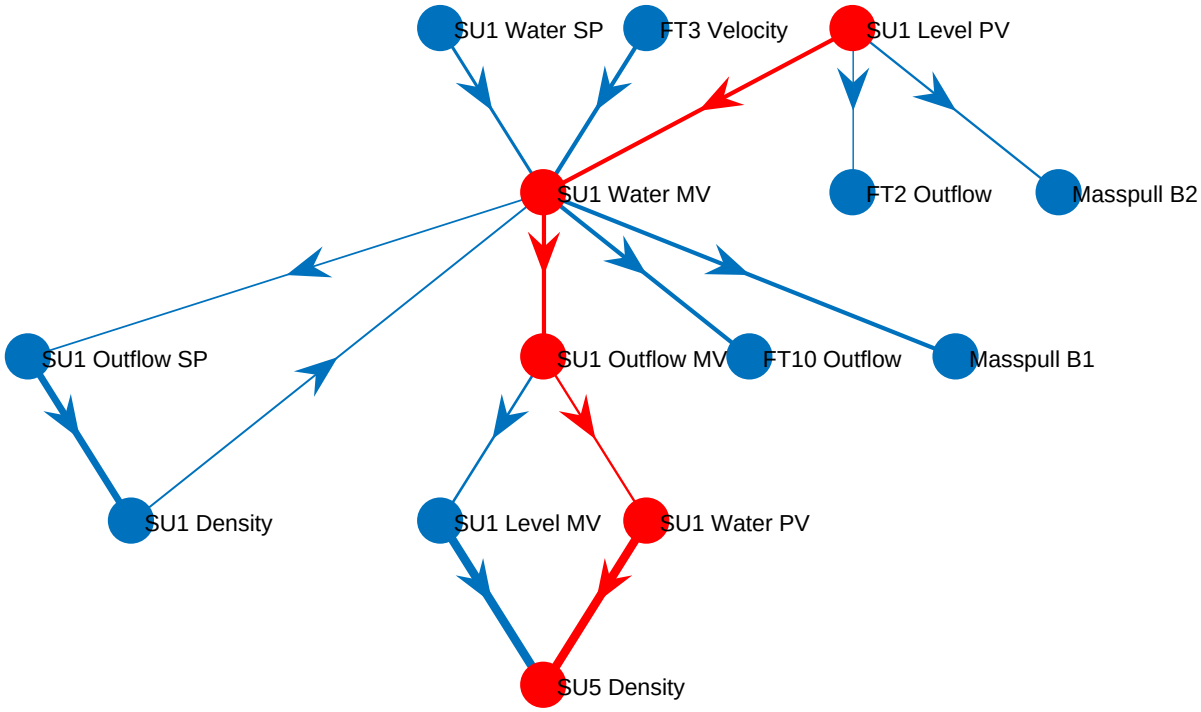

Figure 9.9: *Shortest path from SU1LevelPV to SU5Density*

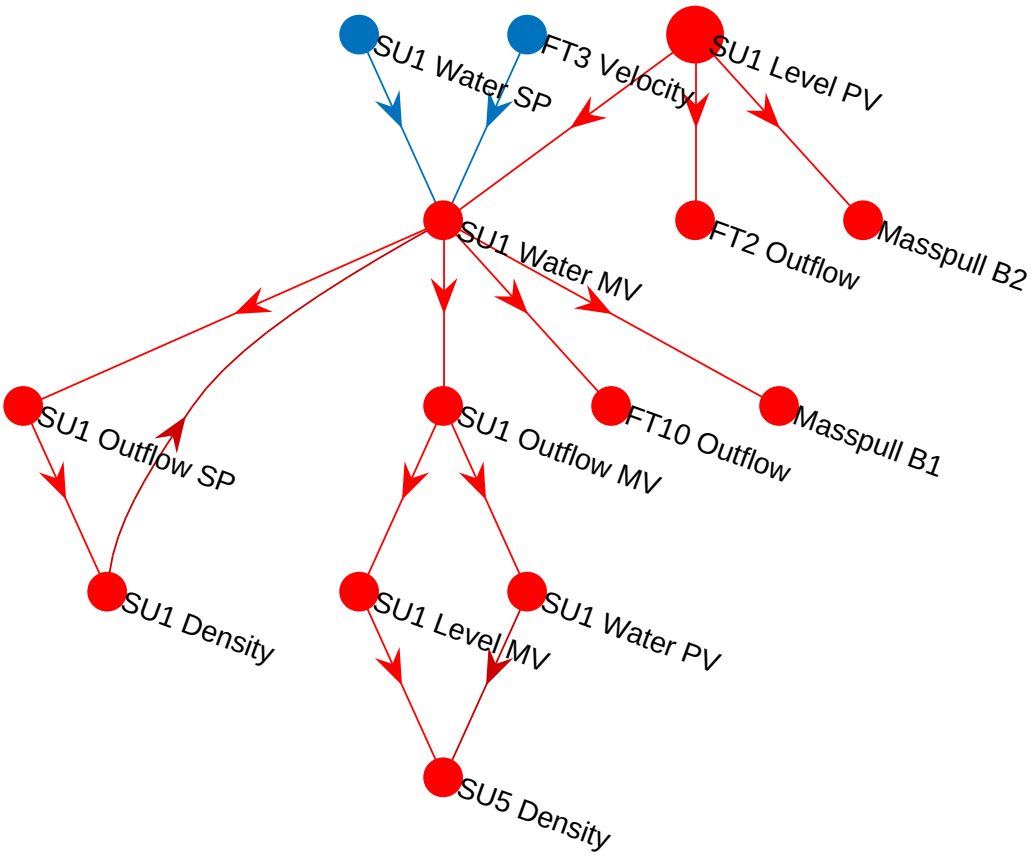

FIGURE 9.10: *All nodes reachable from SU1LevelPV, found using the depth-first search*

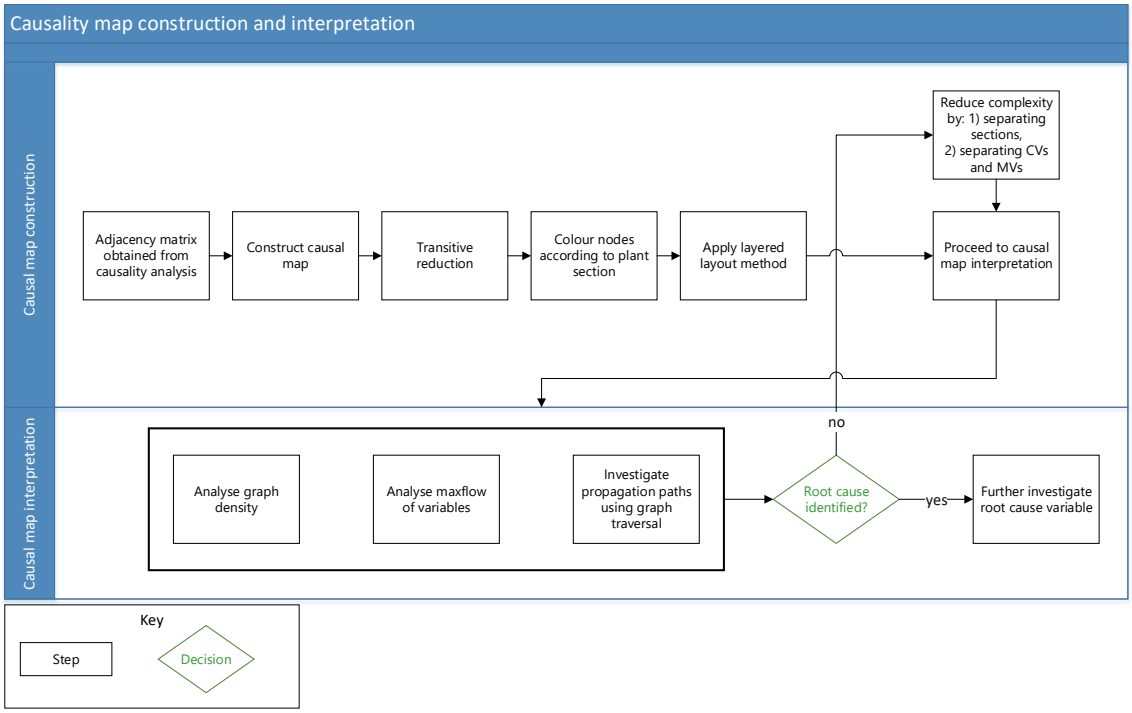

FIGURE 9.11: *Procedure for interpretation of causal maps for fault diagnosis*

9.9 Recommended causal map interpretation procedure

Various tools for constructing causal maps and interpreting the resulting causal maps have been presented, and their usefulness demonstrated. Figure 9.11 now presents the recommended procedure for causal map construction and interpretation. The procedure begins with construction of the causal map from the adjacency matrix derived from the causality analysis. Transitive reduction is then applied as a graph pruning technique to simplify the graph. Graph nodes are then coloured according to the plant section, and the layered layout is applied. All these steps so far have been to construct the causal map in a way that best aids interpretation of the map. The interpretation tools can now be applied. These tools are not presented as steps to be completed in sequence, since there is no particular order to them. The graph complexity metric, the maxflow metric for node importance, and graph traversal techniques are applied. Combining all of this information, the root cause of the fault can be analysed. If a plausible root cause is found, this variable can be investigated further. If not, the graph complexity can be reduced by one of two methods: constructing separate causal maps for each process section; or constructing separate causal maps for CVs and MVs. Then interpretation can be performed again.

9.10 Chapter conclusion

The objective of this chapter was to demonstrate visualisation and algorithmic tools to aid interpretation of causality maps for root cause analysis.

First, the construction of causal maps was discussed. Various graph layout techniques were

presented, and the advantages of each were discussed. The layered technique presents the nodes hierarchically, which presents the propagation paths of faults most clearly. The use of the transitive reduction to remove shortcut nodes was suggested. Transitive reduction effectively reduced the complexity of the graphs, and provided clearer indications of the propagation path of the fault. Methods for grouping and augmenting causality maps based on the variable locations or categories. Augmenting the causality maps with different colours for different variable groupings aided interpretation of the graphs. Separating nodes according to different variable groupings aided the interpretation of the maps by reducing the density of the graphs.

Secondly, methods for interpretation of causal maps were discussed. The maxflow method for assigning node importance was presented. A graph complexity metric was presented, that was shown to be useful for determining whether a causal map could be easily interpreted by a user. Finally, graph traversal techniques, such as the depth-first search were presented, and it was illustrated how these techniques are useful for analysing propagation paths in a process.

The recommended procedure for causal map interpretation based on these presented methods was presented in Figure 9.11.

Now that this chapter has addressed the final component of causality analysis for fault diagnosis, the overall conclusions of this dissertation can be presented in Chapter 10.

CHAPTER 10

Conclusions

Contents

10.1 Dissertation summary . . . 153
10.2 Objective I conclusion . . . 153
10.3 Objective II conclusion . . . 155
10.4 Objective III conclusion . . . 155
10.5 Objective IV conclusion . . . 156
10.6 Fulfilment of overall project aim . . . 156
10.7 Appraisal of dissertation contributions . . . 157
10.8 Suggestions for future work . . . 157

10.1 Dissertation summary

This dissertation investigated, and improved on, existing causality analysis techniques for fault diagnosis.

The objectives of this dissertation are repeated here as a reminder.

Objective I. To *investigate* the factors that affect performance of causality analysis techniques.

Objective II. To *design* a systematic workflow for application of causality analysis for fault diagnosis.

Objective III. To *design* a tool to aid the decision of which causality analysis method to select.

Objective IV. To *present* tools for interpretation of causal maps for root cause analysis.

Figure 10.1 illustrates the components of causality analysis investigated in Chapter 2 that were identified as needing improvement. The chapter where each of these improvements was addressed is noted on the figure, as well as which objective covers each of these components.

10.2 Objective I conclusion

The first objective of this dissertation was to determine the factors that affect the performance of causality analysis techniques.

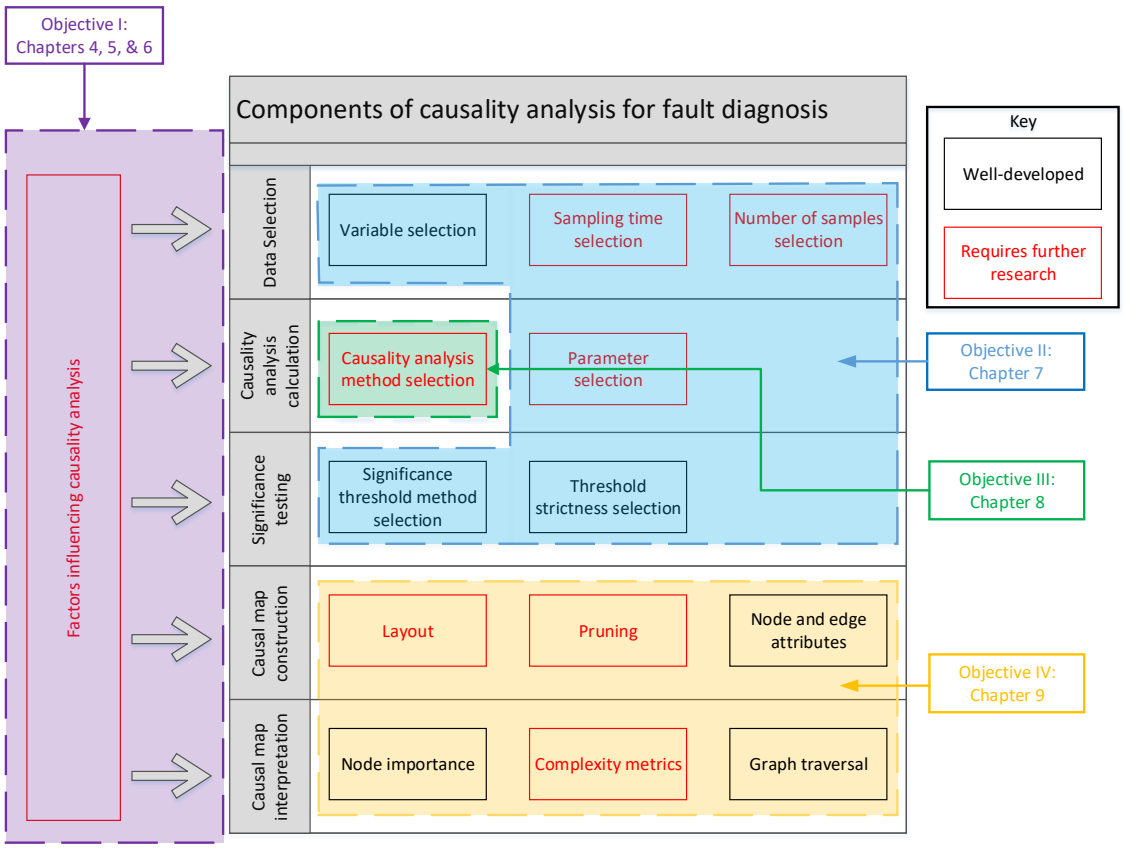

FIGURE 10.1: *Overview of chapters addressing components of causality analysis based fault diagnosis.*

Chapter 4 presented an example of causality analysis used for fault diagnosis of oscillations in a minerals concentrator plant. This case study demonstrated the effectivity of causality analysis for fault diagnosis. However, this case study demonstrated that the implementation of causality analysis is complicated, with numerous steps where the optimal data selection, parameter selection, and interpretation of the results are ambiguous. The case study it also demonstrated the need for careful consideration of process knowledge for meaningful interpretation of the results from otherwise automated techniques.

To address Objective I, Chapter 5 defined the desired performance criteria of causality analysis techniques in terms of: general applicability; automatability; interpretability; accuracy; precision; and computational complexity. Although some of these performance criteria are subjective, such as interpretability, and some are quantifiable, such as accuracy, careful evaluation of techniques based on these criteria can reveal the strengths and weaknesses of each approach. The factors affecting the performance of causality analysis techniques were discussed. Identified factors affecting the performance included: noise; fault types; process interactions; time series characteristics; and parameter selection.

Once the performance criteria had been established, Chapter 6 investigated the impact of some of the process characteristics on the performance of causality analysis techniques. The process conditions investigated were: the effect of step and oscillatory perturbations; the impact of feedback control; and the impact of noise. The ability of Granger causality and transfer entropy to accurately identify known causal connections in a simulated process influenced by these different

conditions was evaluated. For a wide range of process conditions the causality measures were robust, giving significant values for a known causal connection, with some logically consistent exceptions. For oscillatory conditions, high frequencies resemble noise, and therefore give lower causality measures. The effect of low frequency oscillations is so gradual that the observed window used by the causality measures are too small to detect a causal relationship. Closed loop operation attenuates slow acting oscillations and step perturbations, disguising causal relationships.

Some points of comparison of Granger causality and transfer entropy were highlighted from this investigation. Granger causality gave more consistent responses than transfer entropy for a wide range of oscillatory conditions, indicating reliability. Transfer entropy was less affected by the influence of the controller in detecting the causal connection. Transfer entropy appeared much more sensitive to the influence of additional noise.

In Section 7.4, an analysis of variance was performed to quantify the impact of different process conditions, and parameters on transfer entropy. The main purpose of this analysis was to establish guidelines for parametrisation (in fulfilment of Objective II), however, it also revealed the sensitivity of the optimal parameters for transfer entropy to different process conditions.

10.3 Objective II conclusion

The second objective of this dissertation was to develop a systematic workflow for the application of causality analysis techniques for fault diagnosis.

To address Objective II, a systematic workflow for the application of transfer entropy for oscillation diagnosis was developed in Chapter 7. This workflow exploited the relationships between the underlying process dynamics and the parameters required for calculation of transfer entropy to establish guidelines for parameter selection. A significant novel contribution from the investigation of these relationships was that a linear relationship could be fit to predict the optimal time interval given the oscillation period and time delay. The workflow using the developed guidelines was applied to an oscillation diagnosis case study from a minerals concentrator plant. The workflow provided a systematic approach to accurately determining the fault propagation path.

10.4 Objective III conclusion

The third objective of this dissertation was to develop a tool to aid the decision of which causality analysis method to select.

Chapter 8 presented a comparative analysis of Granger causality and transfer entropy used for fault diagnosis in industrial processes. The comparison was based on the desired performance characteristics outlined in Chapter 5.

Transfer entropy was found to be more generalisable, and visually interpretable. However, Granger causality was found to be easier to automate, much less computationally expensive, and easier to interpret the meaning of the values obtained. To directly address the the accuracy and precision of Granger causality and transfer entropy, their ability to find true connections in a simulated process was tested. The results indicated that Granger causality was more accurate, while transfer entropy showed higher precision.

A decision flow was developed from these comparisons to aid users in deciding when to use Granger causality or transfer entropy, as well as to aid in the interpretation of the causality maps obtained from these techniques.

The features of Granger causality and transfer entropy were illustrated on an industrial case study of oscillations in a mineral processing plant. In this case study, the causal map obtained from the transfer entropy analysis showed two root cause variables associated with the same unit in the process. The transfer entropy results were able to provide useful information for further analysis into the cause of the fault. Granger causality, on the other hand, showed a large number of spurious connections, and gave no clear indication of the root cause.

The developed guidelines provided useful information for selecting which causality analysis technique to use in specific scenarios. However, this investigation was limited to Granger causality and transfer entropy. The reason for limiting the investigation to these two techniques was that the literature review showed these two to be the most popular, and therefore the most industrially mature techniques. However, other techniques may be useful in specific scenarios, and these still have to be compared in the comprehensive way presented here.

10.5 Objective IV conclusion

The fourth objective of this dissertation was to present tools and develop guidelines for interpretation of causal maps for root cause analysis.

Chapter 9 investigated visualisation and algorithmic tools to aid interpretation of causality maps for root cause analysis.

First, the construction of causal maps was discussed. Various graph layout techniques were presented, and the advantages of each were discussed. The layered technique presents the nodes hierarchically, which presents the propagation paths of faults most clearly. The use of the transitive reduction to remove shortcut nodes was suggested. Transitive reduction effectively reduced the complexity of the graphs. Methods for grouping and augmenting causality maps based on the variable locations or categories. Augmenting the causality maps with different colours for different variable groupings aided interpretation of the graphs. Separating nodes according to different variable groupings aided the interpretation of the maps by reducing the density of the graphs.

Secondly, methods for interpretation of causal maps were discussed. The maxflow method for assigning node importance was presented. A graph complexity metric was presented, that was shown to be useful for determining whether a causal map could be easily interpreted by a user. Finally, graph traversal techniques, such as the depth-first search were presented, and it was illustrated how these techniques are useful for analysing propagation paths in a process.

A recommended procedure for causal map interpretation based on these presented methods was presented. This procedure may be limited by the fact that it does not provide definite steps to follow for the interpretation of causal maps. It focuses, instead, on presenting relevant and useful tools for a user to apply their engineering reasoning. In future, more automated procedures for this interpretation can be developed.

10.6 Fulfilment of overall project aim

The research hypothesis presented in Chapter 1 was:

> Performance of data-based causality analysis for fault diagnosis can be improved and made more accessible to the process engineering industry by developing systematic procedures for application and interpretation of results.

The aim of the project was to investigate the limitations of the causality analysis procedures currently available to process engineers as fault diagnosis tools and design an evaluate improvements to these tools. All the objectives defined were addressed satisfactorily. A systematic workflow for application of causality analysis techniques was developed and shown to be useful for application to an real world case study of oscillations in a mineral processing concentrator plant. The guidelines for choosing between Granger causality and transfer entropy provide a useful tool for engineers to decide which method to use. The tools for interpretation of causality analysis results presented provide useful aids for engineers.

10.7 Appraisal of dissertation contributions

Figure 10.1 illustrates the components of causality analysis investigated in Chapter 2 that were identified as needing improvement. This serves as an illustration of the contributions of this dissertation.

The novel contributions of this project are:

1. Application of causality analysis is complicated, with multiple decision-making steps that could affect the results. In the literature of causality analysis for fault diagnosis, no systematic framework addressing these numerous, complicated steps has been presented. Chapter 7 provides a systematic workflow addressing all these steps.

2. The accuracy of causality analysis techniques is sensitive to data selection and parameter selection. Chapter 7 provides an analysis of variance on the impact that process and fault dynamics and calculation parameters have on transfer entropy. These results are used to provide guidelines for the above-mentioned workflow. This approach of parametrisation of causality analysis techniques based on process dynamics is novel, and is shown to be effective.

3. The comparative analysis of Granger causality and transfer entropy based on all desired performance criteria for causality analysis techniques presented in Chapter 8 is novel. This comparison was used to provide useful guidelines for selection of which causality analysis technique to use and how to interpret the results.

4. Construction and interpretation of causality maps is an important step for root cause analysis using these methods that has been neglected in fault diagnosis literature, with most authors providing *ad-hoc* interpretations of results. Chapter 9, provides novel guidelines for construction and interpretation of causality maps based on existing techniques.

10.8 Suggestions for future work

The objectives of this dissertation were successfully met. However, candid scrutiny of the results did highlight areas that still require further work.

The interpretation of causal maps still requires further work. The tools and guidelines presented in Chapter 9 present a good starting point to aid engineers in interpreting the results. However,

the interpretation still requires subjective interpretation in cases where the propagation paths are ambiguous. Therefore, more rigorous automated graph interpretation techniques could be applied. Specifically, tools exploiting connection strengths as an indication of likely propagation paths could be utilised. The difficulty of this approach is that causality measures do not directly translate to connections strength. In some cases the causality measure can be used to represent relative connection strengths.

Time series signals are complex, with numerous drivers impacting their responses. These signals can be decomposed into their constituent components using spectral decomposition techniques such as Singular Spectrum Analysis (SSA). Applying causality analysis to each of the decomposed components may provide insight into which of the drivers are responsible for the structure observed in the causal map. This can improve interpretation of the causal map. It could also be used for fault diagnosis in the presence of multiple faults. For example, when multiple oscillations are present in a process, SSA can be sued to decompose the signals into components for each frequency of oscillation. A causal map could then be constructed for each oscillation.

References

Aftab MF, Hovd M & Sivalingam S, 2017, *Convergent cross mapping (CCM) based approach for isolating the source of plant-wide disturbances*, Proceedings of the 2017 IEEE Conference on Control Technology and Applications (CCTA), IEEE, Mauna Lani Resort, HI, USA, pp. 1492–1498.

Aho A, Garey M & Ullman J, 1972, *The Transitive Reduction of a Directed Graph*, SIAM Journal on Computing, **1(2)**, pp. 131–137.

Akaike H, 1974, *A New Look at the Statistical Model Identification*, IEEE Transactions on Automatic Control, **19(6)**, pp. 716–723.

Alcala C & Qin S, 2009, *Reconstruction-based contribution for process monitoring*, Automatica, **45(7)**, pp. 1593–1600.

Arroyo E, Schulze D, Christiansen L, Fay A & Thornhill NF, 2014, *Derivation of Diagnostic Models Based on Formalized Process Knowledge*, IFAC Proceedings Volumes, **47(3)**, pp. 3456–3464.

Arroyo Esquivel E, 2017, *Capturing and Exploiting Plant Topology and Process Information as a Basis to Support Engineering and Operational Activities in Process Plants*, Doctoral Dissertation, Helmut Schmidt University, Hamburg.

Baccal LA & Sameshima K, 2001, *Partial directed coherence: a new concept in neural structure determination.*, Biological cybernetics, **84(6)**, pp. 463–474.

Bang-Jensen J, 2010, *Digraphs : theory, algorithms, and applications*, 2nd Edition, London : Springer, London.

Barnett L, Barrett A & Seth A, 2009, *Granger causality and transfer entropy Are equivalent for gaussian variables*, Physical Review Letters, **103(23)**.

Barnett L & Seth AK, 2014, *The MVGC multivariate Granger causality toolbox: A new approach to Granger-causal inference*, Journal of Neuroscience Methods, **223**, pp. 50–68.

Barnett L & Seth AK, 2017, *Detectability of Granger causality for subsampled continuous-time neurophysiological processes*, Journal of Neuroscience Methods, **275**, pp. 93–121.

Bauer M, Cox JW, Caveness MH, Downs JJ & Thornhill NF, 2007a, *Finding the Direction of Disturbance Propagation in a Chemical Process Using Transfer Entropy*, IEEE Transactions on Control Systems Technology, **15(1)**, pp. 12–21.

Bauer M, Cox JW, Caveness MH, Downs JJ & Thornhill NF, 2007b, *Nearest Neighbors Methods for Root Cause Analysis of Plantwide Disturbances*, Industrial & Engineering Chemistry Research, **46(18)**, pp. 5977–5984.

Bauer M & Thornhill NF, 2008, *A practical method for identifying the propagation path of plant-wide disturbances*, Journal of Process Control, **18(78)**, pp. 707–719.

Birk W, Castao M & Johansson A, 2014, *An application software for visualization and control configuration selection of interconnected processes*, Control Engineering Practice, **26(Supplement C)**, pp. 188–200.

Box GEP, 2008, *Time series analysis : forecasting and control*, 4th Edition, Hoboken, N.J. : John Wiley, Hoboken, N.J.

Bressler SL & Seth AK, 2011, *Wiener - Granger Causality: A well established methodology*, NeuroImage, **58(2)**, pp. 323–329.

Bryan K & Leise T, 2006, *The USD25,000,000,000 eigenvector: The linear algebra behind Google*, SIAM Review, **48(3)**, pp. 569–581.

Cao L, 1997, *Practical method for determining the minimum embedding dimension of a scalar time series*, Physica D: Nonlinear Phenomena, **110(1-2)**, pp. 43–50.

Chiang LH, Jiang B, Zhu X, Huang D & Braatz RD, 2015, *Diagnosis of multiple and unknown faults using the causal map and multivariate statistics*, Journal of Process Control, **28**, pp. 27–39.

Chiang LH, Russell EL & Braatz RD, 2000, *Fault diagnosis in chemical processes using Fisher discriminant analysis, discriminant partial least squares, and principal component analysis*, Chemometrics and Intelligent Laboratory Systems, **50(2)**, pp. 243–252.

Clark AT, Ye H, Isbell F, Deyle ER, Cowles J, Tilman GD & Sugihara G, 2015, *Spatial convergent cross mapping to detect causal relationships from short time series*, Ecology, **96(5)**, pp. 1174–1181.

Cui L, Zhao J & Zhang R, 2010, *The integration of HAZOP expert system and piping and instrumentation diagrams*, Process Safety and Environmental Protection, **88(5)**, pp. 327–334.

Deloitte, 2018, (Unpublished) , Technical report, Available from `https://www2.deloitte.com/za/en/pages/energy-and-resources/articles/the-future-of-mining-in-south-africa.html`.

Di Geronimo Gil G, Alabi D, Iyun O & Thornhill N, 2011, , pp. 15–21.

Dong Y & Qin SJ, 2017, *Dynamic latent variable analytics for process operations and control*, Computers & Chemical Engineering.

Duan P, 2014, *Information Theory-based Approaches for Causality Analysis with Industrial Applications*, Thesis, University of Alberta.

Duan P, Chen T, Shah SL & Yang F, 2014, *Methods for root cause diagnosis of plant-wide oscillations*, AIChE Journal, **60(6)**, pp. 2019–2034.

Duan P, Yang F, Chen T & Shah SL, 2013, *Direct Causality Detection via the Transfer Entropy Approach*, IEEE Transactions on Control Systems Technology.

Duan P, Yang F, Shah S & Chen T, 2015, *Transfer Zero-Entropy and Its Application for Capturing Cause and Effect Relationship Between Variables*, IEEE Transactions on Control Systems Technology, **23(3)**, pp. 855–867.

Faes L, Porta A & Nollo G, 2010, *Testing Frequency-Domain Causality in Multivariate Time Series*, IEEE Transactions on Biomedical Engineering, **57(8)**, pp. 1897–1906.

Ge Z & Song Z, 2013, *Distributed PCA Model for Plant-Wide Process Monitoring*, Industrial & Engineering Chemistry Research, **52(5)**, pp. 1947–1957.

Gibbons AAM, 1985, *Algorithmic graph theory*, Cambridge, England : Cambridge University Press, Cambridge, England.

Gigi S & Tangirala AK, 2010, *Quantitative analysis of directional strengths in jointly stationary linear multivariate processes*, Biological Cybernetics, **103(2)**, pp. 119–133.

Girod B, 2001, *Signals and systems*, Wiley, Chichester.

Govindan R, Raethjen J, Kopper F, Claussen J & Deuschl G, 2005, *Estimation of time delay by coherence analysis*, Physica A: Statistical Mechanics and its Applications, **350(2-4)**, pp. 277–295.

Granger CWJ, 1969, *Investigating Causal Relations by Econometric Models and Cross-spectral Methods*, Econometrica, **37(3)**, pp. 424–438.

Hajihosseini P, Salahshoor K & Moshiri B, 2014, *Process fault isolation based on transfer entropy algorithm*, ISA Transactions, **53(2)**, pp. 230–240.

Hill RC, 2011, *Principles of econometrics*, 4th Edition, Hoboken, NJ : Wiley, Hoboken, NJ.

Hlavackov-Schindler K, 2011, *Equivalence of granger causality and transfer entropy: A generalization*, Applied Mathematical Sciences, **5(73-76)**, pp. 3637–3648.

Hodouin D, 2011, *Methods for automatic control, observation, and optimization in mineral processing plants*, Journal of Process Control, **21(2)**, pp. 211–225.

Horch A, Cox J & Bonavita N, 2007, *Peak performance*, ABB Review, **(1)**, pp. 24–29.

Hu W, Wang J, Chen T & Shah SL, 2017, *Cause-effect analysis of industrial alarm variables using transfer entropies*, Control Engineering Practice, **64**, pp. 205–214.

Hume D, 2008, *An enquiry concerning human understanding*, Oxford : Oxford University Press, Oxford.

Iri M, Aoki K, O'Shima E & Matsuyama H, 1979, *An algorithm for diagnosis of system failures in the chemical process*, Computers & Chemical Engineering, **3(14)**, pp. 489–493.

Isermann R, 2006, *Fault-diagnosis systems : an introduction from fault detection to fault tolerance*, Springer Berlin Heidelberg, Berlin.

Jiang H, Patwardhan R & Shah SL, 2009, *Root cause diagnosis of plant-wide oscillations using the concept of adjacency matrix*, Journal of Process Control, **19(8)**, pp. 1347–1354.

Jiang H, Shoukat Choudhury M & Shah SL, 2007, *Detection and diagnosis of plant-wide oscillations from industrial data using the spectral envelope method*, Journal of Process Control, **17(2)**, pp. 143–155.

Kantz H & Schreiber T, 1997, *Nonlinear Time Series Analysis*, Cambridge University Press, New York, USA.

Keim D, Kohlhammer J, Ellis G & Mansmann F, 2010, *Mastering the Information Age Solving Problems with Visual Analytics*, Eurographics Association.

Kourti T & MacGregor JF, 1995, *Process analysis, monitoring and diagnosis, using multivariate projection methods*, Chemometrics and Intelligent Laboratory Systems, **28(1)**, pp. 3–21.

Kuhnert C, 2013, *Data-driven Methods for Fault Localization in Process Technology*.

Kuhnert C & Beyerer J, 2014, *Data-Driven Methods for the Detection of Causal Structures in Process Technology*, Machines, **2(4)**, pp. 255–274.

Landman R & Jamsa-Jounela SL, 2016, *Hybrid approach to casual analysis on a complex industrial system based on transfer entropy in conjunction with process connectivity information*, Control Engineering Practice, **53**, pp. 14–23.

Landman R, Kortela J, Sun Q & Jamsa-Jounela SL, 2014, *Fault propagation analysis of oscillations in control loops using data-driven causality and plant connectivity*, Computers & Chemical Engineering, **71**, pp. 446–456.

Lewis D, 1973, *Causation*, The Journal of Philosophy, **70(17)**, pp. 556–567.

Li Q & Racine J, 2011, *Nonparametric econometrics: Theory and practice*, Nonparametric Econometrics: Theory and Practice.

Li W, Yue H, Valle-Cervantes S & Qin S, 2000, *Recursive PCA for adaptive process monitoring*, Journal of Process Control, **10(5)**, pp. 471–486.

Lindner B & Auret L, 2015, *Application of data-based process topology and feature extraction for fault diagnosis of an industrial platinum group metals concentrator plant*, IFAC-PapersOnLine, **28(17)**, pp. 102–107.

Lindner B, Auret L & Bauer M, 2017a, *Investigating the Impact of Perturbations in Chemical Processes on Data-Based Causality Analysis. Part 1: Defining Desired Performance of Causality Analysis Techniques*, IFAC-PapersOnLine, **50(1)**, pp. 3269–3274.

Lindner B, Auret L & Bauer M, 2017b, *Investigating the Impact of Perturbations in Chemical Processes on Data-Based Causality Analysis. Part 2: Testing Granger Causality and Transfer Entropy*, IFAC-PapersOnLine, **50(1)**, pp. 3275–3280.

Lindner B, Auret L & Bauer M, 2018a, *A systematic workflow for oscillation diagnosis using transfer entropy*, IEEE Transactions on Control Systems Technology, manuscipt accepted for final submission.

Lindner B, Auret L & Knoblauch N, 2014, *Exploiting process topology for fault diagnosis in a simulated pressure leaching system*, Proceedings of the Proceedings of International Minerals Processing Conference (IMPC 2014).

Lindner B, Chioua M, Groenewald J, Auret L & Bauer M, 2018b, *Diagnosis of Oscillations in an Industrial Mineral Process Using Transfer Entropy and Nonlinearity Index* , IFAC-PapersOnLine, **51(24)**, pp. 1409–1416.

Lindner BS & Auret L, 2014, *Data-driven fault detection with process topology for fault identification*, IFAC Proceedings Volumes, **47(3)**, pp. 8903–8908.

Liu Y, Wang FL & Chang YQ, 2013, *Reconstruction in integrating fault spaces for fault identification with kernel independent component analysis*, Chemical Engineering Research and Design, **91(6)**, pp. 1071–1084.

Lizier JT, 2014, *JIDT: An information-theoretic toolkit for studying the dynamics of complex systems*, Frontiers in Robotics and AI, **1**.

Luo L, Cheng F, Qiu T & Zhao J, 2017, *Refined convergent cross-mapping for disturbance propagation analysis of chemical processes*, Computers & Chemical Engineering, **106**, pp. 1–16.

MacGregor JF, Jaeckle C, Kiparissides C & Koutoudi M, 1994, *Process monitoring and diagnosis by multiblock PLS methods*, AIChE Journal, **40(5)**, pp. 826–838.

MacGregor JF & Kourti T, 1995, *Statistical process control of multivariate processes*, Control Engineering Practice, **3(3)**, pp. 403–414.

Madsen H, 2008, *Time series analysis*, Boca Raton : Chapman & Hall/CRC, Boca Raton.

Maurya MR, Rengaswamy R & Venkatasubramanian V, 2003, *A Systematic Framework for the Development and Analysis of Signed Digraphs for Chemical Processes. 1. Algorithms and Analysis*, Industrial & Engineering Chemistry Research, **42(20)**, pp. 4789–4810.

Mead RR, 2012, *Statistical principles for the design of experiments*, Applications to real experiments, Cambridge : Cambridge University Press.

Muller D, de Villiers PGR & Humphries G, 2010, *A Holistic Approach to Flotation Mass Pull and Grade Control*, IFAC Proceedings Volumes, **43(9)**, pp. 133–136.

Naghoosi E, Huang B, Domlan E & Kadali R, 2013, *Information transfer methods in causality analysis of process variables with an industrial application*, Journal of Process Control, **23(9)**, pp. 1296–1305.

Odiowei PEP & Yi Cao, 2010, *Nonlinear Dynamic Process Monitoring Using Canonical Variate Analysis and Kernel Density Estimations*, Industrial Informatics, IEEE Transactions on, **6(1)**, pp. 36–45.

Olivier LE & Craig IK, 2017, *Should I shut down my processing plant? An analysis in the presence of faults*, Journal of Process Control, **56**, pp. 35–47.

Pearl J, 2003, *Statistics and causal inference: A review*, Test, **12(2)**, pp. 281–345.

Pearl J, 2009, *Causal inference in statistics: An overview*, Statistics Surveys, **3**, pp. 96–146.

Qin SJ, 2003, *Statistical process monitoring: Basics and beyond*, Journal of Chemometrics, **17(8-9)**, pp. 480–502.

Qin SJ, 2012, *Survey on data-driven industrial process monitoring and diagnosis*, Annual Reviews in Control, **36(2)**, pp. 220–234.

Rashidi B, Singh DS & Zhao Q, 2018, *Data-driven root-cause fault diagnosis for multivariate non-linear processes*, Control Engineering Practice, **70**, pp. 134–147.

Reis M & Gins G, 2017, *Industrial Process Monitoring in the Big Data/Industry 4.0 Era: from Detection, to Diagnosis, to Prognosis*, Processes, **5**, p. 35.

Renyi A, 1961, *On Measures of Entropy and Information*, Proceedings of the Proceedings of the Fourth Berkeley Symposium on Mathematical Statistics and Probability, Volume 1: Contributions to the Theory of Statistics, University of California Press, California, pp. 547–561.

Romero D, Graven TG & Thornhill N, 2014, *Towards the development of a tool for visualising plantwide dependencies*, Proceedings of the 2014 IEEE Emerging Technology and Factory Automation (ETFA), pp. 1–4.

Romero DD & Graven TG, 2013, *Visual representation of connectivity information for efficient system understanding*, Proceedings of the Human Factors and Ergonomics Society Annual Meeting, **57(1)**, pp. 2012–2016.

Romero DD & Thornhill NF, 2014, , IEEE, pp. 743–748.

Schreiber T, 2000, *Measuring Information Transfer*, Physical Review Letters, **85(2)**, pp. 461–464.

Schreiber T & Schmitz A, 2000, *Surrogate time series*, Physica D: Nonlinear Phenomena, **142(3-4)**, pp. 346–382.

Sderstrm T, 1989, *System identification*, New York, N.Y. : Prentice-Hall, New York, N.Y.

Shannon CE, 1948, *A mathematical theory of communication*, The Bell System Technical Journal, **27(3)**, pp. 379–423.

Shiozaki J, Matsuyama H, O'Shima E & Iri M, 1985, *An improved algorithm for diagnosis of system failures in the chemical process*, Computers and Chemical Engineering, **9(3)**, pp. 285–293.

Shu Y & Zhao J, 2012, *Data-driven causal inference based on a modified transfer entropy*, Computer Aided Chemical Engineering, **31**, pp. 1256–1260.

Shumway RH & Stoffer DS, 2014, *Time Series Analysis and Its Applications*, Springer.

Silverman BW, 1986, *Density estimation for statistics and data analysis*, 1st Edition, London : Chapman and Hall, London.

Sinnott RK, 2009, *Chemical engineering design*, fifth edition. Edition, Butterworth Heinemann, Oxford.

Skogestad S, 2010, *Multivariable feedback control : analysis and design*, 2nd Edition, Chichester : John Wiley, Chichester.

Stockmann M, Haber R & Schmitz U, 2012, *Source identification of plant-wide faults based on k nearest neighbor time delay estimation*, Journal of Process Control, **22(3)**, pp. 583–598.

Streicher SJ, Wilken SE & Sandrock C, 2014, *Eigenvector Analysis for the Ranking of Control Loop Importance*, Proceedings of the Kleme JJ, Varbanov PS & Liew PY (Eds), Computer Aided Chemical Engineering, volume 33, Elsevier, pp. 835–840.

Sugihara G, May R, Ye H, Hsieh CH, Deyle E, Fogarty M & Munch S, 2012, *Detecting causality in complex ecosystems*, Science, **338(6106)**, pp. 496–500.

Sugiyama K, Tagawa S & Toda M, 1981, *Methods for Visual Understanding of Hierarchical System Structures*, IEEE Transactions on Systems, Man, and Cybernetics, **11(2)**, pp. 109–125.

Takens F, 1981, *Detecting strange attractors in turbulence*, pp. 366–381 in *Dynamical Systems and Turbulence, Warwick 1980*, volume 898, pp. 366–381. Springer Berlin Heidelberg, Berlin, Heidelberg.

Tarjan R, 1972, *Depth-First Search and Linear Graph Algorithms*, SIAM Journal on Computing, **1(2)**, p. 15.

Thambirajah J, Benabbas L, Bauer M & Thornhill NF, 2009, *Cause-and-effect analysis in chemical processes utilizing XML, plant connectivity and quantitative process history*, Computers & Chemical Engineering, **33(2)**, pp. 503–512.

Thornhill N, 2005, *Finding the source of nonlinearity in a process with plant-wide oscillation*, IEEE Transactions on Control Systems Technology, **13(3)**, pp. 434–443.

Thornhill NF & Horch A, 2007, *Advances and new directions in plant-wide disturbance detection and diagnosis*, Special Issue - International Symposium on Advanced Control of Chemical Processes (ADCHEM) ADCHEM 2006 International Symposium on Advanced Control of Chemical Processes (ADCHEM), **15(10)**, pp. 1196–1206.

Van den Kerkhof P, Vanlaer J, Gins G & Van Impe JFM, 2013, *Analysis of smearing-out in contribution plot based fault isolation for Statistical Process Control*, Chemical Engineering Science, **104**, pp. 285–293.

Venkatasubramanian V, Zhao J & Viswanathan S, 2000, *Intelligent systems for HAZOP analysis of complex process plants*, Computers and Chemical Engineering, **24(9-10)**, pp. 2291–2302.

Vicente R, Wibral M, Lindner M & Pipa G, 2010, *Transfer entropya model-free measure of effective connectivity for the neurosciences*, Journal of Computational Neuroscience, **30(1)**, pp. 45–67.

Wakefield BJ, Lindner BS, McCoy JT & Auret L, 2018, *Monitoring of a simulated milling circuit: Fault diagnosis and economic impact*, Minerals Engineering, **120**, pp. 132–151.

Wang F, Gao J & Wang H, 2012, *A new intelligent assistant system for HAZOP analysis of complex process plant*, Journal of Loss Prevention in the Process Industries, **25(3)**, pp. 636–642.

Wang J, Yang F, Chen T & Shah SL, 2016, *An Overview of Industrial Alarm Systems: Main Causes for Alarm Overloading, Research Status, and Open Problems*, IEEE Transactions on Automation Science and Engineering, **13(2)**, pp. 1045–1061.

Westerhuis JA, Kourti T & MacGregor JF, 1998, *Analysis of multiblock and hierarchical PCA and PLS models*, Journal of Chemometrics, **12(5)**, pp. 301–321.

Wibral M, Vicente R & Lindner M, 2014, *Transfer Entropy in Neuroscience*, pp. 3–36 in Wibral M, Vicente R & Lizier JT (Eds), *Directed Information Measures in Neuroscience*, Understanding Complex Systems, pp. 3–36. Springer Berlin Heidelberg.

Wiener N, 1956, *The theory of prediction*, Modern mathematics for engineers, **1**, pp. 125–139.

Wills BABA, 2007, *Wills' mineral processing technology an introduction to the practical aspects of ore treatment and mineral recovery*, 7th Edition, Amsterdam : Elsevier Science & Technology, Amsterdam.

Wold S, Kettaneh N & Tjessem K, 1996, *Hierarchical multiblock PLS and PC models for easier model interpretation and as an alternative to variable selection*, Journal of Chemometrics, **10(5-6)**, pp. 463–482.

Xiao Y & He Y, 2011, *A novel approach for analog fault diagnosis based on neural networks and improved kernel PCA*, Neurocomputing, **74(7)**, pp. 1102–1115.

Yang F, Chen T, Shah SL & Duan P, 2014, *Capturing Connectivity and Causality in Complex Industrial Processes*, SpringerBriefs in Applied Sciences and Technology, Springer, Cham.

Yang F, Shah SL, Xiao D & Chen T, 2012, *Improved correlation analysis and visualization of industrial alarm data*, ISA Transactions, **51(4)**, pp. 499–506.

Yang F, Sirish LS & Deyun Xiao, 2010, , pp. 387–392, conference Proceedings.

Yang F & Xiao D, 2012, *Progress in Root Cause and Fault Propagation Analysis of Large-Scale Industrial Processes*, Journal of Control Science and Engineering, **vol. 2012**, pp. Article ID 478373, 10 pages.

Ye H, Deyle E, Gilarranz L & Sugihara G, 2015, *Distinguishing time-delayed causal interactions using convergent cross mapping*, Scientific Reports, **5**.

Yim SY, Ananthakumar HG, Benabbas L, Horch A, Drath R & Thornhill NF, 2006, *Using process topology in plant-wide control loop performance assessment*, Computers & Chemical Engineering, **31(2)**, pp. 86–99.

Yingwang X & Ying D, 2013, *Combination method of kernel principal component analysis and independent component analysis for process monitoring*, Applied Mechanics and Materials, **249-250**, pp. 153–158, monograph.

Yu J, 2012, *A nonlinear kernel Gaussian mixture model based inferential monitoring approach for fault detection and diagnosis of chemical processes*, Chemical Engineering Science, **68(1)**, pp. 506–519.

Yuan T & Qin SJ, 2014, *Root cause diagnosis of plant-wide oscillations using Granger causality*, Journal of Process Control, **24(2)**, pp. 450–459.

Zhang L, Zheng J & Xia C, 2015, *Propagation Analysis of Plant-Wide Oscillations Using Partial Directed Coherence*, Journal of Chemical Engineering of Japan, **48(9)**, pp. 766–773.

Zhang Y, Cen Y & Luo G, 2018, *Causal direction inference for network alarm analysis*, Control Engineering Practice, **70**, pp. 148–153.

Zhang Y, Li S, Hu Z & Song C, 2012, *Dynamical process monitoring using dynamical hierarchical kernel partial least squares*, Chemometrics and Intelligent Laboratory Systems, **118**, pp. 150–158.

Zhang Y & Ma C, 2012, *Decentralized fault diagnosis using multiblock kernel independent component analysis*, Chemical Engineering Research and Design, **90(5)**, pp. 667–676.

APPENDIX A

Analysis of variance for parametrisation relationships

For the development of the workflow for application of transfer entropy in Chapter 7, an analysis of variance (ANOVA) approach was used to screen the important factors and provide insight into the relationships between process conditions and calculation parameters. The ANOVA included process condition factors (namely the oscillation period, time delay, and residence time) and calculation parameter factors (namely the number of samples, sampling time, time interval, and embedding dimensions) for a total of 8 factors. Table A.1 displays the selected levels for each factor included in the ANOVA.

A full factorial design was implemented with 5 repetitionsMead [2012]. Random process noise is simulated, with different random seeds, so that repeated experiments can be performed for this ANOVA. This came to a total of $4^6 \times 2 \times 2 \times 5 = 81920$ runs. Up to two-way interactions were considered. Higher order interactions can be investigated in further analysis. The results of the ANOVA are shown in Table A.2.

The responses of transfer entropy to individual factors can be observed by plotting their mean values for each level of the factor. These plots are provided in Figure A.1.

TABLE A.1: *Design of ranges for factors used in analysis of variance.*

Factor	**Symbol**	**Range**	**Units**
Oscillation period	P	[1 30]	$[min]$
Time delay	T_D	[0.2 6]	$[min]$
Residence time	τ_p	[5 15]	$[min]$
Number of samples	N_S	[100 5000]	$[samples]$
Sampling time	T_S	[0.1 1]	$[min]$
Time interval	τ	[1 100]	$[samples]$
Embedding dimension for Y	K	[0 1]	$[samples]$
Embedding dimension for X	L	[1 2]	$[samples]$

TABLE A.2: *ANOVA results.*

Factor	**Sum Sq.**	**d.f.**	**Mean Sq.**	F	**Prob**$> F$
P	12149.6	3	4049.9	0.35	0.7868
T_D	17449.9	3	5816.6	0.51	0.6772
τ_p	34546.2	3	11515.4	1	0.3895
N_S	486061	3	162020.3	14.13	0
T_S	8594.6	3	2864.9	0.25	0.8614
τ	187418.3	3	62472.8	5.45	0.001
K	12288.9	1	12288.9	1.07	0.3005
L	732757.5	1	732757.5	63.92	0
$P * T_D$	127569.8	9	14174.4	1.24	0.267
$P * \tau_p$	113951	9	12661.2	1.1	0.3554
$P * N_S$	139078.9	9	15453.2	1.35	0.206
$P * T_S$	106449.5	9	11827.7	1.03	0.4113
$P * \tau$	140848.7	9	15649.9	1.37	0.1976
$P * K$	130.9	3	43.6	0	0.9997
$P * L$	81383.2	3	27127.7	2.37	0.0688
$T_D * \tau_p$	153206.9	9	17023	1.48	0.1468
$T_D * N_S$	73899.2	9	8211	0.72	0.6945
$T_D * T_S$	101472.1	9	11274.7	0.98	0.4511
$T_D * \tau$	127457.5	9	14161.9	1.24	0.2677
$T_D * K$	29307.2	3	9769.1	0.85	0.4652
$T_D * L$	26381	3	8793.7	0.77	0.5123
$\tau_p * N_S$	91184.5	9	10131.6	0.88	0.5388
$\tau_p * T_S$	90548.6	9	10061	0.88	0.5444
$\tau_p * \tau$	89470.3	9	9941.1	0.87	0.5539
$\tau_p * K$	23364.9	3	7788.3	0.68	0.5645
$\tau_p * L$	27834	3	9278	0.81	0.4884
$N_S * T_S$	62216.4	9	6912.9	0.6	0.7956
$N_S * \tau$	811191.2	9	90132.4	7.86	0
$N_S * K$	243525.1	3	81175	7.08	0.0001
$N_S * L$	149386.7	3	49795.6	4.34	0.0046
$T_S * \tau$	41204.6	9	4578.3	0.4	0.936
$T_S * K$	18047.1	3	6015.7	0.52	0.6652
$T_S * L$	46448.8	3	15482.9	1.35	0.2559
$\tau * K$	154236	3	51412	4.48	0.0038
$\tau * L$	464765.5	3	154921.8	13.51	0
$K * L$	127557.8	1	127557.8	11.13	0.0009
Error	936881620.5	81727	11463.6		
Total	942035003.8	81919			

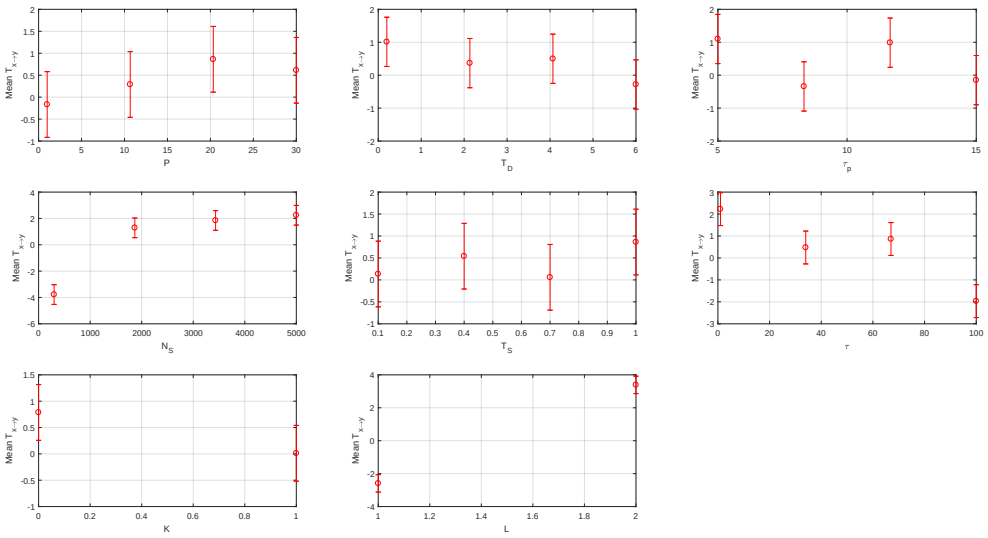

(a) *Mean transfer entropy values for each factor's levels.*

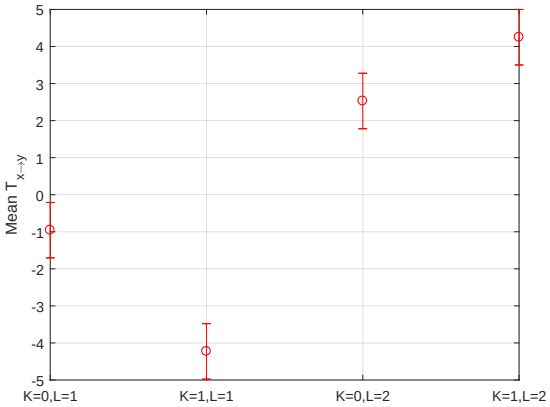

(b) *Mean transfer entropy values for each interaction between K and L.*

FIGURE A.1: *ANOVA results for different levels of each factor.*

APPENDIX B

Transfer entropy application procedure

Chapter 7 presented a systematic workflow for the application of transfer entropy for diagnosis of plant-wide oscillations. This workflow was used to analyse the oscillations discussed in Chapter 8.

B.1 Detect fault

Oscillations were observed in the mass pull variable. These oscillations persisted for over 12 hours. To find the possible suspect variables one can look at upstream and downstream sections to determine whether any of their KPIs showed oscillations. Upstream of the flotation circuit is the milling circuit.

B.2 Perform spectral analysis

Once the oscillation has been detected, additional information on the nature of the oscillation may be discerned using spectral analysis. Using the fast-Fourier transform to find the peak oscillation frequencies it was observed that 27 of the selected trends displayed a common oscillation period of 69 min.

- **Oscillatory variables:** The variables that shared this oscillation period are shown in Figure 8.8. This includes variables from the primary milling circuit, flotation circuit, and secondary milling circuit.
- **Oscillation period:** $P = 69min$.

B.3 Select data for transfer entropy

The suspect variables were identified in Section 7.5.2 included variables from the primary milling, flotation, and secondary milling circuit.

- **Sampling time:** $T_S = 10s$.
- **Number of samples:** $N_S = 4530$ samples.

- **Suspect variables:** 27 variables shown in Figure 8.8.

B.4 Determine process dynamics

Suspect variables were narrowed down during the spectral analysis. For each pair of these variables, system identification was performed to fit a first order plus time delay model. This basic model gave a rough estimate of the time constants of the time delays between the variables. The *System Identification Toolbox* in MATLAB was used to determine the time delay estimates (T_D, in seconds) for each pair of candidate variables.

B.5 Select parameters for transfer entropy

The time delay and the oscillation period can be used to get parameters for transfer entropy.

$$\hat{\tau}_{max} = 0.33P + 0.53T_D + 0.66 \tag{B.1}$$

- **Embedding dimension for input:** $K = 1$.
- **Embedding dimension for output:** $L = 2$.
- **Time interval:** The time interval can be calculated from T_D and P using Equation 7.1.
- **Prediction horison:** $H = \tau$.

B.6 Perform transfer entropy analysis

Once all the parameters have been selected for each pair of variables the transfer entropy analysis can be performed. The causality map shown in Figure 8.9 was obtained.